Mechanical Behavior and Radiation Effects
2017 Principal Investigators' Meeting

September 19-21, 2017
Washington Marriott, Gaithersburg, MD

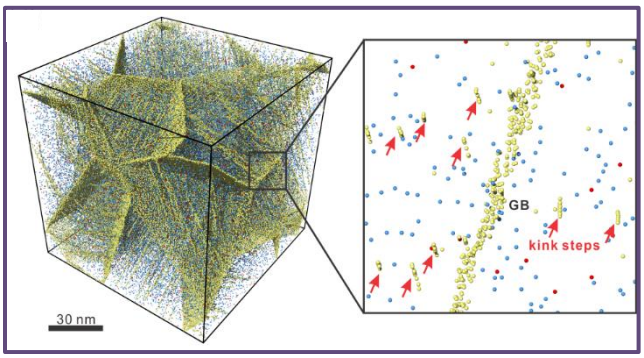

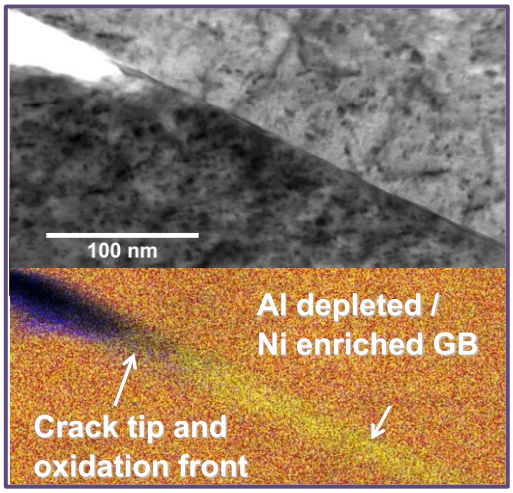

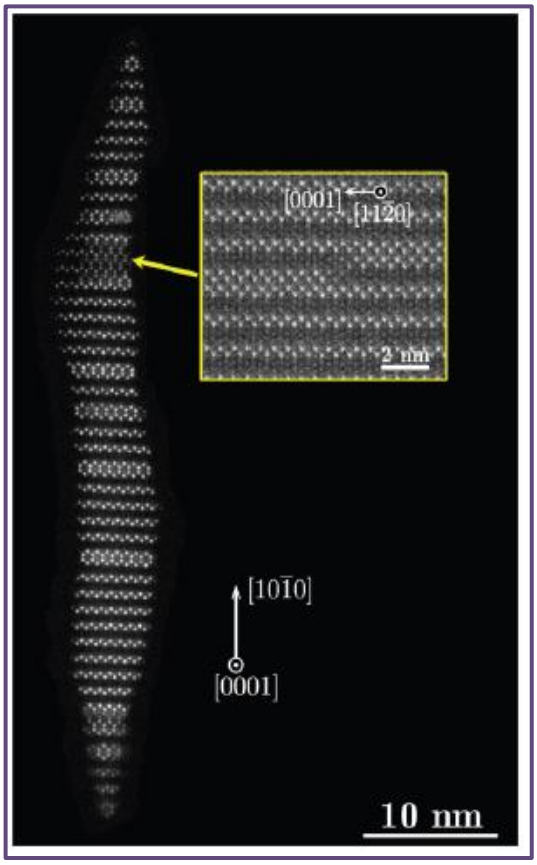

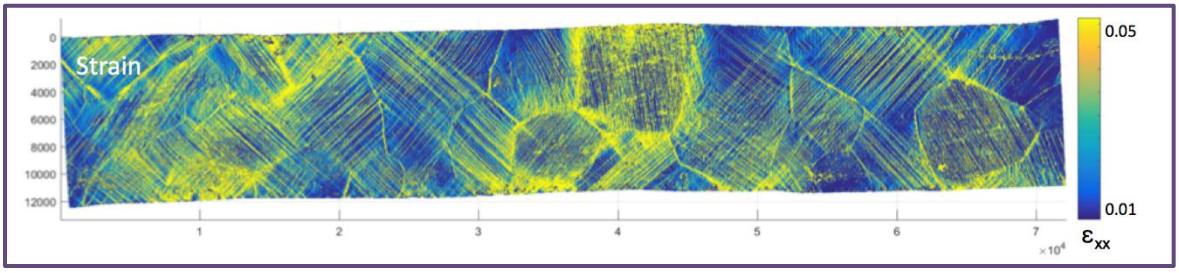

U.S. DEPARTMENT OF ENERGY | Office of Science

Materials Sciences and Engineering Division
Office of Basic Energy Sciences

Cover

Top Left: Hybrid Monte-Carlo/molecular-dynamics simulations of segregation of 0.8 at. % Cu atoms in nanotwinned Ag at 500 K. Equilibrium Cu atom distribution in large-scale nt-Ag model showing simultaneous Cu segregation to GBs and TB defects. Cu atoms segregated to kink steps and GBs are colored in yellow, atoms moved to coherent TB segments in red, and other atoms staying in solution in blue. (Sansoz, University of Vermont)

Right: HAADF-STEM image of precipitate ordering in a dilute Mg-Nd alloy. The bright spots signify Nd atoms. The precipitate (ordered pattern) is coherently embedded in an HCP Mg matrix (dark region surrounding the precipitate) (Marquis et al., University of Michigan)

Middle Left: Stress Corrosion Crack in Ni-4Al sample stressed in 330°C hydrogenated water. ATEM reveals ~20nm crack tip with $NiAl_2O_4$, limited grain boundary migration and Al depletion to ~100 nm ahead of tip. (Bruemmer et al., PNNL)

Bottom: SEM-Digital Image Correlation data of a 99.99% Al oligocrystalline specimen after straining (Field of View approx. 5 mm x 1 mm) (Daly, University of California, Santa Barbara)

This document was produced under contract number DE-SC0014664 between the U.S. Department of Energy and Oak Ridge Associated Universities.

The research grants and contracts described in this document are supported by the U.S. DOE Office of Science, Office of Basic Energy Sciences, Materials Sciences and Engineering Division.

Foreword

This volume comprises the scientific content of the 2017 Mechanical Behavior and Radiation Effects Principal Investigators' (PI) Meeting sponsored by the Division of Materials Sciences and Engineering (DMS&E) in the Office of Basic Energy Sciences (BES) of the U. S. Department of Energy (DOE). The meeting, held on September 19–21 at the Washingtonian Marriott, Gaithersburg, Maryland, is the sixth such meeting on this topic and is one among a series of research theme-based PI meetings being held by DMS&E. The meeting's focus is on research in mechanical behavior and radiation effects of materials, and it also features research that cuts across several other BES core research program areas and Energy Frontier Research Centers where appropriate and relevant.

The studies of mechanical behavior and radiation effects have a long and important history at DOE and its predecessors. It is a tribute to the researchers that the field has continued to move forward into a number of important areas, as can be seen by the diversity of projects being presented at this meeting. Attendees will note a number of new projects and research directions since the 2015 meeting including two new recipients of the Early Career Research Program award. These new projects add to the exciting areas of research and cutting-edge techniques that are a hallmark of this program.

The purpose of the Mechanical Behavior and Radiation Effects PI Meeting is to bring together researchers funded by DMS&E in this important area of research on a periodic basis (approximately every two years) in order to facilitate the exchange of new results and research highlights, to nucleate new ideas and collaborations among the participants, and to identify needs of the research community. The meeting will also help DMS&E in assessing the state of the program, identifying new research directions and recognizing programmatic needs.

I would like to express my sincere thank all of the attendees for their active participation and for sharing their ideas and new research results. Additional thanks go to Professors Samantha Daly and Reiner Dauskardt, who have helped to chair this meeting and provided a number of good suggestions of how to improve the overall flow. I would also like to express my sincere gratitude to Ms Teresa Crockett in DMS&E, and Ms Linda Severs (plus others) of the Oak Ridge Institute for Science and Education (ORISE) for their dedicated and outstanding work in taking care of all the logistical aspects of the meeting.

John Vetrano
Program Manager
Mechanical Behavior and Radiation Effects
Division of Materials Sciences and Engineering
Office of Basic Energy Sciences
U.S. Department of Energy

Agenda

Mechanical Behavior and Radiation Effects
Principal Investigators' Meeting Agenda

Tuesday, September 19, 2017

7:30 – 8:30 am	**Breakfast**
8:30 – 8:40 am	*Welcome from Meeting Chairs* **Samantha Daly and Reinhold Dauskardt**
8:30 – 9:00 am	*Introductory Remarks and Program Overview* **John Vetrano**
Session I	Chair: **Reiner Dauskardt,** Stanford
9:00 – 9:20 am	**Easo George,** ORNL *Multiscale Mechanical Properties and Alloy Design*
9:20 – 9:40 am	**Xinghang Zhang,** Purdue *Deformation Mechanisms of Nanotwinned Al and Binary Al Alloys*
9:20 – 9:40 am	**Elisa Riedo,** CUNY *NanoMechanics: Elasticity and Friction in Nano-Objects*
9:40 – 10:00 am	**Jan Schroers,** Yale *Effect of Chemical Composition and Fabrication Method on the Fracture Toughness of Metallic Glasses*
10:00 – 10:20 am	**Coffee Break**
Session II	Chair: **Julia Greer,** Cal Tech
10:20 – 10:40 am	**Cate Brinson,** Northwestern / **Aaron Stebner**, Colorado School of Mines *Microstructure Anisotropy Effects on Fracture and Fatigue Mechanisms in Shape Memory Alloy Martensites*
10:40 – 11:00 am	**Alejandro Strachan,** Purdue *Understanding, Controlling and Creating Martensitic Phase Transformation in Nanostructured Polycrystals and Metamaterials*
11:00 – 11:20 am	**Bilge Yildiz,** MIT *Chemomechanics of Far-From-Equilibrium Interfaces (COFFEI)*
11:20 – 11:40 am	**Rob Ritchie,** LBNL *Mechanical Behavior of Materials Program*
11:40 – 12:00 pm	**New Project Introductions** (three @5 min each El-Azab, Greer, Kacher)
12:00 – 1:15 pm	**Working Lunch**

Session III	Chair: **Amit Misra,** Michigan
1:15 – 1:40 pm	**Linda Horton,** BES-DMSE Director *Overview of BES Materials Sciences Division*
1:40 – 2:00 pm	**Izabela Szlufarska,** Wisconsin *Coupled Effects of Radiation and Chemical Environment on Interfaces in SiC*
2:00 – 2:20 pm	**Blas Uberuaga,** LANL *The Relationship Between Defect Kinetics and Crystalline Disorder*
2:20 – 2:40 pm	**John Allison,** Michigan *Software Center for Predictive Theory and Modeling*
2:40 – 3:00 pm	**Poster Introductions** (10 @ 2 min each)
3:00 – 3:30 pm	**Break for Discussions/Posters**
Session IV	Chair: **Anter El-Azab,** Purdue
3:30 – 3:50 pm	**Steve Bruemmer,** PNNL *Crack-Tip Mechanisms Driving Environmental Degradation*
3:50 – 4:10 pm	**Gary Was,** Michigan *Localized Deformation and Intergranular Fracture of Irradiated Alloys Under Extreme Environmental Conditions*
4:10 – 4:30 pm	**Qizhen Li,** Washington State *Low Temperature Cyclic Deformation Behavior of Ultrafine-grained Pure Magnesium*
4:30 – 6:30 pm	**Free Time** (posters up but not manned)
6:30 – 8:00 pm	**Dinner and Discussion**
8:00 – 9:30 pm	**Poster Session**

Wednesday September 20, 2017

8:00 – 8:40 am	**Breakfast**
Session V	Chair: **Sam Daly,** UC-Santa Barbara
8:40 – 9:00 am	**Maryam Ghazisaeidi,** Ohio State *Atomic Scale Computational and Experimental Investigation of Twinning Mechanisms in HCP Systems*
9:00 – 9:20 am	**Carl Boehlert,** Michigan State *Characterization and Modeling of Deformation Induced Damage in Hexagonal Metals*
9:20 – 9:40 am	**Reiner Dauskardt,** Stanford *Molecular Origins and Design of Hybrid Films with Unusual Mechanical Properties*
9:40 – 10:00 am	**Karl Sieradzki,** Arizona State *Dynamic Fracture in Dealloying Induced Stress Corrosion Cracking*
10:00 – 10:20 am	**Break**
Session VI	Chair: **Chris Schuh,** MIT
10:20 – 10:40 am	**Carlos Tome,** LANL *Multi-Scale Study of the Role of Microstructure in the Deformation Behavior of Hexagonal Material*
10:40 – 11:00 am	**Stefanos Papanikolaou,** West Virginia *Nanoindentation of Micrograins in Polycrystals Under Multiaxial Stress: Control of Abrupt & Stochastic Plastic Events*
11:00 – 11:20 am	**Lin Li,** Alabama *Multiscale Modeling of Shear Banding in Metallic Glasses*
11:20 – 11:40 am	**Frederic Sansoz,** University of Vermont *Strengthening Nanotwinned Metals beyond the Hall-Petch Limit*
11:40 – 12:00 pm	**New Project Introductions** (3 @ 5 min each, Misra, Schuh, Sheldon)
12:00 – 1:30 pm	**Working Lunch**

Session VII	Chair: **Josh Kacher,** Georgia Tech
1:40 – 2:00 pm	**Richard LeSar,** Ames *Competition and Correlation Among Length Scales: Mesostructure and Mechanical Properties*
2:00 – 2:20 pm	**Mike Mills,** Ohio State *Nanostructured High Temperature Shape Memory Alloys: Integrated Experiments and Simulations*
2:20 – 2:40 pm	**Jessica Krogstad,** UIUC *Dynamic, Robust, Radiation-Resistant Ceramics: Harnessing Thermodynamic and Kinetic Driving Forces*
2:40 – 3:00 pm	**Poster Introductions** (10 @ 2 min each)
3:00 – 3:30 pm	**Break for Discussions/posters**
Session VIII	Chair: **Brian Sheldon,** Brown
3:30 – 3:50 pm	**Wei Cai,** Stanford *Thermal Activation in Dislocation Dynamics of Face-Centered Cubic Metals*
3:50– 4:10 pm	**David Fullwood,** Brigham Young *Fundamental Mechanisms Controlling Dislocation-Obstacle Interactions in Metals and Alloys*
4:10 – 4:40 pm	**Brad Boyce,** SNL *Nanomechanics and Nanometallurgy of Boundaries*
4:40 – 5:00 pm	**Pascal Bellon,** UIUC *Materials for Extreme Irradiation Environments*
5:00 – 6:45 pm	**Free Time** (posters up but not manned)
6:45 – 8:00 pm	**Dinner and Continued Discussions**
8:00 – 9:30 pm	**Poster Session II**

Thursday September 21, 2017

7:30 – 8:20 am	**Breakfast**
Session IX	Chair: **Laurent Capolungo,** LANL
8:20 – 8:40 am	**Kevin Hemker,** Johns Hopkins University *Nanoscale Characterization of Intragranular and Intergranular Deformation Mechanisms*
8:40 – 9:00 am	**Tim Rupert,** UC-Irvine *Doping Metallic Grain Boundaries to Control Atomic Structure and Damage Tolerance*
9:00 – 9:20 am	**Katerina Aifantis,** University of Florida *The Role of Grain Boundary Structure and Chemistry in Materials Failure*
9:20 – 9:40 am	**Jian Gan,** Idaho National Laboratory *The Role of Anisotropy on the Self-Organization of Gas Bubble Superlattice*
9:40 – 10:00 am	**Vaclav Vitek,** University of Pennsylvania *Atomistic Study of Plastic Deformation of Transition Metal Alloys Including High Entropy Alloys*
10:00 – 10:40 am	**Break**
Session X	Chair: **TS Byun,** PNNL
10:40 – 11:00 am	**Lin Shao,** Texas A&M *Radiation Response of Low Dimensional Carbon Systems*
11:00 – 11:20 am	**Bill Weber,** Oak Ridge National Laboratory *Electronic and Atomic Response of Ceramic Under Irradiation*
11:20 – 11:40 am	**Samantha Daly,** UC-Santa Barbara / **Michael Sangid**, Purdue *Deformation Mechanisms at Grain Boundaries in Polycrystals*
11:40 – 12:00 pm	**Eric Homer,** Brigham Young *Computational and Experimental Investigation of Cryogenic Grain Boundary Motion for Enhanced Mechanical Properties*
12:00 – 12:15 pm	**Closing Remarks by John Vetrano**

Poster List

Mechanical Behavior and Radiation Effects Principal Investigators' Meeting

POSTER SESSION I
Tuesday, September 19, 2017

1) **Dislocation in Patterning in Deforming Crystals: Theory, Computational Predictions, and Validation**
   Anter El-Azab, Purdue University

2) **A Fundamental Study on the Link between Mechanical Properties and Atomic-level Microstructure in Nano-sized Metallic Glasses**
   Julia Greer, California Institute of Technology

3) **Fundamental Study of Fatigue Crack Initiation at Grain Boundaries in Austenitic Stainless Steel**
   Josh Kacher, Georgia Institute of Technology

4) **The Role of Grain Boundary Structure and Chemistry in Materials**
   Stephen Hackney, Michigan Tech and Katerina Aifantis, University of Florida

5) **Software Center for Predictive Theory and Modeling**
   Steve DeWitt and John Allison, University of Michigan

6) **Materials for Extreme Irradiation Environments**
   John Beach and Pascal Bellon, University of Illinois, Urbana-Champaign

7) **Characterization and Modeling of Deformation Induced Damage in Hexagonal Metals**
   Martin Crimp and Carl Boehlert, Michigan State University

8) **Chemomechanics of Far From Equilibrium Interfaces (COFFEI)**
   Frank McGorgan, Bilge Yildiz and Harry Tuller, Massachusetts Institute of Technology

9) **Nanoindentation of Micrograins in Polycrystals Under Multiaxial Stress: Control of Abrupt & Stochastic Plastic Events**
   Hengxu Song and Stefanos Papanikolaou, Johns Hopkins University

10) **Nanomechanics and Nanometallurgy of Boundaries**
    Stephen Foiles and Brad Boyce, Sandia National Laboratories

11) **Crack-Tip Mechanisms Driving Environmental Degradation**
    Dan Schreiber and Stephen Bruemmer, PNNL

12) **The Role of Anisotropy on the Self-Organization of Gas Bubble Superlattices**
    Yongfeng Zhang and Jian Gan, Idaho National Laboratory

13) **Multiscale Mechanical Properties and Alloy Design**
    Jamie Morris, Easo George, Yuri Osetskiy, Hongbin Bei and George Pharr, ORNL

14) **Energy Dissipation to Defect Evolution (EDDE) EFRC**
    Yanwen Zhang, Oak Ridge National Laboratory

POSTER SESSION II
Wednesday, September 20, 2017

1) **Plasticity of High-Strength Multiphase Metallic Composites**
   Amit Misra, University of Michigan

2) **Microparticle Supersonic Impact: A Testbed for the Exploration of Metals under Extreme Conditions**
   Chris Schuh, Massachusetts Institute of Technology

3) **Toughening Mechanisms in Ceramic Nanocomposites with One and Two Dimensional Reinforcements**
   Brian Sheldon, Brown University

4) **Deformation Mechanisms at Grain Boundaries in Polycrystals**
   Michael Sangid, Purdue University and Sam Daly, UCSB

5) **Dynamic Fracture in Dealloying Induced Stress Corrosion Cracking**
   Erin Karasz and Karl Sieradzki, Arizona State University

6) **Nanostructured High Temperature Shape Memory Alloys: Integrated Experiments and Simulations**
   Peter Anderson and Mike Mills, The Ohio State University

7) **The Role of Microstructural Neighborhoods in Forming and Evolving Slip Localization in Polycrystalline Metals during Cyclic Plasticity**
   Matthew Miller, Cornell University

8) **Atomistic Study of Plastic Deformation of Transition Metal Alloys Including High Entropy Alloys**
   Yi-Shen Lin and Vasek Vitek, University of Pennsylvania

9) **Localized Deformation and Intergranular Fracture of Irradiated Alloys Under Extreme Environmental Conditions**
   Diana Farkas, Virginia Tech and Gary Was, University of Michigan

10) **Mechanical Behavior of Materials**
    Thomas Pekin, Jun Ding and Rob Ritchie, Lawrence Berkeley National Laboratory

11) **Competition and Correlation Among Length Scales: Mesostructure and Mechanical Properties**
    Richard LeSar, Ames Laboratory

12) **Multi-Scale Study of the Role of Microstructure in the Deformation Behavior of Hexagonal Material**
    Laurent Capolungo and Carlos Tomé, Los Alamos National Laboratory

13) **The Relationship Between Defect Kinetics and Crystalline Disorder**
    Romain Perriot and Blas Uberuaga, Los Alamos National Laboratory

14) **Electronic and Atomic Response of Ceramic Under Irradiation**
    Neila Sellami-Bouachir and Bill Weber, Oak Ridge National Laboratory

Table of Contents

Table of Contents

Abstracts

Energy Dissipation to Defect Evolution – an Energy Frontier Research Center

Yanwen Zhang, Director, Oak Ridge National Laboratory

Program Scope

EDDE's Mission is to develop a fundamental understanding of energy dissipation and defect evolution mechanisms in tunable concentrated solid solution alloys (CSAs), and ultimately to control defect evolution in a radiation environment. Our goal is to reveal energy dissipation mechanisms through electrons, phonons, and magnons, and utilize this knowledge to understand the process of radiation damage formation and evolution in its early stages. We aim to design materials that can intrinsically recover from the damaged state.

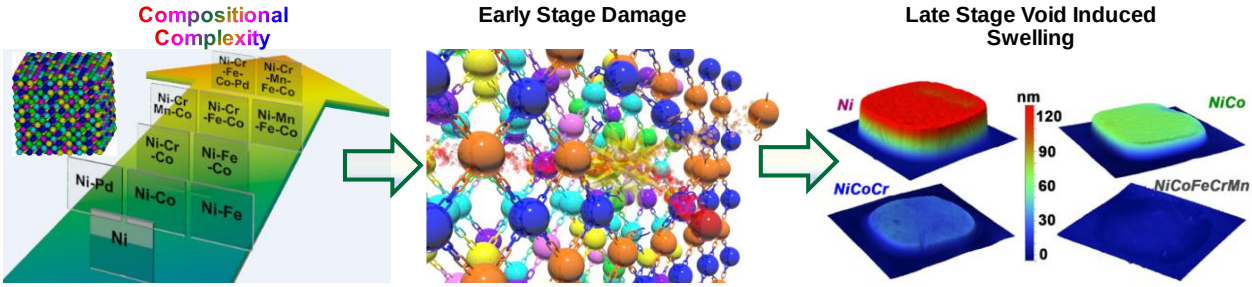

Figure 1. EDDE hypothesis: modifying alloy chemical complexity will enable us to control defect production and dynamics at the early stage of damage and ultimately enhance late stage radiation tolerance under extreme radiation conditions.

Recent Progress

Performance enhancement of structural materials in extreme environments has been actively investigated for many decades. Recently developed single-phase CSAs exhibit significant chemical disorders and inhomogeneous lattice distortions. While it has long been recognized that specific compositions of traditional alloys have enhanced radiation resistance and impact on structural modification, it remains unclear how the atomic-level alloying affects defect formation, damage

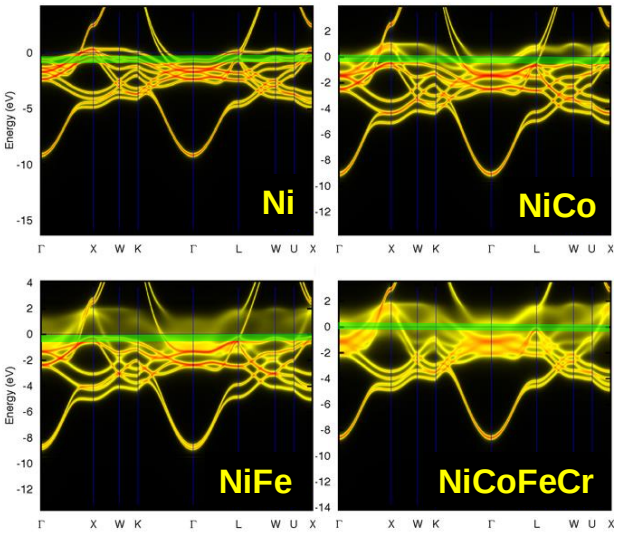

Figure 2. Large degree of disorder smearing (broadening) in alloys leads to much shorter mean free path than in Ni.

accumulation, and microstructural evolution.

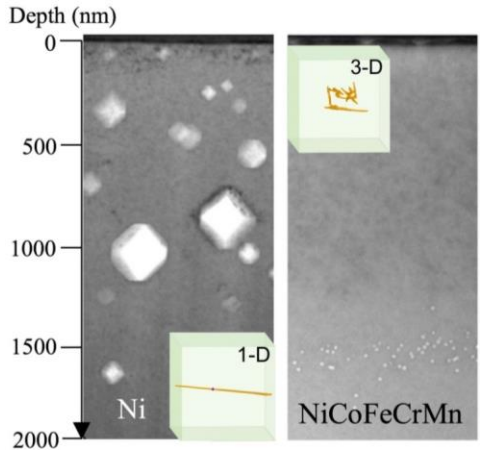

Figure 3. Void distributions in under 3 MeV 5×10^{16} cm^{-2} Ni irradiation at 773 K.

EDDE researchers investigate the fundamental processes involved in radiation damage in CSAs (Figure 1), with the goal of developing a new class of alloys that will be used in fission and fusion reactors. The research is organized around two interconnected thrusts. In Thrust 1: Energy Dissipation, advanced theoretical methods are paired with novel experimental approaches to understand how input energy is partitioned among the electronic, magnetic, and atomic degrees of freedom, how this energy is ultimately dissipated in disordered alloys, and the role of compositional disorder on energy dissipation. In Thrust 2 Defect Evolution, advanced computational methods are used in conjunction with state–of–the–art materials characterization methods to how energy exchange between atoms and electrons influences the formation, nature, and time evolution of defects in irradiated alloys and, in particular, how compositional complexity alters defect processes.

Two distinctive intrinsic properties are expected due to extreme chemical complexity in CSAs. At the level of electrons, disordered local chemical environments significantly enhance electron scattering and affect energy dissipation, and at the level of atoms, chemical disorder leads to complex energy landscapes and affect defect evolution. In Thrust 1, significant reduction of electrical and thermal conductivities (1st distinctive intrinsic property) is discovered (Figure 2). Substantial electronic-level modification and significant reduction of energy dissipation rate through coupled electronic and magnetic interactions in model alloys are demonstrated. In Thrust 2, site-to-site chemical disorder and non-periodic energy landscapes (2nd distinctive intrinsic property) result in substantially improved radiation resistance. High atomic-level stresses facilitate rapid annealing and prevent extended dislocation formation. Increasing compositional complexity in CSAs can significantly suppressed void swelling, by two orders of magnitude at elevated temperatures (Figure 3).

Our recent progress and discoveries increasingly support the EDDE hypothesis that tuning chemical complexity represents a powerful tool for enhancing radiation tolerance in alloys by reducing the rate of Energy Dissipation (Thrust 1) and suppressing Defect Evolution (Thrust 2). Understanding how materials properties can be tailored by alloy complexity and their influence on defect dynamics and structural stability may pave the way for new design principles of materials with unique functionalities or radiation–tolerant structural alloys.

Collaborative Research: The Role of Grain Boundary Structure and Chemistry in Materials Failure project

PI: K.E. Aifantis, Uni. Florida, co-PIs: S.A. Hackney, E. Hebert, Michigan Tech Univ

Program Scope: The hypothesis of this project is that the contribution of interface deformation in materials failure can be described by a modified internal interface (or grain boundary) tension term (ξ_{gb}), defined as the derivative of the interface energy/area (γ_{gb}) with plastic strain (ε^p): $x_{gb} = \P g_{gb} / \P e^p$. This new term ($\xi_{gb}$) has been introduced within the concept of gradient plasticity [1] to predict the critical stress (grain boundary yield stress, σ_{gb}) at which grain boundaries begin deforming plastically through dislocation transmission or absorption. It should be noted that in [1] ξ_{gb} is incorporated through a mechanically induced interface energy $\Phi(\varepsilon^p)$. Consideration of $\Phi(\varepsilon^p)$ and ξ_{gb} has made it possible to capture experimental data [2,3] that could not be interpreted by existing theoretical frameworks, however, the physical interpretation of both quantities remains ambiguous. The scope of this project is to provide a physical interpretation for these parameters and relate them to existing known material properties such as the Burgers vector, chemistry, shear modulus, dislocation spacing, Hall-Petch slope, as well as misorientation and grain size. The approach is three-fold, as experiments (nanoindentation, scanning and transmission electron microscopy), continuum/dislocation mechanics and simulations (atomistic and dislocation dynamics) are used to understand dislocation-interface interactions, which is the physical mechanism giving rise to ξ_{gb}. Of particular interest is the effect that segregate atoms have on ξ_{gb}, as their existence can tune interface properties. Therefore, from a materials science perspective the broader impact of this project is that it will connect the energy minimizing the structural configuration of grain boundaries with aspects of the mechanical property enhancement embodied by the Hall-Petch equation. There is substantial evidence in the literature that solute additions will generally increase the Hall-Petch slope even though the average slip transfer geometry across the grain boundary is expected to be unaffected [4-5]. An interpretation of these results through the Gibbs absorption isotherm leads to the hypothesis that stabilizing the atomic scale structure of the grain boundary via segregation can enhance the dislocation transfer resistance by inhibiting local structural changes within the boundary. Such an idea is supported by DDD results on grain boundary strengthening which reveal a strengthening term correlated with a change in grain boundary energy with plastic strain [6]. To test these concepts the local mechanical behavior of grain boundaries relative to small scale mechanical testing of the relevant grain interiors is studied as a function of chemistry. Results of the grain boundary strength dependence on its chemistry and geometric characteristics are analyzed using discrete dislocation models together with atomistic simulations.

Recent Results:

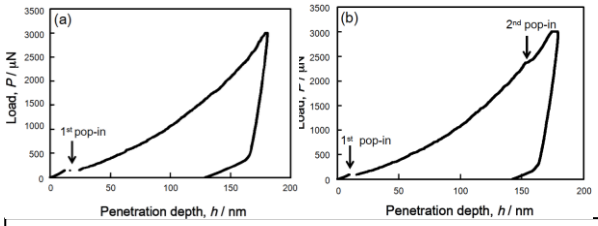

Fig. 1: (a) away from the grain boundary, (b) in close proximity to the grain boundary.

1. Grain boundary yielding/slip transmission through nanoindentation experiments: One of the first experiments to capture grain boundary yielding was nanoindentation near grain boundaries [2]. Nanoindentation experiments are characterized by plateaus (pop-ins) in the load vs. tip-displacement plots. These plateaus indicate movement of dislocations underneath the indenter tip and can therefore

indicate grain yielding. It has been observed, however, that indentations near grain boundaries, such as for Fe-Si alloys and Nb give rise to a second plateau or pop-in [2]. These distinct pop-ins near grain boundaries have been proposed to indicate dislocation motion into the grain boundary and possible emission into the adjacent grain. Despite being a powerful tool nanoindentation is plagued by sample preparation artifacts. A detailed study, therefore, of the role of sample processing on nano-indentation results at the grain boundary and grain interior has been examined for high purity α-Fe. Particularly, indentation of surfaces with unresolved surface deformation due to mechanical polishing have been compared to the same sample surfaces annealed at a high temperature in a reducing atmosphere. Behaviors of interest include discontinuities in P-h curves at grain boundaries versus grain interiors and any variance in the indentation size effect. The differences in indentation behavior with annealing time and temperature are correlated with electron backscatter diffaraction as an independent measure of the surface layer crystallinity. Concurrently with the attempts to find an optimum surface preparation method, nanoindentation experiments were carried out on Fe-2.3% Si tri-crystals in order to capture the effect that the grain boundary misorientation (22.5, 42, 44.6 degrees) has on grain boundary yielding (slip transmission). All Fe-Si samples exhibited a 2nd pop-in near grain boundaries as shown in Fig. 1(a). This is consistent with previous nanoindentation studies [2] near grain boundaries of Fe-Si. However, no experimental evidence has been able to verify the occurrence of such slip with imaging. In the present study, hence, after performing the indentations, scanning probe microscopy and backscatter electron imaging were performed. It is seen in Figs 2(a)&(b) that for the indentation corresponding to Fig. 1(a), which resulted in only one pop-in, the plastic deformation accumulated from the indenter tip to the grain boundary, without transmitting to the adjacent grain. While in Figs 2(c)&(d), which correspond to an indent that displayed a second pop-in (Fig. 1b), it is evident that the plastic flow was transmitted across the boundary. From these images it is not possible to obtain the dislocation mechanism by which slip

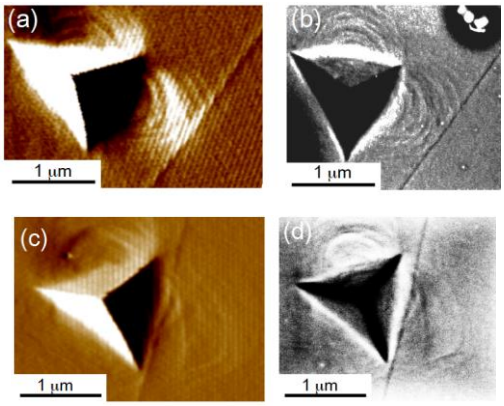

Fig. 2: SPM and BSE images of the indentations. (a)&(b) Correspond to the load-displacement curve of Fig. 1a; (c)&(d) correspond to the load displacement curve of Fig. 2b exhibiting the two pop-ins.

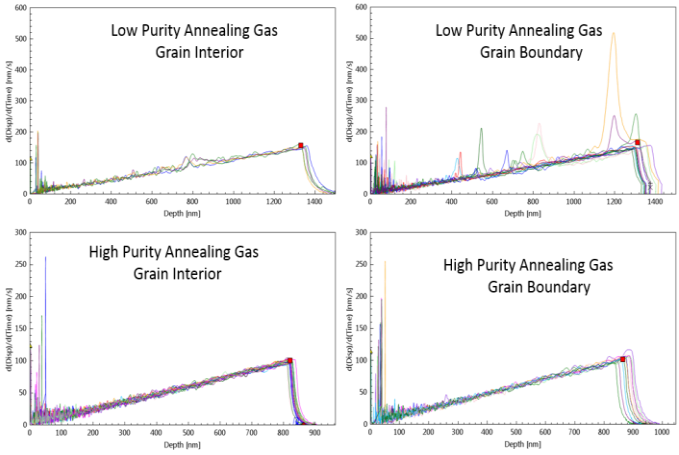

Figure 3: Tip velocity vs indentation depth for grain interior and grain boundary indentations.(a) grain interior indentations with low purity (10 ppm carbon) annealing gas (b) grain boundary indentations with low purity annealing gas (c) grain interior indentations with high purity annealing gas (d) grain boundary indentations with high purity annealing gas.

transmission occurred, i.e. through dislocation emission by the grain by the grain boundary or dislocation transmission, but it is verified for the first time that 2nd pop-ins, near grain boundaries, do indeed correspond to grain boundary yielding.

To further examine the role of grain boundary energy (Φ) changes with plastic strain, the introduction of grain boundary chemistry as an experimental variable is being developed. The idea is that grain boundary segregation will stabilize the boundary structure, making slip transmission more difficult. Our initial results show that the addition of carbon to high purity Fe via the gas phase results in P-h curve 'wiggles' for indentations near the boundary that do not occur in the grain interior or at any point in the "undoped" high purity Fe, as seen in Fig. 3. We note that the grain boundary effect in the carbon doped Fe occurs at a much greater indentation depth and with a much lower amplitude in tip velocity change as compared to the Fe-3%Si which may be related to the much smaller Hall-Petch slope for mild steel compared to silicon steels. The effect is best seen in the tip velocity vs indentation depth presented in Fig. 3

2. Determination of the modified internal interface tension (ξ_{gb}) from gradient plasticity and dislocation mechanics: Tabor's rule states that the yield stress underneath the indenter is $\sigma_{yield}=H/3$, where H is the hardness under the tip. The hardness is defined as $H=P/A$, where P is the applied load, and A is the contact area of the indentation during the pop-in. Hence, it is possible to estimate the value of σ_{gb} through the 2nd pop-in of Fig. 1. In Fig. 4, σ_{gb} is plotted against the grain boundary-to-indenter tip distance at which the 2nd pop-in occurred. It is seen that σ_{gb} is inversely proportional to L, which is reminiscent of the analytical expression predicted by gradient plasticity for grain boundary yielding: $\sigma_{gb}= \xi_{gb} \coth(L/l)/(2l)$ [2], where l is the internal length. Quite good fits are obtained in Fig. 4 by fitting this expression to the data, allowing for values to be obtained for ξ_{gb} and l, which are experimentally related as $\xi_{gb}=2.7l$.

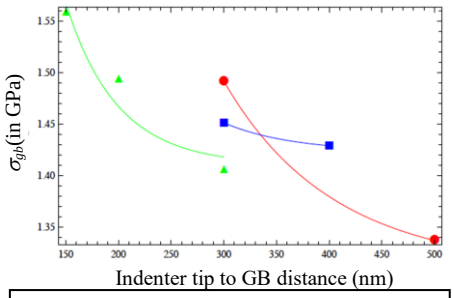

Fig. 4: Experimentally obtained grain boundary yield stress (dots) and fits.

To further rationalize this observation a simple analytical model that combines the concepts of [7-8] is used. Hirth and Lothe [7] developed an analytical formulation for a tilt boundary stress field and specific energy assuming discrete dislocations, which has been shown to fit experimental data. By using the Hirth and Kamat [8] work as our starting point for defining the grain boundary energy, we were able to calculate the grain boundary energy required to remove a dislocation from a tilt boundary, essentially forcing it to yield. This allowed to obtain through dislocation mechanics an expression for the grain boundary yield stress, which could be related with the phenomenological expression from gradient plasticity in order to define ξ_{gb} and l as a function of dislocation and material parameters: $l = d \cdot ln\left(\frac{d^2 + D^2}{d^2}\right)$ and $\xi = l \cdot \frac{G \cdot b}{2 \cdot d \cdot \pi \cdot (1 - \nu)}$, where d is the dislocation spacing, D the distance by which the dislocation is displaced from the grain boundary, b the Burgers vector and G the shear modulus. Numerical plots of these expressions indicate an "almost" linear relationship between ξ_{gb} and l, as the fits from Fig. 4 suggest ($\xi_{gb}=2.7l$.).

3. Determination of the mechanically induced interface energy through simulations: Atomistic/Molecular Dynamics simulations have been extensively employed to capture dislocation-grain boundary interactions. However, they have not been used to our knowledge to deduce the change of the grain boundary energy due to slip transmission. This change of grain boundary energy as a function of dislocation absorption/emission can provide a measure of the mechanically induced interface energy $\Phi(\varepsilon^p)$.As a first step, we performed simulations for an Al crystal, containing three grain boundaries, as potentials are well defined. The energy of the grain boundary was calculated before and after grain boundary absorption for the cases where the grain boundary was $\Sigma3$, $\Sigma9$ and $\Sigma19$. For the case that the absorbed dislocation was screw the change in Φ was found to be 3.60 meV/nm^2 for all types of Σ boundaries considered.

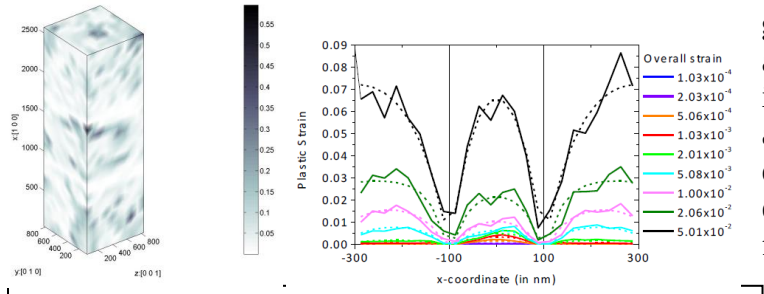

Fig. 5: Left) Strain distribution throughout an Al tricrystal in DDFD, Right) Fit of analytical expressions of the plastic strain from gradient plasticity (solid lines) to DDFD data (doted lines).

4. Grain boundary strength bs on grain size and misorientation: In addition to examining the local interface behavior through atomistics, the overall effect of dislocation motion was also examined by dislocation density functional dynamics (DDFD) simulations for Al tricrystals. Results such as those shown in Fig. 5 indicate that the plastic strain profile obtained from DDFD is in good agreement with the prediction of gradient plasticity, verifying the validity of our model.

Future Directions: Specific Fe grain boundaries with and without an alloying component (Si, P, C) will be studied via nanoindentation and compared with the corresponding grain interior behavior, so as to obtain similar plots as Fig 3, but with a significantly higher amount of data points and numerous materials selections. These studies will be complimented by TEM microstructural analysis of these same boundaries extracted by focused ion beam (FIB). The localized FIB sample preparation will allow the determination of grain boundary-dislocation structure within the plastic cavity of the indenter as compared with the structure outside the plastic cavity. Atomic resolution STEM EDS/EELS mapping at the boundary will be utilized to measure the degree of solute segregation at the boundary both inside and outside the plastic cavity. Furthermore, atomistic simulations, similar to those in Section 3 above, will be performed for Fe systems segregated with C, Si, P and the mechanically induced interface energy as a function of segregation content and grain boundary type will be determined. Also DDFD or discrete dislocation dynamics (DDD) will be formed for Fe crystals with impurities so as to predict the materials response. The simulations and experiments will be directly related in order to obtain values for the parameters ξ and Φ, which allow the characterization of boundaries.

Refs: [1]Aifantis K.E., et al *J Mech Phys Solids* 53, 1047, 2005; [2]Aifantis K.E, et al *Matls Sci & Eng A* 459, 251, 2007; [3]Zhang X., et al *Matls Sci & Eng A* 591, 38, 2014; [4]W. Koster, W, et al Metallkd, 56, 585, 1965; [5]Takeda K., et al ISIJ Inst. 48,1122, 2008; [6] Zhang X., et al *Matls Sci & Eng A* 631, 27, 2015; [7]Hirth J.P., Lothe J., Theory of Dislocations 2nd ed., p. 76 and p. 783; [8]Kamat, Hirth J.P. Scripta Met & Mat, 32, 1795, 1995.

Publications

K.E. Aifantis, H. Deng, H. Shibata, S. Tsurekawa, S.A. Hackney, Relating slip transmission to excess grain boundary energies in sub-micron scale crystals – A Fe-3%Si case study, Under Review.

Center for PRredictive Integrated Structural Materials Science – PRISMS Center

PI: J. Allison, University of Michigan (UM)
Co-PIs: S. Daly, University of California-Santa Barbara (UCSB), K. Garikipati (UM), V. Gavini (UM), M. Hedstrom (UM), H. V. Jagadish (UM); J. W. Jones (UM), E. Marquis (UM), A. Misra (UM), L. Qi (UM), V. Sundararaghavan (UM), K. Thornton (UM), A. Van der Ven (UCSB).

Program Scope

The overarching goal of the PRISMS Center is to establish a unique scientific platform that will enable accelerated predictive materials science. The platform has three key thrust areas:

1. **PRISMS Integrated Computational Software:** Develop and establish a suite of integrated, multi-scale, open-source computational tools for predicting the microstructural evolution and mechanical behavior of structural metals.
2. **PRISMS Integrated Science Use Cases:** The use cases demonstrate the application of the integrated PRISMS platform of experiments, theory and simulation for making major advances in the quantitative and predictive understanding of microstructural evolution and mechanical behavior of magnesium alloys.
3. **The Materials Commons:** Develop and deploy "The Materials Commons," a knowledge repository and virtual collaboration space for curating, archiving and disseminating information from experiments and computations.

Recent Progress and Future Plans

Established in 2012, the PRISMS Center has four full time staff members and eighteen graduate students and post-doctoral fellows. We hold an annual workshop to develop our external PRISMS collaborative community and to train external users of PRISMS software tools and Materials Commons and have trained more than 120 users. We have an external advisory board comprised of internationally recognized researchers in our fields of study which meets annually. Additional information can be found at http://prisms-center.org.

PRISMS Integrated Computational Software

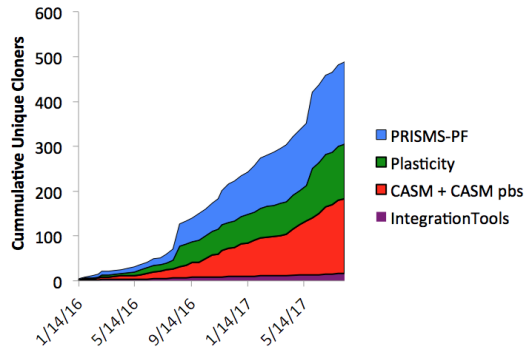

Figure 1. Cumulative clones of PRISMS codes since January 2016.

Currently three primary codes make up the PRISMS Open Source Integrated software: CASM, PRISMS-PF and PRISMS-Plasticity are available on GitHub (see descriptions below). These codes were released in 2015 and have all had at least two major upgrades since then. The GitHub pages for these codes have been viewed more than 15500 times and over 550 clones (copies) have been downloaded by users as shown in Figure 1. Each software package includes a substantial user manual, formulation notes, commented source code and unit tests. A beta version of a new advanced code, DFT-FE (see below), was released in August 2017. In addition, three advanced research codes for phase field crystal, variational multi-scale and mechano-chemistry have been developed/evaluated.

CASM, a Clusters Approach to Statistical Mechanics: CASM provides functionality for symmetry identification, enumeration of symmetrically unique supercells and configurations, use

of automatically determined or custom reference states for formation energy calculation, and convex hull identification. Future planned releases include kinetic Monte Carlo calculations of non-dilute diffusion coefficients. *https://github.com/prisms-center/CASMCode*

PRISMS-PF: The PRISMS phase field code uses the finite element (FE) method, and is a massively scalable numerical framework for implementing phase field models for the multiscale materials modeling effort of PRISMS. The PRISMS FE framework using the deal.ii open-source finite element library has been implemented. Plans for future release include implicit time-stepping and active parameter tracking. *https://github.com/prisms-center/phaseField*

PRISMS-Plasticity: The PRISMS-Plasticity code is a massively parallel numerical framework for implementing continuum and crystal plasticity finite element (CPFE) models using the deal.ii open source library. Various crystal and continuum plasticity material models have been developed, including a backstress formulation for simulating cyclic loads and the capability to model two-phase microstructures. The ability to carry out simulations using gradient plasticity and crack paths is planned for future release. *https://github.com/prisms-center/plasticity*

DFT-FE: Finite element based, real-space methods are being developed for density functional theory simulations containing tens of thousands of atoms. Besides enabling large-scale real-space DFT calculations, these developments will enable an accurate study of the energetics of dislocations and their interactions with other defects.

PRISMS Use Cases

The PRISMS Use Cases serve as demonstrations and test beds for the development and demonstration of the PRISMS platform combining experiments, theory and simulation. Highlights from these use cases are summarized below. In following years, we plan to focus similar integrated efforts on new Mg alloy use cases including microstructural effects on corrosion, strength and fatigue behavior and quaternary alloy optimization.

Precipitate Evolution Use Case

High strength in Mg alloys is achieved by complex precipitation sequences exhibited by a variety of Mg-rare earth (RE) alloys. We have completed a major study integrating CASM, PRISMS-PF and experiments for characterizing precipitation in supersaturated solid solutions of Mg-rich Mg-RE alloys to establish thermodynamic driving forces for Guinier-Preston zone and precipitate formation. The CASM software package was used to construct a cluster expansion Hamiltonian and to perform Monte Carlo simulations to calculate a metastable HCP temperature-composition phase diagram (Figure 2) and energetic information which was passed to PRISMS-PF for simulating precipitate evolution. Aging studies were performed in parallel on dilute Mg-Nd and Mg-Y alloys that were then characterized with HAADF-STEM, an example of which is shown in Figure 3. This integrated experimental-computational study has revealed that the early stage decomposition of these alloys is dominated by the thermodynamic stability of a unique hierarchy of Nd orderings on the HCP crystal structure, which we label β’’’. High-throughput first-principles studies of ordering tendencies in all first-row Mg-RE binary alloys were completed that demonstrated that the coherency strains that arise during precipitate evolution are highly dependent on the alloying system and fall into two classes; alloys that have lenticular precipitates (e.g. β’’’ in Mg-Nd) and those that develop

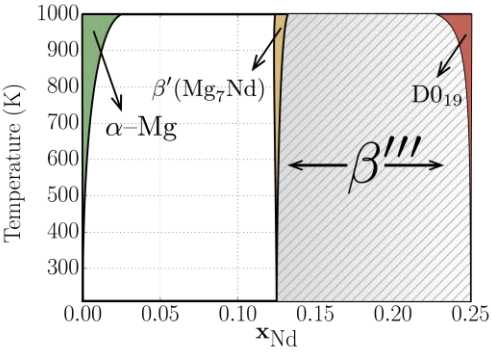

Figure 2*. Mg-Nd phase diagram predicted by CASM showing new metastable phase* β’’’.

rod-like precipitates (e.g. β′ in Mg-Y). This was demonstrated by the PRISMS-PF simulation of metastable precipitates as shown in Figure 4.

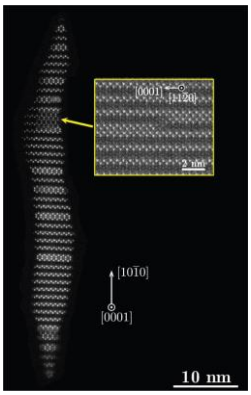

Figure 3. *HAADF-STEM image of precipitate ordering in a dilute Mg-Nd alloy. The precipitate is coherently embedded in an HCP Mg matrix.*

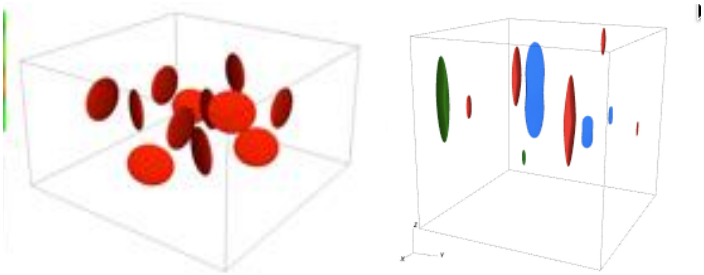

Figure 4. *PRISMS-PF predicted morphology of metastable* β‴ or β′ *precipitates in Mg-Nd and Mg-Y alloys, respectively.*

Tensile Behavior Use Case

This use case integrates results from atomistic simulations with dislocation dynamics and crystal plasticity (PRISMS-Plasticity). This multi-scale modeling capability is linked with unique experimental capabilities for measuring dislocation interactions with precipitates and local strain gradients (SEM-DIC). At the dislocation-precipitate level, we are using ParaDiS as the primary dislocation dynamics code to be integrated into the PRISMS framework, in collaboration with LLNL. A methodology has been developed to determine critical resolved shear stress for dislocations on the basal plane moving through a distribution of precipitates. These simulations are being validated by in-situ and ex-situ TEM investigations of dislocation interaction with precipitates in Mg-RE alloys. As a demonstration, quantitative precipitate morphologies for a Mg-Al-Zn alloy were mapped to ParaDiS and the critical resolved shear stress determined and, when combined with other strengthening mechanisms, the computed estimates for yield strength were within 5% of the experimentally measured value. We plan to complete simulations of dislocation interactions using precipitate distributions mapped from the PRISMS-PF simulations and combine with PRISMS-Plasticity predictions for stress-strain response. Results at the precipitate level are provided as inputs at the higher length scale represented by PRISMS-Plasticity (CPFE). A method was developed using SEM-DIC and PRISMS-Plasticity to iteratively improve on the determination of CRSS for twins and non-basal slip systems. We also use SEM-DIC data to validate the grain-to-grain strains predicted by the CPFE simulation. Using PRISMS-Plasticity, tensile test data and experimental EBSD (texture) map, we have developed crystal plasticity parameters for a Mg-Nd-Y alloy in a variety of aging conditions. Validation of crystal plasticity parameters was performed by comparing predicted displacement fields on a microstructure with corresponding high resolution SEM-DIC data. The PRISMS-Plasticity code also predicts strain distributions within grains, as shown in Figure 5.

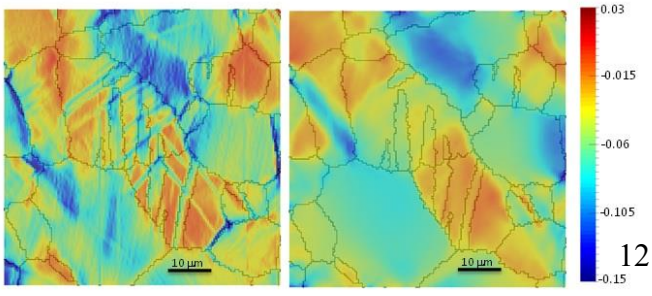

Figure 5. *Comparison of SEM-DIC measured strain map (left) and the PRISMS-Plasticity CPFE simulation (right) for compression of Mg WE43.*

Fatigue Behavior Use Case

The Fatigue Behavior Use Case group is developing capabilities for predicting the role of alloying and microstructure on the low cycle fatigue response and the growth of microstructurally small fatigue cracks in Mg alloys. In this use case, we make use of a unique ultrasonic fatigue scanning electron microscope (UFSEM) to quantify the growth rates of cracks as they advance through grains and across grain boundaries. A cyclic cohesive zone model for prediction of microstructural crack trajectories under high cycle fatigue has been developed and parameters for crack propagation along various slip systems have been obtained using experimental (micro-beach marking) measurements of local crack growth rates within a grain. This is coupled with an analytical model for the effect of grain boundaries on crack paths, including prediction of grain boundary blocking or transmission of cracks based on tilt and twist angles made by the crack planes with respect to the grain boundary. An example of the simulation and experiments is given in Figure 6. We have also recently completed high energy synchrotron experiments at CHESS for characterizing twinning and dislocation accumulation during cyclic loading of pure Mg and APS for characterizing 3D crack paths. Future plans include extending these experiments and developing and validating a more robust method for simulating twinning and 3D fatigue crack growth within PRISMS-Plasticity.

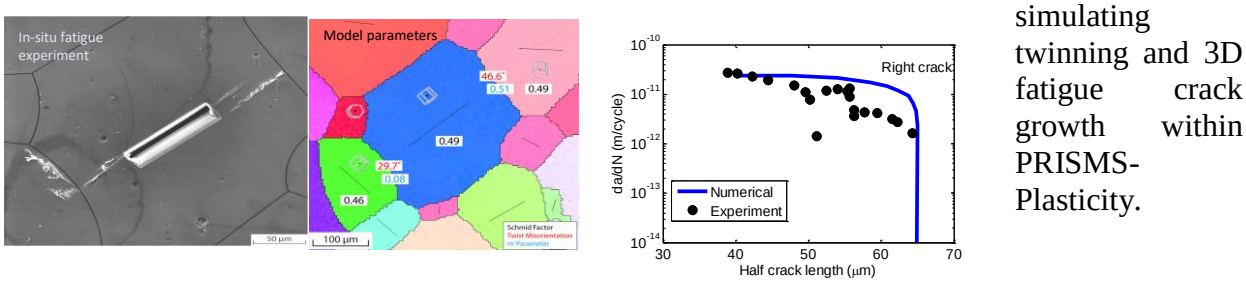

Figure 6*. Experiment and analytical model for predicting blocking versus transmission of cracks across a grain boundary.*

The Materials Commons *https://materialscommons.org*

The Materials Commons is a new information repository and virtual collaboration space for curating, storing and disseminating materials information from experiments and computations. It has been designed to explicitly cover the entire data lifecycle, from data acquisition through sharing and analysis to reuse. The Materials Commons provides a common site for materials researchers to store, share, curate, analyze, publish, and reuse experimental and computational materials data collaboratively. The uniqueness and strength of the Materials Commons is that it is both a collaboration space and an information repository, where the types of collaborations supported are familiar tasks in materials research and the underlying data model for the information repository is tailored for materials data, workflow, and analysis. Provenance is captured automatically and seamlessly as part of the scientific workflow. The Materials Commons is being used by PRISMS use case groups as a means of collaboration and storing and sharing information. It was made publically available in August 2016 and has over 150 registered users who have uploaded more than 1.1 million files in 150 datasets. Future plans for the Materials Commons include establishment of communities of practice for PRISMS Software and other areas using our new Materials Commons API, as well as integration of Materials Commons with Globus for faster upload/download of large files and with the national Materials Data Facility for enhanced data discovery and mining.

2015-2017 PRISMS Center Publications acknowledging DOE-BES support

1. M. Iyer, B. Radhakrishnan, V. Gavini, "Electronic structure study of an edge dislocation in aluminum and the role of macroscopic deformations on its energetics", J. Mech. Phys. Solids 76 (2015) 260-275.
2. E. Sitzmann and E. A. Marquis, “Chemistry and morphology of □' precipitates in an aged Mg-Nd-Y-Zr alloy”, 95(1) 7-13, Philosophical Magazine Letters, (2015).
3. Sambit Das, Mrinal Iyer, Vikram Gavini, “Real-space formulation of orbital-free density functional theory using finite-element discretization: The case for Al, Mg, and Al-Mg intermetallics”, Phys. Rev. B 92, 014104 (2015).
4. A. Natarajan, E. Solomon, B. Puchala, E. Marquis, A. Van der Ven, “On the precipitation sequence in dilute Mg-Nd alloys” Acta Mat, 108, 367-379 (2016).
5. E. Solomon, E.A. Marquis, The structure of ß” and ß’ in an Aged Mg-Nd Alloy, Magnesium Technology. 151-154 (2016)
6. S. Sun and V. Sundararaghavan, "Modeling crack propagation in polycrystalline microstructure using variational multi-scale method", Mathematical Problems in Engineering Volume 2016, Article ID 4715696, 14 pages, (2016).
7. S. Rudraraju, A. Van der Ven, K. Garikipati, “Mechano-chemical spinodal decomposition: A phenomenological theory of phase transformations in multi-component, crystalline solids” Nature Computational Materials, **2**, 16012 (2016).
8. B. Puchala, G. Tarcea, E. A. Marquis, M. Hedstrom, H. V. Jagadish and J. E. Allison, “The Materials Commons: A collaboration platform and information repository for the global materials community”, JOM, 68, 2035-44, 2016.
9. Z. Wang, S. Rudraraju, K. Garikipati, “A three-dimensional field formulation, and isogeometric solutions to point and line defects using Toupin’s theory of gradient elasticity at finite strains” Journal of the Mechanics and Physics of Solids, **94**, 336-361 (2016).
10. P. Acar, V. Sundararaghavan, A linear solution scheme for microstructure design with process constraints, AIAA Journal, 54(12), pp. 4022-4031 (2016).
11. J. Adams, J. Allison, J. W. Jones, “The effects of heat treatment on very high cycle fatigue behavior in hot-rolled WE43 magnesium” International Journal of Fatigue, 93 (2) 372-386, 2016.
12. K. Sagiyama, S. Rudraraju, K. Garikipati, “Unconditionally stable, second-order accurate schemes for solid state phase transformations driven by mechano-chemical spinodal decomposition” Computer Methods in Applied Mechanics and Engineering, **311**, 556-575 (2016).
13. P. Acar, V. Sundararaghavan, Uncertainty Quantification of Microstructural Properties due to Variability in Measured Pole Figures, Acta Materialia, v. 124, p. 100-108, 2017
14. S. Panwar, S. Sun, V. Sundararaghavan, "Modeling fatigue failure using variational multiscale method", Engineering Fracture Mechanics, 162, p. 290-308, 2016
15. P. Acar, V. Sundararaghavan, Uncertainty Quantification of Microstructural Properties due to Experimental Variations, AIAA Journal, Vol. 55, No. 8 (2017), pp. 2824-2832
16. T. Jiang, A. Roy, S. Rudraraju, A. Van der Ven, K. Garikipati, M. Falk, “A multi-physics study of lithium ion battery electrode $Li_{1+x}T_2O_4$”, Journal of Chemical Physics C, **120**, 27871-27881 (2016).
17. G. Teichert, S. Rudraraju, K. Garikipati, “A variational treatment of interface motion and microstructural change as problems of evolving configurations”, Journal of the Mechanics and Physics of Solids, **99**, 338-356 (2016).

18. A. Githens, S. Daly. Patterning Corrosion-Susceptible Metallic Alloys for Digital Image Correlation in a Scanning Electron Microscope. Strain. 2017; 53, e12215 (2016)
19. E. Solomon, V. Araullo-Peters, J.E. Allison, E.A. Marquis, Early precipitate morphologies in a Mg-Nd-(Zr) Alloys. Scripta Materialia 128;14-17 (2017)
20. G. H. Teichert, N. S. H. Gunda, S. Rudraraju, A. R. Natarajan, B. Puchala, K. Garikipati, A. Van der Ven, "A comparison of Redlich-Kister polynomial and cubic spline representations of the chemical potential in phase field computations", Comp. Mater. Sci. **128**, (2017) 127-139.
21. C. Heinrich, V. Sundaraghavan, "A method to predict fatigue crack initiation in metals using dislocation dynamics" Corrosion Reviews, in press, 2017.
22. A. R. Natarajan, A. Van der Ven, "A unified description of ordering in HCP Mg-RE alloys" Acta materialia, 124, p620-632, (2017).
23. S. DeWitt and K. Thornton "Phase Field Modeling of Microstructural Evolution" *Computational Materials System Design*, D. Shin and J. Saal, Eds., Springer Nature, London, (2017).
24. S. DeWitt, E. Solomon, A. Natarajan, V. Araullo-Peters, S. Rudraraju, L. Aagesen, E. Marquis, A. van der Ven, K. Thornton, and J. Allison, " Misfit-Driven β''' Precipitate Composition and Morphology in Mg-Nd Alloys" Acta Mat. (2017)
25. E. Solomon, T. Chan, A Chen, B Uttal-Veroff, E. Marquis "Aging behavior of Mg alloys containing Nd and Y" Magnesium Technology. (2017)
26. P. Acar, S. Srivastava, V. Sundararaghavan, Stochastic Design Optimization of Microstructures with Utilization of a Linear Solver, AIAA Journal, in press, 2017.
27. A. R. Natarajan, A. Van der Ven, "First principles investigation of phase stability in the Mg-Sc binary alloy," Physical Review B, (2017).
28. J. C. Thomas, A. Van der Ven, "The exploration of nonlinear elasticity and its efficient parameterization for crystalline materials," Journal of the Mechanics and Physics of Solids, Vol 107, p76-95, 2017.
29. Z. Wang, J. Siegel, K. Garikipati, "Intercalation driven porosity effects on the electro-chemo-thermo-mechanical response in continuum models for battery material electrodes," Journal of the Electrochemical Society, **164**, A2199-A2212, 2017.
30. K. Sagiyama, S. Rudraraju, K. Garikipati , **"**A numerical study of branching and stability of solutions to three-dimensional martensitic phase transformations using gradient-regularized, non-convex, finite strain elasticity**",** submitted to Journal of the Mechanics and Physics of Solids,(2017).
31. E.L.S. Solomon, E.A Marquis, "Deformation behavior of β' and β''' precipitates in Mg-RE alloys", submitted to Materials Letters (2017).
32. P-W Chu, E. LeMire, E.A. Marquis, "Microstructure of Localized Corrosion Front on Mg Alloys and the Relationship with Anodic Hydrogen Evolution", submitted to Corrosion Science (2017).
33. S. Das, V. Gavini, "Electronic structure study of screw dislocation core energetics in Aluminum and core energetics informed forces in a dislocation aggregate", J. Mech. Phys. Solids, 104, 115-143 (2017).
34. Z.Huang, J. E. Allison, A.Misra, "Interaction of Glide Dislocations with Extended Precipitates in Mg-Nd alloys", submitted to Acta Mater (2017).
35. P. Acar, V. Sundararaghavan, Stochastic Design Optimization of Microstructural Features using Linear Programming for Robust Material Design, sumitted to Acta Materialia, (2017).

36. L.K. Aagesen, J. Miao, J. E. Allison, S. Aubry, A. Arsenlis, "Prediction of Precipitation Strengthening in the Commercial Mg Alloy AZ91 Using Dislocation Dynamics", submitted to Met Trans. (2017).
37. A. R. Natarajan, J. C. Thomas, B. Puchala, A. Van der Ven, Symmetry adapted order parameters and free energies for solids undergoing order-disorder phase transitions, submitted to Physical Review B (2017).

Materials for Extreme Irradiation Environments

Pascal Bellon[1], Robert S. Averback[1], Shen J. Dillon[1], William P. King[2], Dallas R. Trinkle[1]

[1] Department of Materials Science and Engineering, University of Illinois at Urbana-Champaign, Urbana, IL.

[2] Department of Mechanical Science and Engineering, University of Illinois at Urbana-Champaign, Urbana, IL.

Program Scope

This program has been developing a new approach to the design of radiation resistant materials, based on concepts of nanostructuring and self-organization. While focus is on nuclear applications, we expect that the scientific advancements brought forth by this Cluster will have broad impact on materials needs for a number of other advanced energy technologies. The Cluster focuses on the fundamental processes controlling the formation of novel, self-organized, nanostructured materials, their long-term structural and dimensional stability, and the relationships between the nanoscale features and the macroscopic properties. The research combines irradiation experiments, *in situ* and *ex situ* characterization of microstructure and properties, and atomistic simulations and continuum modeling.

The program builds on our past work on self organization in binary alloys, extending the approach to ternary and quaternary alloy systems that form stable compounds, in particular silicides, e.g., Cu-M-Si (M=W, Mo, Nb) systems. While these systems add complexity, they offer new degrees of freedom, which greatly expand our control of the stability and properties of these materials. The research additionally explores the roles of sinks and defect fluxes on phase stability and self-organization, using samples fabricated with nanometer precision and characterized by advanced transmission electron microscopy. In the past two years, we have expanded our investigation of self-organization to the case of alloys processed by severe plastic deformation. The cluster also evaluates the properties of these new materials: their mechanical strength and their resistance to irradiation-induced creep, with deformation and irradiation performed at elevated temperatures both *in situ* in a TEM and *ex situ*. This research integrates experiments with atomistic and continuum modeling for elucidating mechanisms, analyzing results and designing experiments. The modeling combines first principles calculations with atomistic and continuum modeling, emphasizing the coupling between point defects, solute atoms, defect sinks, and applied and internal stresses. We presently investigate non-equilibrium segregation to sinks and its effects on climb and creep rates model on Ni-Si alloys. The model

will soon be extended to Cu-Si alloys with nanoprecipitate defect sinks, and compared with our own experimental measurements on irradiation creep rate in nanostructured Cu-Si-X alloys.

Recent Progress

1. Compositional patterning in ternary alloys.

We showed that nanostructuring by intracascade precipitation, which we originally observed in highly immiscible binary alloys such as Cu-W and Cu-Mo, could also be extended to compound-forming systems, resulting in the formation of high number density of nanoscale carbides and silicides. In the current funding cycle, we have focused on two systems, Cu-Mo-Si and Cu-Nb-Si, to take advantage of the high thermal stability of Mo and Nb silicides to suppress the coarsening of these phases. This nanoprecipitation and the remarkable stability of the nanoprecipitates is illustrated in Fig. 1, for $Cu_{90}Si_{6.5}Mo_{3.5}$ thin films, A quantitative analysis of the thermal coarsening results indicated that the remarkable resistance to thermal coarsening stemmed from two factors, first and foremost the reduction of Mo solubility in Cu by 2 to 3 orders of magnitude in the presence of Mo silicides, and to a lesser extent the narrow particle size distribution introduced by RT irradiation.

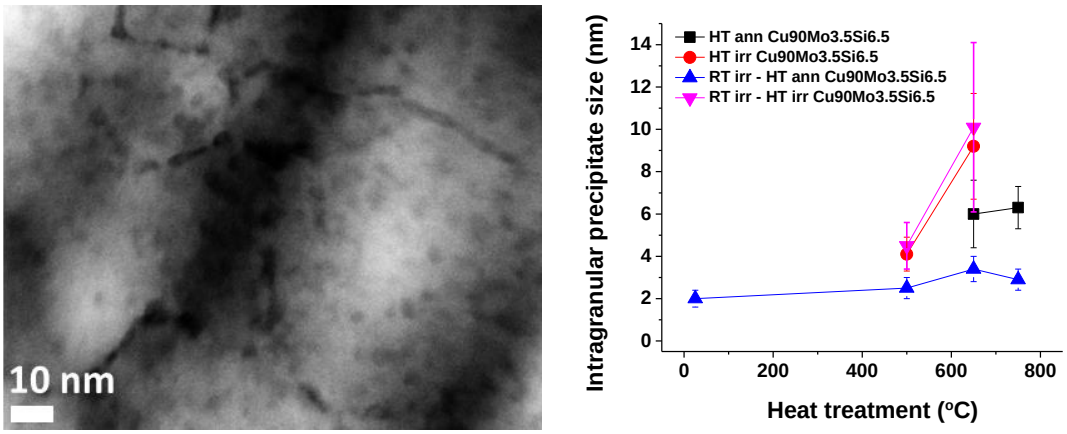

Fig. 1. *(left) HAADF-STEM images from plane view sample of* $Cu_{89}Si_{7.5}Mo_{3.5}$ *irradiated at RT with 1.8 MeV Kr ions to doses of* 2×10^{16} *ions/cm*^{2} *(equivalent to 50 dpa): (right)* Precipitate size evolution in $Cu_{89}Si_{7.5}Mo_{3.5}$ *after direct high temperature annealing for 1 hr (HT ann), RT irradiation followed by high-temperature annealing (RT irr – HT ann) or high temperature irradiation (RT irr - HT irr), or direct high temperature irradiation (HT irr). Note the remarkable coarsening resistance of the RT-irr samples.*

We have also established that self-organized compositional patterns can form in similar alloys by subjecting them to severe plastic deformation (SPD). We have used ball-milling and high-pressure torsion on Cu-Mo, Cu-Nb, and several ternary alloys, including Cu-Mo-Ni, Cu-Mo-O, Cu-Nb-O. The research addresses how ternary alloying elements can be used to increase the density, the stability, or the functionality of nanoprecipitates. Atomistic simulations have been used to elucidate the origins of this self-organization under SPD, analyzed as a competition between superdiffusive mixing of solute in the matrix and clustering induced by chemically-biased solute motion at structurally disordered locations such as grain boundaries and amorphous spots, see Fig. 2. The simulations have also established that these non-equilibrium systems obey

a lever rule and reach steady states that are independent of their initial state. This new knowledge is guiding the selection of alloying element and alloying composition.

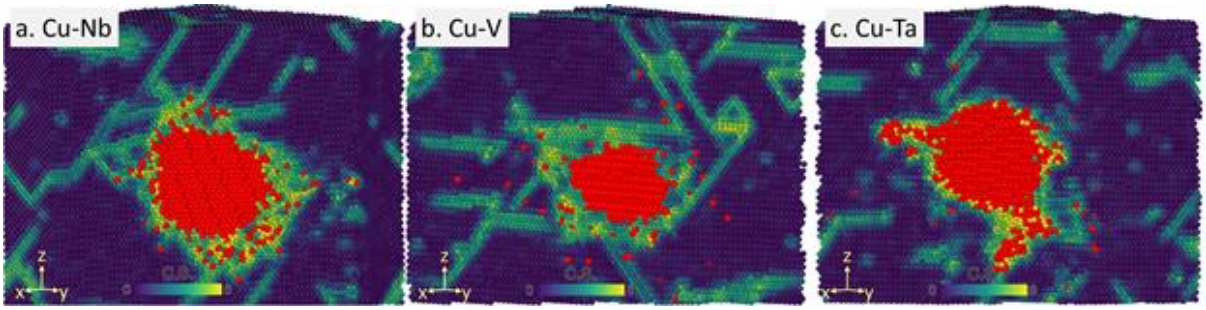

Fig. 2. *a-c Molecular dynamics of various Cu-X binary systems: Snapshots of a (110) cut through the simulated system at a strain of 40. Coloring is indicative of centro-symmetry, with blue marking atoms at perfect crystalline positions and light shades of green atoms indicative of lower symmetry. Non-Cu atoms are displayed with large red symbols. Notice the re-solution of solute atoms into the matrix, and the nucleation of new clusters in Cu-Ta.*

2. Strength in nc-Cu alloys

This work investigates the relative contributions to strengthening from twinning, solid-solution, precipitation, and irradiation hardening mechanisms in sputtered Cu–W thin films irradiated to different doses. A nanograin solid solution strengthening mechanism with a linear compositional dependence is observed for the as-grown alloys and for the alloy samples irradiated to 0.5 dpa. Solid solution strengthening is the major strengthening mechanism for Cu99.5W0.5 at all irradiation doses. Irradiation induces precipitation in samples with W concentrations greater than or equal to 1% at doses above 0.5 dpa. The growth of 1–4 nm precipitates enhances the hardness of these alloys, and the degree of strengthening is determined by the interparticle spacing. While the alloys exhibit steady-state properties after a relatively low dose (0.01 dpa), the different time scales associated with detwinning and damage accumulation in pure Cu lead transients at higher doses (.5 dpa)[1].

3. Modeling of alloy kinetics near dislocation cores.

Building on our past work on effect of strains on defect and solute transport, we have modeled the evolution of the silicon and vacancy distribution under irradiation and including the effect of dislocation climb. We show that below of transition temperature of 1060 K, vacancies could drag solutes through flux coupling, resulting in an segregation inversion, placing silicon on the thermodynamically unstable side of the dislocation core. We have developed coupled discrete (near the core) / continuum (away from the core) treatment to accurately model the dislocation core. A surprising result is the segregation inversion created by irradiation would lead to solute induced acceleration of climb: the irradiation induced solute distribution exerts a force on the dislocation in the same direction as the climb force created by the osmotic pressure of the excess vacancies, see Fig. 3.

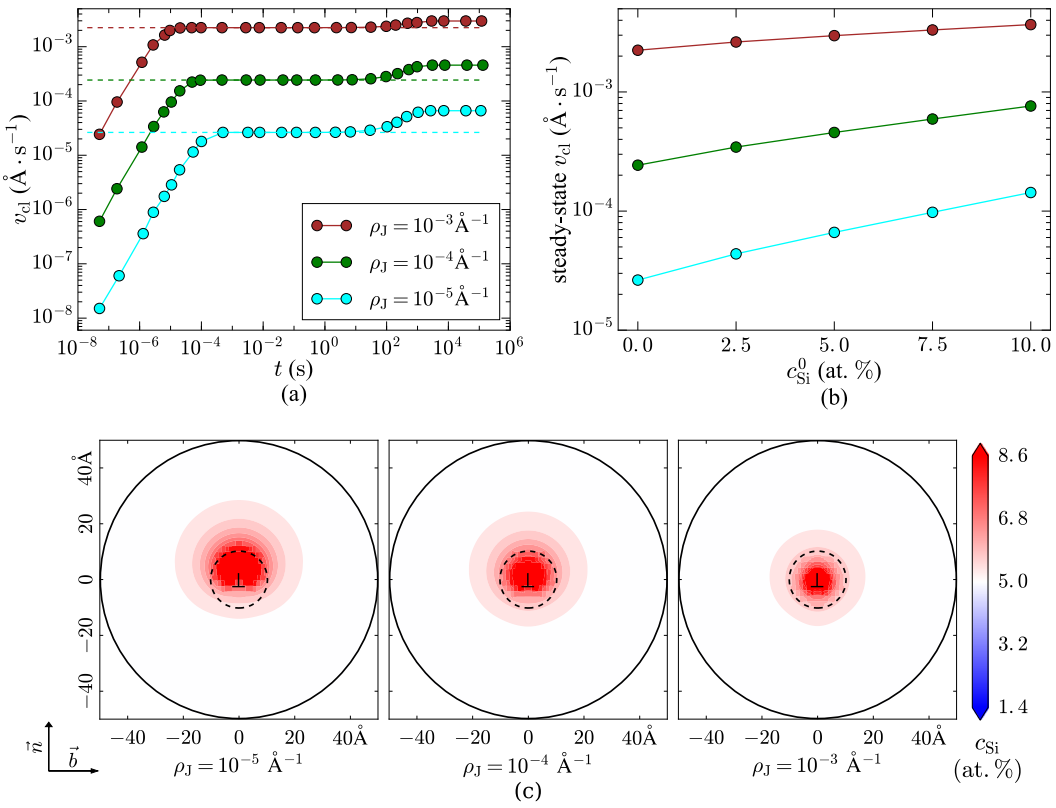

Fig. 3. *. Irradiation-induced dislocation climb velocities as functions of (a) time and (b) far-field solute concentration, and (c) contour plots of the steady-state Si concentration distribution at 960K for three different jog densities. The climb velocity shows three different behaviors: a linear growth immediately following irradiation, a quasi steady-state before Si evolution, the final steady-state after the Si evolves. (c) Steady-state silicon distribution in the moving frame of the dislocation. Silicon is segregated to the opposite side from thermodynamic equilibrium, accelerating dislocation climb.*

Future Plans

The Cluster will continue to investigate irradiation-induced self-organization in complex alloys, the stability and the properties of these nanostructures under elevated temperature irradiation and annealing. We will take advantage of a novel sample synthesis approach, relying on severe plastic deformation, to increase the grain sizes from ≈ 50 nm to above 200 nm. The irradiated microstructures may then contain defect clusters such as dislocation loops and voids. We will investigate the dynamical interactions between self-organized nanoprecipitates and these defect clusters, including sink efficiency and radiation-induced segregation. We will study the effect of particle structure (elemental phase versus intermetallics), coherency (by varying its size), and core/shell structuring on sink strength. We will extend our in-situ irradiation creep experiments to elevated temperatures. Lastly, we will develop new models coupling atomistic and continuum scales for investigating chemical and microstructural evolution under irradiation and applied stress, so as to determine dislocation climb rate in alloys with and without nanostructuring. These predictions will be compared to our experimental measurements and guide the design of critical experiments.

Publications (last 2 years)

[1] G. S. Jawaharram, R. S. Averback, and S. J. Dillon, Hardening Mechanisms in Irradiated Cu-W Alloys, J. Mater. Res. , in press (2017).

[2] A. J. Ardell and P. Bellon, Radiation-induced solute segregation in metallic alloys, Curr Opin Solid St M **20**, 115 (2016).

[3] Z. B. Li and D. R. Trinkle, Kinetic Monte Carlo investigation of tetragonal strain on Onsager matrices, Phys Rev E **93** (2016).

[4] S. Ozerinc, R. S. Averback, and W. P. King, In situ Measurements of Irradiation-Induced Creep of Nanocrystalline Copper at Elevated Temperatures, Jom-Us **68**, 2737 (2016).

[5] D. R. Trinkle, Diffusivity and derivatives for interstitial solutes: activation energy, volume, and elastodiffusion tensors, Philos Mag **96**, 2714 (2016).

[6] W. Z. Yang, S. M. Mao, J. Yang, T. Shang, H. G. Song, J. Mabon, W. Swiech, J. R. Vance, Z. F. Yue, S. J. Dillon, H. X. Xu, and B. X. Xu, Large-deformation and high-strength amorphous porous carbon nanospheres, Sci Rep-Uk **6**, 24187 (2016).

[7] Y. Ashkenazy, N. Pant, J. Zhou, P. Bellon, and R. S. Averback, Phase evolution of highly immiscible alloys under shear deformation: Self-organization, steady states, and the lever-rule, Acta Mater **139**, 205 (2017).

[8] J. A. Beach, M. Wang, P. Bellon, S. J. Dillon, J. Ivanisenko, T. Boll, and R. S. Averback, Self-organized, size-selection of precipitates during severe plastic deformation of dilute Cu-Nb alloys at low temperatures, Acta Materialia, under review (2017).

[9] S. J. Dillon, D. C. Bufford, G. S. Jawaharram, X. Y. Liu, C. Lear, K. Hattar, and R. S. Averback, Irradiation-induced creep in metallic nanolaminates characterized by In situ TEM pillar nanocompression, J Nucl Mater **490**, 59 (2017).

[10] J. Lee, J. Beach, P. Bellon, and R. S. Averback, High thermal coarsening resistance of irradiation-induced nanoprecipitates in Cu-Mo-Si alloys, Acta Mater **132**, 432 (2017).

[11] Z. B. Li and D. R. Trinkle, Mesoscale modeling of vacancy-mediated Si segregation near an edge dislocation in Ni under irradiation, Phys Rev B **95**, 144107 (2017).

[12] X. Y. Liu, R. Hao, S. M. Mao, and S. J. Dillon, Shear strengths of FCC-FCC cube-on-cube interfaces, Scripta Mater **130**, 178 (2017).

[13] T. Schuler, D. R. Trinkle, P. Bellon, and R. Averback, Design principles for radiation-resistant solid solutions, Phys Rev B **95**, 174102 (2017).

Characterization & Modeling of Deformation Induced Damage in Titanium Alloys

Principal Investigators: C.J. Boehlert, T.R. Bieler, M.A. Crimp, and P. Eisenlohr
Michigan State University, 428 S. Shaw Lane, Rm 2100, East Lansing, Michigan 48824

Program Scope

We are using a synergistic experimental and computational approach to identify and examine processes that cause damage nucleation at interfaces in single and two-phase structural alloys. We have systematically studied a near-α phase Ti alloy (Ti-5Al-2.5Sn(wt.%), henceforth referred to as Ti525) and compared the results with work on commercially pure (CP) Ti in order to determine how differences in composition and microstructure affect the processes that cause damage nucleation at interfaces at ambient and elevated temperature. We have also developed dislocation characterization approaches for studying slip behavior using cross-correlation electron backscatter diffraction (cc-EBSD) and electron channeling contrast imaging (ECCI). We have characterized heterogeneous deformation behavior and slip system activity as a function of temperature using slip trace analysis, as well as instances of slip transfer and grain boundary deformation behavior. Using this knowledge to examine the deformation behavior in more complex and multi-phase structural alloys is an objective. Successful completion of this research program will establish a modeling paradigm in which the physical processes responsible for damage nucleation in polycrystals can be simulated.

Recent Progress

We have developed a combined experimental and statistical approach to identify relative slip activity in Ti alloys. We have examined what is needed to do a credible simulation of a microstructural patch, so that weak links in the microstructure can be predicted with confidence. We know that combining slip trace analysis, differential aperture X-ray microscopy (DAXM), and microstructure patch simulation can identify mechanistic phenomena not easily explained using only experimental or modeling approaches alone; for example providing the means to explain the origin of large shear step observations in Ti525. More recent modeling progress has introduced slip transfer, informed by the geometry of active slip systems, into the model. We have identified grain boundaries that are more likely to exhibit slip transfer than others, but the effect is still rather dilute, so further amplification of this effect without losing numerical stability is a goal.

Methodology Improvement for Evaluation of Critical Resolved Shear Stress Ratios

Previously in this program, a methodology to relate critical resolved shear stress (CRSS) ratios to the statistics of surface slip trace observations in unidirectionally deformed samples of hexagonal (Ti) alloys has been reported [1]. During the current reporting period, we improved on one critical assumption made in the original method, which corrected the typically large spread of CRSS values resulting formerly. Furthermore, we investigated the inherent uncertainty of the method itself. At its core, the methodology compares the probability of actually observed slip traces per slip family to their expected values based on the globally applied (unidirectional) stress. Differences between observation and expectation can originate from a systematic diminishing in the activity of lowly stressed systems as well as from different CRSS values per slip family. Both aspects were separately taken into account to isolate the contribution postulated as being due different (relative) CRSS values. To better analyze this methodology, the deformation of a virtual polycrystalline volume, containing 400 randomly oriented grains, was simulated by full-field crystal plasticity with particular CRSS ratios prescribed between <a> slip on basal, prismatic and (first-order) pyramidal

planes, as well as <c+a> slip on the latter plane. Datasets of slip trace observations were generated, and they differed by their respective threshold values that triggered the "observability" of slip activity in each grain. Based on these datasets, it turned out that the inherent uncertainty of the method is likely on the order of a factor of three. Hence, care must be exercised when comparing results obtained for different materials that fall within such margin of error.

Characterization of Dislocations and their Distribution Across Grain Boundaries

One of the subprojects of this program was to evaluate the nature of dislocation shear transfer across grain boundaries, and this is being investigated by examining the dislocation characteristics (Burgers vectors, line directions, and slip planes) and the distributions of the dislocations that are involved in strain-transfer events. The results are then being used to assess the effectiveness of simple slip transfer criteria, such as the Livingston-Chalmers m' criteria [2] and the Lee-Robertson-Birnbaum (LRB) criteria [3], that predict the ease of slip for different combinations of slip systems due to varying grain misorientations. In this subproject, we are studying the slip transfer in CP Ti that has been deformed to ~2% tensile strain by four-point bending at room temperature. Slip planes are identified through slip trace analysis, while the dislocations are directly imaged in the near-surface regions of the grains using electron channeling contrast imaging (ECCI), which facilitates Burgers vector (**b**) and line directions determination. An example of this analysis is shown in Figure 1, which shows a series of images taken along a slip band and interactions at two boundaries in CP Ti. ECCI analysis has revealed that the dislocations in this slip band have **b**=[1-210]. Figure 1b shows a very narrow slip band that nucleated from dislocations in the upper left grain impinging on the boundary. The slip band remains fairly narrow across the grain, but then

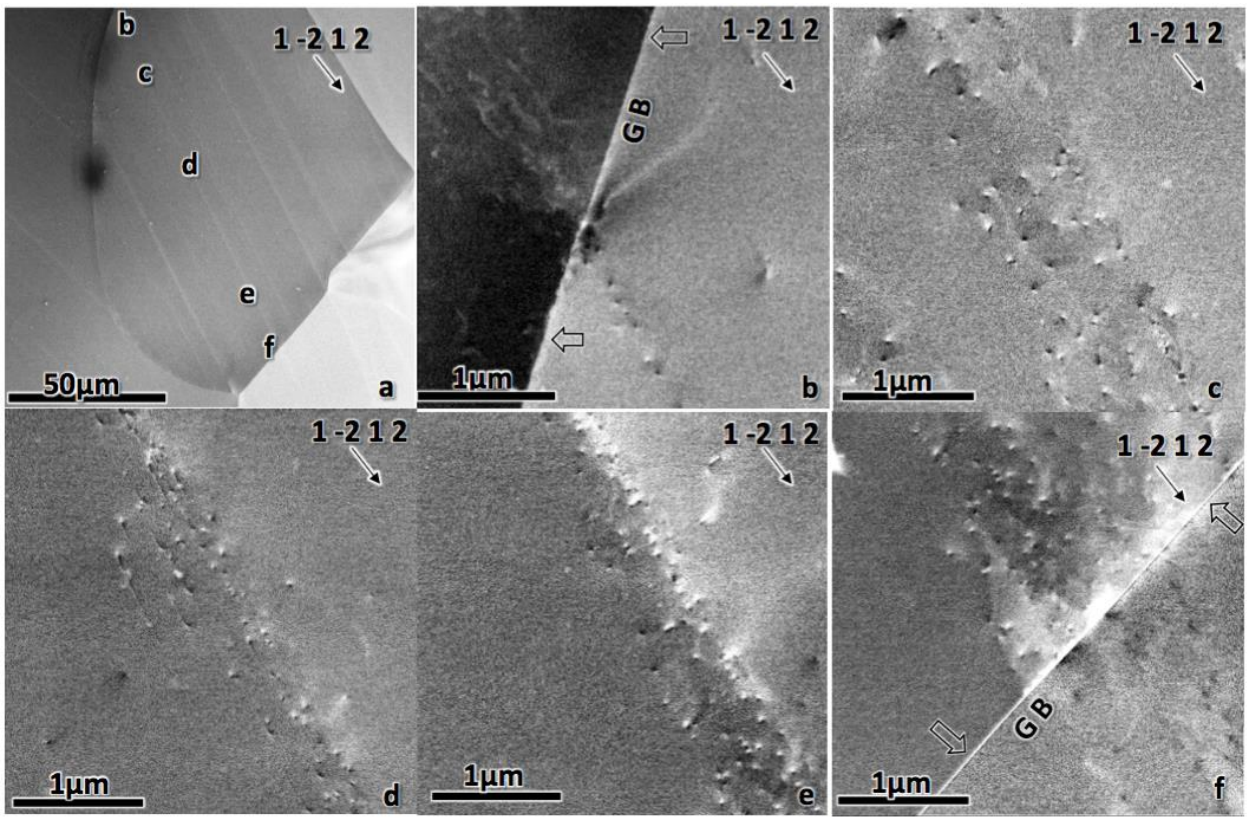

Figure 1. ECC images of dislocation distributions across a grain in a bulk four-point bend CP Ti sample deformed at room temperature. (b) shows the nucleation of a slip band as a result of strain transfer from the dislocations in the upper left grain. (f) shows the resulting pile up as the slip band impinges the lower right grain boundary. The effective width of the slip band increases from the source at the upper left, particularly as the dislocations approach the boundary at the lower right. **g•b**=0 invisibility contrast analysis reveals the dislocations have **b**= [1-210].

spreads out when in reaches the lower right hand side grain boundary (Figure 1f), suggesting relaxation of the pile-up stress may occur by cross-slip or climb near the boundary. Such a mechanism might also mitigate local damage nucleation associated with slip transfer. Currently, studies are underway to characterize the dislocations in the neighboring grains and to assess them in terms of the m' and LRB parameters. This ongoing work is intended to enhance the understanding of grain boundary transfer and the development of grain boundary transfer models already underway, such as that found in [4].

Non-destructive characterization of subsurface dislocation structure using Differential Aperture X-ray Microscopy

Knowledge of subsurface dislocation structure is critical in order to rationalize surface damage nucleation sites observed during bending experiments. Two Differential Aperture X-ray Microscopy (DAXM) based methodologies using the Central Super Dislocation model (CSD) and the Frank-Bilby equation (FBE) [5,6] were developed to non-destructively characterize the subsurface dislocation structure by analyzing the peak streak in the micro-Laue diffraction patterns. For validation purposes, two proposed DAXM methodologies and standard characterization techniques using focused ion beam (FIB) microscopy and transmission electron microscopy (TEM) were used to characterize the subsurface dislocation structure of the same Ti525 room-temperature tensile deformed sample. The results demonstrate that the CSD based method can provide a rapid identification of the Burgers vector for the dominant slip system whereas the FBE-based method can provide a spatially resolved dislocation density map, but with relatively high computational cost. The subsurface dislocation structure, characterized using the proposed methodologies, was largely in agreement with the FIB-TEM analysis, except for few special cases where the assumed kernel structure of the dislocation distribution could have potentially skewed the calculated dislocation structure.

Simulation of slip transfer using the Luster-Morris m' parameter in a bicrystal

In anticipation of installing slip transfer capability into a crystal plasticity model suitable for large-scale simulation, the logic needed to consider each slip system interaction in the boundary was developed and assessed in several virtual experiments using bicrystal samples. The key to this modeling strategy is to efficiently address the absence of natural boundary barriers in the phenomenological power-law based crystal plasticity model, which unrealistically assumes no barrier to slip across the boundary. Thus, the logic was made to harden the near-boundary regions by impeding all the slip systems for material points near boundaries (to mimic the Hall-Petch effect), except for slip systems with high m' values. Computational simulations show notable changes in the overall stress tensor shape and magnitude due to implementation of this crystal plasticity model enhanced with the slip transfer capability.

Dislocation Characterization using ECCI/EBSD

Characterizing dislocations using electron microscopy is traditionally carried out using TEM. The sample preparation required for TEM thin foils can be cumbersome and can lead to the introduction of defects. Also, due to the size limitations of thin foils, it can be difficult to obtain a statistical representation of the bulk material. In comparison, the techniques of ECCI and cross-correlation electron backscattered diffraction (CC-EBSD) can be carried out on bulk samples, allowing for a more statistical representation, and the required sample preparation is less demanding. Characterization using ECCI is similar to TEM in that dislocations are imaged using diffraction contrast. CC-EBSD is similar to standard EBSD, however, the EBSD patterns are saved and later cross-correlated to calculate the elastic strains based of the subtle shifts in the EBSD patterns. The

measuring of elastic strains essentially leads to the determination of the geometrically necessary dislocation (GND) content. In order to verify if the two techniques of ECCI and CC-EBSD give the same results, nanoindentation was carried out, using a conical spherical tip, in body centered cubic tantalum (Ta). An indent was made in the middle of a grain oriented with a plane normal of [011]. Figure 2a shows the dislocations imaged at the top left of the indentation using ECCI and Figure 2b shows the CC-EBSD derived GND density of the same area. In general, the ability of the two techniques to map dislocation distributions in terms of location and relative density is comparable. They do not however, correspond one to one. In areas of low dislocation density, the CC-EBSD measurements of dislocations gets lost in the noise; suggesting that ECCI is better for characterizing dislocations in areas of lower dislocation density and CC-EBSD is better suited for characterizing dislocations in areas of higher dislocation density. This subproject was carried out in collaboration with the research group of Dr. David Fullwood, who was supported by Department of Energy grant DE-SC0012587.

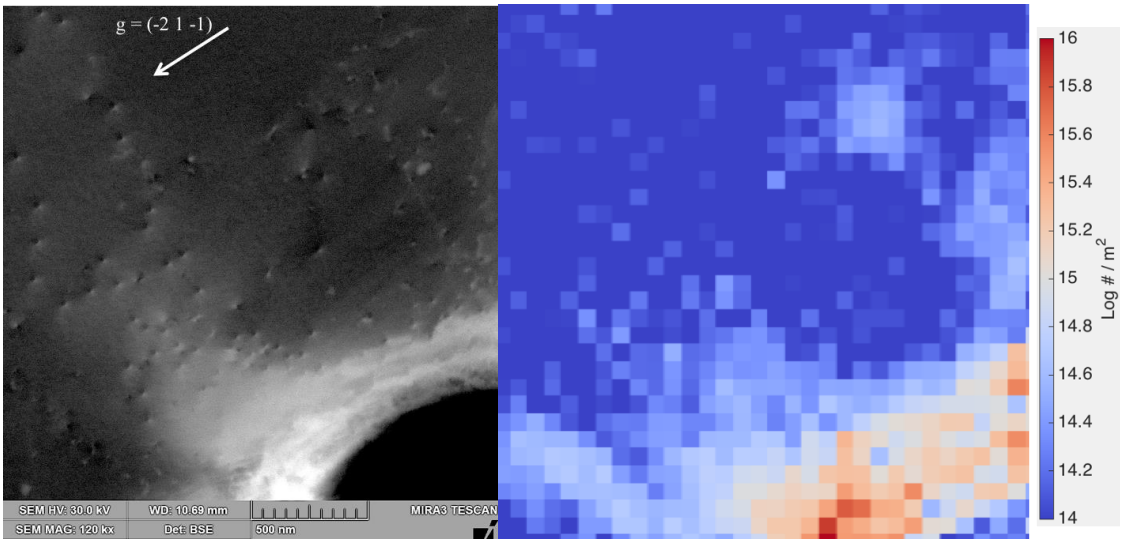

(a) (b)

Figure 2. a) ECCI image of the top left of an indent in high purity Ta. b) CC-EBSD calculated GND density map of the same area.

Future Plans

We have been developing an integrated experimental measurement and modeling approach that can provide information to assist interpretation of detailed mechanisms of deformation at the mesoscale. Now that this infrastructure is in place, it will be possible to identify discrepancies between mathematical models and experimental observations with a degree of confidence not achieved in the past, focusing on Ti alloys and slip and grain boundary sliding mechanisms. From discrepancies between observations and models, new insights about deformation modes are possible. These insights can be used to more rapidly explore the physical reality that occurs in heterogeneous deformation and damage nucleation processes, and future work will concentrate on obtaining these insights.

References

1. H. Li *et al*., Acta Materialia 61, (2013) 7555-7567.
2. J. Livingston and B. Chalmers, Acta Metall. 5 (1957) 322–327.
3. T.C. Lee, I.M. Robertson, and H.K. Birnbaum. Scr. Metall. 23 (1989) 799–803.
4. T.R. Bieler *et al*., Current Opinion Solid State Materials Science 18(4) (2014) 212-226.
5. F.C. Frank, *Symposium on the Plastic Deformation of Crystalline Solids* (Office of Naval Research Pittsburgh, Pennsylvania, 1950), p. 150
6. B.A. Bilby, *Report on the Conference on Defects in Crystalline Solids* (The Physical Society, London, 1955), p. 123

Publications (2015-2017)

I.G. Dastidar, A.L. Pilchak, T.R. Bieler, V. Khademi, M.A. Crimp, and C.J. Boehlert, "The Tensile and Tensile-Creep Deformation Behavior of Ti-8Al-1Mo-1V(wt.%)", Materials Science and Engineering A, Vol. 636 (2015) 289-300. doi: 10.1016/j.msea.2015.03.059

H. Li, C.J. Boehlert, T.R. Bieler, and M.A. Crimp, "Analysis of the Deformation Behavior in Tension and Tension-Creep of Ti-6Al-4V(wt.%) at 298K and 728K Using *In-Situ* SEM Experiments", Philosophical Magazine, Vol. 95 no. 7 (2015) 691-729. http://dx.doi.org/10.1080/14786435.2014.1001459

C. Zhang, H. Li, P. Eisenlohr, W. Liu, C.J. Boehlert, M.A. Crimp, T.R. Bieler, "Effect of Realistic 3D Microstructure in Crystal Plasticity Finite Element Analysis of Polycrystalline Ti-5Al-2.5Sn", International Journal of Plasticity, Vol. 69 (2015) 21-35. http://dx.doi.org/10.1016/j.ijplas.2015.01.003

V. Khademi, C.J. Boehlert, and M. Ikeda, "The tensile deformation behavior of beta titanium alloys at elevated temperatures", *Proceedings of the Twenty-Fourth International Symposium on Processing and Fabrication of Advanced Materials (PFAM XXIV)*, editors: M. Ikeda, T. Haruna, M. Niinomi, and T.S. Srivatsan, Organized by Kansai University (Osaka, Japan), 2016, pp. I-X.

V. Khademi, M. Ikeda, and C.J. Boehlert, "The Effect of Temperature on the Tensile Deformation Behavior of Ti-13Cr-1Fe-3Al(wt.%)", *Proceedings of the 13th World Conference on Titanium (Ti-2015)*, Edited by: Vasisht Venkatesh, Adam L. Pilchak, John E. Allison, Sreeramamurthy Ankem, Rodney Boyer, Julie Christodoulou, Hamish L. Fraser, M. Ashraf Imam, Yoji Kosaka, Henry J. Rack, Amit Chatterjee, and Andy Woodfield, TMS (The Minerals, Metals & Materials Society), 2016, p. 1109-1116. DOI: 10.1002/9781119296126.ch188

H. Li, C.J. Boehlert, T.R. Bieler, and M.A. Crimp, "The Distribution of the Deformation Systems in Tension in Alpha+Beta Titanium Alloys at Temperatures Ranging between 296K-728K", *Proceedings of the 13th World Conference on Titanium (Ti-2015)*, Edited by: Vasisht Venkatesh, Adam L. Pilchak, John E. Allison, Sreeramamurthy Ankem, Rodney Boyer, Julie Christodoulou, Hamish L. Fraser, M. Ashraf Imam, Yoji Kosaka, Henry J. Rack, Amit Chatterjee, and Andy Woodfield, TMS (The Minerals, Metals & Materials Society), 2016, p. 1103-1108. DOI: 10.1002/9781119296126.ch187

B.E. Dunlap, T.J. Ruggles, D.T. Fullwood, B. Jackson, M.A. Crimp, "Comparison of Dislocation Characterization by Electron Channeling Contrast Imaging and Cross-Correlation Electron Backscattered Diffraction", accepted for publication in Ultramicroscopy.

C. Zhang, S. Balachandran, P. Eisenlohr, M.A. Crimp, C. Boehlert, R. Xu, T.R. Bieler, "Comparison of dislocation content measured with transmission electron microscopy and micro-Laue diffraction based streak analysis", submitted to Scripta Materialia.

Nanomechanics and Nanometallurgy of Boundaries

Brad Boyce, Principal Investigator
Sandia National Laboratories, Albuquerque, NM 87185-0889

Program Scope

Deformation of metals and grain growth are often considered unrelated; the two subjects are invariably taught in separate courses. However, in nanocrystalline metals, deformation is facilitated by grain boundary mediated mechanisms including both the shear sliding and normal motion of grain boundaries [1]. While the deformation-induced grain growth process can enhance ductility in nanocrystalline metals [2], it has also been associated with premature failure by facilitating fatigue crack initiation [3] and wear-induced delamination [4]. These failure mechanisms are specifically associated with abnormal grain growth (AGG) [5], where a rare minority of susceptible grains result in a bimodal grain size distribution. Recent evidence suggests that AGG kick-starts with a rare boundary type that possesses exceptionally high mobility (or mechanical coupling) at room temperature and below. This project combines Sandia's strengths in computational and experimental nanomechanics to understand the heterogeneous properties of grain boundaries that vary widely depending on their structure and the resulting implications for mechanically-driven motion. By departing from most conventional thermodynamic and kinetic models of boundary processes which treat all boundaries with single-valued properties, this heterogeneous framework is expected to reframe the thinking of mechanisms associated with mechanically-induced grain growth and illuminate pathways to avoid catastrophic AGG processes while still enabling strain accommodation via other boundary-mediated deformation mechanisms. While our modeling modalities are limited to observing boundary response under monotonic conditions, the atomic scale models have provided atomic-scale resolution on the complex mechanisms that cause a rare minority of boundaries to move extremely fast at low temperatures – a phenomenon that we hypothesize is underpinning the mechanically-induced growth process.

Recent Progress

Recent work has focused on understanding the role of heterogeneous boundary character on microstructural evolution under thermal and mechanical stimuli. In pure metals, we have focused on the role of grain boundary character. While a planar grain boundary can be described with 5-degrees of freedom, it is more commonly reduced to scalar metrics such as misorientation angle. Building off of recent work that has attempted to describe grain boundary properties such as energy and mobility within the framework of a two-dimensional fundamental zone [6], we are examining the possibility that the boundary stiffness is the controlling property that can be described in low-dimensional space. We have found that certain grain boundaries display "ultrafast" motion in response to an applied driving force [7]. While the precise atomistic

mechanism for the motion differs for different grain boundary types, they all share a common militaristic (diffusionless) local reordering process to facilitate the ultrafast motion (Fig 1). It is this rare ultrafast motion that is thought to be influencing mechanical response at room temperature and below.

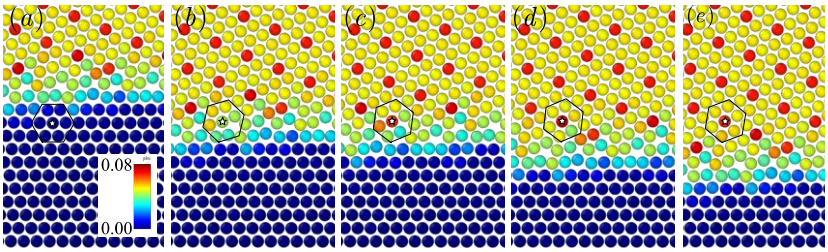

Figure 1. Snapshots of the motion of a Σ7 (12 3 1)/(9 8 3) boundary motion where the atoms are colored by local microrotation. The star is a fiduciary mark and the hexagon highlights atoms undergoing a concerted rotation.

However, most grain boundaries are more complex than even the 5-angle description of their orientation. Local curvature, the primary cause of thermally-driven instability, is the result of faceting and associated boundary defects which interact with the deformation-induced defects to drive material response. The facets and their associated junction defects are dictated by the stiffness of the various grain boundary planes [8].

Chemical segregation at grain boundaries is also considered as a stabilizing effect on boundary response in the context of Zener pinning, solute drag (in the case of a precipitate or 2nd phase), or reduction of the thermodynamic driving force [9]. While our group has studied the stabilization of a number of binary alloy systems [10-12], we have recently focused on the Pt-Au system [13]. Pt-Au is the most noble binary alloy available, and as such, it is the least susceptible to oxygen uptake and oxide-induced stabilization. Yet in our thermal studies we have found that the Pt-Au alloy is substantially more stable than a pure-Pt equivalent. Atomistic and mesoscale modeling frameworks have been used to further elucidate these binary alloy systems. Departing from conventional thermodynamic and kinetic models for grain growth, both our experiments and simulations show that segregation is highly heterogeneous: not all grain boundaries segregate equally. For this reason, true thermodynamic stabilization of a grain structure may never be achievable.

Ultimately, the project seeks to tie understanding of boundary stability to mechanical properties. Using in-situ x-ray diffraction we have observed the onset and kinetics of the abnormal grain growth process on fatigue crack initiation [14]. This observation has confirmed that the grain-growth process starts well in advance of crack initiation under high-cycle fatigue conditions. Moreover, the grain-growth process can be used to predict the crack initiation event, and even interrupt a test just prior to crack initiation. In-situ transmission electron microscopy was further used to confirm the grain growth process and map the local crystallographic reorientations that take place as a fatigue crack propagates (Figure 2) [15]. Perhaps the most exciting result is the new observations of friction and wear behavior in nanocrystalline metals. Based on previous results, we hypothesize that there is an equilibrium grain size under tribological loading: depending on loading conditions, nanocrystalline grains grow whereas

coarse-grains refine through cell formation [12]. By stabilizing the grains through alloying, we have shown a nanocrystalline Pt-Au allow with specific wear rates that are comparable to diamond-like carbon, orders of magnitude lower than any previously reported metallic system.

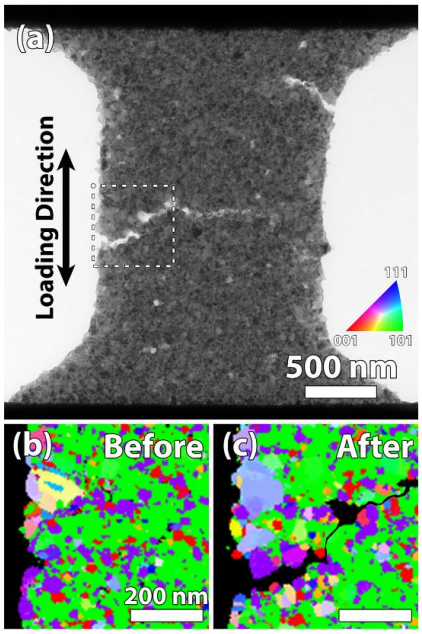

Figure 2. Nanocrystalline Cu after failing at 357,000 loading cycles with corresponding precession electron diffraction orientation maps before and after fatigue illustrating the grain growth process.

Future Plans

There are several pathways for continued investigation. While in the near-term we continue to explore the role of heterogeneous grain boundaries on thermal and mechanical response of pure metals and binary nanocrystalline alloys, ultimately we will broaden these observations to other material systems: e.g. nanotwinned metals, nanocrystalline metals with amorphous grain boundaries, and nanoporous metals. We seek to extend the concept of an equilibrium grain size to fatigue loading conditions, and directly observe defect-boundary interactions under thermal and mechanical loading using in-situ TEM and SEM observation. We will use grain mapping techniques such as precession electron diffraction to understand the role of grain boundary character on the subsequent evolution.

In addition to our thermal and mechanical studies on nanocrystalline metals, we are proposing an expansion to explicitly study ion irradiation stability of nanocrystalline metals. Our hypothesis in that proposed expansion is that different grain boundary types will respond very differently to irradiation: with some grain boundaries accelerating motion while others slow down due to the change in character/defect state/chemistry of the boundary. This investigative pathway will take advantage of Sandia's unique in-situ ion irradiation TEM capability.

To understand grain boundary stability through simulation, we have largely focused on monotonic thermal models for boundary motion. Moving forward, we will work towards superimposed mechanical descriptions for boundary motion and a generalized framework for describing susceptibility. We will seek to describe how grain boundary defects and defect-boundary interactions serve to mobilize (or immobilize) grain boundaries, and the role of grain boundary heterogeneities. Finally, we are beginning to explore modeling frameworks that can describe multi-cycle evolution for the purpose of developing a more fundamental understanding of evolution that takes place under cyclic fatigue and wear loading conditions.

Acknowledgements

Sandia National Laboratories is a multimission laboratory managed and operated by National Technology and Engineering Solutions of Sandia, LLC., a wholly owned subsidiary of Honeywell International, Inc., for the U.S. Department of Energy's National Nuclear Security Administration under contract DE-NA-0003525.

References

[1] J. W. Cahn, Y. Mishin, and A. Suzuki, "Coupling grain boundary motion to shear deformation," Acta materialia, vol. 54, pp. 4953-4975, 2006.
[2] D. Gianola, S. Van Petegem, M. Legros, S. Brandstetter, H. Van Swygenhoven, and K. Hemker, "Stress-assisted discontinuous grain growth and its effect on the deformation behavior of nanocrystalline aluminum thin films," Acta Materialia, vol. 54, pp. 2253-2263, 2006.
[3] B. L. Boyce and H. A. Padilla, "Anomalous fatigue behavior and fatigue-induced grain growth in nanocrystalline nickel alloys," Metallurgical and Materials Transactions A, vol. 42, pp. 1793-1804, 2011.
[4] H. A. Padilla, B. L. Boyce, C. C. Battaile, and S. V. Prasad, "Frictional performance and near-surface evolution of nanocrystalline Ni–Fe as governed by contact stress and sliding velocity," Wear, vol. 297, pp. 860-871, 2013.
[5] A. Rollett, D. J. Srolovitz, and M. Anderson, "Simulation and theory of abnormal grain growth—anisotropic grain boundary energies and mobilities," Acta metallurgica, vol. 37, pp. 1227-1240, 1989.
[6] E. R. Homer, S. Patala, and J. L. Priedeman, "Grain boundary plane orientation fundamental zones and structure-property relationships," Scientific reports, vol. 5, 2015.
[7] C. O'Brien and S. Foiles, "Exploration of the mechanisms of temperature-dependent grain boundary mobility: search for the common origin of ultrafast grain boundary motion," Journal of materials science, vol. 51, pp. 6607-6623, 2016.
[8] F. Abdeljawad, D. L. Medlin, J. A. Zimmerman, K. Hattar, and S. M. Foiles, "A diffuse interface model of grain boundary faceting," Journal of Applied Physics, vol. 119, p. 235306, 2016.
[9] C. C. Koch, R. O. Scattergood, M. Saber, and H. Kotan, "High temperature stabilization of nanocrystalline grain size: thermodynamic versus kinetic strategies," Journal of Materials Research, vol. 28, pp. 1785-1791, 2013.
[10] B. G. Clark, K. Hattar, M. T. Marshall, T. Chookajorn, B. L. Boyce, and C. A. Schuh, "Thermal stability comparison of nanocrystalline Fe-based binary alloy pairs," JOM, vol. 68, pp. 1625-1633, 2016.

[11] M. Kapoor, T. Kaub, K. A. Darling, B. L. Boyce, and G. B. Thompson, "An atom probe study on Nb solute partitioning and nanocrystalline grain stabilization in mechanically alloyed Cu-Nb," Acta Materialia, vol. 126, pp. 564-575, 2017.
[12] N. Argibay, T. Furnish, B. Boyce, B. Clark, and M. Chandross, "Stress-dependent grain size evolution of nanocrystalline Ni-W and its impact on friction behavior," Scripta Materialia, vol. 123, pp. 26-29, 2016.
[13] F. Abdeljawad, P. Lu, N. Argibay, B. G. Clark, B. L. Boyce, and S. M. Foiles, "Grain boundary segregation in immiscible nanocrystalline alloys," Acta Materialia, vol. 126, pp. 528-539, 2017.
[14] T. Furnish, A. Mehta, D. Van Campen, D. Bufford, K. Hattar, and B. Boyce, "The onset and evolution of fatigue-induced abnormal grain growth in nanocrystalline Ni–Fe," Journal of materials science, vol. 52, pp. 46-59, 2017.
[15] D. C. Bufford, D. Stauffer, W. M. Mook, S. Syed Asif, B. L. Boyce, and K. Hattar, "High cycle fatigue in the transmission electron microscope," Nano letters, vol. 16, pp. 4946-4953, 2016.

Publications

[1] M. Kapoor, K. Darling, T. Kaub, B. L. Boyce, and G. B. Thompson, "An Atom Probe Study on the Nanocrystalline Grain Stabilization and Nb Solute Partitioning in Mechanically Alloyed Cu-Nb," Acta Materialia, vol. 126, pp. 564-575, 2017.
[2] J. Kacher, K. Hattar, and I. M. Robertson, "Initial texture effects on the thermal stability and grain growth behavior of nanocrystalline Ni thin films," Materials Science and Engineering A, vol. 675, pp. 110-119, 2017.
[3] J. Gruber, H. Lim, F. Abdeljawad, S. Foiles, and G. J. Tucker, "Development of physically based atomistic microstructures: The effect on the mechanical response of polycrystals," Computational Materials Science, vol. 128, pp. 29-36, 2017.
[4] S. J. Dillon, D. C. Bufford, Q. S. Jawaharram, X. Liu, C. Lear, K. Hattar, et al., "Irradiation-induced creep in metallic nanolaminates characterized by In situ TEM pillar nanocompression," Jounral of Nuclear Materials, 2017.
[5] F. F. Abdeljawad, P. Lu, N. Argibay, B. G. Clark, B. L. Boyce, and S. M. Foiles, "Grain boundary segregation in immiscible nanocrystalline alloys," Acta Materialia, vol. 126, pp. 528-539, 2017.
[6] T. A. Furnish, D. Van Campen, A. Mehta, D. C. Bufford, and K. Hattar, B. L. Boyce, "The onset and evolution of abnormal grain growth during high cycle fatigue of nanocrystalline Ni-Fe," Journal of Materials Science, 2016
[7] B. G. Clark, K. Hattar, M. T. Marshall, T. Chookajorn, B. L. Boyce, and C. A. Schuh, "Thermal Stability Comparison of Nanocrystalline Fe-Based Binary Alloy Pairs," JOM, vol. 68, pp. 1625-1633, 2016.

[8] C. J. O'Brien and S. M. Foiles, "Exploration of the Mechanisms of Temperature Dependent Grain Boundary Mobility: Search for the common origin of ultrafast grain boundary motion," Journal of Materials Science, vol. 51, pp. 6607-6623, 3/31/2016 2016.

[9] T. A. Furnish, B. L. Boyce, J. A. Sharon, C.J. O'Brien, B.G. Clark, C. Arrington, J. Pillars, "Fatigue stress concentration and notch sensitivity in nanocrystalline metals," Journal of Materials Research, vol. 31, 2016.

[10] D. C. Bufford, D. Stauffer, W. M. Mook, S. A. S. Asif, B. L. Boyce, and K. Hattar, "High cycle fatigue in the transmission electron microscope," Nano Letters, 2016.

[11] F. Abdeljawad and S. M. Foiles, "Interface-driven Phenomena in Solids: Thermodynamics, Kinetics and Chemistry," JOM, 2016.

[12] G. Mohanty, J. Wehrs, B. Boyce, A. Taylor, M. Hasegawa, L. Phillippe, J. Michler, "Room temperature stress relaxation in nanocrystalline Ni measured by micropillar compression and miniature tension," Journal of Materials Research, vol. 31, 2016.

[13] Y. Chen, N. Li, D. C. Bufford, J. Li, K. Hattar, H. Wang, X. Zhang, "In situ study of heavy ion irradiation response of immiscible Cu/Fe multilayers," Journal Of Nuclear Materials, 2016.

[14] N. Argibay, T. A. Furnish, B. L. Boyce, B. G. Clark, and M. Chandross, "Stress-dependent grain size evolution of nanocrystalline Ni-W and its impact on friction behavior," Scripta Materialia, 2016.

[15] B. Muntifering, S. J. Blair, C. Gong, A. Dunn, R. Dingreville, J. Qu, et al., "Cavity Evolution at Grain Boundaries as a Function of Radiation Damage and Thermal Conditions in Nanocrystalline Nickel," Materials Research Letters, vol. 4, pp. 96-103, 2016.

[16] S. A. Briggs, C. M. Barr, J. Pakarine, M. Mamivand, K. Hattar, D. D. Morgan, et al., "Observations of defect structure evolution in proton and Ni ion irradiated Ni-Cr binary alloys," NOTE: This peripheral publication was not included in mid-term review. Journal of Nuclear Materials, vol. 479, pp. 48-58, 2016.

[17] S.N. Mathaudhu and B.L. Boyce, "Thermal Stability: the next frontier for nanocrystalline materials", JOM, v. 67(12), pp. 2785-2787, 2015.

[18] D.C. Bufford, F.F. Abdeljawad, S.M. Foiles, and K. Hattar, "Unraveling irradiation induced grain growth with in situ transmission electron microscopy and coordinated modeling", Applied Physics Letters, v. 107, p. 191901, 2015.

[19] P. Sarobol, M. Chandross, J.D Carroll, W.M. Mook, D.C Bufford, B.L. Boyce, K. Hattar, P.G. Kotula, A.C. Hall, "Room temperature deformation mechanisms of alumina particles observed from in situ micro-compression and atomistic simulations", Journal of Thermal Spray Technology, v. 25(1), pp. 82-93, 2015.

[20] F. Abdeljawad and S.M. Foiles: "Stabilization of Nanocrystalline Alloys via Grain Boundary Segregation: A Diffuse Interface Model", Acta Materialia, v. 101, p. 159-171, 2015.

Microstructure Anisotropy Effects On Fracture And Fatigue Mechanisms In Shape Memory Alloy Martensites

PI: Prof. L. Catherine Brinson, Northwestern University

Co-PI: Prof. Aaron P. Stebner, Colorado School of Mines

Program Scope:

The broad goal of this program is to develop a mechanistic understanding of the influence that microstructure anisotropy and the relative size-scale of structural features have on the deformation response of shape memory alloys (SMAs). In the first phase of this program, we documented two deformation phenomena in the high-symmetry cubic phase in superelastic nickel-titanium (NiTi) SMAs: 1) The interaction of structural features (micro-holes) with the grain-scale deformation; 2) The heterogeneity in deformation between free surfaces and the specimen interior during cyclic loading of NiTi.

The current phase is focused on failure mechanisms in the low-symmetry monoclinic martensite phase in NiTi SMAs. Specifically, we are testing the following hypotheses:

1. Due to the high elastic anisotropy of low symmetry martensite phases and more twin systems, but fewer slip systems to activate compared to austenite, the mechanisms that govern crack tip deformation and dictate crack growth paths and velocities will be significantly different in martensites compared to the cubic austenite phase in SMAs.
2. Due to the fewer number of available slip systems, fatigue responses at crack tips in martensites will be governed by martensite-martensite interface nucleation and mobility, with slip playing a secondary role.
3. Due to the saturation of detwinning and reorientation mechanisms after a finite deformation, at higher crack stress intensities, slip will take over as the dominant mechanism determining crack deformation mechanics.
4. Due to a relatively higher constraint on martensite twin motion near high angle grain boundaries inherited from parent austenite structures, martensite fracture mechanics will be driven by the grain boundaries in their proximity.
5. Due to the effect of granular vs. surface constraints on martensite reorientation mechanisms, crack-tip deformation in thin and/or surfaces of specimens will be different than in the bulk.

Recent Progress

In creating materials, we have found that brittle carbide and oxide inclusions (Figure 3(b)) are present in large dendritic networks or as individual brittle inclusions in nearly all of our samples, especially the crystals grown with the modified Bridgman technique. These inclusions are known to be deleterious to the fatigue life of SMAs [2,3]. Therefore, to understand and correctly characterize the behavior of the monoclinic phase, it is necessary to also understand the detailed deformation behavior around these inclusions. This is a modification of our proposed research

plan for this phase, in which we proposed to study pristine monoclinic structures. We are also continuing to work on fabricating samples that have less profound populations of these inclusions toward our original goal of studying the monoclinic structure in isolation; namely we are now employing advanced processing techniques that include sputter deposition as well as strain-annealing of electron beam remelting bar stocks.

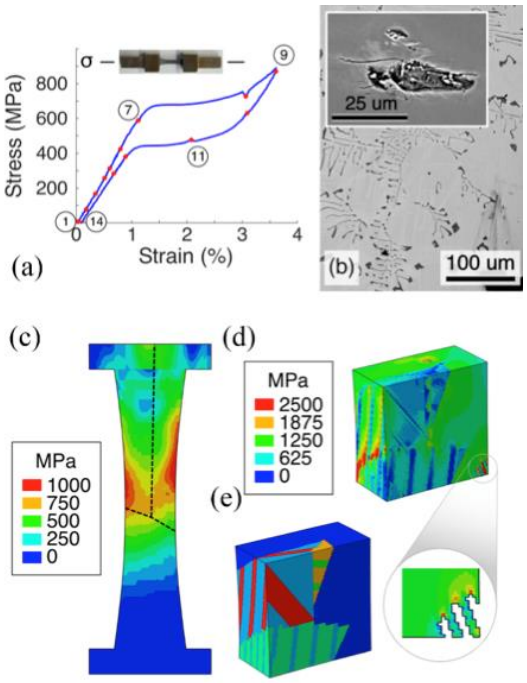

Figure 1:(a) Nominal stress-strain curve (b) SEM images showing dendritic inclusion networks and (inset) a single inclusion (c) Axial stress at 600 MPa macro stress. (d) A section of the gage showing details of local stress at 800 MPa macro stress. The inset shows the heterogeneous axial stress around an inclusion array and (e) The martensitic microstructure corresponding to the section in (d).

Similar to the micro-holes and heterogeneity of grain neighbors studied in Phase 1 of this program, these inclusions also constrain the phase transformation mechanics in NiTi. To elucidate the mechanisms by which the inclusions alter phase transformations, we studied an oligocyrystal sample under superelastic loading, in which the B19' martensite is stressed induced from the B2 austenite. The measured transformation strains in the specimen were half of the theoretically expected values based on the crystallographic theory of martensite [1]. We then used microstructural modeling, informed by in situ high-energy X-ray diffraction microscopy (HEDM) measurements, to obtain the local stress state around the inclusions (Figure 3(c-e)). We found that the regions between inclusion dendrites are shielded from the externally applied stress and thus can lead to the activation of martensite variants that produce low transformation strain**.** Additionally, we found that even in the absence of high angle grain boundaries, austenite-martensite and martensite-martensite interfaces acted as additional sources of constraint. This constraint led to deformation in the martensite phase seen as proportional gradients in rotation and elastic stretch.

In totality, non-optimal martensite variants may nucleate about inclusions. Because inclusions also create stress concentrations, these are often the first martensite nucleation events. Hence these unfavorable variants may consume the entire sample, even far away from the inclusions, resulting in non-optimal transformation strains in the bulk. Still, the variant propagation paths are further constrained by competing austenite-martensite and martensite-martensite interfaces nucleated from other regions, leading to gradients in rotation and stretch to maintain compatibility through the sample. Previously, the predominant explanation for why SMA polycrystals do not exhibit near theoretical transformation strains was texture. These new results

show that there are also competing effects from inclusions that limit the ability to completely transform to theoretically favorable variants.

With the influence of inclusions on the nucleation of transformation structures ascertained, our current work is now focused on characterizing failure mechanisms in martensitic NiTi. To localize deformation in the specimens, we use notched dogbone specimens in uniaxial tension in this set-up. To increase the size of martensite domains for in situ X-ray methods, the material was mostly detwinned before cutting the samples. These detwinned, notched monoclinic samples were subject to two loading scenarios to test the hypotheses listed above:

a. Static load testing, where the specimen was monotonically loaded to failure to observe the anisotropy of the strain field, along with a transition from predominant reorientation and detwinning to plasticity.
b. Low cycle fatigue testing, where the specimens were cyclically loaded to at low loads, to observe the accumulation of deformation over cycles.

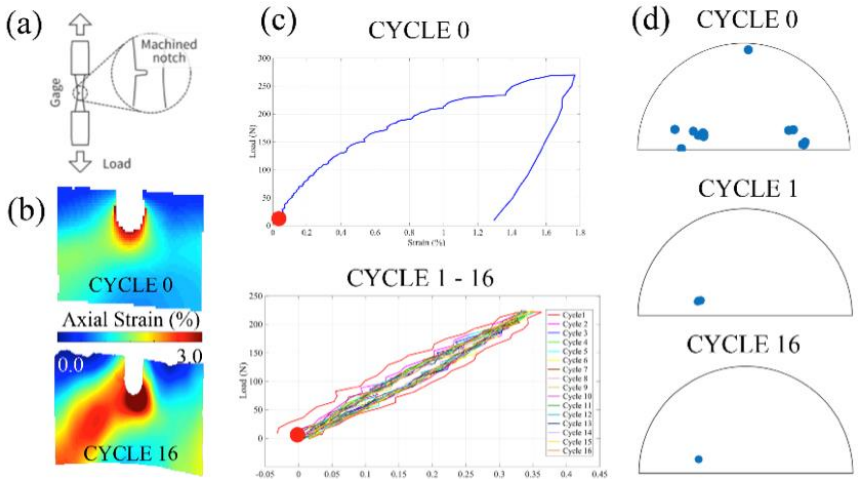

Figure 2: We found that in a martensitic NiTi specimen (a), initially relatively isotropic strain fields developed around a notch-tip (b, Cycle 0), but anisotropy increased as cycling was carried out (b, Cycle 16). This observation is correlated with (d) martensite orientations, where initially many different variants participated in the deformation, but after 1 cycle only a single monoclinic variant was present, leading to increased anisotropy.

Our preliminary results of the cyclic study indicate that the local deformation near a notch loaded similar to Type-I crack loading showed asymmetric strain localization (Figure 4(a-b)). During cyclic loading, the martensite reorientation and detwinning activity occurred primarily in the first cycle as evidenced by the large unrecovered strain in cycle 1 vs. small hysteresis subsequent cycles (Figure 2). This observation was reinforced by the martensite crystal orientations obtained from HEDM. A large number of martensite domains were identified at the beginning of the first cycle, which reoriented to favorable orientations and retained that microstructure upon unloading after successive cycles, as shown in Figure 2(d).

Furthermore, we have begun to understand the source of ductility in NiTi, in particular why a short change in aging time can suddenly cause a 30% or greater increase in failure strains but not effect the failure stress (see Figure 3a). Using geometrical phase analysis of high-resolution TEM images, we have found that coherent Ni_4Ti_3 martensite precipitate structures (as in Figures 3b-c) are critical to ductility. In particular, when the precipitates are small (< 5nm, corresponding to

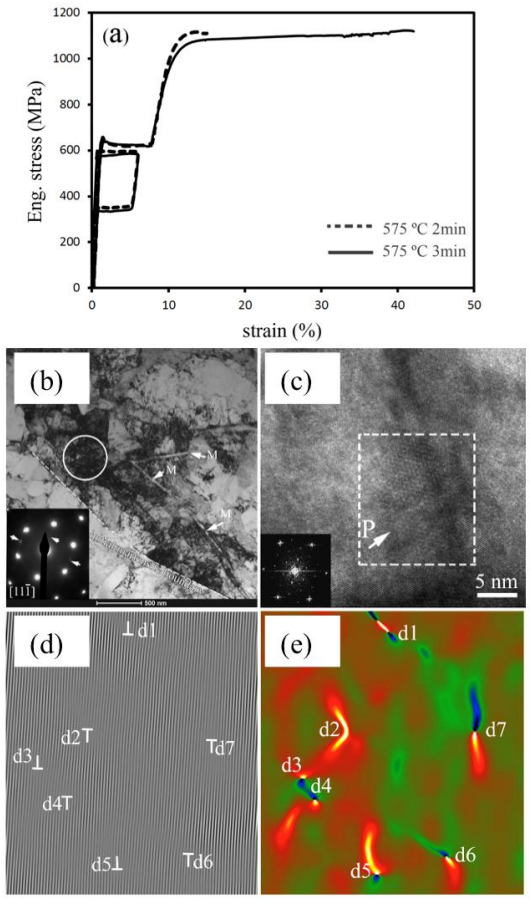

Figure 3: (a) The ductility of NiTi can vary drastically with subtle changes to heat treatments. (b-c) Ni4Ti3 precipitate structures, as imaged here along <111>B2 in a sample that underwent the 3 min heat treatment from (a), must be of a critical size to provide (d-e) Orowan looping to absolve dislocations about their interfaces, and commensurate ductility to the material, else the are sheared and re-dissolved into the matrix (not shown).

the 2 min heat treatment), they are sheared and dissolved back into the matrix as dislocations pass through the material. However, slight growth of the precipitates to ~ 8 to 10 nm prevents them from being sheared, and instead Orowan looping occurs about their interfaces (Figures 3d-e) and they accommodate great amounts of plasticity.

Future Plans

We will perform in situ and ex situ micro-Laue diffraction experiments this fall to more precisely (up to ~200 nm) map the sub-grain structures around the notches and cracks than presented in Figure 2. Concurrently, we will finish the analyses of the HEDM data for the monotonic failure and low cycle failure experiments, and complement the X-ray studies with post mortem electron microscopy techniques and micromechanical modeling. High resolution TEM, in particular, will be needed to examine fine twin structures toward completing our testing of Hypothesis 1. One major challenge toward testing our original hypotheses, which were all written around an assumption of ductile failure, has been the presence of oxides and carbides, which have incited brittle failure in all but samples also aged with Ni_4Ti_3 precipitate structures of critical dimensions to absolve significant amounts of plastic deformation. Thus we are also working on fabricating samples that allow us to complete the testing of our original hypotheses. However, interesting alternate hypotheses have arisen centered around the role of inclusions and coherent precipitates in transformations and failures of SMAs. These are resulting in publications about fatigue and failure mechanisms in the meantime.

References

[1] K. Bhattacharya, Microstructure of Martensite: Why it forms and how it gives rise to the shape-memory effect, Oxford University Press, 2003.

[2] S. W. Robertson, A. R. Pelton, R. O. Ritchie, Mechanical fatigue and fracture of Nitinol, International Materials Reviews 57 (1) (2012) 1–37.

[3] M. Rahim, J. Frenzel, M. Frotscher, J. Pfetzing-Micklich, R. Steegmuller, M. Wohlschlogel, H. Mughrabi, G. Eggeler. Impurity levels and fatigue lives of pseudoelastic NiTi shape memory alloys. Acta Mater 61 (2013) 3667-03686.

Publications

1. H.M. Paranjape, P.P. Paul, H. Sharma, D. Dale, P. Ko, Y.I. Chumlyakov, L.C. Brinson, A.P. Stebner "In-situ 3D Characterization of the Deformation Mechanics of Superelastic NiTi Shape Memory Alloy Oligocrystals Under Multiscale Constraint" submitted to *Acta Materialia*.
2. P.P Paul, H.M Paranjape, B. Amin-Ahmadi, A.P. Stebner, D.C. Dunand, L.C. Brinson "Effect of Machined Feature Size Relative to the Microstructural Size on the Superelastic Performance in Polycrystalline NiTi Shape Memory Alloys" In Revision with *Materials Science and Engineering A.*
3. B. Amin-Ahmadi, A. Shamimi, T.W. Duerig, Stebner, A.P. "Critical Ni4Ti3 Precipitate Structures for Ductility in Nickel-Titanium " submitted to *Scripta Materialia*.
4. B. Amin-Ahmadi, J.G. Pauza, A. Shamimi, T.W. Duerig, R.D. Noebe, Stebner, A.P. "Coherency Strains of H-Phase Precipitates and Their Influence on Functional Properties of Nickel-Titanium-Hafnium Shape Memory Alloys" submitted to *Scripta Materialia*.
5. H. M. Paranjape, P. P. Paul, H. Sharma, P. Kenesei, JS Park, T. W. Duerig, L. C. Brinson, A. P. Stebner (2017). Influences of granular constraints and surface effects on the heterogeneity of elastic, superelastic, and plastic responses of polycrystalline shape memory alloys. *Journal of the Mechanics and Physics of Solids* 102, pp 46-66.
6. A. N. Bucsek, H. M. Paranjape, A. P. Stebner (2016). Myths and Truths of Nitinol Mechanics: Elasticity and Tension-Compression Asymmetry. *Shape Memory and Superelasticity*. DOI 10.1007/s40830-016-0074-z.
7. P. Zhu, Z. Cui, M. S. Kesler, J. A. Newman, M. V. Manuel, M. C. Wright, L. C. Brinson (2016). Characterization and modeling of three-dimensional self-healing shape memory alloy-reinforced metal-matrix composites. *Mechanics of Materials* 103, pp 1-10.
8. A.P. Stebner, H.M. Paranjape, B. Clausen, L.C. Brinson, A.R. Pelton "In-situ Neutron Diffraction Studies of Large Monotonic Deformations of Superelastic Nitinol" 2015 *Shape Memory and Superelasticity* 1:252-267.
9. C. Bewerse, L.C. Brinson, D.C. Dunand (2016). Porous Shape-Memory NiTi-Nb with Microchannel Arrays. *Acta Materialia* 115, pp 83-93.

Crack Tip Mechanisms Driving Environmental Degradation

S.M. Bruemmer, D.K. Schreiber, C. Wang, M.L. Sushko
M.J. Olszta, K. Kruska, M.L. Sushko and K.M. Rosso

Pacific Northwest National Laboratory

Program Scope

Establishing the fundamental processes that control environmental degradation and crack propagation in hostile conditions represents a grand challenge and critical basic science need for current and future energy generating systems. Such linkages are historically elusive and incomplete, as evidenced by the decades-old debate concerning the mechanism(s) of stress corrosion cracking (SCC) in the high-temperature, corrosive environments found in nuclear reactors. In this research program, we leverage advances in site-specific, atomic-level, in-situ and ex-situ analytical microscopy techniques and multiscale mechanistic modeling to explicate the atomistic and molecular processes of material degradation at surfaces, grain boundaries and ultimately nanoscopic crack tips that precede macroscopic material failure.

The central thesis for this work is that common underpinning mechanisms at the atomic scale control the SCC response at the macroscale from high-temperature gaseous to low-temperature aqueous environments. These processes involve selective oxidation, vacancy injection and local composition changes along grain boundaries that cannot be adequately addressed by existing theories of environmental degradation. Our goal, therefore, is to isolate and clarify the roles of these interlinked atomistic phenomena through theory and observation, and develop a new understanding of grain boundary degradation that can be applied to predict and control SCC behavior. We pursue this understanding through three primary research directions:

i) Environment-Induced Degradation and Crack-Tip Nanostructures including quantitative crack-growth-rate testing under controlled environmental conditions and ex-situ characterization of grain boundary oxidation fronts and crack tips using analytical transmission electron microscopy (ATEM) and atom probe tomography (APT) to correlate local structure and chemistry at near-atomic resolution with macroscopic degradation response;

ii) In-Situ Measurement of Selective Oxidation including evaluation of oxide growth and vacancy injection during high-temperature gaseous and aqueous exposures by TEM and APT to interrogate dynamic processes that link to atomistic simulations and macroscale cracking;

iii) Mechanistic Modeling of Grain Boundary Oxidation that focuses on oxide and defect formation, atomistic diffusion, vacancy motion, and metal/oxygen/vacancy interactions at multiple length and time scales that occur at corrosion/oxidation fronts and crack tips.

Recent Progress

Current research has focused on developing a fundamental understanding of the behavior of model Ni-base binary alloys in oxidizing gaseous and aqueous environments, including:

- In-situ TEM oxidation experiments have identified the fundamental steps controlling surface oxidation for Ni-10Cr, Ni-20Cr and Ni-Al alloys in gaseous environments. [1-3]
- First-principles modeling of solute diffusion along grain boundaries has revealed remarkably different activation barriers for Cr and Al that help to explain experimental differences in the intergranular (IG) oxidation behavior. [4] This information has been combined with multiscale modeling to predict porosity formation during grain boundary oxidation in Ni-Cr and Ni-Al alloys. [5] In addition, Cr-O and Cr-S interactions have been modeled in Ni to evaluate the potential for internal IG sulfidation and oxidation. [6] Finally, atomistic modeling of vacancy-mediated diffusion across Cr_2O_3 has been performed examining how O moves through defects in the oxide. [7]
- The importance of creep deformation and grain boundary oxidation promoting IG crack growth in high-purity Ni, Ni-5Cu, Ni-5Fe, Ni-5Cr and Ni-4Al alloys has been elucidated from tests in high-temperature nitrogen gas and hydrogenated water environments. [8]

Our further discussion provide a more in-depth consideration of our new analyses of SCC crack-growth tests and related analytical observations on Ni-Cr alloys. [9] Crack growth response in hydrogenated water and nitrogen gas at temperatures between 300 and 360°C have shown that creep deformation, particularly at grain boundaries, is a dominant mechanism for IG cracking in our high-purity binary Ni-base alloys. [8] A significant change is observed as the alloy Cr concentration increased from 5 to 30 at% with the crack growth measured in nitrogen gas sharply decreasing as the solute content increases. Conversely, the maximum SCC crack growth rate in hydrogenated water is observed for the Ni-20Cr alloy, with lower propagation rates for alloys with either lower (Ni-10Cr and Ni-5Cr) or higher (Ni-30Cr) Cr concentrations. The 5–20 at% alloys exhibit IG attack during water exposures that is consistent with grain boundary selective oxidation of Cr promoting the environment enhanced crack growth. However, the controlling factor for the higher SCC susceptibility for the Ni-20Cr appears to be its matrix strength that creates an increased crack-tip stress intensity and strain rate leading to faster SCC growth. Further raising the bulk concentration of Cr to 30 at% produces the highest matrix strength, however no IG attack is observed along with the lowest SCC growth in hydrogenated water. This dichotomy results from the

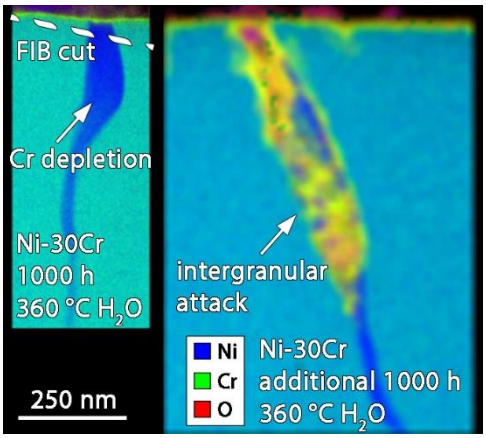

Fig 1. (left) STEM EDS of initial oxidation for Ni-30Cr. A thin, protective Cr_2O_3 film forms with a Cr depleted grain boundary. (right) Removing this oxide by FIB and re-exposing the sample results in intergranular attack. [12]

rapid formation of a continuous protective Cr_2O_3 film for Ni-30 Cr, [10] whereas lower Cr concentrations form non-protective, porous Cr oxides along the grain boundaries. [8,11] This is consistent with recent mesoscale modeling of the Cr-concentration dependence of the IG oxide porosity, wherein a porous oxide forms below 20 at% Cr and a compact oxide for Ni-30Cr. [5]

The formation of a protective oxide is a key aspect of the slip oxidation model for SCC which describes a dynamic process where crack growth occurs only after a protective oxide is broken and continues until the film reforms. For Ni-30Cr, observations of unstressed coupons have revealed formation of this protective film also results in a metallic grain boundary ahead that is severely depleted of Cr. [10] A key issue for SCC propagation is how this Cr-poor grain boundary reacts when the oxide film is broken; a unique "repassivation" experiment was devised to address this aspect. Employing a focused ion beam (FIB), the protective Cr_2O_3 film was removed from above the grain boundary to simulate breaking of the film during SCC. Exposure of the unprotected and Cr depleted grain boundary in hydrogenated water revealed rapid corrosion through the Cr-depleted region (Fig. 1). [12] At the edges of the original Cr-depleted zone, a protective oxide film again forms in conjunction with further Cr-depletion ahead. This experiment demonstrates that rupture of the protective film creates a finite, oxidized zone along the grain boundary which may partially explain IGSCC growth in Ni-30Cr alloys. Importantly, this mechanism is quite different from the lower Cr alloys where preferential grain boundary oxidation occurs continuously and is never inhibited by a protective oxide film.

Future Plans

We plan to extend our SCC testing, advanced in-situ and ex-situ microscopy and multiscale modeling into two new areas: the effect of common second phases in model alloys and direct interrogation of liquid/solid interfaces. We continue to seek insights into processes of selective oxidation, vacancy creation and injection, and atomic diffusion that are accelerated at grain boundaries, interfaces and crystalline defects to control environmental degradation and cracking.

Intergranular secondary phases present possibilities for beneficial and deleterious effects to SCC behavior. For example, while IG Cr carbides are known to impede crack initiation and slow crack growth in Ni-Cr alloys, a debate persists whether this benefit originates from changes in grain boundary corrosion/oxidation or mechanical interaction of the crack tip with the second phase. Experiments will continue in high-temperature water, steam and gas under controlled oxidizing conditions. Preliminary efforts to incorporate such heterogeneities into mesoscale models of grain boundary oxidation have already identified strong differences in elemental potentials as a result of IG precipitates, [13] which correlate with analytical observations in similar alloys. [14]

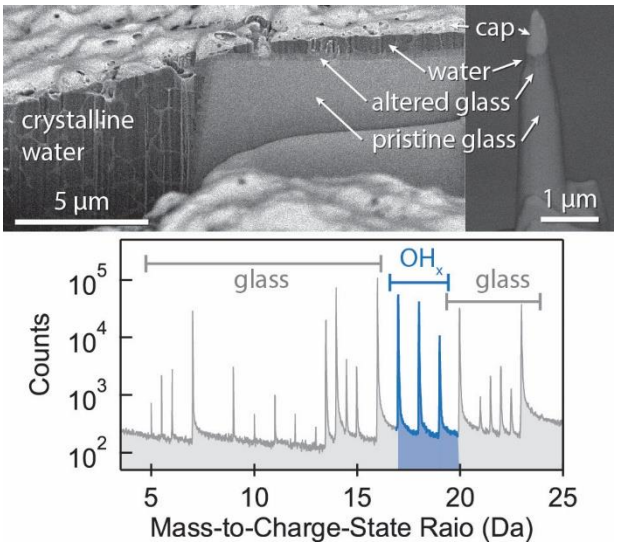

Fig 2. (top) Cryo-FIB/SEM images of APT specimen preparation at the (frozen) water/corroded glass interface. (bottom) Corresponding mass spectrum with the unique "water" peaks highlighted. [15, 16]

A concern when performing ex-situ, static observations of dynamic processes (e.g. oxidation and crack growth) is the alteration of key details when removing the sample from its test environment. In-situ techniques also suffer from degraded resolution or non-standard specimen geometries in comparison to ex-situ testing methods. An exciting new opportunity to bridge ex-situ and in-situ methods is site-specific cryogenic sample preparation. As part of a synergistic EFRC research project, PNNL has developed a novel cryo-FIB/APT specimen preparation and transfer system that is enabling the direct interrogation of (frozen) liquid/solid corrosion interfaces (Fig. 2). [15, 16] Although still in its infancy, this approach can uniquely and directly study corrosion phenomena at liquid/solid interfaces, including crack tips, in native corrosion environments. Our initial goals are to analyze "wet" corroded surfaces of model binary alloys, with the future goal of targeting crack tips for evidence of selective dissolution and hydroxide phases that are not apparent by conventional ex-situ microscopy analyses.

References

[1] C.M. Wang et al., *ACS Applied Materials & Interfaces*, 7 (2015) 17272-17277.
[2] L. Luo et al., *Scripta Materialia*, 114 (2016) 129-132.
[3] L. Luo et al., *Chemical Communications*, 52 (2016) 3300-3303.
[4] V. Alexandrov et al., *Journal of Physical Chemistry Letters*, 6 (2015) 1618-1623.
[5] M.L. Sushko et al., *The Journal of Chemical Physics*, 142 (2015) 214114.
[6] V. Alexandrov et al., *Corrosion Science*, 113 (2016) 26-30.
[7] B. Medasani et al., *Journal of Physical Chemistry C*, 121 (2017) 1817-1831.
[8] S. M. Bruemmer et al., manuscript in review, August 2017.
[9] S. M. Bruemmer et al., manuscript in preparation August 2017.
[10] M.J. Olszta et al., Proc. Corrosion 2014, NACE, San Antonio, Texas, USA, 2014, p. 4251.
[11] D.K. Schreiber et al., *Scripta Materialia*, 89 (2014) 41-44.
[12] K. Kruska et al., manuscript in preparation August 2017.
[13] M. Sushko et al., manuscript in preparation August 2017.
[14] D.K. Schreiber et al., Proc. 18th International Conference on Environmental Degradation of Materials in Nuclear Power Systems - Water Reactors, TMS, Portland, OR, USA, in press.
[15] D.E. Perea et al., *Advanced Structural and Chemical Imaging*, 3 (2017) 12.
[16] D.K. Schreiber et al., manuscript in preparation August 2017.

Publications (2015-Present)

Schreiber, D. K., M. J. Olszta, K. Kruska and S. M. Bruemmer (2017). “Role of Grain Boundary Cr_5B_3 Precipitates on Intergranular Attack in Alloy 600.” Proc. 18th International Conference on Environmental Degradation of Materials in Nuclear Power Systems - Water Reactors, The Minerals, Metals and Materials Society, in press.

Medasani, B., M. L. Sushko, K. M. Rosso, D. K. Schreiber and S. M. Bruemmer (2017). "Vacancies and vacancy-mediated self diffusion in Cr_2O_3: A first-principles study." *The Journal of Physical Chemistry C* 121(3): 1817-1831.

Zhai Z., M. B. Toloczko, M. J. Olszta and S. M. Bruemmer (2017). “Stress Corrosion Crack Initiation of Alloy 600 in PWR Primary Water.” *Corrosion Science* 123: 76-87.

K. Kruska, Z. Zhai and S. M. Bruemmer (2017). “Characterization of SCC Initiation Precursors in Cold-Worked Alloy 690.” Proc. Corrosion 2017, NACE International, Paper 9717.

Zhai Z., M. B. Toloczko, M. J. Olszta and S. M. Bruemmer (2017). “Precursor Evolution and SCC Initiation in Cold-Worked Alloy 690 in Simulated PWR Primary Water.” Proc. Corrosion 2017, NACE International, Paper 9475 and *Corrosion J.* 73-10: 1224-1236.

Alexandrov, V., M. L. Sushko, D. K. Schreiber, S. M. Bruemmer and K. M. Rosso (2016). "Adsorption and diffusion of atomic oxygen and sulfur at pristine and doped Ni surfaces with implications for stress corrosion cracking." *Corrosion Science* 113: 26-30.

Gault, B., D. W. Saxey, M. W. Ashton, S. B. Sinnott, A. N. Chiaramonti, M. P. Moody and D. K. Schreiber (2016). "Behavior of molecules and molecular ions near a field emitter." *New Journal of Physics* 18(3): 033031.

Kaspar, T. C., D. K. Schreiber, S. R. Spurgeon, M. E. McBriarty, G. M. Carroll, D. R. Gamelin and S. A. Chambers (2016). "Built-in potential in Fe_2O_3-Cr_2O_3 superlattices for improved photoexcited carrier separation." *Advanced Materials* 28(8): 1616-1622.

Liu, F., L. Huang, L. M. Porter, R. F. Davis and D. K. Schreiber (2016). "Analysis of compositional uniformity in AlxGa1−xN thin films using atom probe tomography and electron microscopy." *Journal of Vacuum Science & Technology A* 34(4): 041510.

Luo, L., L. Zou, D. K. Schreiber, D. R. Baer, S. M. Bruemmer, G. Zhou and C.-M. Wang (2016). "In-situ transmission electron microscopy study of surface oxidation for Ni–10Cr and Ni–20Cr alloys." *Scripta Materialia* 114: 129-132.

Luo, L., L. Zou, D. K. Schreiber, M. J. Olszta, D. R. Baer, S. M. Bruemmer, G. Zhou and C.-M. Wang (2016). "In situ atomic scale visualization of surface kinetics driven dynamics of oxide growth on a Ni-Cr surface." *Chemical Communications* 52(16): 3300-3303.

Alexandrov, V., M. L. Sushko, D. K. Schreiber, S. M. Bruemmer and K. M. Rosso (2015). "Ab initio modeling of bulk and intergranular diffusion in Ni Alloys." *Journal of Physical Chemistry Letters* 6(9): 1618-1623.

Santhanagopalan, D., D. K. Schreiber, D. E. Perea, R. L. Martens, Y. Janssen, P. Khalifah and Y. S. Meng (2015). "Effects of laser energy and wavelength on the analysis of $LiFePO_4$ using laser assisted atom probe tomography." *Ultramicroscopy* 148: 57-66.

Bruemmer S. M., M. J. Olszta, N. R. Overman and M. B. Toloczko (2015). “Cold Work Effects of Stress Corrosion Crack Growth in Alloy 690 Tubing and Plate Materials.” Proc. 17th International Conference on Environmental Degradation of Materials in Nuclear Power Systems - Water Reactors, Canadian Nuclear Society, Paper 8.

Zhai Z., M. J. Olszta, M. B. Toloczko and S. M. Bruemmer (2015). “Precursor Corrosion Damage and Stress Corrosion Crack Initiation in Alloy 600 During Exposure to PWR Primary Water.” Proc. 17th International Conference on Environmental Degradation of Materials in Nuclear Power Systems - Water Reactors, Canadian Nuclear Society, Paper 58.

Sushko, M. L., V. Alexandrov, D. K. Schreiber, K. M. Rosso and S. M. Bruemmer (2015). "Multiscale model of metal alloy oxidation at grain boundaries." *The Journal of Chemical Physics* 142(21): 214114.

Wang, C. M., D. K. Schreiber, M. J. Olszta, D. R. Baer and S. M. Bruemmer (2015). "Direct in-situ TEM observation of modification of oxidation by the injected vacancies for Ni-4Al alloy using a microfabricated nanopost." *ACS Applied Materials & Interfaces* 7(31): 17272-17277.

Xu, Z., D. Li, D. K. Schreiber, K. M. Rosso and S. M. Bruemmer (2015). "Modeling selective intergranular oxidation of binary alloys." *The Journal of Chemical Physics* 142(1): 014704.

Thermal Activation in Dislocation Dynamics of Face-Centered Cubic Metals

Wei Cai, Stanford University

Program Scope

Dislocation dynamics controls plastic deformation, mechanical strength, and failure of crystalline materials. It also governs fatigue resistance under cyclic loading, creep resistance at elevated-temperature, and radiation resistance for reactor applications. Thermally activated dislocation processes play a critical role in the strain hardening and dislocation patterning behavior of crystals, but are still not well understood. Cross slip and removal of Lomer-Cottrell (LC) junctions are two important thermally activated processes in pure Face-Centered Cubic (FCC) metals. Many fundamental questions regarding these processes still remain open, and our proposed research seeks to provide answers. This project will use dislocation dynamics (DD) simulations and atomistic simulations with advanced sampling techniques to determine the fundamental mechanisms of cross slip and LC junction removal processes and their consequence on strain hardening.

Recent Progress

Over the last two years, we have made significant progress in advancing the capability of dislocation dynamics (DD) simulations of work hardening of single crystals. A sub-cycling integrator has been developed that significantly extends the time step allowed in the DD simulation, allowing us to probe larger plastic strains. More recently, the sub-cycling integrator is implemented on GPUs to overcome the difficult of combining sub-cycling integration with parallel computing. This results in a 20x speed up compared with serial CPU implementation.

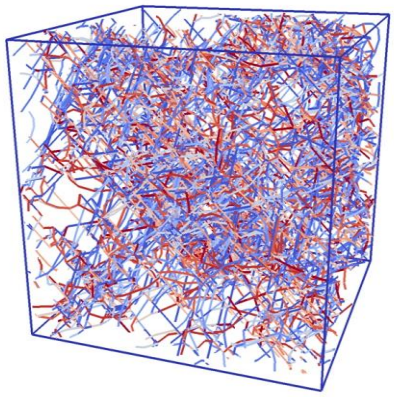

Figure 1. Dislocation structure predicted by large scale DD simulations of single crystal Cu deformed along the [001] axis.

The new DD capability allows us to make discoveries on the nature of dislocation microstructure (Fig.1) and the origin of strain hardening. We found that junction formation between dislocations on different slip planes is not only essential for strain hardening, but also leads to an exponential distribution of the dislocation line lengths between junction pinning points. The exponential length distribution is parameterized by two variables: the total dislocation density ρ, and the nondimensional parameter $\varphi \equiv N^2/\rho^3$, where N is the number of dislocation lines per unit volume. We develop a simple model describing the evolution of a population of dislocation lines, and by using parameters extracted directly from DDD simulations are able to explain both the exponential distribution and the observed hardening rate. We then further examine the relationship between junctions and hardening by conducting specialized DDD simulations where we are able to

prevent specific junction types from forming. We find that among the four types of junctions in FCC crystals, glissile junctions make the dominant contribution to the strain hardening rate.

The ability to generate large dislocation microstructures during strain hardening also provides us new ways to compare theory and simulations with experiments. We are now able to compute virtual X-ray diffraction patterns from the complex dislocation microstructures of DD that can be compared with micro-Laue experiments [1]. X-ray diffraction measurements has the advantage of being a non-destructive method, and has been shown to provide a rich set of information of the microstructure during deformation, including elastic strains, lattice rotations in individual grains. We have developed a method to compute virtual X-ray diffraction patterns based on the non-singular formulation of dislocation fields. The preliminary results show peak broadening, streaking during deformation, as was reported in experiments.

Future Plans

We plan to incorporate the dislocation cross slip rate model constructed based on atomistic simulations into our DD model and use it to predict the effect of thermally activated processes on the temperature/strain rate effects on strain hardening. We will also perform molecular dynamics (MD) simulations of cross slip to reveal any finite temperature effects possibly missed by zero-temperature energy barrier calculations.

We will also test several ideas that can potentially extend the strain range of our DD simulations even further (potentially to 5% or even 10%). These include the possibility of detecting (and perhaps coarse-graining or removing) dense dislocation tangles that develop during plastic deformation but become too costly to handle in a DD simulation.

We also plan to continue our investigation on the geometrical/topological features of the dislocation network predicted by the DD simulations. The goal is identify important coarse-grained variables that can be used to construct continuum theory of strain hardening, as well as to be able to generate statistically representative dislocation microstructures at large strain (without always having to perform DD simulations starting from zero strain).

References

1. H. Van Swygenhoven and S. Van Petegem, The use of Laue microdiffraction to study small-scale plasticity, JOM, 12, 36-43 (2010).

Publications

1. I*ll* Ryu, W. Cai, W. D. Nix, H. Gao, Stochastic behaviors in plastic deformation of face-centered cubic micropillars governed by surface nucleation and truncated source operation, *Acta. Mater.* 95, 176 (2015).

2. I*ll* Ryu, W. Cai, W. D. Nix, H. Gao, Anisotropic size-dependent plasticity in face-centered cubic micropillars under torsion, JOM 68, 253-260 (2015).

3. Ryan Sills and Wei Cai, Solute Drag on Perfect and Extended Dislocations, *Philos. Mag.* 96, 895 (2016).

4. Ryan Sills, Amin Aghaei, and Wei Cai, Advanced Time Integration Algorithms for Dislocation Dynamics Simulations of Work Hardening, *Model. Simul. Mater. Sci. Eng.*, 24, 045019 (2016).

5. Edgar J. L. Borda, Wei Cai, and Maurice de Koning, Dislocation structure and mobility in hcp ^{4}He, *Phys. Rev. Lett.* 117, 045301 (2016).

6. Seunghwa Ryu and Wei Cai, Stability of Eshelby Dislocations in FCC Crystalline Nanowires, *International Journal of Plasticity*, 86, 26 (2016).

7. Ya Gai, Chia Min Leong, Wei Cai, and Sindy K. Y. Tang, Spatiotemporal periodicity of dislocation dynamics in a two-dimensional microfluidic crystal flowing in a tapered channel, *Proc. Natl. Acad. Sci.* 113, 12082 (2016).

8.Wei Cai and William D. Nix, Imperfections in Crystalline Solids, Cambridge University Press, 2016.

9.Ryan Sills, William Kuykendall, Amin Aghaei and Wei Cai, Fundamentals of Dislocation Dynamics Simulations, in Christopher R. Weinberger and Garritt J. Tucker (Eds.), Multiscale Materials Modeling for Nanomechanics, Springer, 2016.

Role of Grain Boundaries in Polycrystalline Deformation

Prof. Michael D. Sangid, Purdue University
Prof. Sam Daly, University of California at Santa Barbara

Program Scope

Polycrystalline deformation is a complex process that has yet to be fully understood. The important deformation mechanisms in a polycrystalline material include slip within grains, transfer of slip across grains, twinning, and grain boundary sliding. However, little is known about the interactions between these mechanisms during plastic deformation. While these deformation mechanisms have been studied individually, the coupling between them has not received much attention, especially at mesoscale. Studying whether these mechanisms are competitive or cooperative is imperative to a better understanding of polycrystalline deformation.

Grain boundaries (GBs) dictate the mechanical response during polycrystalline deformation, by providing a strengthening mechanism as a barrier to dislocation motion. GBs also emit dislocations and allow for relative motion of adjacent grains along their plane. Grain boundary sliding (GBS) becomes significant in nanocrystalline materials and in bulk materials during creep, deformation at high temperatures, and superplastic deformation. Conventionally, crystal plasticity frameworks do not include an explicit description of grain boundaries, or of GBS as a deformation mechanism. Using a combined computational and experimental approach, we aim to include an explicit description of grain boundary elements inside a finite element framework, as well as additional degrees of freedom to account for deformation mechanisms active at grain boundaries, such as GBS. The inclusion of additional degrees of freedom allow for the incorporation of a description of the physics of dislocation-GB interaction into the modeling framework.

Recent Progress

On the modeling front, a framework has been developed to incorporate grain boundary deformation mechanisms, in the form of tuning barriers to slip and grain boundary sliding, within a crystal plasticity finite element model. On the experimental front, the focus has been to achieve high-resolution, wide-area deformation maps, and underlying crystallography maps of test specimens of an idealized model material of columnar, high purity 99.99% aluminum, to identify the underpinning physics of slip-GB and GBS mechanism and to inform modeling efforts.

Overview of Experiments

An experimental procedure was created to produce high-resolution deformation maps on columnar specimens of 99.99% aluminum, in order to provide a unique data set for the crystal plasticity modeling described herein. These experiments are capable of resolving slip traces inside of grain across areas as large as 5 mm x 1 mm. Creating an approach to map deformations

that are sufficiently high resolution to capture slip and grain boundary sliding, but encompass mm-scale field of views (FOVs), on a model system of high-purity (99.99%) columnar aluminum, proved challenging in numerous aspects. In brief, specimens are fabricated in-house by electro-discharge machining with gage dimensions of 5 mm x 1 mm x *t* mm, with thickness *t* ranging from 0.15 - 0.5 mm and annealed. The specimens are then mounted by a custom vacuum setup (due to their sensitivity to plastic deformation), mechanically polished, and chemically patterned with 300 nm nanoparticles for deformation tracking, following which they are tested in-SEM under uniaxial tension. Micrograph-capture has been automated to achieve higher-resolution testing in tractable time frames, and custom codes have been written to stitch the numerous resultant EBSD and DIC fields by calculating cross-coefficients between adjacent image subsets. An example of the resulting EBSD and strain (ε_{xx}) fields across the gage section are shown in Figure 1.

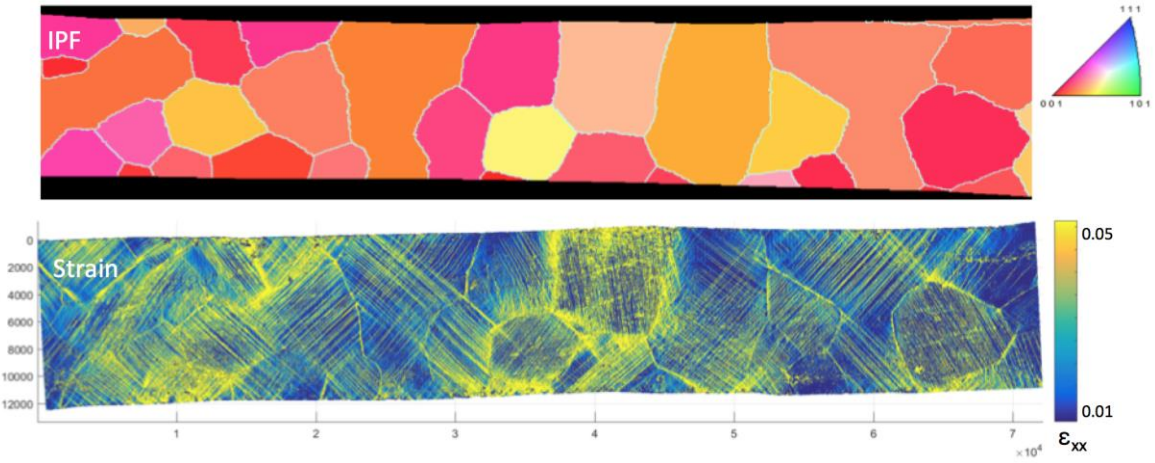

Figure 1: EBSD (top) and SEM-DIC (bottom) data of a 99.99% Al oligocrystalline specimen (FOV approx. 5 mm x 1 mm)

Overview of Modeling

The crystal plasticity model is generated based on the aforementioned DIC experiment. First, a virtual instantiation of the characterized microstructure is developed, where the 3D columnar microstructure is generated from the 2D EBSD scan. The GB normal vectors are determined based on an in-house code, which enables a complete description of the GB with respect to its 5 degrees of freedom. This description of the GB is used to (i) specify the possible plane and directions for GB sliding and (ii) calculate the interfacial energy. The existence of a functional form for the GB energy was first postulated in [1], and was more recently found in [2]. The individual GB energy is determined for each GB characterized within the specimen. Further, based on prior experimental and atomistic simulation studies [3, 4], the GB energy dictates the barriers to slip transmission and GB sliding. Thus, the GB energy is used to determine the strength of each individual GB within the microstructure. Within the finite element model, a mesh is generated explicitly relative to the microstructural features and the GB mantle

and grain cores are defined, such that the strength of the GB is determined based on its GB energy and the additional deformation modes are added to accommodate GB sliding. The framework is shown in Fig. 2.

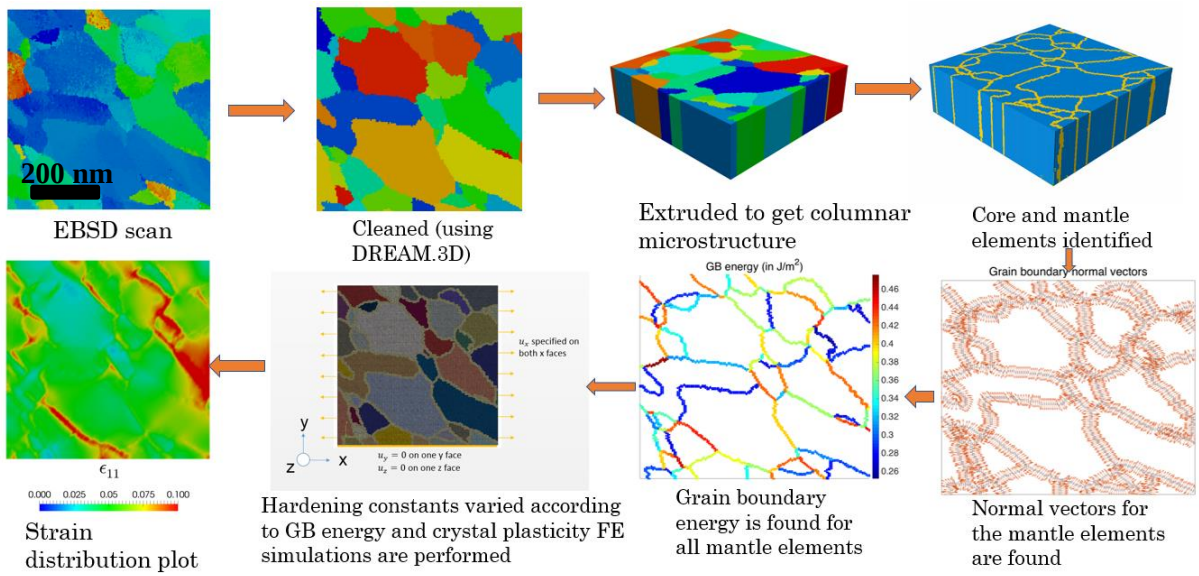

Figure 2: Overview of the modeling framework.

Additionally, the modeling framework has been extended to include temperature and irradiation effects, as experimental characterization will also be conducted at elevated temperatures and on irradiated materials. Specifically, the Kocks-Mecking type hardening equations for crystal plasticity have been selected such that it is inherently temperature dependent. The formulation is adopted based on thermodynamic activation of dislocation segments to promote slip [5], and is modified to include a GB energy term. As shown in Fig 3, the strength of the GB is adjusted based on its interfacial energy and is also artificially, uniformly hardened/softened for demonstration purposes. Based on the results of the experiment, each GB will be tuned to account for the underpinning physics and propensity for coupled slip and GB sliding events. Lastly, an extra term is included in the hardening equation to account for the presence of stacking fault tetrahedra for the irradiated material [6].

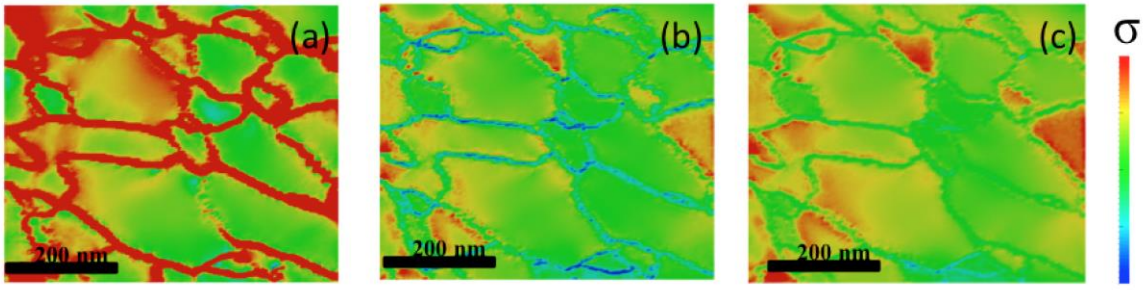

Figure 3: Preliminary model framework results, where the GB strength is (a) uniformly hard, (b) uniformly soft, and (c) adjusted based on individual GB interfacial energy.

Future Plans

In the upcoming months, the focus of this research will be to calibrate the crystal plasticity (CP) model from the experiments currently underway. The CP parameters for crystallographic slip will be calibrated to match the macroscopic stress-strain curves. Afterwards, GBS will be characterized from the DIC experiments and correlations between GB types (i.e. the interfacial energy) and the magnitude of sliding will be determined and used to inform the crystal plasticity parameter selection for the GBS mechanism. A metric for comparison between the strain predicted by the CP model and measured from the experiment is determined based on the spatial summation of error. Regions of high discrepancy, especially near GBs, will be further examined to identify complimentary or competitive deformation modes between crystallographic slip and grain boundary sliding, which will be used to refine the constitutive equations of the CP model. Future experiments will be run at both room temperature and elevated temperatures (~0.5 T_m) in order to activate varied degrees of grain boundary sliding, and to provide multiple specimen datasets under each testing condition. New automated micrograph capture codes will be used to further refine the spatial resolution of the displacement measurements while maintaining the mm-scale coverage of the displacement maps.

References

[1] D. L. Olmsted, S. M. Foiles, and E. A. Holm, "Survey of computed grain boundary properties in face-centered cubic metals: I. Grain boundary energy," *Acta Mater.*, vol. 57, no. 13, pp. 3694–3703, 2009.

[2] V. V. Bulatov, B. W. Reed, and M. Kumar, "Grain boundary energy function for fcc metals," *Acta Mater.*, vol. 65, pp. 161–175, 2014.

[3] M. D. Sangid, T. Ezaz, H. Sehitoglu, and I. M. Robertson, "Energy of slip transmission and nucleation at grain boundaries," *Acta Mater.*, vol. 59, no. 1, pp. 283–296, 2011.

[4] S. Namilae, N. Chandra, and T. G. Nieh, "Atomistic simulation of grain boundary sliding in pure and magnesium doped aluminum bicrystals," *Scr. Mater.*, vol. 46, no. 1, pp. 49–54, 2002.

[5] I. J. Beyerlein and C. N. Tome, "A dislocation-based constitutive law for pure Zr including temperature effects," *Int. J. Plast.*, vol. 24, no. 5, pp. 867–895, 2008.

[6] N. R. Barton, A. Arsenlis, and J. Marian, "A polycrystal plasticity model of strain localization in irradiated iron," *J. Mech. Phys. Solids*, vol. 61, no. 2, pp. 341–351, 2013.

Publications

Publications are underway.

Molecular Design of Hybrid Films with Unusual Mechanical Properties

Professor Reinhold H. Dauskardt
Department of Materials Science and Engineering, Stanford University
Stanford, CA 94305 – 4034, Email: dauskardt@stanford.edu

Program Scope

Our research is focused on fundamental studies related to the molecular design, synthesis, characterization and modeling of molecular-reinforced hybrid glass films for superior mechanical and fracture properties. Molecular-reinforced hybrid glass films exhibit unique electro-optical properties while maintaining excellent thermal stability. They have important technological application for emerging nanoscience and energy technologies including anti-reflective and ultra-barrier layers in photovoltaics and display technologies. However, they are often inherently brittle in nature, do not adhere well to adjacent substrates, and exhibit poor mechanical properties.

Our research brings together a unique combination of internationally recognized thin-film processing and mechanical characterization capabilities coupled with computational modeling that we have pioneered to study hybrid films. Composition and molecular structure are characterized using high resolution X-ray, electron, optical and nuclear spectroscopy. Mechanical properties are studied using acoustic, nanoindentation, force modulated AFM, and thin-film adhesion and cohesion techniques we have pioneered for thin-film structures. We leverage computational modeling capabilities that allow us to understand the complex molecular structure, free volume, cohesive and elastic properties of hybrid molecular materials. This has enabled the molecular design, synthesis, characterization and modeling of hybrid films for superior mechanical and fracture properties.

Recent Progress

Terminal Groups and Elastic Asymmetries: Due to the presence of terminal groups that limit network connectivity, we found that hybrid molecular materials can have a marked asymmetric elastic modulus[1] (wherein the compressive, E_C, and tensile, E_T, moduli are different), which has significant implications for thermomechanical reliability[2] and can ultimately limit their integration into emerging nanotechnologies including dielectrics in microelectronics, antireflective (AR) coatings, protective coatings in flexible electronics, and molecular sieves for biosensing.[3–7] Hybrid materials may contain a range of network terminations that vary in molecular weight and size. These terminal groups affect the material's density, which controls their interaction distance and thus may also affect the resulting elastic asymmetries.

We explored a range of terminal groups (OH, methyl, vinyl, and phenyl) using a consistent molecular architecture to study their effects on the elastic asymmetries. Since the hybrid material density decreases with increasing terminal group size, it was expected that molecular architectures with large terminal groups should result in reduced elastic asymmetries. Contrary to this expectation, we show that hybrid molecular materials with large terminal groups are dense enough to allow significant steric interactions, and, as a result, we show that increasing the terminal group size actually increases the degree of elastic asymmetry even further (**Fig. 1**). Thus, we develop a new design principle that connects more complex terminal groups in the underlying molecular architecture with asymmetric elastic behavior.

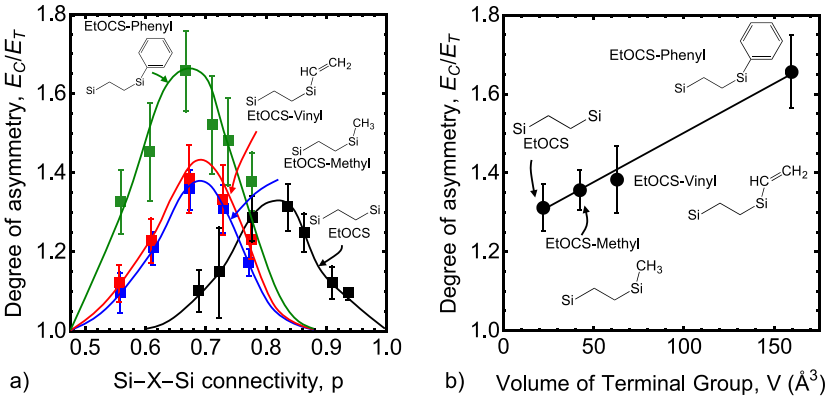

Figure 1: (**a**) The degree of elastic asymmetry, E_C / E_T, as a function of network connectivity, *p*, for the Et-OCS, Et-OCS-methyl, Et-OCS-vinyl, and Et-OCS-phenyl models. (**b**) The maximum degree of elastic asymmetry, E_C / E_T, with respect to the volume of the terminal group in each molecular model: OH (Et-OCS), methyl (Et-OCS-methyl), vinyl (Et-OCS-vinyl), and phenyl (Et-OCS-phenyl).

We explored the effects of porosity on elastic asymmetries and found that terminal groups preferentially situate at internal pore surfaces (**Fig. 2a**). Thus, there is a reduction in the average terminal group cluster size and the number of possible steric interactions, reducing the degree of elastic asymmetry. Porosity can be thought of as increasing the average distance between terminal groups. As a result, increasing volume percentage porosity

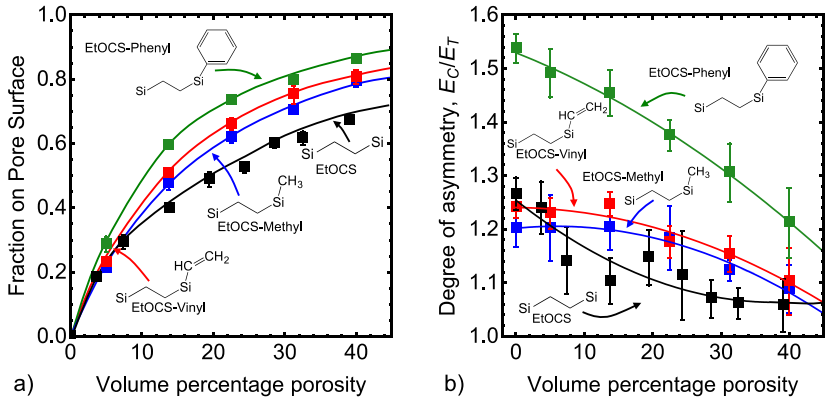

Figure 2: (**a**) The terminal groups for each molecular model (Et-OCS, Et-OCS-methyl, Et-OCS-vinyl, and Et-OCS-phenyl) increasingly situate at internal pore surfaces for increasing volume percentage porosity. (**b**) The degree of elastic asymmetry, E_C / E_T, as a function of the volume percentage porosity.

decreases the degree of elastic asymmetry, E_C / E_T, for each model network (**Fig. 2b**).

Hyperconnected Network Architectures: Designing hybrid glasses to maintain high levels of mechanical strength and stiffness remains a significant challenge that can ultimately limit the integration of these materials into emerging nanotechnologies.

To address this challenge, we exploited the fundamental dependence of the elastic properties on network connectivity by developing a hyperconnected network architecture, wherein the connectivity of a silicon atom within the network extends beyond its chemical coordination number, resulting in exceptional mechanical properties. The concept of silicon network hyperconnectivity is illustrated in **Fig. 3a**,**b** where the potential silicon network connectivity of a silicon atom in an ethylene-bridged glass and a trifunctional 1,3,5-benzene-bridged glass are shown. In glasses with only linear bridges between silicon atoms (e.g. oxygen or ethylene), each silicon atom can connect to a maximum of four nearest silicon neighbors. However, the structure of the 1,3,5-benzene precursor is such that each silicon atom in these networks can potentially connect to five other nearest silicon neighbors: the benzene ring in the 1,3,5-benzene structure connects each silicon atom to two others via carbon bridges, while maintaining the ability of a silicon atom to connect with three others via Si-O-Si bonds. Compared to linearly bridged glass models (methylene, ethylene, 1,4-benzene, 1,3-benzene), the hyperconnected 1,3,5-benzene exhibits exceptionally high stiffness at a density similar to the methylene-bridged material (**Fig. 3c**). Surprisingly, the 1,3,5-benzene glass has a higher modulus but a significantly lower density than amorphous SiO_2.[8–10]

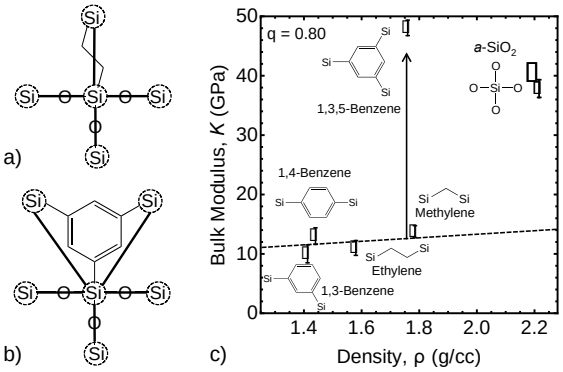

Figure 3: Fully condensed silicon atoms have network connectives of $m_{Si} = 4$ and $m_{Si} = 5$ for (**a**) ethylene-bridged glasses and (**b**) 1,3,5-benzene glasses, respectively. (**c**) The predicted bulk modulus, K, as a function of the predicted mass density, ρ, for model organosilicate glasses with various organic bridges. The experimental[8–10] (open square) and simulated values for amorphous SiO_2 are shown for comparison.

While nanoporosity is an important structural parameter that controls materials properties such as the dielectric constant, it severely degrade the mechanical properties (**Fig. 4a**). However, hyperconnected network architectures significantly enhance the modulus of nanoporous glasses compared to a state-of-the-art nanoporous ethylene-bridged glass (**Fig. 4b**).

Future Plans

We will continue our research to develop hybrid films with improved mechanical and fracture properties. Specifically, we will continue to pioneer molecular design criteria to control the mechanical properties. By leveraging our atmospheric plasma deposition capabilities, we will synthesize hybrid materials with controlled molecular architectures (including a range of terminal groups) to further calibrate our computational models and develop hybrids with well-controlled degrees of elastic asymmetry and exceptional mechanical properties. Furthermore, using our computational tools, we will study the role of bridging in hybrids to build a robust connection between molecular structure and network connectivity with the resulting mechanical properties.

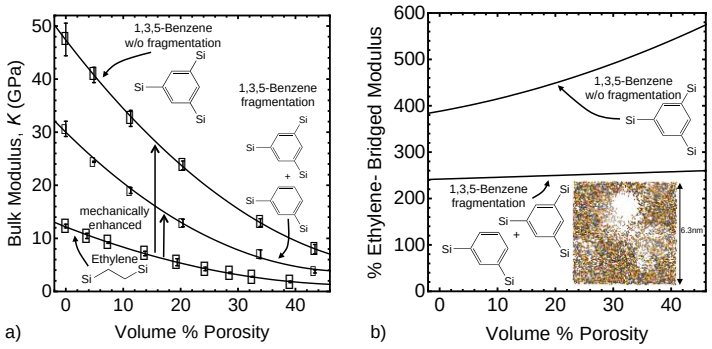

Figure 4: (**a**) The bulk moduli of pure ethylene-bridged, pure 1,3,5-benezne-bridged, and fragmented 1,3,5-benzene-bridged model glasses are plotted against the volume % porosity. (**b**) The moduli of the pure 1,3,5-benzene and fragmented 1,3,5-benzene glasses are shown as the percentage of the ethylene-bridged modulus as a function of volume % porosity.

References

1. Burg, J. A. & Dauskardt, R. H. Elastic and thermal expansion asymmetry in dense molecular materials. *Nature Mater.* **15,** 974–980 (2016).
2. Burg, J. A. & Dauskardt, R. H. Thermomechanical asymmetries in ULK dielectric glasses. in *IEEE Interconnect Technology Conference (IITC/AMC)* 95–97 (2016).
3. Volksen, W., Miller, R. D. & Dubois, G. Low dielectric constant materials. *Chem. Rev.* **110,** 56–110 (2009).
4. Volksen, W., Lionti, K., Magbitang, T. & Dubois, G. Hybrid low dielectric constant thin films for microelectronics. *Scr. Mater.* **74,** 19–24 (2014).
5. Hiller, J. A., Mendelsohn, J. D. & Rubner, M. F. Reversibly erasable nanoporous anti-reflection coatings from polyelectrolyte multilayers. *Nat. Mater.* **1,** 59–63 (2002).
6. Kresge, C. T., Leonowicz, M. E., Roth, W. J., Vartuli, J. C. & Beck, J. S. Ordered mesoporous molecular sieves synthesized by a liquid-crystal template mechanism. *Nature* **359,** 710–712 (1992).
7. Dong, S., Zhao, Z. & Dauskardt, R. H. Dual Precursor Atmospheric Plasma Deposition of Transparent Bilayer Protective Coatings on Plastics. *ACS Appl. Mater. Interfaces* **7,** 17929–17934 (2015).
8. Haynes, W. . *CRC handbook of chemistry and physics*. (CRC press, 2014).
9. Tsou, C., Huang, Y. S., Li, H. C. & Lai, T. H. Determination of thermal expansion coefficient of thermal oxide. *Sensors Mater* **17,** 441–451 (2005).
10. Tsai, H. C. & Fang, W. Determining the Poisson's ratio of thin film materials using resonant method. *Sensors Actuators A Phys.* **103,** 377–383 (2003).

Recent Publications

In press:

1. Joseph A. Burg and Reinhold H Dauskardt, "The Effects of Terminal Groups on Elastic Asymmetries in Hybrid Molecular Materials," **Journal of Physical Chemistry B**, 2017.
2. Joseph A. Burg, Mark S. Oliver, Geraud Dubois, and Reinhold H. Dauskardt, "Hyperconnected Molecular Glass Network Architectures with Exceptional Elastic Properties," **Nature Communications**, 2017.

Published:

3. Siming Dong, Jiahao Han, Zhenlin Zhao and Reinhold H. Dauskardt "Role of Carbon Bridge Length of Organosilicate Precursors on the Atmospheric Plasma Deposition of Transparent Bilayer Protective Coatings on Plastics," **Plasma Processes and Polymers**, 13, 1053–1060, 2016.
4. Joseph Burg and Reinhold H. Dauskardt "Elastic and Thermal Expansion Asymmetry in Dense Molecular Materials" **Nature Materials**, 15 (9), 974-980, 2016.
5. Linying Cui, Geraud Dubois, and Reinhold H. Dauskardt, "Carbon-Bridge Incorporation in Organosilicate Coatings Using Oxidative Atmospheric Plasma Deposition," **ACS Applied Materials & Interfaces**, 8 (2), 1309-1318, 2016.
6. S. Dong, Z. Zhao, R.H. Dauskardt, "Dual Precursor Atmospheric Plasma Deposition of Transparent Bilayer Protective Coatings on Plastics," **ACS Applied Materials & Interfaces**, 2015, 7 (32), pp 17929-17934, 2015.

Self-organized dislocation structures in metals

Anter El-Azab, School of Materials Engineering, Purdue University

Program Scope

This research started in August 2017; it aims to provide a first-principles understanding of the collective dislocation dynamics that lead to dislocation patterning in deforming face centered cubic metals. Of primary interest are the early stages of pattern formation. The fundamental role of spatial and temporal dislocation correlations in dislocation self-organization and in the collective dislocation mobility, short range reactions and cross slip under deformation will be investigated using theory and computations within the recently developed Continuum Dislocation Dynamics (CDD) framework [1]. The enhanced CDD model will be used to predict the ubiquitous patterning of dislocations in Cu, Al and Ni, as a function of deformation strain rate, temperature, and crystallographic orientation. To capture the underlying science of deformation mechanisms on mesoscopic length scales and provide for direct comparisons with deformation measurements, continuum dislocation dynamics simulations will be extended to volumes on the order of 15μm – 25μm on edge and strains up to 5%. These simulations will provide a new level of predictions for comparison with *in situ* and *ex situ* Transmission Electron Microscopy (TEM), Electron Backscattering Diffraction (EBSD), and direct and absolute model validation with 3D Dark Field X-Ray Microscopy (DFXM) and both polychromatic and scanning-monochromatic 3D X-Ray Microscopy (3DXM) experiments using focused synchrotron x-ray beams. The roles of spatial and temporal correlations on the collective dynamics of dislocations will be tested quantitatively by isolating the effects of the collective mechanisms influenced by the correlations, and checking whether they yield results more agreeable with experiments. Open literature TEM data as well as DFXM and 3DXM deformation data provided by collaborators will be used for this purpose. The associated constitutive closure for the CDD framework will be achieved using large scale Discrete Dislocation Dynamics (DDD) simulations and stochastic modeling.

Recent Progress

A detailed plan for year 1 research has been put together. The PI is currently making interviews with the incoming students to identify those who will join this research by mid-August.

Future Plans

The overall research is divided into four areas:

- First principles based bottom-up (re)formulation of the continuum dislocation dynamics to integrate the dislocation correlations, collective dislocation mobility, and short range reactions into the CDD model equations.
- Simulation of temporal and spatial dislocation correlations combined with modeling of the collective mobility of dislocations and their short-range reaction rates to establish closure of the CDD model equations.
- Computational implementation of the updated CDD model equations into a Finite Element Method (FEM) code.
- Investigation of dislocation patterning and the scaling of dislocation microstructure and its dependence on crystal orientation and temperature, and the impact on hardening. Model validation using 3DXM, DFXM, and TEM generated deformation microstructure measurements, as well as data from the open literature on stress-strain behavior of Cu, Al and Ni.

Year 1 of the effort will focus on the theoretical development of continuum dislocation dynamics, the dislocation correlations, and collective dislocation mobility. Large scale discrete dislocation dynamics simulations to collect relevant data for constitutive closure of CDD equations will be started.

References

[1] S. Xia, J Belak, and A. El-Azab, The discrete-continuum connection in dislocation dynamics: I. Time coarse graining of cross slip, Modelling and Simulation in Materials Science and Engineering, 24 (2016) 075007.

Publications

No publications from this project yet.

Fundamental Mechanisms Controlling Dislocation-Obstacle Interactions in Metals and Alloys

[*]David T. Fullwood, [*]Eric R. Homer and [+]Robert H. Wagoner

[*]Mechanical Engineering Department, Brigham Young University, Provo UT 84602, USA, dfullwood@byu.edu
[+]Department of Material Science and Engineering, Ohio State University, 2041 College Rd, Columbus OH 43210, USA

Program Scope

Despite various advances in modeling the behavior of dislocations at the meso-scale, the accurate prediction of bulk dislocation evolution at the sub-grain level remains a challenge. One particular approach – the super-dislocation, or SD model – accounts for elastic forces between populations of dislocations, and has enjoyed various successes in terms of predicting macroscopic material behavior. These accomplishments include prediction of the Hall Petch and Bauschinger effects and the elastic-plastic transition.

This project seeks to test the hypothesis that bulk (meso-scale) grain boundary / dislocation interactions can be predicted using simple geometrical considerations of the relevant slip systems, and/or other local microstructural characteristics. The hypothesis is explored via a combined modeling and experimental approach.

Various potential definitions of transmissivity factor, or obstacle stress, are incorporated into the SD model for prediction geometrically necessary dislocation (GND) content in polycrystals under various strain conditions. Cross-correlation EBSD is used to map actual GND content in order to compare simulated predictions with experimental measurements. The study focuses particularly on grain boundaries, where GND buildup often occurs.

Furthermore, MD simulations of dislocation / GB interactions across a wide number of GB types are used to inform the selection of transmissivity factor, and test the hypothesis at the atomistic and nano-level.

Recent Progress

Details from various central and peripheral findings of earlier stages of this project can be found in the 'Publications' section at the end. This abstract focuses mainly on unpublished results, along with a brief summary of the most recent macro-level achievements of the SD model. Figure 1. illustrates SD-prediction of the detailed form of the Bauschinger effect (i.e. including not only yield, but post-reversal strain hardening) as a function of aging in Al-Ge-Si alloys [1]. In Fig. 1, γ is a measure of

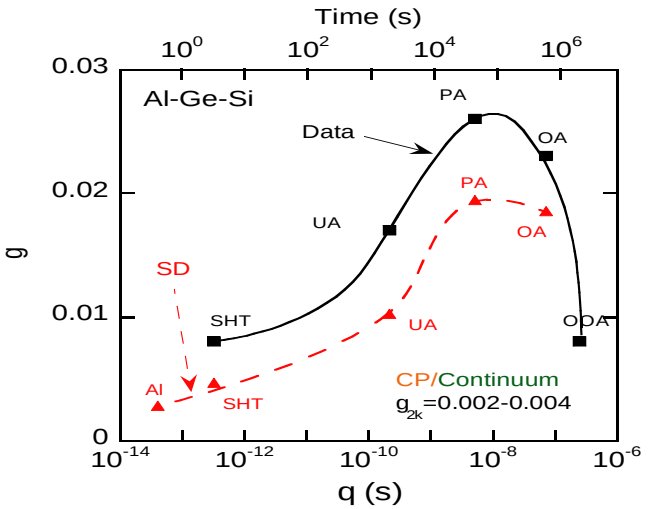

Fig. 1. Predicted and measured transition strain range (γ) following stress reversal for aged Al alloy. CP predicts negligible transition strains.

the transition strain range after reversal. This paper demonstrates the successful implementation of the inter-dislocation and dislocation / obstacle elastic interactions via the SD model, applied to nano-sized microstructures with both grain and phase boundaries controlling the macro properties.

At the other practical extreme of length scale, the SD model predicted the behavior of composite-like DP steel [2]. Figure 2 shows SD predictions and experiments from the literature for the nonlinearity of nominally elastic deformation. The results also show the effect of varying obstacle strength on the simulations, corresponding approximately to various obstacle mechanisms. (Note the red and purple curves corresponding to two obstacle strength scaling magnitudes.)

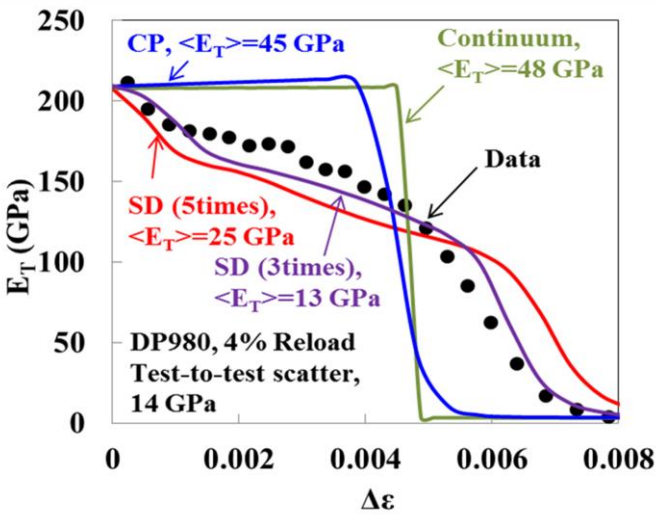

Fig. 2. Modulus change predicted by SD for nominally elastic unloading and reverse loading, compared with parallel standard

In order to test the model assumption and performance at the micro-scale, three Ta oligocrystals, with approximately columnar grains, were pulled in tension to a sufficient strain level to observe dislocation build-up at various grain boundaries. The GND measurements from cross-correlation EBSD were then compared with predictions of GND content using a standard crystal plasticity finite element model (CPFEM), and using the SD model (the same base CPFEM model, but with elastic interactions between sets of dislocations, and between sets of dislocations and GBs, accounted for). The results are shown pictorially in Fig. 3.

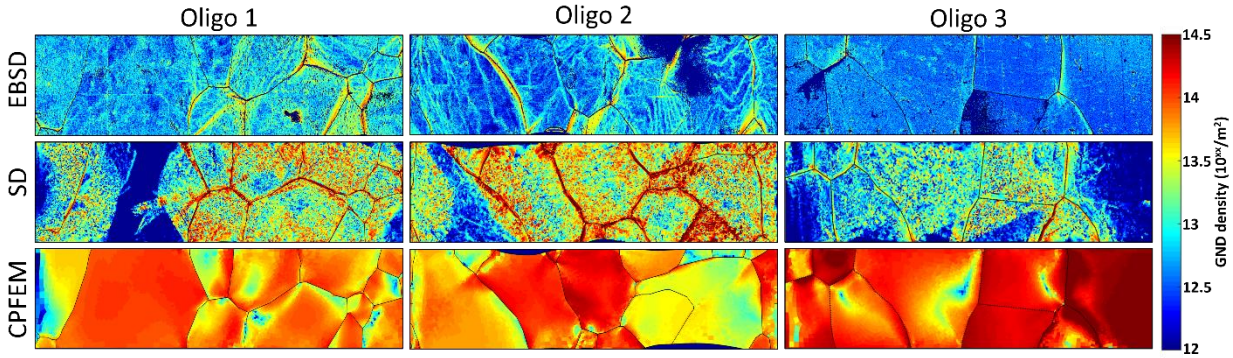

Fig. 3. GND maps constructed using EBSD data (first row), SD model results (second row), and CPFEM results (third row) for specimen 1 at 6.8% strain (first column), specimen 2 at 19.2% strain (second column), and specimen 3 at 5.2% strain (third column). Dark blue regions (1e12 mm^{-2}) in the EBSD generated GND maps indicate points where the diffraction pattern was of too poor of quality for an orientation to be resolved.

As can be seen from the figure, the SD model generally reflects experimental results by predicting buildup of dislocations near the GBs, while CPFEM predicts a more uniform dislocation

distribution throughout each grain. Overall, the SD model predicts average GND content within one order of magnitude of experimental results, while CPFEM predicts it within about two orders of magnitude. Furthermore, the SD model correclty predicts which specific GBs will have pileup 58% of the time; i.e. it is better than random selection, but cannot be considered to accurately reflect dislocation / GB interactions in its current form.

MD simulations of dislocation / GB interactions have been carried out on more than 25 different GBs with the goal of determining the factors that are of greatest importance in the interaction. The MD simulations are examined to determine: the slip system of the incident dislocation, when dislocations impinge on the GB, what resolved shear stresses are associated with its interaction, whether the slip dislocation transmits or not, the slip system and resolved shear stresses of transmitted dislocations. Additionally, other factors are calculated, such as transmissivity [3] and residual dislocation content left behind in the GB following a transmission event [4]. Each simulation cell consists of ~500,000 atoms and has a configuration as shown in Figure 2a; the shape is designed such that uniaxial applied loads, as shown cause nucleation of dislocations at the sharp notch, which then propagate into the GB as shown in Figure 2b.

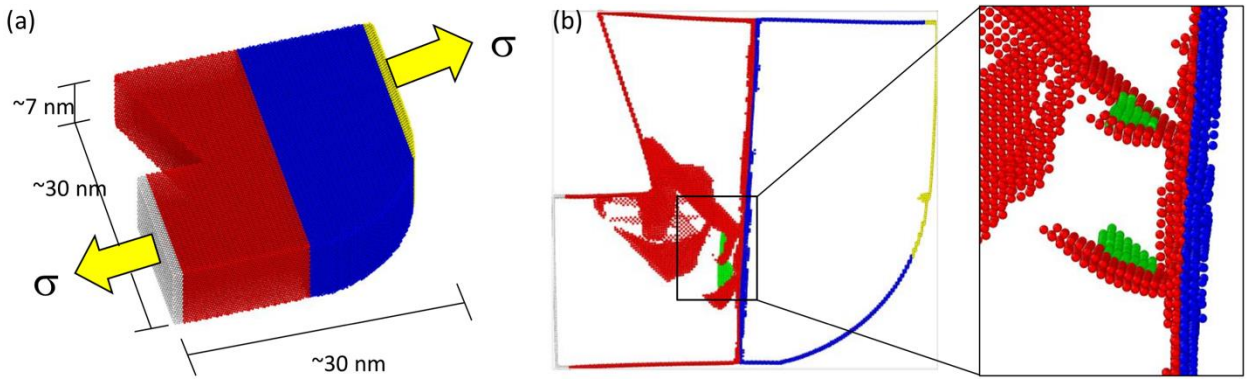

Fig. 4 (a) Depiction of dimensions, shape, and loading of the bicrystal MD simulation. (b) Snapshot of a single MD simulation showing dislocations nucleated from the stress concentration and impinging on the GB. Atoms with perfect FCC structure have been removed to show what is happening in the interior of the bicrystal.

The factors noted above are measured for each of the dislocation / GB interactions. In deforming these 25 GBs, there were 51 different dislocation / GB interactions that were observed. Of these, 27 exhibited transmission with the remaining 25 dislocations becoming pinned or absorbed into the GB without transmitting a dislocation into the other grain. In the initial analysis, there has been no correlation found regarding the magnitudes of the resolved shear stress on a given system and the transmission of a dislocation on the other side of the GB. In fact, some of the highest observed stresses were on systems that have not allowed transmission of a dislocation. However, the transmissivity factor correctly predicts the outgoing slip system for 63% of the transmission events. For another 22% of the cases, the factor correctly predicts the slip plane. Other outgoing dislocations were partial dislocations, which were not considered. Thus only 15 events are incorrectly predicted. Additionally, analysis of the residual Burgers vector indicates that 78% of the transmission events occurred on slip systems that had the minimum residual Burgers vector. On average, the transmitted slip systems had residual Burgers vectors of 0.7Å, while cases with

no transmission had an average residual Burgers vector of 3.8Å on the predicted slip system. In summary, it appears that we should be able to discern which dislocation events will result in transmission based on a combination of the transmissivity factor and the residual Burgers vector. At present, no accurate prediction of the resolved shear stress required for a transmission event has been determined.

Future Plans

An experimental campaign is underway to compile a large dataset of dislocation / GB interactions in BCC and FCC materials. Several terabytes of EBSD data were obtained this summer in collaboration with Sandia National Lab, and samples with varying grain size are currently being polished for scanning. The data will be mined for correlations that infer the form of the correct transmissivity factor / obstacle stress model. Furthermore, specific boundaries that display special characteristics will be selected for more detailed study via more detailed experimental and SD model analysis.

The MD work will proceed with additional GBs, with the goal of examining more than 100 dislocation / GB interactions to determine the factors most critical to predicting slip transmission or the lack thereof, and the stresses associated with the events. Following completion of this work, the MD work will focus on simulating large numbers of dislocations interacting with a single boundary to determine the propensity for building at different GBs. The goal is to see buildup similar to that observed in experiments for interpretation of the results.

References

[1] W. Gan, H.J. Bong, H. Lim, R. Boger, F. Barlat, R.H. Wagoner. Mechanism of the Bauschinger effect in Al-Ge-Si alloys, Materials Science and Engineering A 684 (2017) 353-372.

[2] H.J. Bong, H. Lim, M.-G. Lee, D. Fullwood, E. Homer, R.H. Wagoner. An RVE procedure for micromechanical prediction of mechanical behavior of dual-phase steel, Materials Science and Engineering A (In Review).

[3] Z. Shen, R.H. Wagoner, W.A.T. Clark. Dislocation and grain boundary interactions in metals, Acta Metall. 36 (1988) 3231-3242.

[4] W.Z. Abuzaid, M.D. Sangid, J.D. Carroll, H. Sehitoglu, J. Lambros. Slip transfer and plastic strain accumulation across grain boundaries in Hastelloy X, Journal Of The Mechanics And Physics Of Solids 60 (2012) 1201-1220.

Publications

1. Hyuk Jong Bong, Hojun Lim, Myoung - Gyu Lee, David Fullwood, Eric Homer and R. H. Wagoner, An RVE Procedure for Micromechanical Prediction of Mechanical Behavior of Dual-phase Steel, Materials Science and Engineering A, 695 (2017), 101-111
2. Richard Wyman, David Fullwood, Robert Wagoner, Eric Homer, Variability of non-Schmid effects in grain boundary dislocation nucleation criteria, Acta Materialia, 124C (2017) 588-597, 10.1016/j.actamat.2016.11.005
3. Landon Hansen, Brian Jackson, David Fullwood, Stuart I. Wright, Marc de Graef, Eric Homer, Robert Wagoner, Influence of Noise Generating Factors on Cross Correlation EBSD Measurement of GNDs, Microscopy and Microanalysis, in press, 23 (2017), Issue 3, 460-471, 10.1017/S1431927617000204
4. W. Gan, H.J. Bong, H. Lim, R. Boger, F. Barlat, R.H. Wagoner. Mechanism of the Bauschinger effect in Al-Ge-Si alloys, Materials Science and Engineering A 684 (2017) 353-372. http://dx.doi.org/10.1016/j.msea.2016.12.020
5. Zhong Chen, Hyuk Jong Bong, Dayong Li, R.H. Wagoner, The Elastic - Plastic Transition of Metals, International Journal of Plasticity, International Journal of Plasticity, 83 (2016), 178-201; 10.1016/j.ijplas.2016.04.009
6. T.J. Ruggles, T.M. Rampton, A. Khosravani, D.T. Fullwood, The effect of length scale on the determination of geometrically necessary dislocations via EBSD continuum dislocation microscopy, Ultramicroscopy 164 (2016), 1-10, 10.1016/j.ultramic.2016.03.003
7. T.J. Ruggles, D.T. Fullwood, J. Kysar, Resolving geometrically necessary dislocation density onto individual dislocation types using EBSD based continuum dislocation microscopy, International Journal of Plasticity, 76 (2016), 231, 10.1016/j.ijplas.2015.08.005
8. Brian Jackson, Jordan Christensen, Saransh Singh, Marc De Graef, David Fullwood, Eric Homer and Robert Wagoner, Performance of Dynamically Simulated Reference Patterns for Cross Correlation EBSD, Microscopy and Microanalysis, 22 (2016), 4, 7890802. https://doi.org/10.1017/S143192761601148X
9. Andrew Orme, Isaac Chelladurai, T Rampton, D Fullwood, A Khosravani, M Miles, R Mishra, Insights into Twinning in AZ31 Magnesium: A Combined EBSD and Machine Learning Study, Computational Materials Science, 124 (2016), 353-363. http://dx.doi.org/10.1016/j.commatsci.2016.08.011
10. Khosravani, D. Fullwood, B.L. Adams, T. Rampton, M.P. Miles, R.K. Mishra, Nucleation and propagation of $\{10\bar{1}2\}$ twins in AZ31 magnesium alloy, Acta Materialia, 100 (2015), 202-214. http://dx.doi.org/10.1016/j.actamat.2015.08.024
11. Hardin TJ, Ruggles TJ, Koch, DP, Niezgoda SR, Fullwood DT, Homer ER, Analysis of Traction-Free Assumption in High-Resolution EBSD Measurements. Journal of Microscopy, 260 (2015), 1, 73-85. DOI: 10.1111/jmi.12268
12. David Fullwood, Mark Vaudin, Craig Daniels, Timothy Ruggles, and Stuart I. Wright, Validation of Kinematically Simulated Pattern HR - EBSD for Measuring Absolute Strains and Lattice Tetragonality, Materials Characterization, 107 (2015), 270, 10.1016/j.matchar.2015.07.017

13. Homer ER. Investigating the mechanisms of grain boundary migration in annealing processes using molecular dynamics. 36th Risø International Symposium Proceedings, IOP Publishing, Roskilde, 2015, p. 012006. doi:10.1088/1757-899X/89/1/012006.
14. ER Homer, S Patala, JL Priedeman, Grain Boundary Plane Orientation Fundamental Zones and Structure - Property Relationships, Scientific Reports, 5 (2015), 15476, 10.1038/srep15476

The Role of Anisotropy on the Self-Organization of Gas Bubble Superlattice

J. Gan[1], Y. Zhang[1], C. Sun[1], C. Jiang[1], Y. Gao[1], L. He[1], D. Sprouster[2], L. Ecker[2]
[1]Idaho National Laboratory, [2]Brookhaven National Laboratory

Program Scope

Self-organization of nanoscale void/gas bubble superlattices has been widely observed in irradiation experiments however yet to be well understood. The recent discovery of incoherent face-centered-cubic (fcc) Xe bubble lattice in body-centered-cubic (bcc) UMo challenges the widely accepted coherency between superlattices and matrices. A complete mechanistic understanding of bubble lattice self-organization may have a large impact to materials science and nuclear energy advancement, and is the objective of this project. The knowledge obtained through a coherent integration of experimental and computational approach will advance the current understanding of self-organization mechanisms of nanostructures under irradiation. To realize this goal, two appealing self-organization mechanisms previously proposed in open literatures have been identified: anisotropic elastic interaction between voids and kinetic anisotropy such as one-dimensional (1D) self-interstitial atoms (SIA) diffusion. For the first year, the focus is on the effect 1D diffusion using bcc Mo and W, with the former being elastically anisotropic while the latter isotropic. Efforts have been made to investigate the fundamental interaction between inert gas and metal matrices, the mechanism for void/bubble superlattice formation and their stabilities under irradiation and annealing, and the experimental conditions for bubble superlattice formation and evolution, and to establish advanced characterization techniques for bubble superlattice.

Recent Progress

Helium gas bubble superlattice (GBS) has been successfully produced in pure Mo and W by using ion implantation. Systematical experiments have been performed to determine the optimized implantation conditions for the GBS formation. The injection of helium gas ions to ~ 10 at.% at temperature of 0.2 T_m (T_m: melting temperature) produces well-aligned gas bubbles in both Mo and W. It suggests that the role of elasticity on GBS formation is weaker than that of SIA diffusion. Figure 1 (left) shows representative transmission electron microscopy (TEM) micrographs of GBS in Mo and W, the inset of fast Fourier transform (FFT) suggests a clear evidence of the ordering of helium gas bubbles on {110} planes. The lattice parameter of He GBS, estimated using FFT, is ~ 4.8 nm in Mo and ~ 5.2 nm in W. The average size helium gas bubble is ~ 1.5 nm for both Mo and W. However, the gas bubble lattice parameter strongly depends on the implantation temperature and ion flux. It is known that Xe GBS in irradiated U-10Mo fuel has high thermal stability. In-situ thermal annealing experiment was conducted in TEM to study the thermal stability of He GBS in Mo. The result shows superior thermal stability of He GBS up to 850˚C ($0.39T_m$) as shown in Fig. 1 (center and right). The significance of this thermal stability is on its great potential for broad applications such as for 3D patterning for advanced functional material and the design of the advanced nuclear fuels with inherent property for the development of thermally stable fission gas superlattice, which has high gas inventory capacity operating at high temperature.

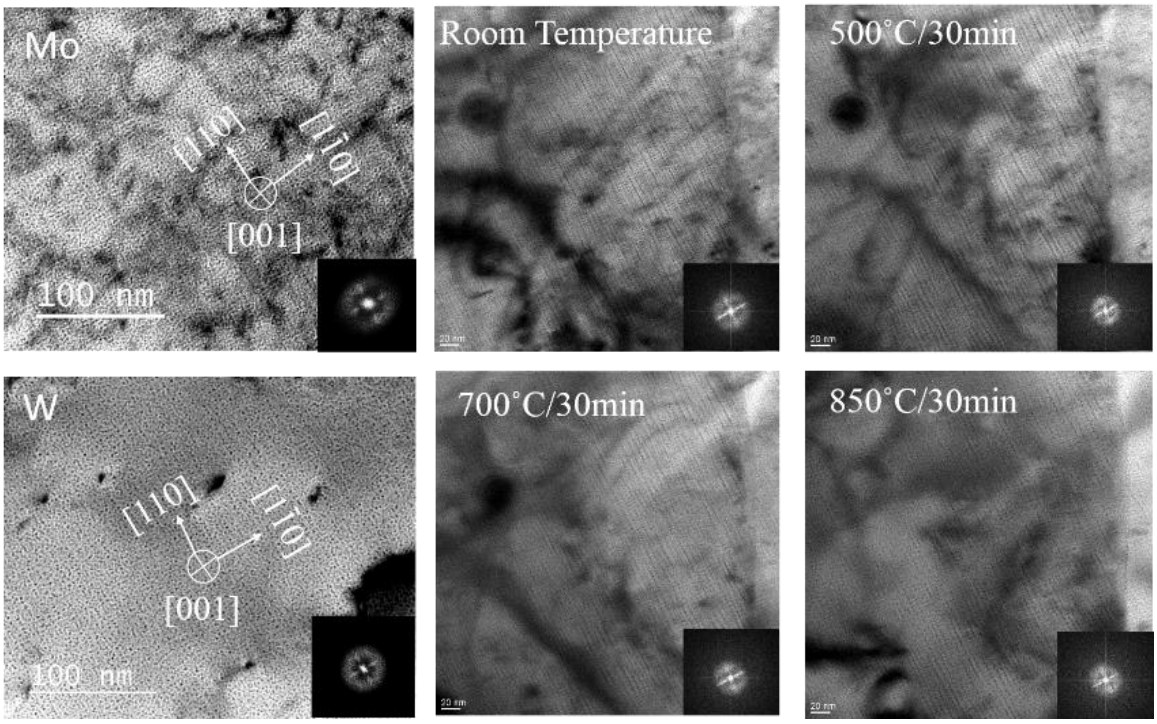

Figure 1. He gas bubble superlattice in Mo and W (left) using ion implantation. Insets with fast Fourier transform (FFT) show bubble ordering. TEM bright field images reveal stable He GBS alignment from in-situ annealing up to 850 ℃ (middle and right).

Irradiation-induced disordering of superlattice has been reported in the literature, for instance, ion irradiation can cause the disorder of L12 structured gamma prime precipitates in Ni-based suepralloy due to creation of point defects and anti-site defects. Here, the first time, the order-disorder transformation of He gas bubble superlattice is observed under Kr ion irradiation. In-situ Kr ion irradiation with energy of 1 MeV using IVEM at ANL was performed on the Mo TEM foil with He GBS. The evolution of gas bubble alignment and FFT clearly suggests that the order-disorder transformation of He gas bubble superlattice under Kr ion irradiation at 300˚C completes at a relatively low dose of 2.5 dpa. This is quite different from Xe GBS in irradiated U(Mo) which is believed to be stable under irradiation.

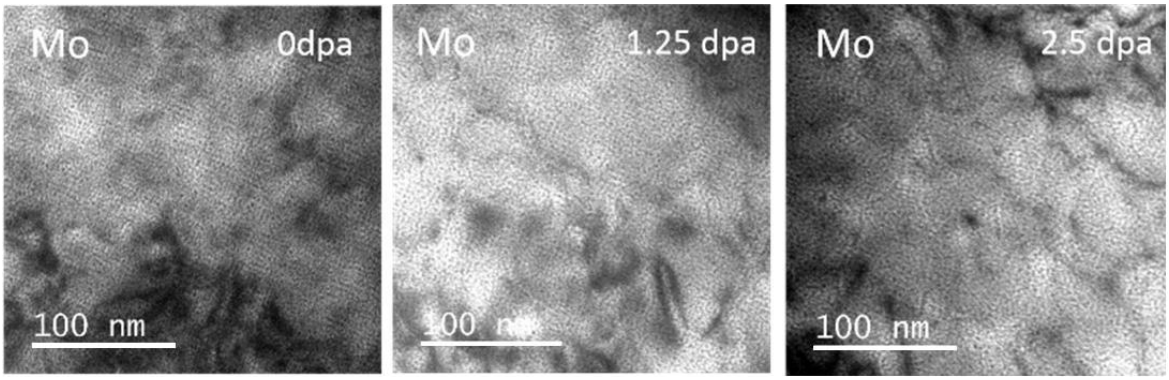

Figure 2. He gas bubble superlattice transformation from order to disorder under 1 MeV Kr irradiation at 300 ℃.

Systematical density functional theory (DFT) calculations have been carried out to explore the thermodynamic stability of inert gases such as He and Xe in group 5B (V, Nb and Ta) and 6B (Cr, Mo and W) metals, as well as the interactions between gas atoms and lattice defects. Some representative results are shown in Fig. 3. It is known that without vacancies the inert gases are found to have high solution energies in these metals. Accordingly, inert gas atoms show strong affinity to vacancies or voids, indicating a strong tendency to precipitate into bubbles. With sufficiently high gas to vacancy ratio in a gas-vacancy cluster, the presence of gas atom can effectively suppress recombination between vacancies and SIAs and stabilize this cluster, as shown by the increase in the interaction energy between a gas-vacancy cluster and a SIA in Fig.3. The results suggest high driving forces, particularly for Xe, to form stable gas bubbles under irradiation by occupying vacancies. These results provided thermodynamic basis for understanding gas behaviors in metal matrices and parameters to be used in atomistic simulations and theoretical analysis. Moreover, very good group trends are obtained in the results, suggesting that the interaction between inert gases and metal matrices may be governed by the electronic configurations of metal atoms.

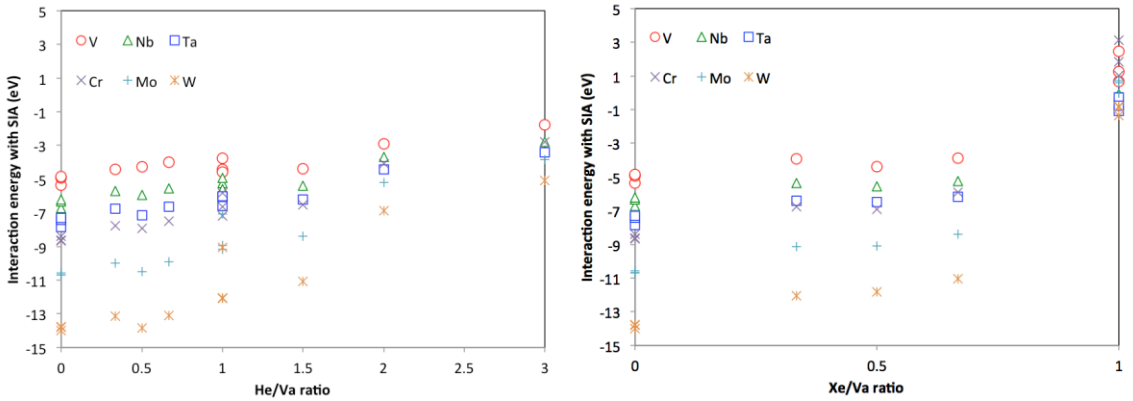

Figure 3. Interaction energies as a function of gas/vacancy ratio between a SIA and a gas-vacancy cluster in group V and VI bcc metals from DFT calculations.

To explore the nucleation process of void superlattice, which may possibly share the same formation mechanism with bubble superlattice, a novel atomic kinetic Monte Carlo (AKMC) method considering 1D SIA diffusion has been developed. In conjunction, theoretical analysis is carried out in analogy to phase separation in regular solution with source and reaction terms. It is predicted by the theoretical analysis that with increasing vacancy concentration, a critical condition will be reached for spontaneous phase separation, which features a characteristic length dependent on defect dynamics. This characteristic length can be stabilized when ordering is induced by kinetic anisotropy such as 1D SIA diffusion. The superlattice symmetry is found to be dictated by 1D SIA diffusion, challenging the widely accepted empirical rule that the superlattice is coherent with the matrix. The nature of spontaneous phase separation for superlattice is clear in AKMC simulations at low temperature and high dose rate, as shown in Fig. 4(a) and (c). With increasing temperature or decreasing dose rate, individual void nucleation and growth weaken the ordering, leading to *defects* formation in the superlattice, as shown in Fig. 4(b).

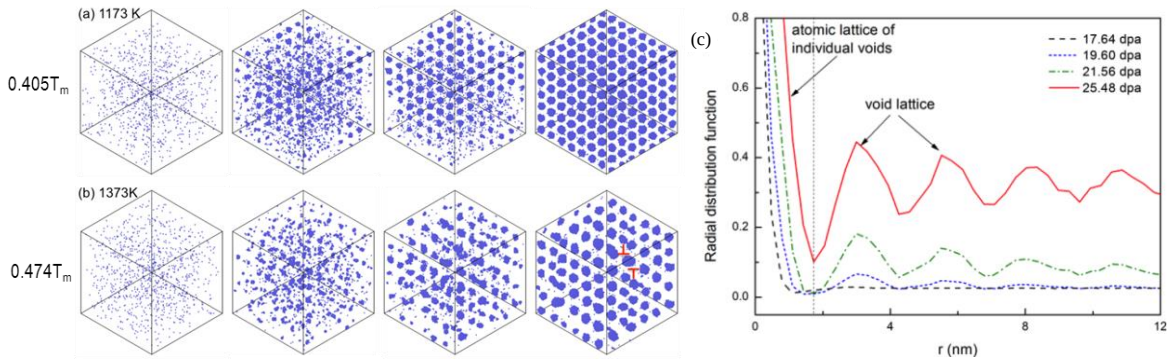

Figure 4. Snapshots of AKMC simulations showing 3D void lattice formation in Mo: (a) at 1173 K spontaneous phase separation leads to a perfect void lattice, and (b) at 1373 K, void nucleation and growth give defects in the void lattice. (c) Radial distribution function of vacancy showing the nucleation and stabilization of a wave length in the AKMC simulation shown in (a).

The theoretical analysis also leads to an analytical prediction of void superlattice parameter based on materials properties and irradiation conditions without any fitting parameters. The unprecedented predictability is demonstrated by comparison to independent experiments in W and Mo and AKMC simulations in Mo shown in Fig. 5. Three important trends regarding the superlattice parameter a_L are predicted: i) a_L increases with increasing temperature, ii) a_L decreases with increasing dose rate, iii) under the same irradiation condition, a_L is larger in materials with higher vacancy diffusivities. The first and the third predictions are validated by the measurements in neutron irradiated Mo and W in literature, and the second one is validated by AKMC simulations. An indirect experimental support to the second prediction is that, in general, at the same temperature the void superlattice parameters produced by ion irradiation are usually smaller than that by neutron irradiation, since the former is usually associated with much higher dose rates. Given the uncertainties in the experiments, quantitative comparison with experiments can be regarded as very good as well. The consistency between theory and experiments, alongside the direct support from AKMC simulations, indicates that the spontaneous phase separation based theory captures the nature of void superlattice formation. It can thus be utilized to tailor desired superlattice in experiments, e.g., by adjusting irradiation conditions and materials properties. This theory is expected to hold and will be extended for bubble superlattice.

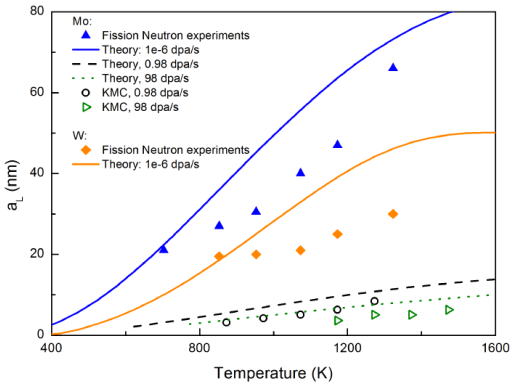

Figure 5. Superlattice parameters as functions of temperature in bcc Mo and W.

The above theoretical analysis also predicts a low temperature boundary for void superlattice formation using the condition that the predicted nearest neighbor distance in the superlattice is no less than twice of the recombination radius. In addition to void superlattice, the irradiation conditions for He gas bubble superlattice in bcc Mo and W have been identified experimentally. For both materials, bubble superlattices have been produced by He ion irradiation. Since both Mo and W have 1D SIA anisotropic diffusion and only Mo is elastically anisotropic, this confirms that indeed 1D SIA diffusion can lead to bubble superlattice formation, consistent with the AKMC simulations. Elastic anisotropy is not suggested as a necessary condition for that.

Synchrotron experiments at the NSLS-II at BNL were performed to nondestructively characterize bubble size, GBS lattice structure and lattice parameter in Mo and W substrates implanted with He ions. These were the first measurements of their kind and capitalized on the ultra-high brightness and small X-ray source size of the NSLS-II. Rapid SAXS and WAXS mapping measurements (< 20 min per sample) at the LiX beamline were performed to determine the spatial distribution of GBS within a series of samples.

An example of the SAXS-WAXS mapping is shown in Fig. 6(a) for a He implanted Mo sample. The mapping of SAXS and WAXS results in 1200 individual scattering/diffraction patterns. The visualization of GBS rich regions was accomplished with an image montage made possible through customized python scripts and ImageJ. The most intense scattering pattern in the center of the SAXS images (shown in red in Fig. 6(b)) is due to the signal from the matrix and He bubbles, while the diffuse diffraction spots observable away from the central pattern are attributed to the diffraction due to the ordering of the He gas bubbles.

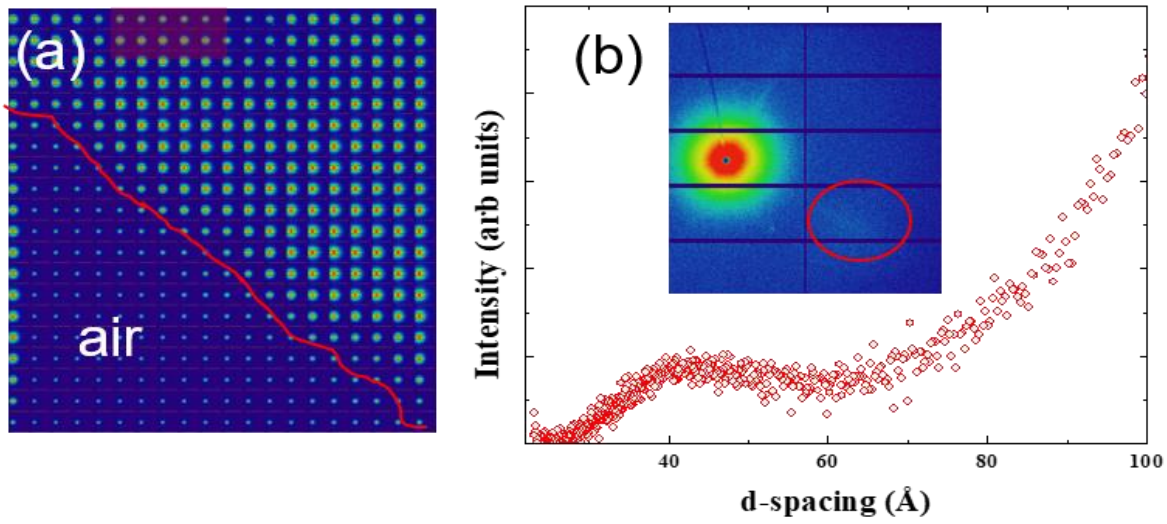

Figure 6. (a) SAXS map (montage of SAXS images) of a He implanted Mo sample. The sample surface is shown by a red line dividing a region with air scatter from the scattering from the sample. A portion of the GBS-rich region is highlighted (transparent red box). One of the integrated scattering patterns within the red box is shown in (b) with the diffraction peak from a plane of He GBS (d-spacing ~3.9 nm).

SAXS-WAXS experiments were also performed on a neutron irradiated U(Mo) nuclear fuel sample with well-developed Xe GBS at the LiX beamline (NSLS-II). Figure 7 shows an example of the scattering signal from the Xe GBS. The sharper, more well-defined diffraction signal is indicative that the fission gas bubbles are highly ordered, and phase identification shows that they are in an FCC arrangement, consistent with past TEM reports. Future synchrotron experiments on this sample include mapping the structural state of the gas in the GBS fine bubbles and in large fission gas bubbles that form in regions of the sample where the GBS has started to collapse with X-ray Absorption Near Edge Spectroscopy.

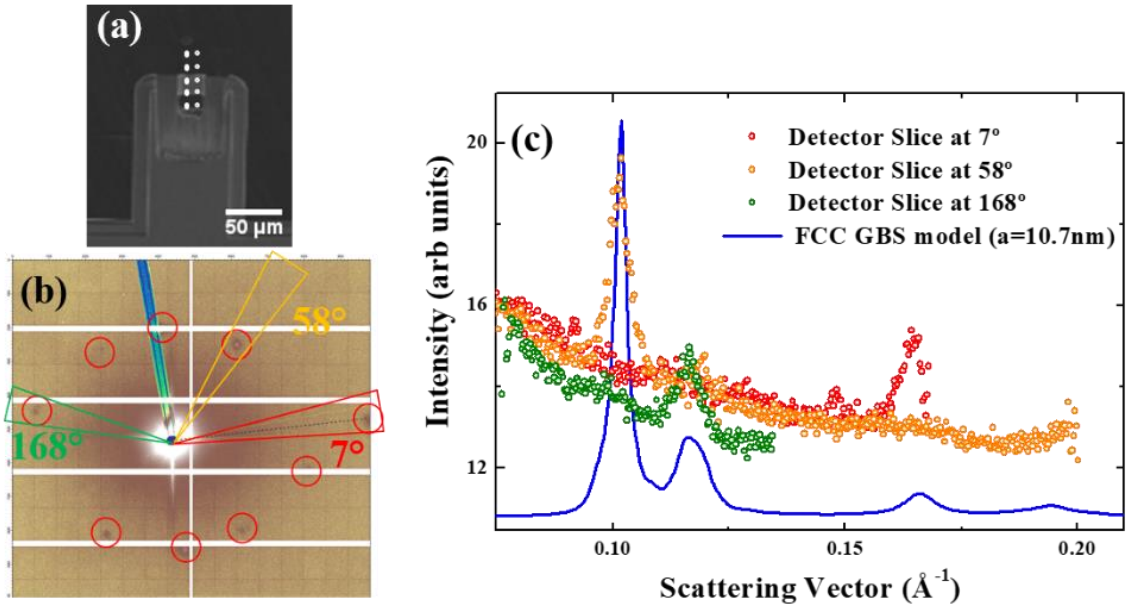

Figure 7. (a) Image of the neutron irradiated UMo fuel sample measured at LiX, (b) Scattering pattern with diffraction spots highlighted, (c) Intensity profiles of individual slices shown in (b) with the superposition of an FCC GBS model.

Future Plans

The accomplishments received so far have significantly advanced the current understanding on void/bubble superlattice formation. In the future, theoretical analysis will be continued to 1) predict superlattice symmetry based on anisotropic SIA diffusion, 2) predict bubble superlattice using the data produced by DFT calculations, and 3) to explore the role of elastic anisotropy. Trends regarding matrix properties, gas element, and irradiation conditions will be predicted. In conjunction, new experiments will be carried out to systematically study the effects of dose rate, temperature, matrix properties and gas elements on the gas bubble superlattice parameter, to validate the predictions by theoretical analysis. Advanced characterizations will also be done to quantify the strain field around the bubble and gas content and pressure in the bubbles.

References

1. J. Gan, D.D. Keiser, B. D. Miller, A. B. Robinson, D. M. Wachs, M. K. Meyer, Thermal stability of fission gas bubble superlattice in irradiated U-10Mo fuel, Journal of Nuclear Materials, 464 (2015): 1-5.
2. C. Sun, M. Kirk, M. Li, K. Hattar, Y. Wang, O. Anderoglu, J. Valdez, B. P. Uberuaga, R. Dickerson, S. A. Maloy, Microstructure, chemistry and mechanical properties of Ni-based superalloy Rene N4 under irradiation at room temperature, Acta Materialia, 95 (2015): 257-265.
3. C. Abromeit, S. Matsumura, Kinetics of antiphase domain boundaries during and L12 order-disorder phase transformation: a Monte Carlo simulation, Philosophy Magazine A, 82 (2002): 2287-2302.
4. J. H. Evans, Nature 29, 403 (1971).
5. N. M. Ghoniem, D. Walgraef, and S. J. Zinkle, Journal of Computer-Aided Materials Design 8, 1 (2001).
6. K. Malen and B. R., in Proc. Int. Conf. on Voids Formed by Irradiation of Reactor Materials, Reading (1971).
7. C. H. Woo and W. Frank, J. Nuclear Materials 137, 7 (1985).
8. J. W. Cahn, Acta Met. 9, 795 (1961).
9. J. Moteff, V. Sikka, and H. Jang, in Consultant Symp. on the physics of irradiation produced voids (1975).
10. J. DiFabio et al, "The Life Science X-ray Scattering Beamline at NSLS-II" AIP Conf. Proc. 1741, 030049 (2016)

Publications (Oct. 2016 – Aug. 2017)

Yipeng Gao, Yongfeng Zhang, Daniel Schwen, Chao Jiang, Cheng Sun, Jian Gan, Xian-Ming Bai, "Self-organization of void superlattices: atomic scale perspective and theoretical prediction", submitted to Nature Communication in August 14, 2017.

There are 4-5 more journal articles in preparation for submission in September 2017.

Multiscale Mechanical Properties and Alloy Design

Easo P. George,[1,2] Hongbin Bei,[1] Yanfei Gao,[2,1] James R. Morris,[1,2] Yuri Osetskiy[1]

[1]Oak Ridge National Laboratory, Materials Science and Technology Division, Oak Ridge, TN 37831; [2]University of Tennessee, Department of Materials Science and Engineering, Knoxville, TN 37996

Program Scope

Our goal is to understand the fundamental factors that govern the phase stability and mechanical behavior of high-entropy alloys (HEAs) and their derivative medium-entropy alloys (MEAs). As opposed to conventional alloys that are based on one or two major elements, HEAs/MEAs comprise multiple principal elements in relatively high concentrations. This opens a vast, unexplored compositional space near the centers of phase diagrams where new alloys with exceptional properties might be lurking waiting to be discovered. Indeed, a few HEAs with striking mechanical properties have already been identified [e.g., 1,2] but much remains to be done. These materials are of fundamental scientific interest because textbook treatments of phase stability, deformation, and diffusion cannot be easily extended to compositionally complex multicomponent alloys. Currently, we are investigating single-phase (solid solution) alloys to avoid the confounding effects of multiple phases in the microstructure; among those, we focus on model alloys with the face-centered cubic (FCC) crystal structure. Careful thermomechanical processing is employed to control their microstructures, followed by analyses using a variety of techniques including X-ray and neutron diffraction, advanced electron microscopy, and atom probe tomography. Mechanical testing is performed as a function of temperature and strain rate to elucidate the effects of composition and microstructure on mechanical behavior. Interrupted tests are used to quantify microstructural evolution with strain to uncover the governing mechanisms at different stages of plasticity. Modeling and simulations based on molecular dynamics as well as *ab initio* calculations are used to develop a deeper understanding of the experimental results. Longer term, we expect our work to lead to the formulation of broad scientific principles for the design of an important new class of structural materials for use in energy-related applications.

Recent Progress

Because of space limitations, we will highlight just a few of our recent results that bear on phase stability and mechanical properties. The original concept behind HEAs was that their high configurational entropies would suppress the formation of harmful intermetallic compounds and stabilize single-phase solid solutions [3]. That turned out not to be the case and contributions to the Gibbs free energy from enthalpy [4,5] and non-configurational entropy [6] appear to be critical in determining the phases present in the microstructure. Among the single-phase HEAs, the

CrMnFeCoNi alloy discovered by Cantor et al. [7] is perhaps the most extensively investigated. Careful analysis utilizing a variety of techniques over multiple length scales, including X-ray diffraction, light microscopy, scanning electron microscopy, transmission electron microscopy, and atom probe tomography have shown that it is a true solid solution down to atomic scales when annealed at temperatures above 800 °C [8,9]. However, at lower temperatures, the solid solution becomes unstable and multiple metallic and intermetallic phases precipitate out [8-10]. Fig. 1 shows an example of this phase decomposition on a grain boundary after a 500-day anneal at 500 °C. Selected area diffraction and energy dispersive X-ray spectroscopy showed that three different precipitates formed: $L1_0$-structured NiMn, B2-structured FeCo and a Cr-rich body-centered cubic phase [8]. After annealing for 500 days at 700 °C, a sigma phase was identified on the grain boundaries with the tetragonal crystal structure of the binary Cr-Fe sigma phase [8]. It contained all five elements of the starting solid solution suggesting that it is a quinary variant of the binary sigma phase, which is not surprising given that the sigma phase forms in all the Cr-X binaries (X = Mn, Fe, Co, or Ni). At both temperatures, the precipitates formed almost exclusively at grain boundaries suggesting that they offer preferential sites for heterogeneous nucleation or faster diffusion pathways. The latter is given some credence by the fact that precipitation occurs very fast (minutes to hours) if this alloy is processed by high-pressure torsion to have nanocrystalline grains [9]; however, it is not known whether the excess stored energy after severe plastic deformation is a contributing factor. The sigma phase also forms at intragranular pores [8], which suggests that heterogeneous nucleation is likely an important factor. Additional studies are needed to disentangle the thermodynamic and kinetic driving forces for phase decomposition. Meanwhile, our studies clearly show the limits of entropic stabilization, which can lead to the formation of embrittling intermetallic phases [9]. Similar instabilities likely occur also in other systems. Therefore, HEAs being considered for elevated temperature applications should be thoroughly investigated for in-service phase decomposition.

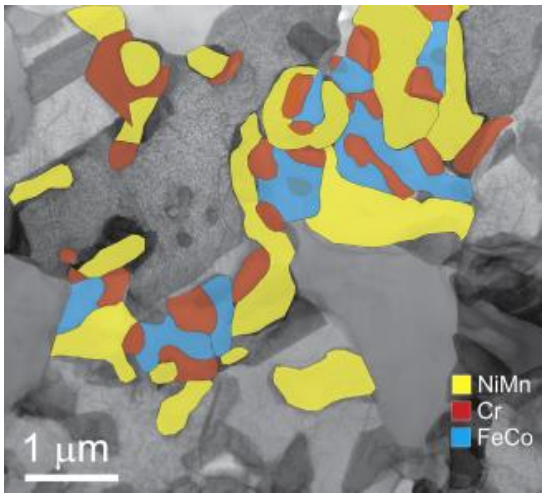

Fig. 1 EDX maps superimposed on STEM image showing three distinct precipitates in the originally single-phase CrMnFeCoNi (FCC) alloy after 500 days at 500 °C [8].

Not all phase instabilities are deleterious; some can have beneficial effects. As discussed later, twinning induced plasticity (TWIP) is a potent mechanism that can defeat the strength-ductility trade-off in certain HEAs and MEAs [1,11]. The local stacking in the twinned regions of FCC alloys is hexagonal close-packed (HCP). Therefore, alloying elements that destabilize FCC relative to HCP are likely to also favor twinning. Another mechanism that has been successfully employed to defeat the strength-ductility trade-off in HEAs [2] is transformation induced plasticity

(TRIP). In this case too, alloying elements that destabilize FCC relative to HCP are desirable since they can induce TRIP effects during plastic deformation.

In the HEA literature, it is often assumed that alloys with higher entropy will exhibit proportionally higher solid solution strengthening [e.g., 12], but a thorough investigation by us of a family of FCC alloys in which potentially confounding factors such as grain size, second phases, etc. were carefully eliminated showed that there is no correlation between configurational entropy (number of constituent elements) and strength or ductility [13]. To obtain a better understanding of alloying effects on solid solution strengthening, we characterized the displacement of atoms from their ideal lattice positions (Fig. 2) because such displacements distort the lattice and contribute to strengthening. The magnitude of the atomic displacement parameter (ADP) at finite temperatures, which was obtained by synchrotron X-ray diffraction for the CrMnFeCoNi HEA [14], is the sum of the squares of the dynamic displacements of the atoms due to thermal vibrations (dynamic disorder) and the static displacement of the mean positions from the ideal lattice positions (static disorder). Consequently, the ADP becomes increasingly dominated by static disorder as the temperature is decreased. For the CrMnFeCoNi HEA, the measured ADP values were 23.5±0.4 and 58.7±0.5 pm^2 at 25 and 300 K, respectively [14]. Assuming that the 25-K value is an upper limit of the static disorder, and taking its square root, one gets a displacement of <5 pm (0.005 nm) averaged over all the atoms in this alloy, which raises the question whether there really is "severe" lattice distortion as is often claimed in the literature. Refinement of the X-ray spectra did not allow us to obtain the independent ADPs for each element (only the average ADP for the entire crystal). Therefore, first-principles total-energy calculations were performed to obtain the mean square atomic displacements (MSADs) of the constituent elements. The MSADs decreased monotonically with *d*-electron concentration from a high of ~43 pm^2 for Cr to a low of ~9 pm^2 for Ni. Interestingly, the MSAD for the CrMnFeCoNi alloy obtained by averaging the computed MSADs of the constituent elements was 25.2 pm^2, which is close to the experimentally determined average ADP value of 23.5 pm^2, giving credence to the first-principles calculations. These calculations can also be used to estimate the effective atomic radii of the constituent elements, which were found to decrease in the order Cr, Ni, Mn, Fe, Co. Interestingly, the largest pair-wise difference in the effective atomic radii was approximately 4.1% (between Cr and Co), which is significantly larger than if the size difference is estimated using the Goldschmidt radii. From micropillar compression experiments, the critical resolved shear stress (CRSS) of the CrMnFeCoNi alloy was shown to be ~33-43 MPa [15], which

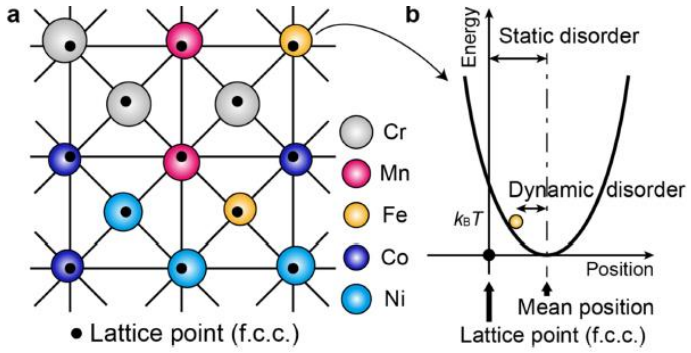

Fig. 2 (a) Schematic illustration of the FCC lattice of the CrMnFeCoNi HEA showing (exaggerated) displacements of the mean positions of atoms from the ideal lattice positions, and (b) schematic potential energy well showing static and dynamic disorder [14].

is an order of magnitude higher than that of pure Ni (~3-4 MPa). Nevertheless, a Labusch-type analysis shows that a hypothetical 50-50 binary alloy with a 4% atomic size difference and the shear modulus of the CrMnFeCoNi alloy gives the right value of yield strength, indicating again that severe lattice distortion need not be invoked to rationalize the high CRSS values of HEAs.

The computed MSAD value of any element in the Cr-Mn-Fe-Co-Ni system depends on the environment of that element. That is, the MSAD value of, say, Mn is not a constant, but depends on which other elements are present in the alloy. For example, in the alloy CrMnFeNi, the MSAD value of Mn is ~61 pm^2, which is more than twice its value (~26 pm^2) in the alloy MnFeCoNi. This is because elements with a large effective atomic radius (such as Cr) tend to displace those with a smaller effective radius (such as Fe and Co) significantly from their ideal lattice position. In the Cr-Mn-Fe-Co-Ni system, Cr thus plays an outsize role in determining the atomic displacements in those alloys in which it is present. Since our earlier work [13] showed that the stronger alloys were generally those containing Cr, regardless of the total number of elements in the alloy, it is of interest to determine whether the reason for that result lies in the MSAD trends described above. However, to rule out any effect of the relatively high shear modulus (μ) of Cr, the yield strength values must first be normalized by μ. Figure 3 shows a plot of the shear modulus normalized yield strengths of several alloys (ternaries to quinary) in the Cr-Mn-Fe-Co-Ni family as a function of the square root of MSAD. The reasonably good linear fit indicates that MSAD is a useful scaling factor to predict the athermal yield stress of HEAs and that the resistance to dislocation motion depends on the degree to which the atoms are displaced from their ideal lattice positions.

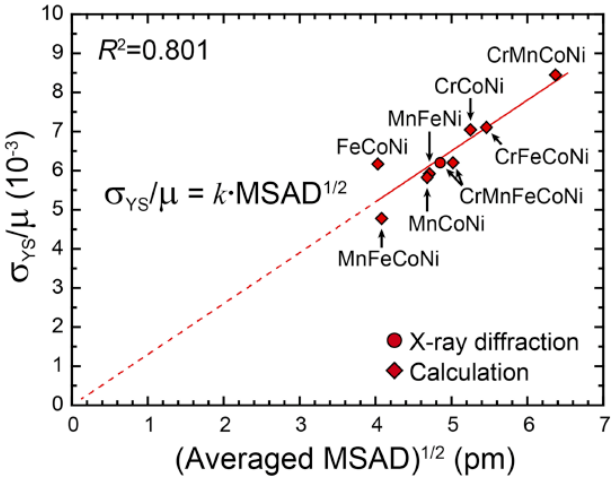

Fig. 3 Shear-modulus-normalized yield strengths at 0 K of the CrMnFeCoNi HEA and its quaternary and ternary MEA subsets vs. square-root of the MSAD averaged over all the elements in each alloy [14].

An intriguing aspect of the MEAs and HEAs investigated by us is that the CrCoNi ternary not only has a higher yield strength than the CrMnFeCoNi quinary, but its ductility [13] and toughness [11] are also higher. Furthermore, ductility/toughness and strength of both alloys increase as the temperature is decreased to the cryogenic range. The key microstructural feature responsible for this behavior is deformation induced twinning and the differences between the two alloys as well as the effects of temperature are directly related to the stress for the onset of twinning and how easy/difficult it is to reach that stress [16]. By interrupting tensile tests after different amounts of strain and examining samples extracted from the gage sections by TEM, it was possible to determine the applied (far-field) stress at which twinning starts in the two alloys [16]. As it turns out, within experimental scatter, the twinning stress is roughly the same in the two alloys. So why

does the CrCoNi MEA twin more easily than the CrMnFeCoNi HEA? Basically, for two reasons: the yield strength of the CrCoNi alloy is higher than that of the CrMnFeCoNi alloy, and the shear modulus of CrCoNi is higher, which makes its work hardening rate higher [16]. In other words, the MEA starts off from a higher base, and then climbs faster, allowing it to reach the threshold stress for twinning earlier.

Future Plans

We plan to experimentally characterize the lattice distortion in the simpler MEAs that are more tractable by synchrotron X-ray diffraction. In the quinary HEAs, only the ADP averaged over the whole crystal could be determined; however, it is of interest to know the displacement of each constituent element and not just that of the average alloy. This will allow robust predictions of how deviations from equiatomic compositions affect solid solution strength. We will also investigate effects of stacking fault energy and phase stability on TWIP and TRIP effects in the Cr-Mn-Fe-Co-Ni system that we have been working on. First-principles calculations will be used to guide alloy selection and deviations from the equiatomic composition to understand how composition can be used to optimize strength and ductility/toughness.

References

1. B. Gludovatz et al. *Science* **345** 1153 (2014).
2. Z. Li et al. *Nature* **534** 227 (2016).
3. J.W. Yeh et al. *Adv. Eng. Mater.* **6** 299 (2004).
4. F. Otto et al. *Acta Mater.* **61** 2628 (2013).
5. M.C. Troparevsky et al. *Phy. Rev. X* **5** 011041 (2015).
6. D. Ma et al. *Acta Mater.* **100** 90 (2015).
7. B. Cantor et al. *Mater. Sci. Eng. A* **375** 213 (2004).
8. F. Otto et al. *Acta Mater.* **112** 40 (2016).
9. B. Schuh et al. *Acta Mater.* **96** 258 (2015).
10. E.J. Pickering et al. *Scripta Mater.* **113** 106 (2016).
11. B. Gludovatz et al. *Nature Comm.* **7** 10602 (2016).
12. J.W. Yeh. *JOM* **67** 2254 (2015).
13. Z. Wu et al. *Acta Mater.* **81** 428 (2014).
14. N.L. Okamoto et al. *AIP Advances* **6** 125008 (2016).
15. N.L. Okamoto et al. *Sci. Reports* **6** 35863 (2016).
16. G. Laplanche et al. *Acta Mater.* **128** 292 (2017).

Publications (since last PI meeting)

Z. J. Zhang, M. M. Mao. J. Wang, B. Gludovatz, Z. Zhang, S. X. Mao. E. P. George, Q. Yu, R. O. Ritchie, "Nanoscale origins of the damage tolerance of the high-entropy alloy CrMnFeCoNi," *Nature Comm.* **6**, 10143 (2015).

Z. Wu, Y. F. Gao, H. Bei, "Single crystal plastic behavior of a single-phase, face-center-cubic-structured, equiatomic FeNiCrCo alloy," *Scr. Mater.* **109**, 108-112 (2015).

B. Schuh, F. Mendez-Martin, B. Völker, E. P. George, H. Clemens, R. Pippan, A. Hohenwarter, "Mechanical properties, microstructure and thermal stability of a nanocrystalline CoCrFeMnNi high-entropy alloy after severe plastic deformation," *Acta Mater.* **96**, 258-268 (2015).

Z. Wu, C. M. Parish, H. Bei, "Nano-twin mediated plasticity in carbon-containing FeNiCoCrMn high entropy alloys," *J. Alloy Compd.* **647**, 815-822 (2015).

B. Gludovatz, E. P. George, R. O. Ritchie, "Processing, microstructure and mechanical properties of the CrMnFeCoNi high-entropy alloy," *JOM* **67**, 2262-2270 (2015).

G. M. Pharr, "Recent advances in small-scale mechanical property testing by nanoindentation," *Curr. Opin. Solid State Mater. Sci.* **19**, 324-333 (2015).

Y. F. Gao, B. C. Larson, "Displacement fields and self-energies of circular and polygonal dislocation loops in homogeneous and layered anisotropic solids," *J. Mech. Phys. Solids* **83**, 104-128 (2015).

M. Sebastiani, K. E. Johanns, E. G. Herbert, and G. M. Pharr, "Measurement of fracture toughness by nanoindentation methods: Recent advances and future challenges," *Curr. Opin. Solid State Mater. Sci.* **19**, 315-316 (2015).

F. L. Meng, J. W. Qiu, I. Baker, H. Bei, "The effects of annealing on the microstructure and mechanical properties of Fe28Ni18Mn33Al21," *J. Mater. Sci.* **50,** 7821-7834 (2015).

B. Mazumder, C. M. Parish, H. Bei, M. K. Miller, "The role of processing route on the microstructure of 14YWT nanostructured ferritic alloy," *J. Nucl. Mater.* **465**, 204-211 (2015).

G. Song, Z. Sun, L. Li, X. Xu, M. Rawlings, C. H. Liebscher, B. Clausen, J. Poplawsky, D. N. Leonard, S. Huang, Z. Teng, C. T. Liu, M. D. Asta, Y. F. Gao, D. C. Dunand, G. Ghosh, M. W. Chen, M. E. Fine, P. K. Liaw, "Ferritic alloy with extreme creep resistance via coherent hierarchical precipitates," *Sci. Rep.* **5**, 16327 (2015).

B. Gludovatz, A. Hohenwarter, K. V. S. Thurston, H. Bei, Z. Wu, E. P. George, R. O. Ritchie, "Exceptional damage-tolerance of a medium entropy alloy CrCoNi at cryogenic temperatures," *Nature Comm.* **7**, 10602 (2016).

F. Otto, A. Dlouhy, K. G. Pradeep, M. Kubenova, D. Raabe, G. Eggeler, E. P. George, "Decomposition of the single-phase high-entropy alloy CrMnFeCoNi after prolonged anneals at intermediate temperatures," *Acta Mater.* **112**, 40-52 (2016).

N.L. Okamoto, S. Fujimoto, Y. Kambara, M. Kawamura, Z. M. T. Chen, H. Matsunoshita, K. Tanaka, H. Inui, E. P. George, *Sci. Reports* **6** 35863 (2016).

N. L. Okamoto, K. Yuge, K. Tanaka, H. Inui, E. P. George, "Atomic displacement in the CrMnFeCoNi high-entropy alloy – A scaling factor to predict solid solution strengthening," *AIP Advances* **6**, 125008 (2016).

H. Bei, Y. Z. Xia, R. I. Barabash, Y. F. Gao, "A tale of two mechanisms: strain-softening versus strain-hardening in single crystals under small stressed volumes," *Scr. Mater.* **110**, 48-52 (2016).

Y. F. Gao, "Deformation fields near a steady fatigue crack with anisotropic plasticity," *Extreme Mech. Lett.* **6**, 45-51 (2016).

D. Yu, K. An, X. Chen, H. Bei, "Phase-specific deformation behavior of a NiAlCr(Mo) lamellar composite under thermal and mechanical loads," *J. Alloys Compd.* **656**, 481-490 (2016).

Y. Z. Xia, Y. F. Gao, G. M. Pharr, H. Bei, "Single versus successive pop-in modes in nanoindentation tests of single crystals," *J. Mater. Res.* **31**, 2065-2075 (2016).

Y. F. Gao, H. Bei, "Strength statistics of single crystals and metallic glasses under small stressed volumes," *Prog. Mater. Sci.* **82**, 118-150 (2016).

Z. Sun, G. Song, T. A. Sisneros, B. Clausen, C. Pu, L. Li, Y. F. Gao, P. K. Liaw, "Load partitioning between the bcc-iron matrix and NiAl-type precipitates in a ferritic alloy on multiple length scales," *Sci. Rep.* **6**, 23137 (2016).

H. Yang, Y. Chen, H. Bei, C. R. dela Cruz, Y. D. Wang, K. An, "Annealing effects on the structural and magnetic properties of off-stoichiometric Fe-Mn-Ga ferromagnetic shape memory alloys," *Mater. Des.* **104**, 327-332 (2016).

Z. Zhang, H. Sheng, Z. Wang, B. Gludovatz, Z. Zhang, E. P. George, Q. Yu, S. X. Mao, and R. O. Ritchie, "Dislocation mechanisms and 3D twin architectures generate exceptional strength-ductility-toughness combination in CrCoNi medium-entropy alloy," *Nature Comm.* **8**, 14390 (2017).

C. L. Tracy, S. Park, D. R. Rittman, S. J. Zinkle, H. Bei, M. Lang, R. C. Ewing & W. L. Mao "High pressure synthesis of a hexagonal close-packed phase of the high-entropy alloy CrMnFeCoNi," *Nature Comm.* **8**, 15634 (2017).

K. V. S. Thurston, B. Gludovatz, A. Hohenwarter, G. Laplanche, E. P. George, R. O. Ritchie, "Effect of temperature on the fatigue-crack growth behavior of the high-entropy alloy CrMnFeCoNi," *Intermetall.* **88**, 65-72 (2017).

W. Skrotzki, A. Pukenas, B. Joni, E. Odor, T. Ungar, A. Hohenwarter, R. Pippan, E. P. George, "Microstructure and texture evolution during severe plastic deformation of CrMnFeCoNi high-entropy alloy," *IOP Conf. Series: Materials Science and Engineering* **194** 012028 (2017).

V. Maier-Kiener, B. Schuh, E. P. George, H. Clemens, A. Hohenwarter, "Nanoindentation testing as a powerful screening tool for assessing phase stability of nanocrystalline high-entropy alloys," *Mater. Des.* **115**, 479-485 (2017).

V. Maier-Kiener, B. Schuh, E. P. George, H. Clemens, A. Hohenwarter, "Insights into the deformation behavior of the CrMnFeCoNi high-entropy alloy revealed by elevated temperature nanoindentation," *J. Mater. Res.* **32**, 2658-2667 (2017).

K. Jin, Y. F. Gao, H. Bei, "Intrinsic properties and strengthening mechanism of monocrystalline Ni- containing ternary concentrated solid solutions," *Mater. Sci. Eng. A* **695**, 74-79 (2017).

J. Miao, C.E. Slone, T.M. Smith, C. Niu, H. Bei, M. Ghazisaeidi, G. M.Pharr, M. J. Mills, "The evolution of the deformation substructure in a Ni-Co-Cr equiatomic solid solution alloy," *Acta Mater.* **132**, 35-48 (2017).

G. Song, Z. Sun, L. Li, B. Clausen, S.Y. Zhang, Y.F. Gao, P.K. Liaw, "High temperature deformation mechanism in hierarchical and single precipitate strengthened ferritic alloys by in situ neutron diffraction studies," *Sci. Reports*, **7**, 45965 (2017).

Atomic Scale Computational and Experimental Investigation of Twinning Mechanisms in HCP Systems

Maryam Ghazisaeidi, Assistant professor, Materials Science and Engineering, Ohio State University (Co-PI: Michael J. Mills, Ohio State University)

Program Scope

The overarching goal of this project is to understand the fundamental reasons underlying different twinning behavior of various hcp metals by comparing twin nucleation and growth mechanisms in these systems. Of particular interest is the effect of alloying on twin nucleation and growth in Ti alloys. This project has three major thrusts: (1) studying twin nucleation as a result of slip transfer at the grain boundaries, using molecular dynamics/statics calculations, (2) quantifying the effect of Al on twin growth in Ti alloys, using *ab initio* calculations and experiments and (3) quantifying oxygen effects on twinning behavior of Ti through *ab initio* calculations and experiments. In this presentation we will mainly focus on thrust (3). We use density functional theory (DFT) to study the structure of the Ti (10-12) twin boundary, and identify all interstitial sites at and around the twin boundary. We then calculate the site energies, as wells as the migration barrier for oxygen to jumps between different sites. Finally, using an exact solution to the master equation for diffusion, we translate the atomic jump rates to the diffusivity near the twin boundary. Our results predict enhanced mobility of O near the twin boundary, facilitating the segregation of oxygen to the twin boundary. This prediction is confirmed experimentally.

Recent Progress

Figure 1 shows the supercell used in our DFT calculations. We used a double-twin-boundary geometry to take advantage of the periodic boundary conditions in the direction perpendicular to the twin. In bulk Ti, O has the lowest energy in octahedral sites and is stable also in hexahedral and crowdion sites. Presence of the twin boundary break the symmetry of the crystal resulting in new interstitial sites. We identified all such sites in and around the twin boundary and in adjacent layers. The atomic layers are divided into 4 regions (L1-L4) according to their distance from the twin boundary, where the bulk geometry is retrieved in L4. Previous DFT calculations by Wu and Trinkle [1] had shown that tetrahedral sites are not stable for O in Ti and relax to the hexahedral sites. Notable new sites around the twin geometry are (1) octahedral sites at the boundary that are more attractive than bulk and (2) stable tetrahedral sites in the first layer.

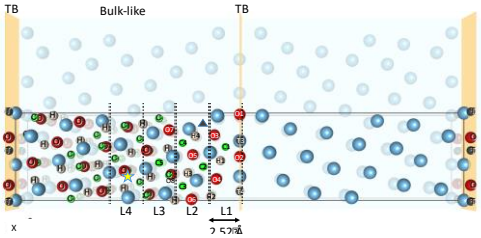

Figure 1 Octahedral, hexaderal and crowdion sites for O near twin boundary. Away from the boundary bulk geometry is retrieved.

Next we calculated the energy barrier for O to jump between various interstitial sites, shown in **Figure 2.** Transition state searches were conducted using the Climbing Image Nudged Elastic band method CI-NEB [2]. **Figure 2**, shows these energy barriers as a function of distance from the twin boundary. The solid line shows the corresponding barriers for O in bulk Ti. First, note that various jump barriers away from the twin agree well with the bulk values, however, the barriers are significantly lower in L1 region in the vicinity of the twin boundary. This is particularly important in case of direct jumps between octahedral sites; in bulk Ti, the barrier for these types of jumps is about a 1 eV higher than the o-h or o-c jumps, suggesting that direct o-o jumps are unlikely. On the other hand, direct o-o jump barriers are of the same order as the o-h or o-c jumps around the twin boundary. This suggests the possibility of an additional network of direct jumps between octahedral sites for O.

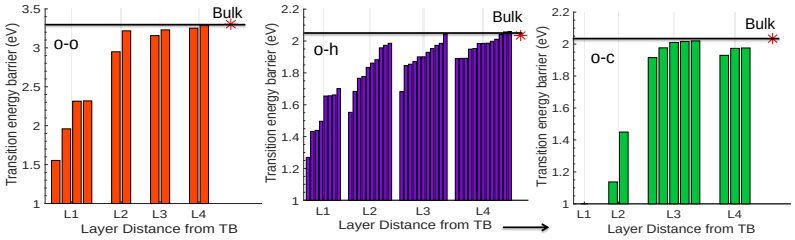

Figure 2 Energy barrier for Octahedral-Octahedral, Octahedral-hexahedral and Octadehdral-Crowdion jumps as a function of distance from the boundary. The solid line shows corresponding barriers in bulk.

Existence of additional interstitial sites, and lower migration barriers around the twin boundary imply higher mobility for O interstitials near twin boundary. We used an analytical approach to obtain the diffusivity of O from DFT values for site energies and transition state energy barriers. This approach is based on an exact solution of the diffusion master equation [3]. **Figure 3** shows the diffusion coefficient as a function of temperature parallel and perpendicular to the twin plane. Bulk diffusivity is also included for comparison. Activation barrier for diffusion is reduced around the twin boundary. Bulk activation barrier of about 2.0 eV is in good agreement with previous DFT predictions and experiments [1]. These results show an increased mobility for O interstitials near the twin boundary, contrary to previous arguments based solely on the crystallographic considerations of octahedral sites in bulk Ti.

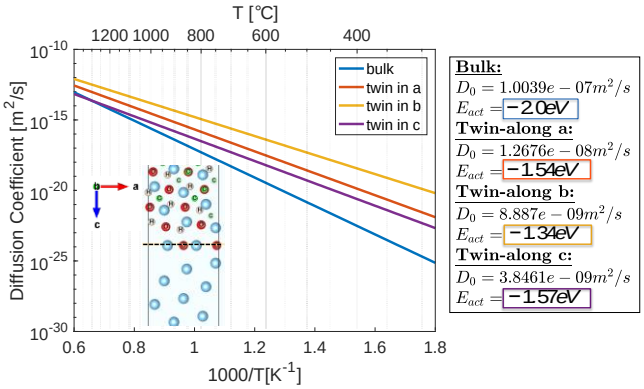

Figure 3 Diffusivity of O along different directions near twin boundary and bulk.

Our results show enhanced diffusivity of O interstitials at the $(10\bar{1}2)$ twin boundary, suggesting the segregation of O to the twin boundaries. This prediction is confirmed experimentally by elemental mapping at the matrix/twin boundary. **Figure 4** shows the

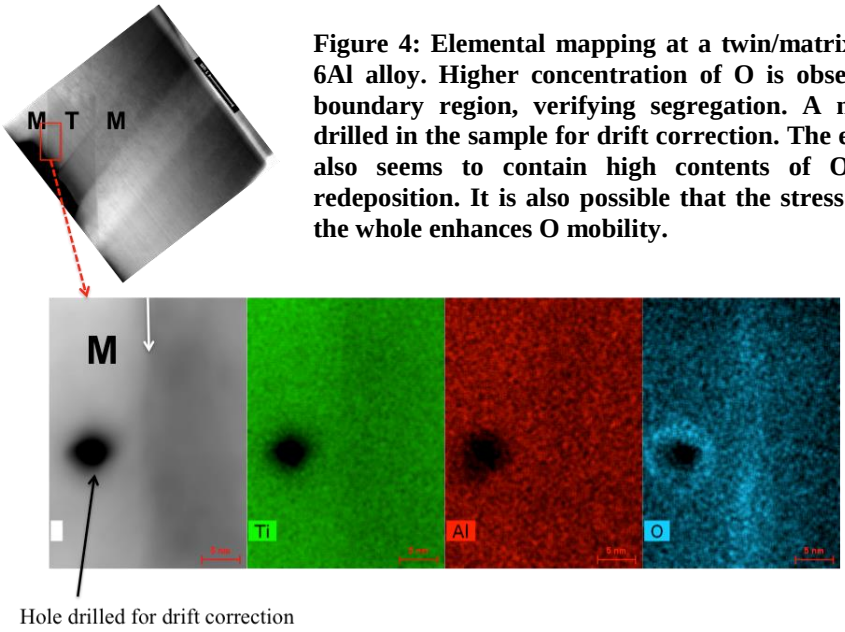

Figure 4: Elemental mapping at a twin/matrix interface in Ti-6Al alloy. Higher concentration of O is observed at the twin boundary region, verifying segregation. A nanoscale hole is drilled in the sample for drift correction. The edge of this whole also seems to contain high contents of O, possibly from redeposition. It is also possible that the stress concentration at the whole enhances O mobility.

elemental maps near an identified twin boundary in a Ti-6Al alloy. Enhanced concentration of oxygen is evident at the twin boundary.

Future plans:

We predicted and confirmed the segregation of O interstitial to the twin $(10\bar{1}2)$ twin boundary in Ti. Our next hypothesis is that, once O segregates to the boundary, it will pose an obstacle to further motion of the twin front; higher stresses are required to move the twin boundary, causing reduced growth under constant loading condition or "strengthening" of the twinning mode. Nie et al have shown the periodic segregation of substitutional solutes to the $(10\bar{1}2)$ win boundary in Mg and demonstrated the pinning effect of segregation on growth of this twinning mode [4]. From the theoretical point of view two modes can be envisioned for twin growth in hcp systems (1) glide of the twinning dislocations (disconnections) on the twin plane which advances one side of the boundary with respect to the other by the step height character of the disconnection and (2) lateral growth by formation of islands (twinning dislocation loops) on already existing boundaries. Segregation of solutes to a subgroup of interstitial sites in or around the boundary affects both. We will calculate the pinning stress that segregated O interstitials exert on both modes of twin growth. Next direction is quantifying the effect of Al and possible short range order formation on twin nucleation and growth in Ti-Al alloys.

Refernces:

[1] H. H. Wu and D. R. Trinkle, the diffusion through interpenetrating pathways: Oxygen in Titanium, Physical Review Letters (107) 045504 (2011)
[2] G. Henkelman, B. P. Uberuaga, Hannes Jonsson, J. Phyc. Chem (113) 9901 (2000)

[3] D. R. Trinkle, Philos. Mag. **96**, 2714-2735 (2016)
[4] J. F. Nie, Y. M. Zhu, J. Z. Liu and X. Y. Fang, Periodic segregation of solute atomsin fully coherent twin boundaries, Science, (24) 957-960 (2013).

Publications:

1. M. S. Hooshmand, M. J. Mills and M. Ghazisaeidi, Atomistic modeling of dislocation interactions with twin boundaries in Ti, Modelling and Simulation in Materials Science and Engineering, 25 (4), 045003
2. M. S. Hooshmand, G. B. Viswanathan, M. Mills and M. Ghazisaeidi, "Diffucion of oxygen near Ti (10-12) twin boundary", to be submitted.

A Fundamental Study on the Link between Mechanical Properties and Atomic-level Microstructure in Nano-sized Metallic Glasses

Julia R. Greer, Principal Investigator, California Institute of Technology

Program Scope

This project seeks to gain a fundamental understanding of the effects of atomic-level microstructure in metallic glasses on its strength and deformability and will offer new directions towards our understanding of the mechanical behavior of amorphous metals. The proposed work is carried out via nano-mechanical quasi-static and damping experiments, microstructural analysis, and modeling. Efforts are dedicated to investigating the effects of deposition technique on the mechanical response of nano-sized metallic glasses and to establish the link between the atomic-level detail and internal energy state with deformability, ductility, damping, and failure strength. We are performing nano-tensile experiments on samples with dog-bone shaped geometries with dimensions ~500nm and mechanical damping experiments on metallic glass nano-cantilevers. These samples are fabricated by sputtering and post-annealing processing followed by lithography to produce a wide range of dimensions, initial free volume distributions and energy states. All nano-mechanical specimens are subjected to different degrees of annealing post-deposition to map a parameter space for the mechanical and microstructural investigations. Experimentally determined stress-strain relationships are enhanced by *in-situ* SEM observations coupled with X-ray Synchrotron experiments performed at Argonne National Lab. Atomistic simulations (Molecular Dynamics) are performed to quantify the free volume distribution and mechanical properties of experimentally studied samples. These efforts promise to provide a new step in our understanding of mechanical properties of amorphous metals.

Recent Progress

We investigated the mechanical behavior and atomic-level structure of glassy Zr-Ni-Al nano-tensile specimens with widths between 75 and 215 nm. We focused our studies on two different energy states: (1) as-sputtered and (2) sputtered then annealed below the glass transition temperature (*Tg*). In-situ tensile experiments conducted inside a scanning electron microscope (SEM) revealed substantial tensile ductility, in some cases reaching >10% engineering plastic strains, >150% true plastic strains, and necking down to a point during tensile straining in specimens as wide as ~150 nm. We found the extent of ductility to depend on both the specimen size and the annealing conditions. Using molecular dynamics (MD) simulations, transmission electron microscopy (TEM), and synchrotron x-ray diffraction (XRD), we explained the observed mechanical behavior through changes in free volume as well as short- and medium-range atomic-level order that occur upon annealing. This work demonstrates the importance of carefully choosing the metallic glass fabrication method and post-processing conditions for

achieving a certain atomic-level structure and free volume within the metallic glass, which then determines the overall mechanical response. An important implication of these results is that sputter deposition may be a particularly promising technique for producing thin coatings of metallic glasses with significant ductility, enabled by the high level of disorder and excess free volume associated with the sputtering process.

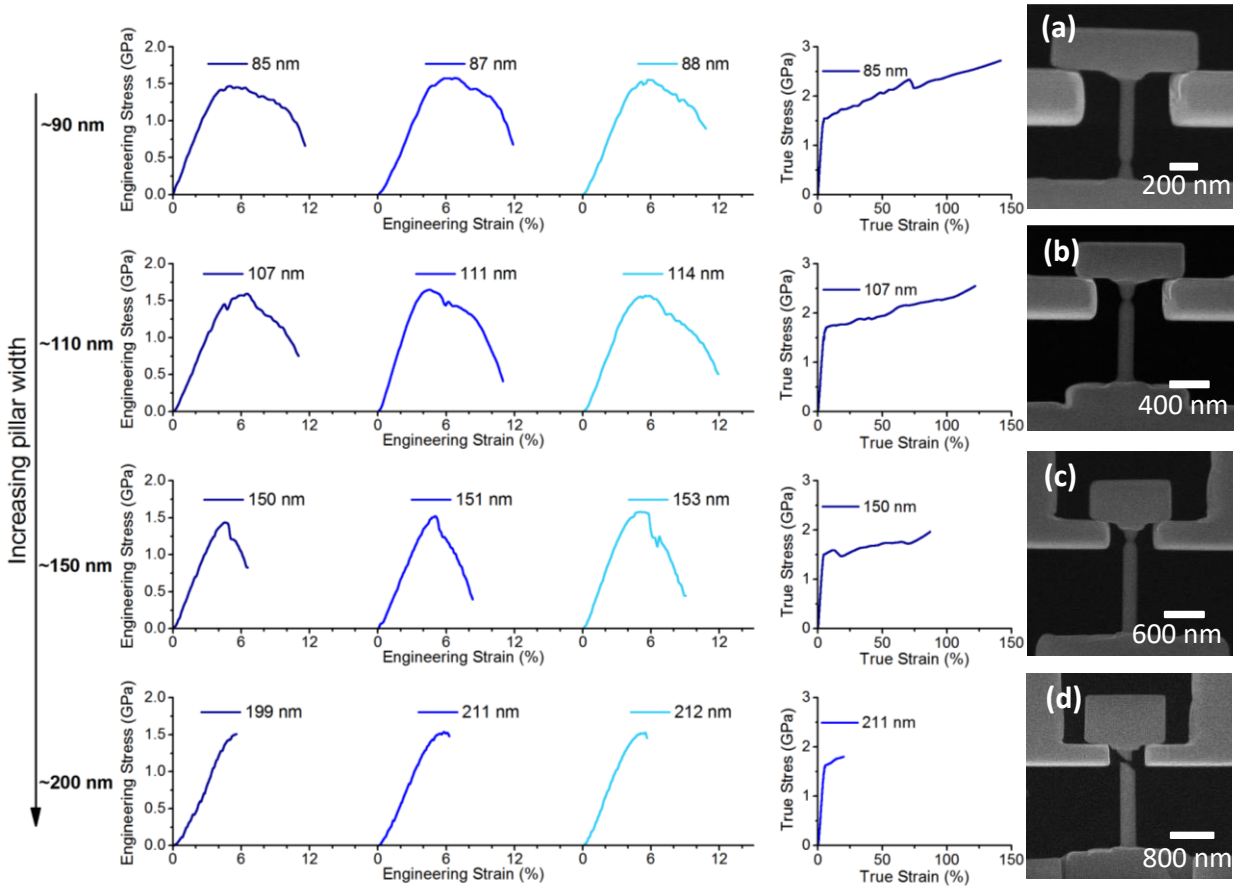

Figure 1. Uniaxial tensile experiments on the as-sputtered Zr-Ni-Al metallic glass samples, including **(left)** engineering stress-strain data, **(center)** true stress-strain data, and **(a-d)** SEM images from in-situ videos around the time of sample failure. The data is grouped by specimen size with ~90 nm wide specimens in the top row, ~110 nm wide specimens in the top-middle row, ~150 nm wide specimens in the bottom-middle row, and ~200 nm wide specimens in the bottom row.

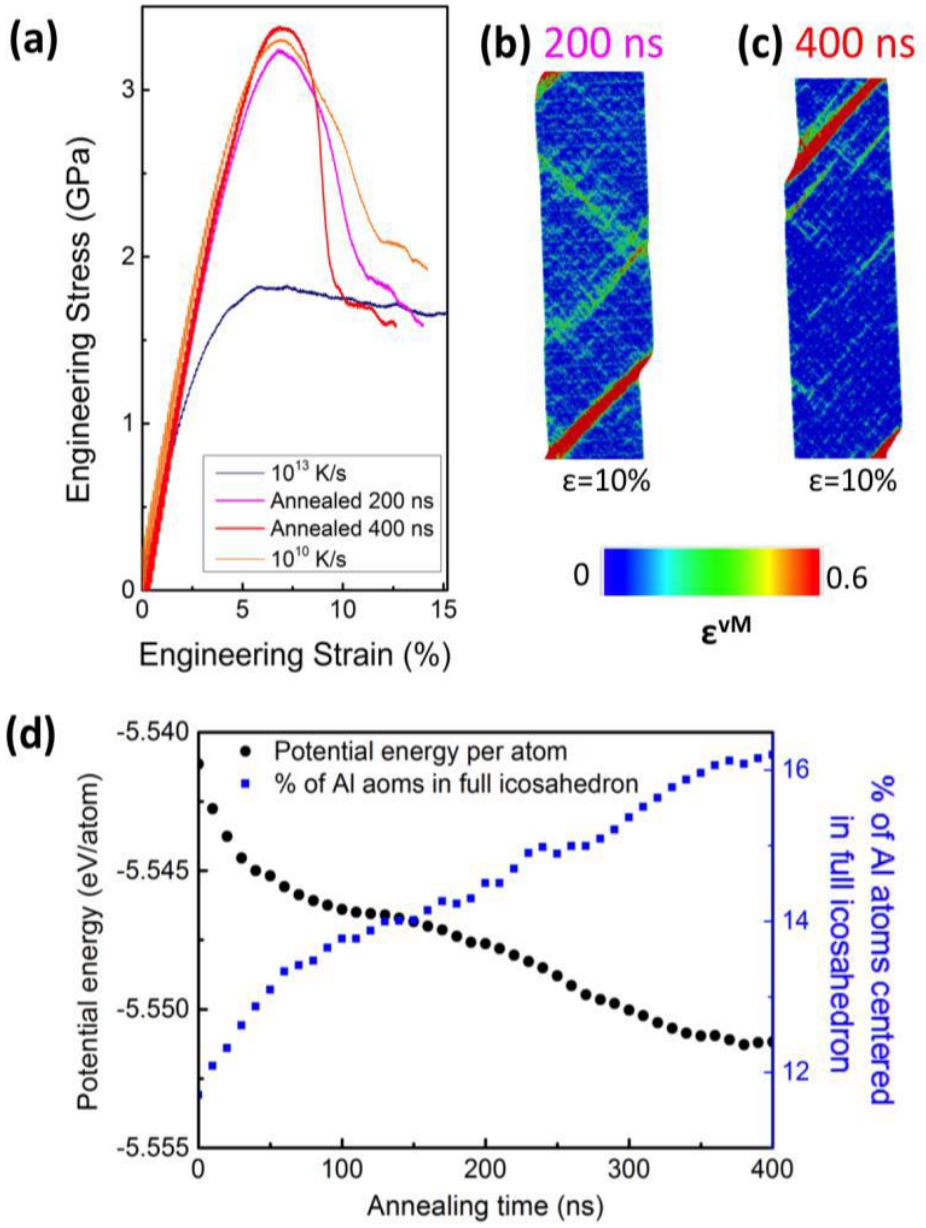

Figure 2. MD simulations on the effect of annealing on the mechanical behavior and atomic structure of Zr-Ni-Al metallic glass. Specimens have diameters of 40 nm and heights of 120 nm. The annealing was conducted at T=850K (80% of simulated Tg). (a) Tensile engineering stress-strain response of the initial as-quenched sample formed with a cooling rate of 1013 K/s, after annealing for 200 ns, after annealing for 400 ns, and for comparison the sample formed with a cooling rate of 1010 K/s. (b-c) Visualization of atomic von Mises shear strains of the samples annealed for (b) 200 ns and (c) 400 ns. (d) Structural evolution of the metallic glass during annealing at 850 K as measured by the average atomic potential energy (PE) of the system (left axis) as well as the fraction of Al-centered full-icosahedra clusters (right axis).

Future Plans

These initial efforts under the auspices of this program demonstrated the "smaller is more ductile" size effect present in Zr-Ni-Al metallic glass nanopillars, which exhibited substantial necking for certain nanopillar sizes. Importantly, we discovered that it was not only the sample size that influenced the necking behavior but also the processing conditions. Samples in an as-sputtered state exhibited substantially more ductility than those in an annealed state; and

synchrotron XRD revealed a significant increase in short- and medium-range order upon annealing, thereby linking the state of atomic order in a metallic glass with its ductility.

Future efforts will involve further characterization of sputtered metallic glasses (Ni-Al-Zr) in terms of correlating their microstructure with mechanical properties (specifically, ductility, deformability and strength) and density. New efforts will be made to measure absolute density using cantilever damping experiments, which we have not performed before. These measurements will provide further fundamental insights into the microstructure of metallic glasses as a function of processing conditions and will link it to the ensuing mechanical properties.

References and Publications

1. R. Liontas, M. J. Zadeh, Q. Zeng[c], Y.-W. Zhang, W. L. Mao, J. R. Greer "Extreme tensile ductility in sputtered Zr-Ni-Al nano-sized metallic glasses" ***Acta Mater.*** **118**, 270-285 (2016)

Nanoscale characterization of intragranular and intergranular deformation mechanisms

Kevin J. Hemker
Departments of Mechanical Engineering and Materials Science and Engineering,
Johns Hopkins University, 3400 N Charles St., Baltimore MD 21218. hemker@jhu.edu

Program Scope

Enabled by rapid advances in computational horsepower and ever-increasing model sophistication, multi-scale modeling can be used to illuminate the complex interplay between material processing, structure and properties in fundamentally new ways, but doing so requires quantitative microstructural information for both model input and validation. Historical approaches to microstructural characterization provide volume-average representations of the material through microstructural parameters such grain size. While these approaches are of great utility, it is clear that many important problems in materials science require a more sophisticated representation of the underlying microstructure. This demand for meaningful heterogeneous representations of material microstructures and properties is further compounded by the need to benchmark models at length scales that are appropriate for the phenomena being modeled. Empirical models relating macroscopic properties (e.g. yield strength) to average microstructural parameters (e.g. inverse square root grain size) have served us well, but the future lies in being able to predict local phenomena such as the coalescence of dislocation populations within grains or the nucleation of twins or voids at grain boundaries. Such predictions require detailed understanding of both local structure and the local stress state.

Having developed experimental tools to characterize the small-scale and scale-specific mechanical behavior of MEMS materials and nanocrystalline thin films, the current study is aimed at quantifying, locally and at the nanoscale, the influence that stress and microstructure have on the deformation behavior of polycrystalline metals and alloys. The activities undertaken here offer unique opportunities to advance experimental capabilities for both nanoscale characterization and benchmarking. Two new TEM-based techniques, automated crystal orientation mapping (ACOM) and elastic strain mapping made possible by the recently released Topspin AutoSTRAIN acquisition & analysis module, offer the opportunity to map lattice distortions, stress concentrations, and defect populations with unprecedented spatial resolution. Successful application of these techniques will offer a unique complement to more established diffraction techniques and provide the local details needed to underpin predictive physics-based constitutive models of twinning and plasticity. The current study involves in situ and post mortem characterization of polycrystalline ceramics, metals, alloys and thin films deformed to varying degrees. High-resolution maps are being collected and used to elucidate nanoscale details such as: the role of grain orientation and grain boundary misorientation; local stress concentrations in nascent twin formation; and the redistribution of local stress during grain boundary migration, twinning, and dislocation pileups.

Recent Progress

In a series of experiments that combined in situ straining with TEM-based automated crystal orientation mapping (ACOM) we documented microstructural evolution of with nanoscale resolution at sequential stages of deformation. Orientation maps of freestanding annealed nanocrystalline Cu films have been collected, and the resultant datasets provide direct measures of grain size, shape and orientation as well as local grain boundary character and position at various stages of applied strain. Although a global increase in grain size was not observed, numerous local examples of stress-driven grain boundary and twin boundary migration were recorded and studied. Detailed analysis of the misorientation of mobile and immobile grain boundaries provided clear experimental evidence that a broad range of grain boundaries are susceptible to stress-assisted migration but that there is not a dominant or magic grain boundary that triggers grain growth. That is to say that no general correlation between grain boundary misorientation and mobility was detected (Fig. 1). Incoherent ∑3 boundaries were observed to be significantly more mobile than coherent ∑3 twin boundaries. Nevertheless, deformation twins were observed to nucleate and grow from grain boundaries and triple points.

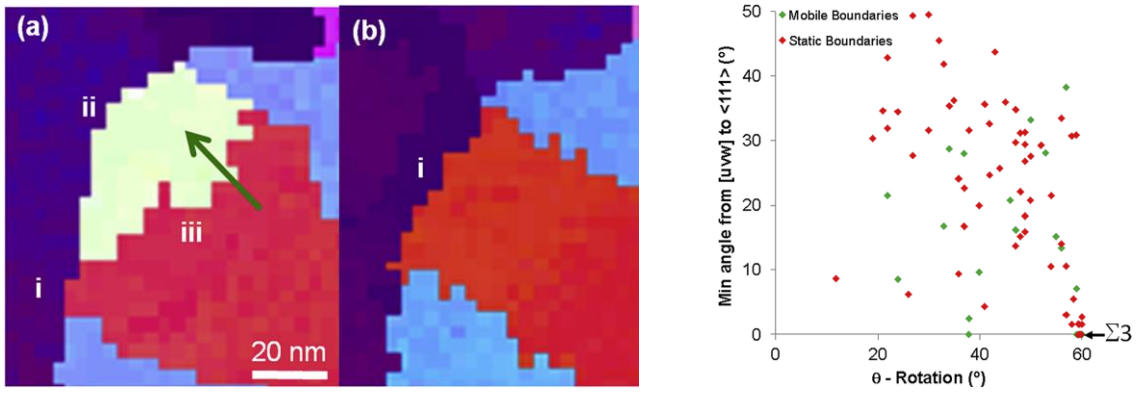

Figure 1: *Comparison orientation maps with a straining increment between showing annihilation of a smaller grain upon straining. Plot comparing axis-angle defined misorientations of mobile and static grain boundaries. No clear correlation between misorientation and grain boundary mobility was uncovered. [1]*

The as-deposited Cu films were found to contain multiple grains through the film thickness and were not amenable to ACOM orientation mapping, but films annealed for 1 hour at 300ºC exhibited modest grain growth and were well suited for ACOM. The grain size increased from 29 ± 14 nm to 57 ± 22 nm and the fraction of twin-containing grains increased from 0.18 to 0.70. Thus, this thermally-assisted grain growth provided an experimental compliment simulations of twin junction formation by Srolovitz [2]. Our experimental observations of twin and twin junction formation (Fig. 2) have been directly compared with the MD predictions in a way that was not been previously possible for nanocrystalline materials. These comparisons show that the types and relative frequency of twin junctions predicted to appear upon annealing by MD simulations [2] are experimentally observed [3]. The in situ ACOM maps also indicate that the twin junctions that are formed during thermal annealing can be removed upon straining.

More recently, we have focused on utilizing automated nanobeam electron diffraction to locally measure elastic strains in polycrystalline metals and ceramics. We have successfully measured baseline strain resolutions in polycrystalline films that are comparable to that reported by the developers of the technique for single-crystalline silicon. Beyond this, we have sought to measure elastic strains near defects and to correlate the measured elastic strain with the strain calculated by other means. Early examples include grain boundary facets in polycrystalline boron carbide and dislocations and low-angle boundaries in magnesium.

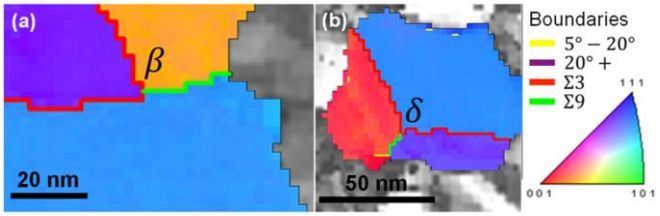

Figure 2: *Orientation maps of grains and specific twin junctions. The grain shown in (a) contains a β junction, and the grain shown in (b) contains a δ junction. [3]*

Previous to its acquisition at JHU, the Topspin automated nanobeam electron diffraction (NBED) strain measurement system was developed for, and used exclusively to study, semiconductor materials. The strains near epitaxial interfaces were of particular interest, and the developers of the technique quote a standard deviation of 0.02%, which corresponds to a strain resolution of 0.08% assuming a normal distribution and a ±2σ (95%) confidence threshold. The Si devices typically studied via Topspin are particularly well-suited for the technique because there is a very large region with the same orientation that can be used to obtain a strain-free reference, they are nearly defect-free, and the epitaxial strain is very high. We first set out to determine if similar strain resolution can be obtained for polycrystalline samples, where it is harder to identify a strain-free reference, and where microstructural defects (e.g. boundaries, dislocations) impose measurable amounts of strain on the surrounding crystalline regions.

We started with a polycrystalline boron carbide sample that contained many precipitate and defect free grains. A strain map recorded from the center of such a grain provided a good strain baseline. Using a step size of 10 nm and a precession angle of 0.8°, a strain map was calculated from a rectangular region in the center of the grain, using a SAED pattern near the center of the scan as the reference. In total, 16,824 points were measured and a histogram of the strain values plotted. Assuming a normal distribution, 95% of strain values fell within ±2σ which corresponds to a range of 0.100%. This corresponds well to the reported strain resolution (0.1%) values for conventional NBED and the strain resolution reported by the Topspin developers. Similar experiments, performed on rolled and annealed Cu sheets yielded strain resolution of 0.156%, which is slightly higher, likely due to the retention of dislocations after the anneal. Nevertheless, the results are encouraging for the study of metallic polycrystalline samples with this technique.

The boron carbide sample also provided us with a quantitative benchmark with which to test the ability of the Topspin technique to measure inhomogeneous strains in polycrystalline samples. There is a significant difference between the thermal expansion of the a and c axis in rhombohedral boron carbide, and the difference in orientation between neighboring grains results

in residual elastic stresses and strains upon cooling. Strain maps were collected to determine (1) if the elastic strains created by thermal mismatch could be detected above the strain baseline we determined for boron carbide and (2) if the sign and magnitude of the measured strains correlate with what is expected from the thermal mismatch.

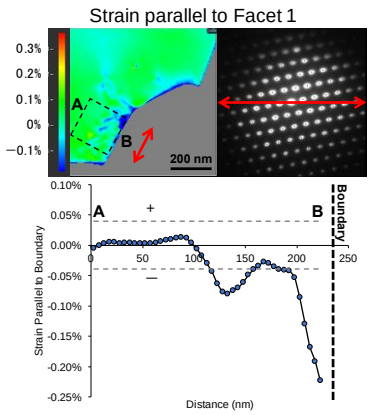

Figure 3: *Elastic strain map near a GB facet. Plot of the evolution of the strain as the GB is approached. The strain is clearly compressive and greater than 2σ.*

A map of the elastic strain near one GB facet is shown in Fig. 3. The strain for this facet goes compressive near the GB, and similar maps for the other two facets show tensile and no elastic strains. These measurements show that, as expected, elastic strains of differing sign and magnitude develop and are dependent on the misorientation of the grains and the geometry of the facets. A simple model was developed to predict the strain in boron carbide bicrystals for various grains and facet orientations, and the predicted trends are in good agreement with the measurements. Additional observations of elastic stress fields around low-angle boundaries and individual dislocations have also been collected and are being analyzed.

Future Plans

We are collecting stress maps around dislocations in Cu and twins in Mg and are working to benchmark those observations, and by extension the Topspin technique, with quantitative models. We recently reported on the synthesis of NiMoW films with sputter deposition that results in fully dense, <111> textured films with oriented nanotwins and exhibit ultra-high tensile strengths exceeding 3 GPa, highly anisotropic plastic behavior, exceptional thermal and mechanical stability, low CTE and high electrical conductivity [4]. This unusual balance of properties arises from its textured and nanotwinned microstructure, and we intend to employ orientation and stress mapping to better understand and model this hierarchical nanoscale material.

References

[1] PF Rottmann, KJ Hemker, Experimental quantification of mechanically induced boundary migration in nanocrystalline copper films, *Acta Materialia* **140** (2017) 46-55.

[2] SL Thomas, AH King, DJ Srolovitz, When twins collide: Twin junctions in nanocrystalline nickel, *Acta Materialia* **113** (2016) 301-310.

[3] PF Rottmann, KJ Hemker, Experimental observations of twin formation during thermal annealing of nc copper films using orientation mapping, *Scripta Materialia* **141** (2017) 76-79.

[4] GD Sim, JA Krogstad, KM Reddy, KY Xie, GM Valentino, TP Weihs, KJ Hemker, Nano-twinned metal MEMS films with unprecedented strength and stability, *Science Adv.* **3** (2017) e1700685.

Publications

Paul F Rottmann, Kevin J Hemker, Experimental quantification of mechanically induced boundary migration in nanocrystalline copper films, *Acta Materialia* **140** (2017) 46-55.

Paul F Rottmann, Kevin J Hemker, Experimental observations of twin formation during thermal annealing of nanocrystalline copper films using orientation mapping, *Scripta Materialia* **141** (2017) 76-79.

David Raciti, Liang Cao, Kenneth J. T. Livi, Paul F. Rottmann, Xin Tang, Chenyang Li, Zachary Hicks, Kit H. Bowen, Kevin J. Hemker, Tim Mueller, Chao Wang, Low-Overpotential Electroreduction of Carbon Monoxide Using Copper Nanowires, *ACS Catal.* **7** (2017) 4467−4472.

Paul F Rottmann, Kevin J Hemker. In Situ Analysis of the Fracture Behavior of Nanocrystalline Copper Using Precession-Assisted Crystal Orientation Mapping. *Microscopy and Microanalysis* **21**(S3) (2015) 273-274.

Computational and Experimental Investigation of Cryogenic Grain Boundary Motion for Enhanced Mechanical Properties

Eric R. Homer
Department of Mechanical Engineering, Brigham Young University, Provo, UT, 84602
eric.homer@byu.edu

Program Scope

The major goal of the project is to determine the feasibility of cryogenic processing to obtain enhanced mechanical properties by influencing the microstructural network of grain boundaries (GBs). GBs have a significant influence on numerous material properties, including strength and ductility. Thermomechanical processing frequently modifies these material properties by altering GB networks through the motion of GBs. This processing is facilitated by the thermally activated motion of large populations of GBs, making it difficult to control the resulting microstructure. In contrast, at cryogenic temperatures, GB motion has been observed in a subset of select GBs [1-4]. This difference in GBs that are mobile at cryogenic temperatures presents a transformational opportunity to create different microstructural networks that have enhanced strength and ductility.

The specific goals and tasks associated with the project are to (i) observe and measure cryogenic GB mobilities and mechanisms, (ii) identify crystallographic trends of cryogenically mobile GBs, and (iii) determine cryogenic processing-structure-property relationships. The work combines simulation, which can investigate the atomic mechanisms that would enable cryogenic GB migration, with experiments, which can provide evidence of the phenomena observed in simulations and other published work.

Recent Progress

Significant progress has been made in understanding the mechanisms associated with non-thermally activated GB motion, that would enable cryogenic processing. In the past year, work has been focused on (1) the role of crystallography and the mechanisms associated with migration of incoherent twin GBs at cryogenic temperatures, (2) CSL pinning and ordered atomic motions associated with non-thermally activated mobility in Σ7 and Σ9 GBs, (3) discovering the building blocks of GB systems using machine learning and the role of those building blocks in non-thermally activated mobility, and (4) proof of concept testing for direct observation of cryogenic grain boundary motion in collaboration with Peter Hosemann at UC-Berkeley. Each of these efforts is described in additional detail in the paragraphs below.

(1) In simulations, some incoherent twin grain boundaries (GBs) have demonstrated a remarkable ability to migrate at cryogenic temperatures. With twin grain boundaries playing an important role in numerous materials, it is important to understand their behavior across the full range of possible grain boundary plane orientations. This work examined the migration of 41

computed Σ3 nickel grain boundaries over a range of temperatures. The boundary plane orientation appears to play the determining role in the nature of the migration observed, which is evident when the data are plotted in the fundamental zone of possible boundary plane orientations, as shown in Figure 1. GBs whose boundary plane lie between $(1\,1\,1)$ and $(2\,\bar{1}\,\bar{1})$ exhibit thermally activated migration and the atoms do not move in a coordinated fashion. The remaining GBs, including the $(1\,0\,\bar{1})$ GB, exhibit some form of thermally damped migration. The thermally damped migration is characterized by inverse temperature dependence where the GBs migrate faster at lower temperatures (down to 100 K) and move in a coordinated fashion involving Shockley partial dislocations. The inverse temperature dependence, which is confirmed by random walk simulations, appears to be consistent with dislocation drag, which could be related to the Shockley partial dislocations. At least one GB exhibits mixed mobility trends due to the presence of both thermally activated and thermally damped migration characteristics.

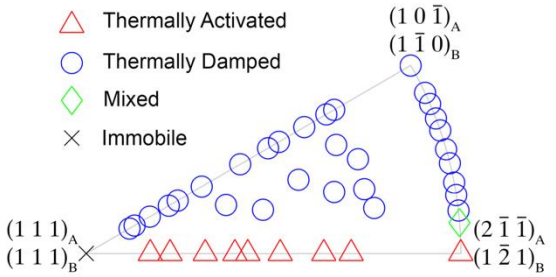

Figure 1 – Plot indicating the role of the boundary plane orientation in determining the grain boundary migration mechanisms for the Σ3 misorientation.

(2) Past molecular dynamics simulations of mobility in Σ7 and Σ9 grain boundaries (GBs) have indicated an ability to migrate at cryogenic temperatures [5], and CSL boundaries have been shown to play a role in cryogenic GB migration at cryogenic temperatures [3,4]. This work examines GB migration in Σ7 and Σ9 nickel bicrystals at temperatures ranging from 100 to 1000 K. For GBs that exhibit non-thermally activated migration, the atomic mechanisms indicate that CSL atoms act as pinning points for GB migration. In essence, there is a two-part mechanism for migration, unpinning of the GB and then fast migration of the GB until it is pinned again [6]. Interestingly, the higher temperatures prolong the pinning and slow the migration, leading to inverse temperature dependence. This mechanism is consistent with previous work [7] and supports the hypothesis of the Σ3 GBs that show an ordered mechanism is a necessary but not sufficient condition for cryogenic GB migration.

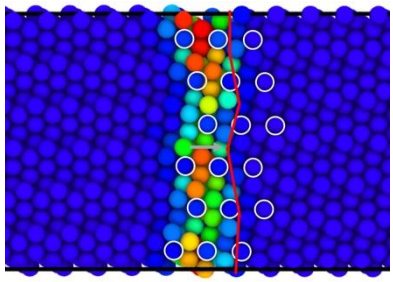

Figure 2 – Depiction of CSL atoms pinning the migration of a Σ7 GB.

(3) The efforts here have been performed in collaboration with Gus Hart and PhD student Conrad Rosenbrock at BYU and with Gábor Csányi at Cambridge University. Machine learning has proven to be a valuable tool to approximate functions in high-dimensional spaces. Unfortunately, analysis of these models to extract the relevant physics is never as easy as applying machine learning to a large dataset in the first place. This effort used a description of atomic systems that generates machine learning representations with a direct path to physical

interpretation. While the work demonstrated its usefulness as a universal descriptor of grain boundary systems, it is widely applicable to atomic systems of any nature. Grain boundaries in crystalline materials are a quintessential example of a complex, high-dimensional system with broad impact on many physical properties including strength, ductility, corrosion resistance, crack resistance, and conductivity. The method uses the smooth overlap of atomic positions (SOAP) to characterize the structure of the GBs [8], and a comparison of local atomic environments leads to a finite set of 'building blocks' that comprise a large dataset of GBs. The machine learning not only provides predictions of various properties, including GB energy and mobility type, but also provides insight into the physical building blocks that influence each of these properties. This opens the way to discover the underlying physics behind a variety of behaviors by understanding which building blocks map to particular properties. In the long run, understanding of these building blocks will allow optimization of materials for desirable behaviors.

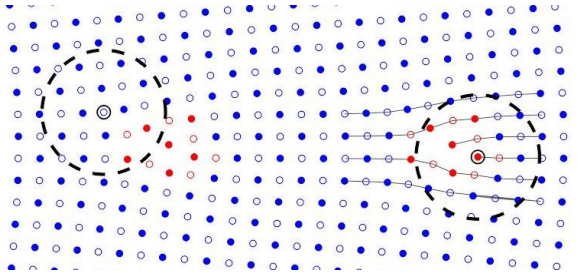

Figure 3 – Atomic structure of a symmetric tilt GB with two of the most important 'building blocks' associated with thermally activated migration identified. The right structure includes an array of edge dislocations while the left structure is a newly identified structure that is very important for thermally activated migration.

(4) Experimental efforts described here have been performed by PhD student David Frazer working under the direction of Peter Hosemann at the University of California, Berkeley. Micropillars created out of ECAP copper, using FIB, have been cooled to -145 ºC using a custom-built device and subjected to compression using a Hysitron PI-85. EBSD is performed prior to and at various loading steps to determine microstructural evolution. Two tests to date have refined the procedures for this attempt at direct observation of cryogenic grain growth. While no viable data has demonstrated the phenomena, the tests serves as evidence that the experimental approach is possible and minor corrections should lead to improved future efforts.

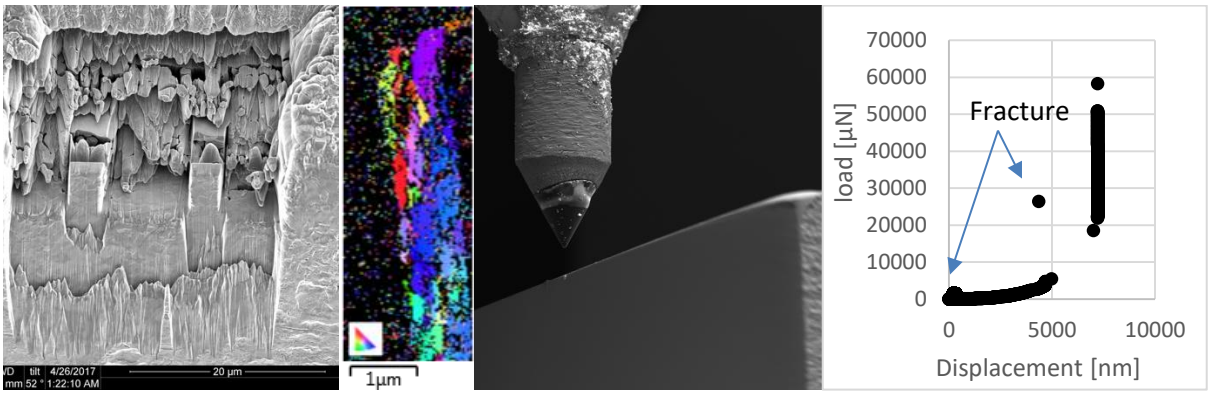

Figure 4 – From left to right the figure shows the micropillars, EBSD performed at cryogenic temperatures, the indentation using the Hysitron PI-85, and the load displacement data from the test.

Future Plans

The first year of the grant has focused heavily on the simulation work. During the coming year, the experimental work will become an important focus. Collaboration with Peter Hosemann will continue, and a new collaboration with Greg Thompson at Alabama will commence. Efforts will also be started to examine cryogenic GB migration at BYU. Simulation work will continue at BYU, with a focus on understanding the building block discovered as part of the machine learning effort. Ongoing discussion with Brad Boyce (Sandia), Khalid Hattar (Sandia), and Greg Thompson (Alabama) ensure that the project efforts remains focused the goal of the work.

References

[1] K. Zhang, J.R. Weertman, J.A. Eastman, The influence of time, temperature, and grain size on indentation creep in high-purity nanocrystalline and ultrafine grain copper, Appl Phys Letters. 85 (2004) 5197–5199.

[2] K. Zhang, J.R. Weertman, J.A. Eastman, Rapid stress-driven grain coarsening in nanocrystalline Cu at ambient and cryogenic temperatures, Appl Phys Letters. 87 (2005) 061921. doi:10.1063/1.2008377.

[3] J.G. Brons, H.A. Padilla II, G.B. Thompson, B.L. Boyce, Cryogenic indentation-induced grain growth in nanotwinned copper, Scripta Mater. 68 (2013) 781–784. doi:10.1016/j.scriptamat.2012.12.026.

[4] J.G. Brons, J.A. Hardwick, H.A. Padilla II, K. Hattar, G.B. Thompson, B.L. Boyce, The role of copper twin boundaries in cryogenic indentation-induced grain growth, Materials Science & Engineering A. 592 (2014) 182–188. doi:10.1016/j.msea.2013.11.005.

[5] E.R. Homer, E.A. Holm, S.M. Foiles, D.L. Olmsted, Trends in grain boundary mobility: Survey of motion mechanisms, Jom. 66 (2014) 114–120. doi:10.1007/s11837-013-0801-2.

[6] F. Ulomek, V. Mohles, Separating grain boundary migration mechanisms in molecular dynamics simulations, Acta Materialia. 103 (2016) 424–432. doi:10.1016/j.actamat.2015.10.021.

[7] C.J. O'Brien, S.M. Foiles, Exploration of the mechanisms of temperature-dependent grain boundary mobility: search for the common origin of ultrafast grain boundary motion, J Mater Sci. 51 (2016) 6607–6623. doi:10.1007/s10853-016-9944-1.

[8] A.P. Bartók, R. Kondor, G. Csányi, On representing chemical environments, Phys Rev B. 87 (2013) 184115. doi:10.1103/PhysRevB.87.184115.

Publications

[1] J.L. Bair, E.R. Homer, *CSL Pinning and Ordered Atomic Motions Associated with Non-Thermally Activated Mobility in Σ7 and Σ9 Grain Boundaries*, Acta Materialia. (2017) under review.

[2] C.W. Rosenbrock, E.R. Homer, G. Csányi, G.L.W. Hart, *Discovering the building blocks of atomic systems using machine learning: application to grain boundaries*, npj Computational Materials. 3 (2017) 29. doi:10.1038/s41524-017-0027-x.

[3] Y.B. Zhang, J.D. Budai, J.Z. Tischler, W. Liu, R. Xu, E.R. Homer, et al., *Boundary migration in a 3D deformed microstructure inside an opaque sample*, Scientific Reports. 7 (2017) 4423. doi:10.1038/s41598-017-04087-9.

[4] J.L. Priedeman, D.L. Olmsted, E.R. Homer, *The role of crystallography and the mechanisms associated with migration of incoherent twin grain boundaries*, Acta Materialia. 131 (2017) 553–563. doi:10.1016/j.actamat.2017.04.016.

Fundamental Study of Fatigue Crack Initiation at Grain and Twin Boundaries in Austenitic Stainless Steel

Josh Kacher
Georgia Institute of Technology

Program Scope

Fatigue damage under cyclic loading conditions is an inherently multiscale process, with defect interactions occurring across hundreds of microns but crack initiation processes occurring at the nanoscale. To understand these fatigue damage processes, experimental approaches that reflect this multiscale behavior are needed. In this project, novel *in situ* scanning and transmission electron microscopy deformation experiments capable of resolving information across length scales, including the evolution of the local defect state and the accompanying stress fields, will be developed. Focused ion beam machining will be used to link the length scales, allowing direct integration of nanoscale-processes with the surrounding mesoscale microstructural and stress state. The objective of this project is to understand the evolution of the defect state leading to fatigue crack initiation with an emphasis on understanding the role of twin and grain boundaries on the crack initiation process. This includes determining what local mechanisms drive the crack initiation process and how damage accumulation and failure initiation is influenced by the surrounding microstructure. The primary material that will be investigated in this research is 316L stainless steel, a broadly-used structural steel alloy, though many of the observed mechanisms are expected to be applicable to a range of engineering alloys.

Dynamic, robust, radiation-resistant ceramics: harnessing thermodynamic and kinetic driving forces

Jessica A. Krogstad
Department of Materials Science and Engineering
University of Illinois, Urbana-Champaign

Program Scope

Porosity is an inherent feature of ceramic materials, which can be difficult to eliminate completely. There are many applications that, instead, capitalize on the relative stability of porous structures at elevated temperatures, ranging from catalysis to filtration, bone scaffolding and thermal barrier coatings [1]. To date, porosity and void evolution within nuclear ceramics–fuels, cladding or waste containment schemes–has remained difficult to characterize and control, making it just one of many deleterious consequences of the extreme thermal, mechanical and irradiative conditions [2]. However, as the mechanisms for radiation damage and recovery within ceramics continue to be clarified [3, 4], one route for additional radiation tolerance may stem from engineered porosity. Numerous strategies aimed at reducing radiation damage involve the incorporation of a high density of defect sinks, typically grain boundaries within single or multi-phase systems [5]. A pore surface is an infinite defect sink, provided that the defects have sufficient mobility to reach it and that the pore itself does not migrate, shrink/coarsen or otherwise drastically change its morphology. Stabilizing a highly porous microstructure, wherein diffusion behavior is significantly altered by both heterogeneous radiation induced defects and strong thermal gradients, requires a more in depth examination of the mechanisms responsible for stabilizing or destabilizing ceramic microstructures under a combination of these conditions.

The *overarching objective* of this project is to establish a class of structural ceramics with enhanced radiation tolerance based on a dynamic microstructure by harnessing the synergistic effects of radiation enhanced diffusion, capillarity and thermally induced mass transport on microstructural evolution. Specifically, we aim to (i) quantify changes in mass transport behavior that may influence the microstructural evolution of ionic/covalent ceramic materials subjected to irradiation (ii) quantify how surface energy and local curvature resulting from porosity may further influence local mass transport behavior (iii) quantify mass transport behavior under large thermal gradients that may further influence microstructural evolution and damage accumulation and (iv) finally to assess the synergistic interactions of these contributing factors.

Recent Progress

The first year of this project has focused on aims (i) and (ii). Specifically, we have begun to quantify changes in mass transport of irradiation-induced defects in the vicinity of certain

microstructural features, namely pores and grain boundaries. Two approaches have been used so far: *ex situ* ion irradiation of nanocrystalline 20YSZ and *in situ* ion irradiation of the same nanocrystalline 20YSZ. To date, both of these techniques have been limited to room temperature so far, but will be extended to elevated temperatures (see Future Plans). Figure 1 provides an example of the *in situ* ion irradiation damage progression in the vicinity of two adjacent pores. There are several qualitative observations that can be immediately extracted from this time series. Given that the contrast changes here arise largely from the build up of radiation-induced point and line defects, the overall damage incurred by the bridging ligament/strut is considerably less than that of the nearby larger grain (lower left corner). Localized strain and bending may also contribute to the contrast changes, which has complicated defect-tracking analyses. However, from preliminary defect tracking analysis we have learned two important lessons. First, images were only collected every 5 minutes during this extended irradiation experiment (9 hours), which seems to be a limitation in that many defects are annihilated during this time span, thus confusing the image analysis algorithms applied. The second key outcome is a function of the specimen geometry. Even though the interpore spacing in this case is only ~300nm, the significant surface area on the top/bottom of the ~200nm thick TEM specimen acts as a more efficient defect sink. This is unavoidable in this experimental configuration; however, we anticipate that a more rapid image acquisition and elevated temperatures to promote lattice diffusion biased by the curvature of the pores will allow us to track defect migration towards pores in future experiments.

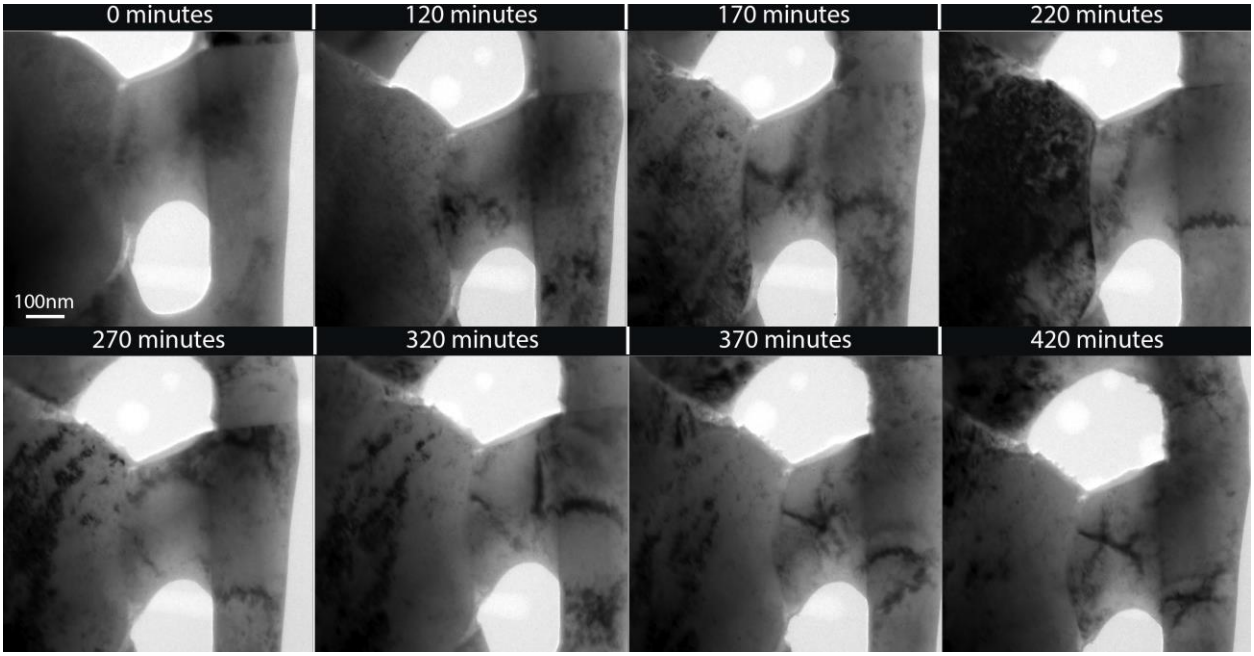

Figure 1 – Time series of in situ (TEM) room temperature ion irradiation (2.8MeV Au, 4 nA, 9 hours) of porous 20YSZ using the I^3TEM at Sandia National Laboratory (in collaboration with Khalid Hattar). This area was selected to highlight a narrow interpore ligament (strut) of approximately 300nm. Compare the constrast changes in the ligament to the larger nearby grains that accumulate more damage before recovery. More complete analysis of the residual defects is underway, as well as defect tracking via image analysis over the course of the exposure.

Ex situ irradiation of bulk 20YSZ pellets has also been conducted with the help of K. Hattar at Sandia National Laboratories. Ceramic pellets with an average grain size of 400nm and 92% of the theoretical density were pre-characterized using microCT at the University of Illinois to identify the position and size of as sintered porosity. Post-irradiation analysis of the microstructures is currently underway.

Future Plans

Over the next year, we plan to continue our efforts to understand the interplay between radiation-induced defects and microstructural features within porous 20YSZ, specifically emphasizing behavior at elevated temperatures. Elevated temperatures are anticipated to not only enhance the lattice diffusivity and accelerate the rates for irradiation-induced defect recombination/annihilation, but may also disrupt microstructurally stabilizing space charge regions near grain boundaries and pores. This later hypothesis will be further explored through post-mortem correlative TEM/APT characterization of specific grain boundaries. Futhermore, we plan to work with Prof. J.M. Zuo (UIUC) to develop a more sophisticated image analysis tool that is more robust against bending and strain induced contrast and enable rigorous defect tracking relative to microstructural features.

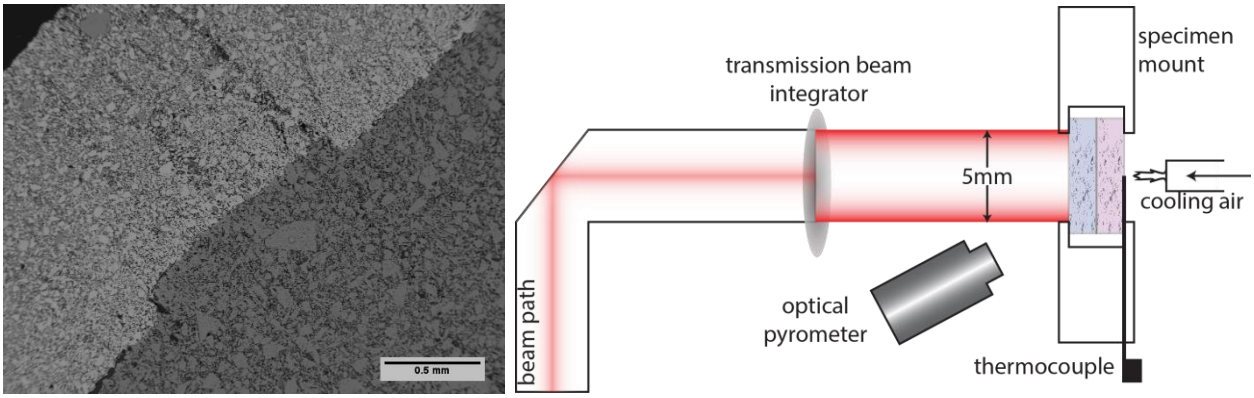

Figure 2 – (a) SEM micrograph of preliminary YSZ/YbSH diffusion couple from which interdiffusion coefficients will be extracted and used as baseline data for future thermal gradient diffusion couples. (b) Schematic of one version of the thermal gradient experimental set up utilizing laser heating. A second proposed set up uses a microheater to reduce thermal shock and minimize sample volume. Currently both configurations are being pursued with insight provided by researchers at UCSB who currently operate a similar laser-based rig.

We have also begun to characterize diffusion couples consisting of yttrium-stabilized zirconia/ytterbium-stabilized hafnia (cf Figure 2a), which will ultimately be studied under an imposed thermal gradient. An in house, thermal gradient rig (cf. Figure 2b) is currently underdevelopment and should be commissioned within the coming year. In following years, this diffusion data and the thermal gradient rig, will be used to study microstructural evolution under strong thermal gradients.

References

[1] P. Colombo, "Engineering porosity in polymer-derived ceramics," *Journal of the European Ceramic Society*, vol. 28, no. 7, pp. 1389–1395, 2008.

[2] D. R. Olander, "Fundamental aspects of nuclear reactor fuel elements," tech. rep., California Univ., Berkeley (USA). Dept. of Nuclear Engineering, 1976.

[3] K. E. Sickafus, H. Matzke, T. Hartmann, K. Yasuda, J. A. Valdez, P. Chodak III, M. Nastasi, and R. A. Verrall, "Radiation damage effects in zirconia," *Journal of Nuclear Materials*, vol. 274, no. 1, pp. 66–77, 1999.

[4] S. Zinkle, V. Skuratov, and D. Hoelzer, "On the conflicting roles of ionizing radiation in ceramics," *Nuclear Instruments and Methods in Physics Research Section B: Beam Interactions with Materials and Atoms*, vol. 191, no. 1, pp. 758–766, 2002.

[5] W. Han, M. J. Demkowicz, N. A. Mara, E. Fu, S. Sinha, A. D. Rollett, Y. Wang, J. S. Carpenter, I. J. Beyerlein, and A. Misra, "Design of radiation tolerant materials via interface engineering," *Advanced materials*, vol. 25, no. 48, pp. 6975–6979, 2013.

Publications

Krogstad, J.A. "Is there room for porosity in nuclear ceramics? What we can learn from dynamic microstructures in extreme conditions." *Ceram. Bull*. 96 (2017) 30-34. **Link**.

Competition and Correlation Among Length Scales: Mesostructure and Mechanical Properties

Peter Collins, Alex King, Richard LeSar (Lead), Mikhail Mendelev, and Ryan Ott
Ames Laboratory

Program Scope

We have developed an integrated experimental and modeling program to examine the underlying mechanisms of plasticity in nanotwinned materials. We create systems with differing twin morphologies and microstructures and characterize their structures using techniques that range from electron microscopy to synchrotron scattering. Mechanical testing of these samples is carried out in a novel tensile strain stage that enables accurate measurements of stress-strain behavior with concurrent *in situ* transmission electron microscopy (TEM) observations of evolving microstructures. We use a temperature-controlled nanoindenter to characterize the thermal dependence of the mechanical properties, from which we can extract activation energies and volumes and identify the deformation mechanisms. The experiments are coupled with a modeling and simulation program that includes atomistics and discrete dislocation simulations. Through the close coupling of experiment and modeling, the program has shed new light on plasticity in nanotwinned materials. Our overall objective, however, is to **systematically** identify and characterize the deformation processes for a series of materials systems.

Recent Progress

Integrating experiment and computation, we initially focused on determining the deformation mechanisms in nanotwinned (NT) materials, starting with nanotwins in pure silver. We extended that work in a study of the effects of solutes on the deformation in nanotwinned materials. Figure 1, shows the dramatic effect of Cu solutes on NT silver samples, in which small additions lead to greatly decreased twin spacings and grain sizes, with a corresponding increase in hardness. Combining experiments with detailed atomistic simulations [1], we find that doping with a small amount of copper results in grain sizes and twin spacings well below those previously obtained for pure silver and a hardness value (3.3 GPa) about 50% higher than the previously recorded value. The doped materials also exhibit high thermal stability and retain good electrical conductivity [1]. Molecular dynamics simulations [1] suggest that the strengthening may arise from solute atoms segregating to higher energy grain boundaries (GB), reducing strain concentrations and

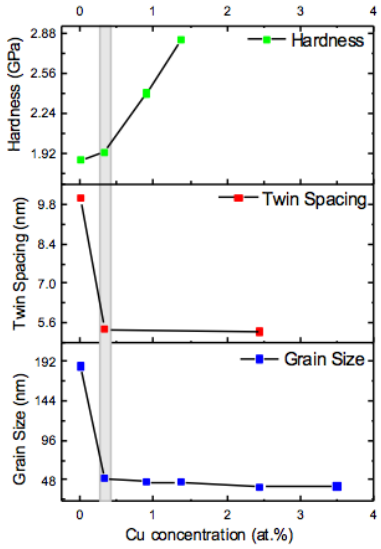

Figure 1: Effect of Cu solutes on structure and strength in nano twinned silver.

suppressing dislocation nucleation. More detailed atomistic simulations on bicrystals [2] show that oversized (Ag in Cu) or undersized (Cu in Ag) solutes can dramatically increase the yield stress, which is attributed to changes in the GB structure that occur during dislocation emission, leading to increases in the heat of segregation, and thus the energy barrier for dislocation nucleation. From room-temperature and high-temperature nanoindentation measurements, we determined the activation volumes [3] and activation energies [4-5] of the deformation, respectively. The results are consistent with dislocation nucleation being the dominant rate-limiting mechanism of deformation in nanotwinned silver. In [6], we discuss these results in the context of strengthening in nanoscale multilayers.

To extend our studies, we are focusing on systems in which the correlations between mechanisms can be deconvolved to eliminate the competition between length scales and we can thus focus on one mechanism at a time. Recognizing the critical importance of the *dynamics* of deformation, we are extending our program to include time-dependent measurements. To extend the applicability of the results to a broad range of technologically important materials, we are focusing on multiphase systems in which phase boundaries are important. Tackling these problems will require a new suite of characterization and modeling tools, which we have been developing.

Synthesis and mechanical testing: To date, we have created nanotwinned materials using magnetron sputtering, which enables the close control of concentration and, through the deposition rate, the grain size and twin-boundary spacing. To extend the studies to new systems, we are using Equal Channel Angular Pressing (ECAP) (Dr. T. Lowe, Colorado School of Mines), which enables us to obtain large samples with controlled microstructures. Mechanical testing will be done by using a FIB to machine samples and using the *in-situ* system described above. We will also continue with high-temperature nanoindentation measurements now that we have established its reliability for inferring deformation mechanisms. To rapidly study damage accumulation in materials with characteristic length scales that are equivalent to those in materials in real world uses, we are using ultrasonic fatigue testing as shown schematically in Figure 2. This approach will allow for a more rapid transition of our results.

Characterization: A major activity in this program is to relate dislocation structures to the deformation mechanisms, which requires robust methods for determining the dislocation structures. One of our challenges is that dislocation structures are dependent on the scale of the microstructure. Thus, we need to consider a range of methods. Precession electron diffraction (PED) enables the determination of local crystal orientations at a resolution of a few nanometers. From these, five of the nine components of the dislocation density (Nye) tensor can be determined, which has information about the Burgers vector and line direction of the dislocations [7]. We are using a combination of dislocation simulations and experiment to extend

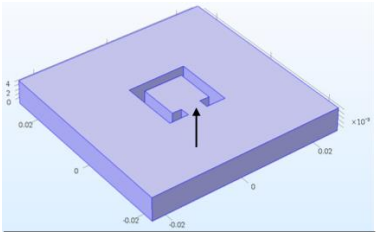

Figure 2: Simulation showing a configuration for ultrasonic fatigue testing.

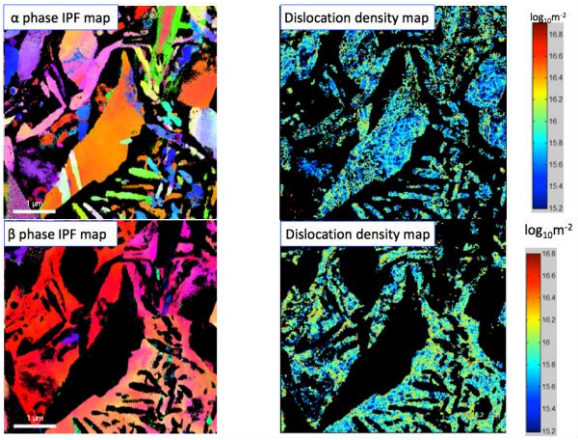

Figure 3: Orientation and dislocation density maps for a two-phase material determined using precession electron diffraction.

PED to determine all nine components, which will provide more complete information about local dislocation structures.

Our long-range goal is determine fundamental deformation mechanisms at the nanoscale and then evaluate those mechanisms for applicability in larger samples. One of the challenges has been the determination of the crystal orientation for large samples. We will use electron backscatter diffraction EBSD in the mid-range of sample sizes, on the order of a few hundred microns. However, to extend to even larger samples, we will use a recently-developed method, spatially resolved acoustic spectroscopy (SRAS) [8]. SRAS is a technique for material characterization based on measuring the surface acoustic wave velocity. In Figure 4, we show an example of a SRAS measurement of crystal orientations — length scales in the many mm range are possible.

Modeling: In an on-going collaboration with the BES program of Dr. Laurent Capolungo at Los Alamos, we have implemented an FFT-based dislocation dynamics (DD) model [9,10] within the FFT-based crystal plasticity (CP) formalism [11]. An example of the DD-CP method is shown in Figure 5 [12]. This approach will enable, for the first time, the ability to examine the dynamic development of dislocation substructures within polycrystalline materials and microstructures under appropriate loading scenarios. The results from these simulations will be closely tied to the experimental characterization of such structures, as described above, shedding light on mechanisms not seeable experimentally.

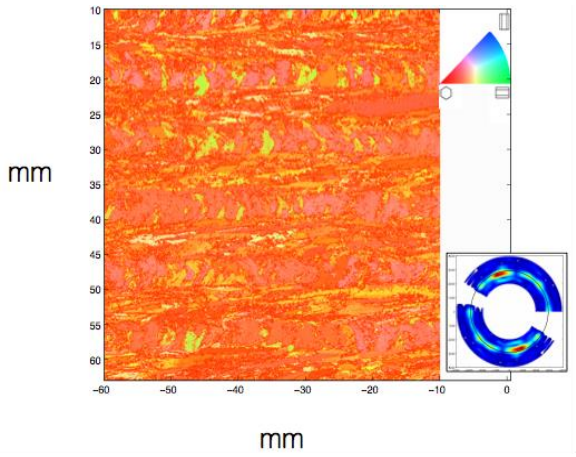

Figure 4: Large orientation map (~2750 mm^2) determined using spatially resolved acoustic spectroscopy (SRAS). The resolution of this scan is ~100 μm, with a possibility of increasing it to 50 μm using current approaches. It may be possible to increase the resolution to 2-3 μm, allowing for simultaneous fatigue and measurements while in lab air and not vacuum. Inset figure shows the "slowness" map for the surface acoustic waves for a (0001) orientation.

Future Plans

Using an integrated computation and experimentation approach, we are beginning to answer important questions in materials deformation that involve both strain and time. This work has required the development of truly cutting edge tools that span across length and time scales.

We now have those tools in place. The goal is to use them to identify synergies between deformation mechanisms, enabling a multiscale, multi-physics, systems description of deformation.

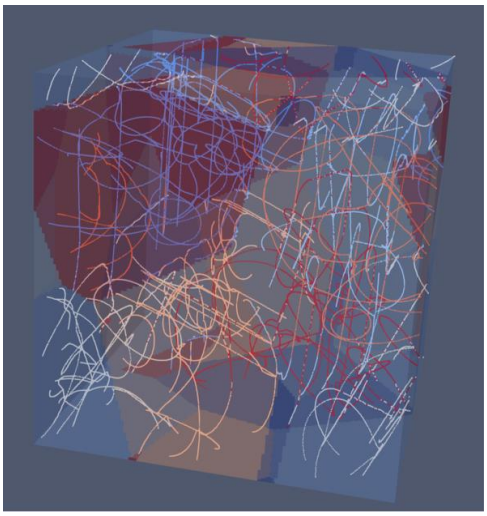

Figure 5: Snapshot of a crystal plasticity calculation based on discrete dislocation dynamics simulations. The sample is a cube 1.5 μm on a side with six grains with random orientations. The dislocations are colored according to the grain.

References

1. J. Ye, X. Ke, J. Geng, F. Liu, D. Qu, J. Marian, A. Caro, R. T. Ott, F. Sansoz, and Y. M Wang, Strengthening metals beyond the Hall-Petch limit, in preparation
2. V. Borovikov, M. I. Mendelev, and A. H. King, Effects of solutes on dislocation nucleation from grain boundaries, Inter. J. Plasticity 90, 146-155 (2017)
3. H. Yavas, J. Geng, R. T. Ott, M. F. Besser, K. Rajan, and R. LeSar, Strain rate sensitivity and activation volume of nanotwinned Ag-Al films via nanoindentation (in preparation).
4. H. Yavas, R. T. Ott, M. F. Besser, J. Geng, K. Rajan, and R. LeSar, Effects of Cu-solute addition on microstructural and mechanical properties of nanotwinned silver films, submitted to Phil. Mag. Lett. (2017)
5. H. Yavas, M. F. Besser, R. T. Ott, J. Geng, K. Rajan, and R. LeSar, Dependence of the Mechanical Properties of Nanotwinned Silver Films on Temperature and Texture, submitted to Phil. Mag. Lett. (2017)
6. S. Subedi, I. J. Beyerlein, R. LeSar, and A. D. Rollett, Strength of nanoscale metallic multilayers, Scripta Mater. (2017). http://dx.doi.org/10.1016/j.scriptamat.2017.04.009
7. I. Ghamarian, P. Samimi, Y. Liu, B. Poorganji, V. K. Vasudevan, and P. C. Collins, Characterizing the nano-structure and defect structure of nano-scaled non-ferrous structural alloys, Mater. Character. 113, 222-231 (2016)
8. R. J. Smith, M. Hirsch, R. Patel, W. Li, A. T. Clare, and S. D. Sharples, Spatially resolved acoustic spectroscopy for selective laser melting, J. Mater. Process. Tech. 236, 93-102 (2016)
9. J. Graham, A. D. Rollett, and R. LeSar, "Fast-Fourier transform discrete dislocation dynamics," Model. Simul. Mater. Sci. Engin. 24, 085005 (2016)
10. N. Bertin, M. V. Upadhayay, C. Pradalier, and L. Capolungo, "A FFT-based formulation for efficient mechanical fields computation in isotropic and anisotropic periodic discrete dislocation dynamics," Model. Simul. Mater. Sci. Engin. 23, 065009 (2015)
11. R. A. Lebensohn, A. K. Kanjarla, and P. Eisenlohr, "An elasto-viscoplastic formulation based on fast Fourier transforms for the prediction of micromechanical fields in polycrystalline materials," Inter. J. Plasticity 32-33, 59-69 (2012)
12. J. Graham, R. LeSar, and L. Capolungo, "A FFT-based method for coupling discrete dislocation dynamics within polycrystal plasticity," in preparation (2017)

Multi-scale Modeling of Shear Banding in Metallic Glasses

PI: Lin Li The University of Alabama

Program Scope

The overarching goal of this research project is to develop an understanding of the microstructural features and deformation mechanisms that control shear banding in metallic glasses (MGs), which will enable the development of MGs with enhanced plasticity. To achieve the goal, this project includes the following thrusts: (1) development of a structure-enriched multi-scale modeling framework; (2) determination of the formation mechanisms for shear bands in presence of structural heterogeneity; (3) determination of the relationship between structural evolution and macroscopic mechanical responses of MGs, particularly MG plasticity improvement through structural rejuvenation. In the current work, we focus on thrusts (1) and (2). Particularly, we study the effect of spatial heterogeneity of elasticity, resulting from the inherently inhomogeneous amorphous structures, on the deformation behaviors of a model Cu64Zr36 MG, by using multi-scale modeling methods.

Recent Progress

The spatial heterogeneity of elastic property at nanoscale A highly heterogeneous shear modulus distribution at the nanoscale, following a Gaussian-type, is revealed by the molecular dynamics (MD) simulations of Cu64Zr36 MG with 32,000 atoms. The simulations were performed using the optimized embedded atom method (EAM) potential [1], and the melt was equilibrated at high temperature and then quenched to room temperature (300 K) at a cooling rate of 10^9 K/s. Additionally, we evaluate the local elasticity from the atomic scale to that of the coarse-grained sub-cells using [2], so that the local shear modulus can be analyzed with adequate spatial resolution to reflect its heterogeneous distribution. Fig. 1(a) shows this measured distribution of local shear moduli (for a sub-cell size of ~ 8 Å), which fits the Gaussian function with an average value of 25.9 GPa and a standard deviation of 4.44 GPa (black line). Fig. 1(b) illustrates the coarse-grained map of atomic elastic modulus, with the red and blue colors respectively representing the high and low shear modulus regions.

Such nanoscale heterogeneity in MGs underpins the ‘soft spots’ that likely undergo stress-driven shear transformation to carry plastic flow. To coordinate them for ductility at large scale, the control of heterogeneity needs to be committed to the level from nanometer-scale shear transformation zones (STZs) to their organization into shear band patterns. We adapt a meso-scale STZ dynamics model [3-4], extending the modeling framework by incorporating an elastic heterogeneity at nanoscale. This is achieved by assigning a Gaussian-type shear modulus distribution to local elements/sites, and further turning the spatial heterogeneity of the local shear moduli for a specific correlation length ξ following the definition of spatial autocorrelation function (ref. to Fig. 1(d)). Fig. 1(c) illustrates the map of local shear moduli distribution within the model samples with ξ = 0.5 and 5 nm, respectively. Clearly, as the spatial correlation length increases, both elastically soft and hard sites aggregate, giving rise to the larger clustering regions with similar local shear moduli.

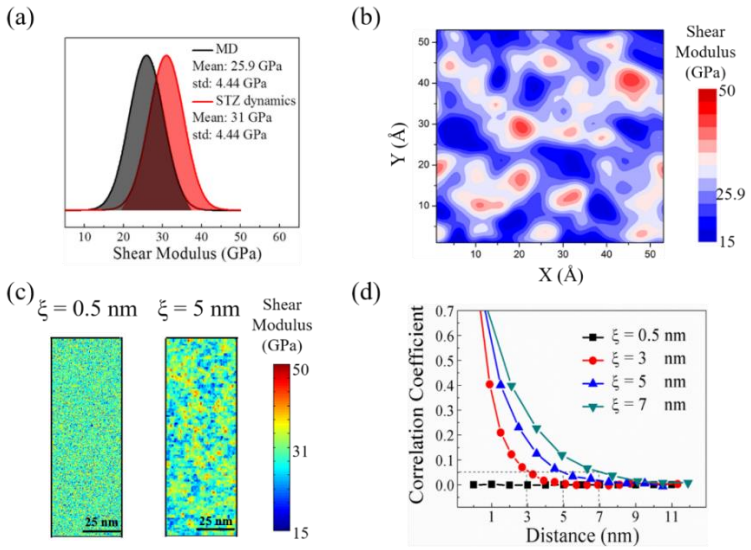

Figure 1: The spatial heterogeneity of elastic property at nanoscale. (a) The Gaussian distributions of local shear moduli of Cu64Zr36 MG obtained by MD simulations (in black) and used in the STZ dynamics simulations (in red). (b) The coarse-grained map of local shear moduli obtained by MD simulations. (c) The spatial distributions of local shear moduli of the samples with correlation lengths of 0.5 and 5 nm, respectively. (d) The correlation coefficient as a function of distance for various STZ dynamics samples.

Macroscopic stress-strain responses in presence of elastic heterogeneity We further use the developed STZ dynamics model to study the effect of the spatial heterogeneity of elasticity on the macroscopic deformation behavior of MGs. Fig 2(a) illustrates the tensile stress-strain responses of the simulated MGs with various correlation lengths. A transition from stress-overshoot to elastic-perfect plastic flow is observed as the spatial correlation length increases. Correspondingly, the deformation morphology changes from one dominate shear band to the formation of multiple shear bands, as shown in Fig. 2(b). Moreover, a critical spatial correlation length of local shear moduli is identified, dividing the dependence of mechanical properties of MGs on the spatial correlation into two regimes (ref. to Fig. 2(c) & (d)). In the weak correlation Regime I, the strength decreases and ductility increases as the correlation length increases. In strong correlation Regime II, the strength remains constant and ductility decreases as correlation length increases.

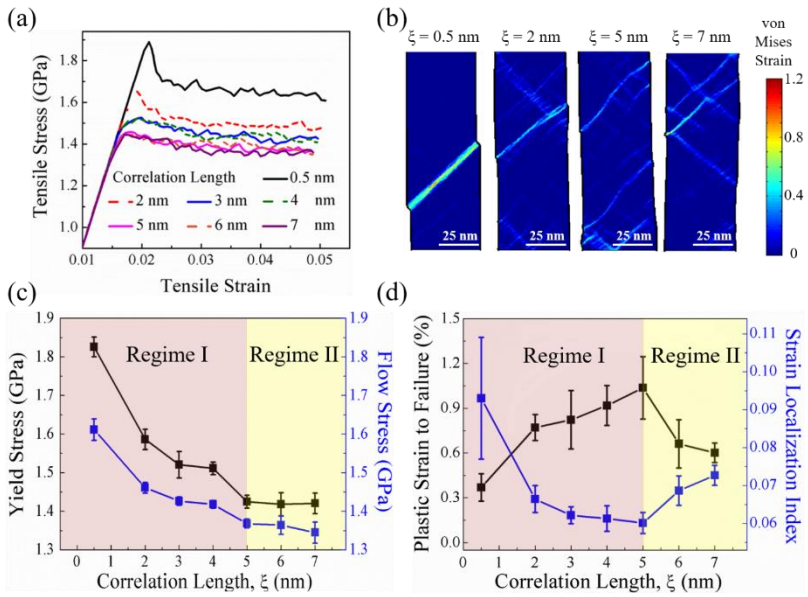

Figure 2: Mechanical behaviors of the simulated MGs at various correlation lengths. (a) The representative tensile stress-strain curves of the simulated Cu64Zr36 MGs. (b) The von Mises strain snapshots of the samples at the total strain of 0.04. (c) The yield stress and the flow stress versus the correlation length. (d) The macroscopic plastic strain to failure and the microscopic strain localization index versus the correlation length.

Shear band formation in presence of elastic heterogeneity We study into details the process of shear band formation and its correlation with elastic heterogeneity. *At weak spatial correlation*, in the case of correlation length $\xi = 0.5$ nm, one dominant shear band is formed even in the presence of elastic heterogeneity, as shown in Fig. 3. The shear banding process follows the two-stage model [5], in which the stress drives the formation/nucleation of a shear band embryo before it rapidly grows into a dominant band. The nucleation and growth stages are well distinguished, coming in sequence over the course of deformation. The nucleation stage prefers the soft sites but the propagation exhibits no preference, involving both soft and hard driven by the concentrated local stress field. Thus, in the case of $\xi = 0.5$ nm, even though the existence of structural heterogeneity offers a decent amount of elastically soft sites that could facilitate strain delocalization, the spatial correlation is not strong enough to do so. Therefore, the concentrated stress in front of the shear band embryo drives the rapid growth of one dominant shear band in the sample.

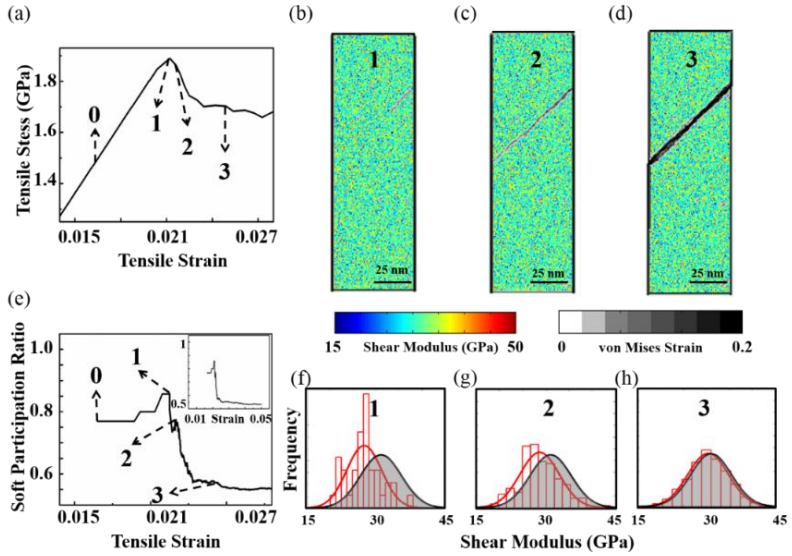

Figure. 3 The formation of one dominant shear band in the simulated MG with correlation length of 0.5 nm. (a) The stress-strain response marked with the critical moments of shear banding. (b) - (d) The snapshots of von Mises strain distribution, overlapped on the shear moduli distributions (e) The evolution of the soft site participation ratio. (f)-(h) The shear modulus distribution of the local sites that have undergone STZ transition at the critical moments, along with the local shear modulus distribution within the whole samples in black.

At strong spatial correlation when the spatial correlation length reaches the critical value (i.e., ξ = 5 nm), multiple shear bands are formed to carry plastic flow as shown in Fig. 4. Upon yielding, the STZs are triggered in several soft sites and evolve into shear band embryos. Further straining, the embryos penetrate the surrounding locations clustered with relatively low shear moduli and form several incipient shear bands. Eventually, the incipient bands connect with each other and develop a percolated strain path throughout the sample to conduct steady plastic flow. Over the course of shear band formation, the stress barely changes after yielding, the flow stress is close to the yield stress in the stress-strain response. Different from weak correlation case, the nucleation and growth stages of forming one band are not distinct and might disappear. Instead, several shear band embryos nucleate at elastically soft sites, and the formation of the shear bands is via connecting/percolating the shear band embryos [5]. Above the critical correlation length, the MG still deforms by forming multiple shear bands, but the number of the bands is reduced. It is anticipated that the further increase of spatial correlation results in the aggregation of soft

regions/clusters enlarged in size but reduced in number. Consequently, fewer soft clusters are now available for the nucleation of shear band embryos.

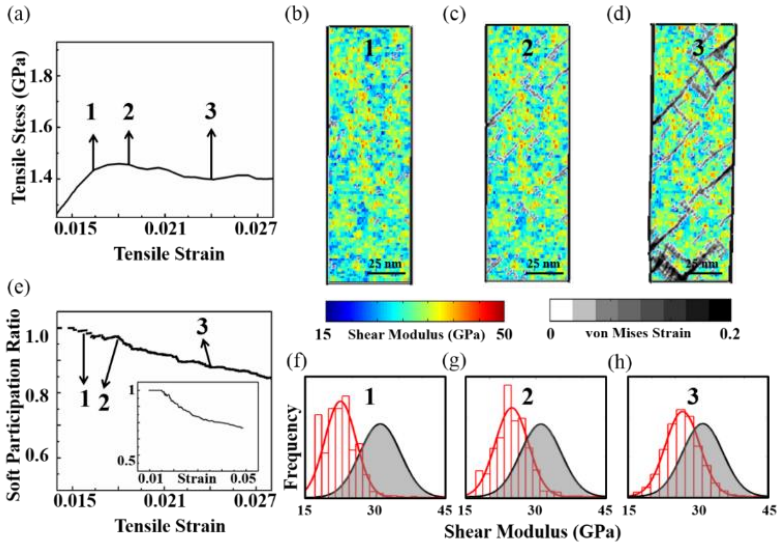

Figure 4 The formation of multiple shear bands in the simulated MG at the critical correlation length 5 nm. (a) The stress-strain response (b) - (d) The snapshots of von Mises strain distribution, overlapped on the shear moduli distributions (e) The evolution of the soft site participation ratio. (f)-(h) The shear modulus distribution of the local sites that have undergone STZ transition at the critical moments.

The spatial correlation can control the organization of STZs into shear band pattern, leading a transition of shear band formation from stress-dictated nucleation and growth to structure-dictated strain percolation. We hypothesize that the critical shear band nucleus size is an underlying cause of the transition of deformation behaviors. Below the critical size, the increase in correlation length enlarges the size of soft clusters, facilitating the nucleation of incipient shear bands, delocalizing plastic flow and enhancing ductility. Above the critical size, the increase in correlation length decrease the number of soft clusters, limiting strain percolation paths to form shear bands, intensifying the extent of strain localization and reducing the ductility of MGs.

Future Plans

Our results clearly underscore the importance of nanoscale elastic microstructure on controlling the deformation behavior of monolithic MGs. The next step is to study the evolution of structural heterogeneity upon thermo-mechanical processing and its relationship with macroscopic mechanical responses of MGs. Three specific will be targeted: (1) The atomistic simulations are performing to establish the correlation between glass local structure and activation energies for shear transformation events. (2) The mesoscale shear transformation zone dynamics model will be extended to incorporate state variables, reflecting the dynamics of structural evolution. (3) Experimentally, atomic force microscope will be performed to evaluate the elastic heterogeneity of Zr-based MGs and the heterogeneity evolution upon sub-T_g relaxation.

References

1. Cheng, Y. Q., Ma, E., Sheng, H. W., Phys. Rev. Lett. 102, 245501 (2009).
2. Cheng, Y. Q., Ma, E., Phys. Rev. B **80**, 064104 (2009).
3. E.R. Homer, C.A. Schuh, Acta Mater. 57 (2009) 2823–2833.
4. L. Li, E.R. Homer, C. A. Schuh, Acta Mater. 61 (2013) 3347–3359
5. A.L. Greer, Y.Q. Cheng, E. Ma, Mater. Sci. Eng. R Reports. 74 (2013) 71–132.

Publications

1. Sterwerf, C., Kaub, T., Thompson, G., Deng, C., Li, L., “Transition of Deformation Behaviors in Amorphous/Crystalline Cu45Zr55/Cu Multilayers”. Thin Solid Films, 2017
2. Wang N, Ding J, Yan F, Asta M, Ritchie R.O., Li L, “Spatial correlation of elastic heterogeneity tunes the deformation behaviors of metallic glasses” (in preparation)
3. Choi, C., Ding, J., Li, L., “Structural characteristics at the saddle state of Cu64Zr36 metallic glasses using activation-relaxation technique” (in preparation)

Low Temperature Cyclic Deformation Behavior of Ultrafine-grained Pure Magnesium

PI: Qizhen Li, Washington State University

Program Scope

Magnesium (Mg), as the known lightest structural metal, is attracting considerable research interest. Mg with ultrafine grains is especially appealing since grain refinement can overcome its relatively low ductility caused by the material's HCP structure and limited slip systems [1-5]. This project aims at exploring the cyclic mechanical properties of ultrafine-grained (UFG) pure Mg at low temperatures and uncovering the corresponding fundamental fatigue deformation mechanisms. This research aim will be accomplished through fatigue testing and microstructure characterization of UFG Mg specimens. The research results will reveal the detailed activities of dislocations, twins, and grain boundaries in UFG Mg at the studied temperatures and cyclic loading conditions and will be able to provide new insight on the low temperature fatigue deformation mechanisms. The underlying understanding of the mechanisms will greatly contribute to the research community and allow us to take full advantage of this type of novel material.

Recent Progress

The important finding from the recent research is the inhomogeneous microstructure of ECAPed samples and the relation between the inhomogeneous microstructure and the processing.

- The microstructure analysis of commercially pure magnesium deformed through one cycle of ECAP present inhomogeneous microstructure generated by the processing. A large number of deformation twins were generated in most of the grains. Shear bands and the breakdown of grains were observed on the cross-section plane right around the center of the sample height. The deformation was severer along the inner surface of the ECAP mold channel.

- The texture analysis of the annealed sample before experiencing ECAP processing, the sample experienced one cycle of ECAP processing, and the sample experienced eight cycles of ECAP processing shows that the highest intensities for these three samples fall in the range of $60^{o} \sim 75^{o}$ from the north pole of the pole figures. There is no significant difference in the texture for these samples, although the grain size is significantly reduced after eight cycles of ECAP processing.

- Although the microstructure was inhomogeneous for the sample experienced one cycle of ECAP processing, the sample showed homogeneous equiaxed grains with uniformly distributed twins after experienced eight cycles of ECAP processing.

Inhomogenous Microstructure of Magnesium Experienced One Cycle of ECAP:

Figure 1(b) and 1(c) present the magnified microstructure of the mostly deformed regions in two cross-section planes. One plane (Plane I) is at about a quarter of the height of the sample, and the other plane (Plane II) is at around the center of the sample. The microstructure of the sample before experiencing the ECAP processing is shown in Figure 1(a) to show the initial microstructure with sparsely-distributed twins. Clearly, the grains were deformed more severely in Plane II than those in Plane I.

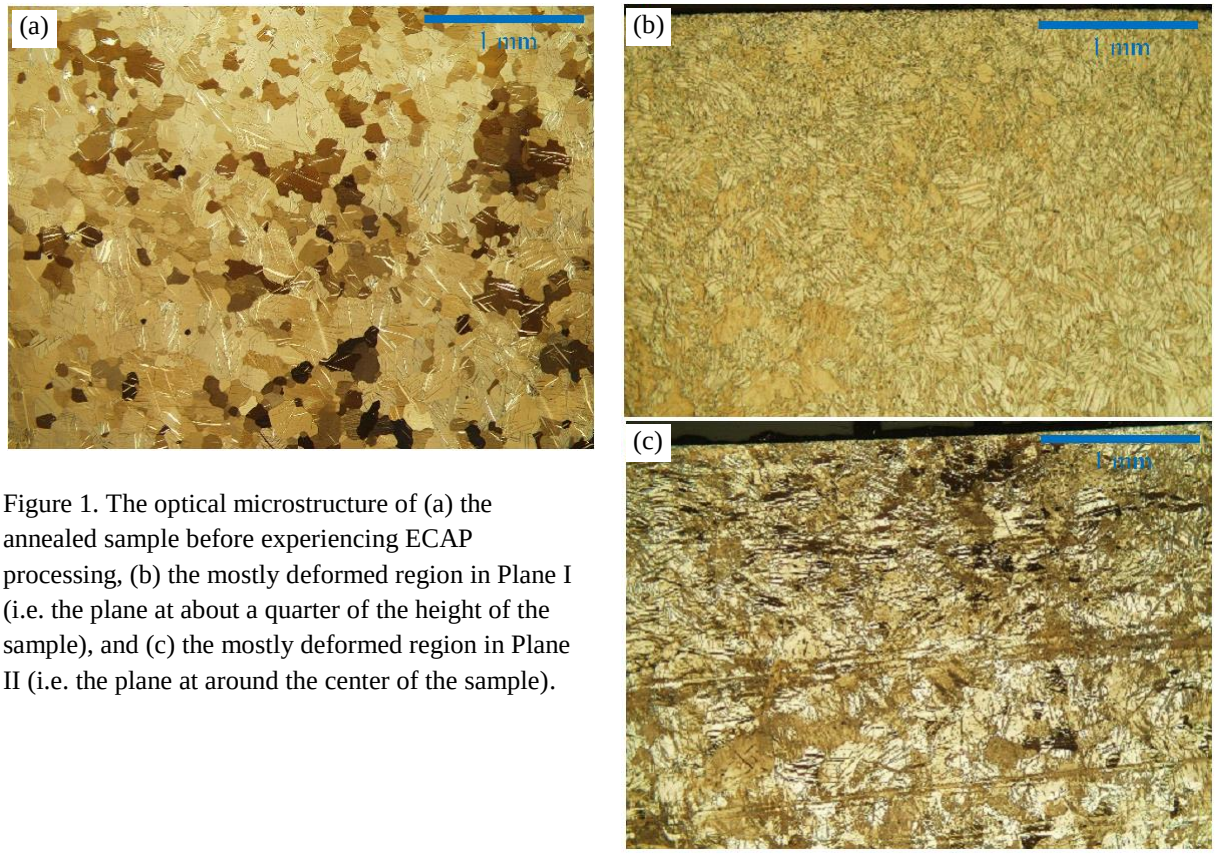

Figure 1. The optical microstructure of (a) the annealed sample before experiencing ECAP processing, (b) the mostly deformed region in Plane I (i.e. the plane at about a quarter of the height of the sample), and (c) the mostly deformed region in Plane II (i.e. the plane at around the center of the sample).

Microstructure of Magnesium Experienced Various Cycles of ECAP:

Followed the pressing Route Bc with 90^{o} sample rotation between two consecutive ECAP passes, the samples were processed for 1, 2, 4, and 8 passes. Figure 2(a) provides the EBSD image of the microstructure of the samples before experiencing any ECAP processing and after being heat treated at 300^{o}C for 12 hours. The grains in Figure 2(a) are approximately equiaxed,

and the average grain size is on the order of 100μm. After experienced eight cycles of ECAP processing, the sample showed almost equiaxed grains with uniformly distributed twins in Figure 2(b).

The 0002 and 10-10 pole figures were obtained for the annealed sample before experiencing ECAP processing, the sample experienced one cycle of ECAP processing, and the sample experienced eight cycles of ECAP processing respectively. The highest intensities for these three samples fall in the range of $60^{o} \sim 75^{o}$ from the north pole of the pole figures. There is no significant difference in the texture for these samples, although the grain size is significantly reduced after eight cycles of ECAP processing.

Although the microstructure was inhomogeneous for the sample experienced one cycle of ECAP processing as shown in Figure 1(b) and 1(c), the sample showed homogeneous equiaxed grains with uniformly distributed twins after experienced eight cycles of ECAP processing as shown in Figure 2(b).

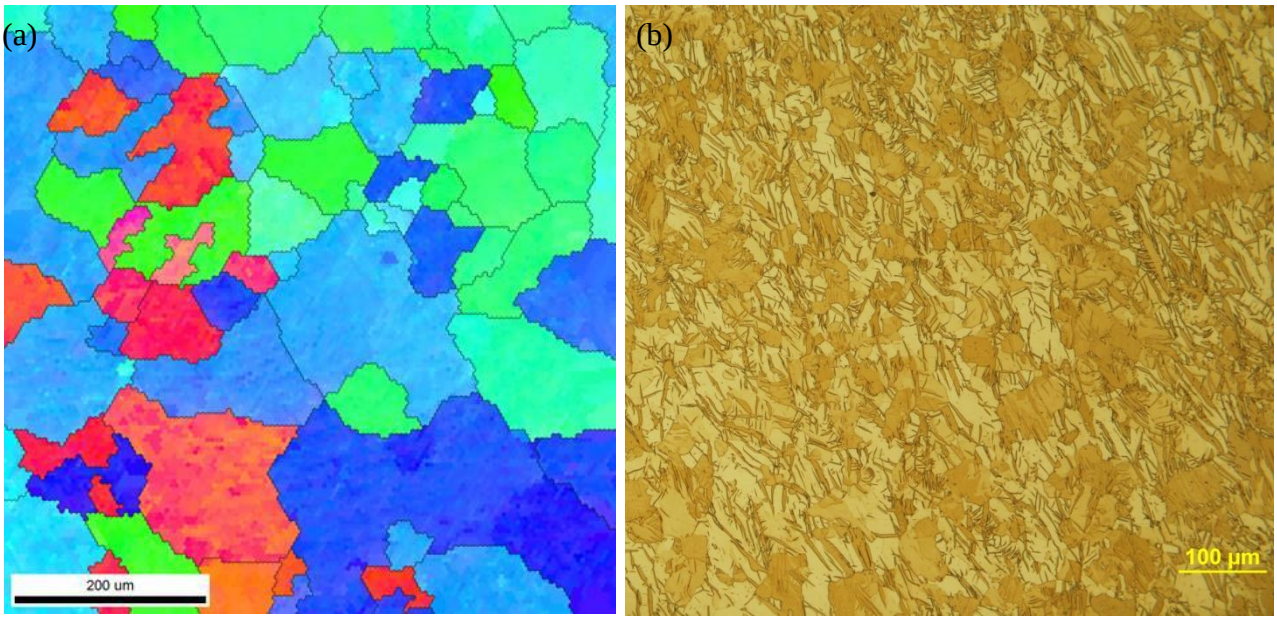

Figure 2. (a) EBSD image of the annealed sample before experiencing ECAP processing, (b) Optical micrograph of the sample experienced eight cycles of ECAP processing.

Future Plans

Low temperature testing equipment was ordered and will be shipped to Washington State University soon. We will get it set up in the PI's lab. More ECAPed samples will be prepared. Further research will be performed to study fatigue properties of the UFG pure Mg at low testing temperatures.

References

[1] M. Avedesian, and H. Baker, Magnesium and magnesium alloys, Materials Park, OH: ASM International, 1999

[2] M.T. Perez-Prado, J.A. del Valle, O.A. Ruano, Grain refinement of MG-Al-Zn alloys via accumulative roll bonding, Scripta Materialia 51, 2004, pp. 1093

[3] L. Jin, D.L. Lin, D.L. Ma, X.Q. Zeng, W.J. Ding, Mechanical properties and microstructure of AZ31 Mg alloy processed by two-step equal channel angular extrusion, Materials Letters 59, 2005, pp. 2267

[4] Y. Yoshida, K. Arai, S. Itoh, S. Kamado, Y. Kojima, Realization of high strength and high ductility for AZ61 magnesium alloy by severe warm working, Science and Technology of Advanced Materials 6, 2005, pp. 185

[5] W.M. Gan, M.Y. Zheng, H. Chang, X.J.Wang, X.G. Qiao, K.Wu, B. Schwebke, H.G. Brokmeier, Microstructure and tensile property of the ECAPed pure magnesium, Journal of Alloys and Compounds 470, 2009, pp. 256

Publications

Q.Z. Li, X. Jiao, Characterization of Inhomogeneous Microstructure of Ultrafine Grained Magnesium, accepted by 2017 Sustainable Industrial Processing Summit, Cancun, Mexico, October 22-26, 2017

X. Jiao, Q.Z. Li, Microstructure Evolution of Pure Magnesium Processed by different ECAP Routes, to be submitted

Understanding Microplasticity Processes Related to Fatigue Damage Using High Energy X-Rays and a Crystal-Based Modeling Formulation

Matthew Miller[1], Paul Dawson[1], Ulrich Lienert[2], Jim Williams[3], Mark Obstalecki[1] and Robert Carson[1]
[1]Sibley School of Mechanical and Aerospace Engineering, Cornell University, Ithaca, NY
[2]Deutsches Elektronen-Synchrotron, Hamburg, Germany
[3]Materials Science Department, The Ohio State University, Columbus, OH

Program Scope

A long-standing materials science challenge is the ability to predict failure under cyclic loading, where a wide range of materials and structures operate in engineering environments. Fatigue of ductile metal polycrystals is a microstructure-sensitive localization process beginning with cyclic plasticity-driven production of substructural inhomogeneities that eventually develop into cracks. Understanding the processes leading to fatigue crack initiation, the formation of aggregate wide slip bands, in ductile metals such as copper or nickel, with enough detail to allow prediction is the overall objective of this project. **In this project, our aim is to develop a predictive capability for the heterogeneous cyclic plastic deformation processes that lead to the formation of slip bands that begin at the grain scale and then extend throughout a polycrystalline aggregate, eventually becoming a crack.** The ubiquitous persistent slip bands (PSBs) observed in single crystals aligned for single slip from early fatigue research are examples of the plastic localization that occurs before a fatigue crack initiates. Since the transmission of slip and eventual localization must involve clusters of grains, this project has focused on developing an understanding of cyclic slip processes and the evolution of grain-scale structures and mechanical environments during cyclic loading. We have created and advanced new experimental and modeling methods for studying cyclic plasticity within an entire polycrystalline aggregate with single crystal resolution.

Recent Progress

Experimental In our previous work we examined a precipitation-hardened alloy, OMC copper. Recently, we conducted in situ cyclic loading experiments on OFHC copper, a purely strain hardening material. Our experiments have focused on the response of each crystal within the aggregate, namely the spreads in the diffracted intensity distributions for the peaks within each crystal measured using high energy x-ray diffraction (HEXD). We have linked the spread in the HEXD data to heterogeneous plastic straining, which is a precursor to fatigue crack initiation. We conducted near- and far-field diffraction experiments on the OFHC sample, which yield grain maps and orientation spread information, respectively. Figure 1 depicts the OFHC grain maps. The beam used in the experiment was 125 μm tall and 1mm wide. Four “slices” were interrogated in the experiment.

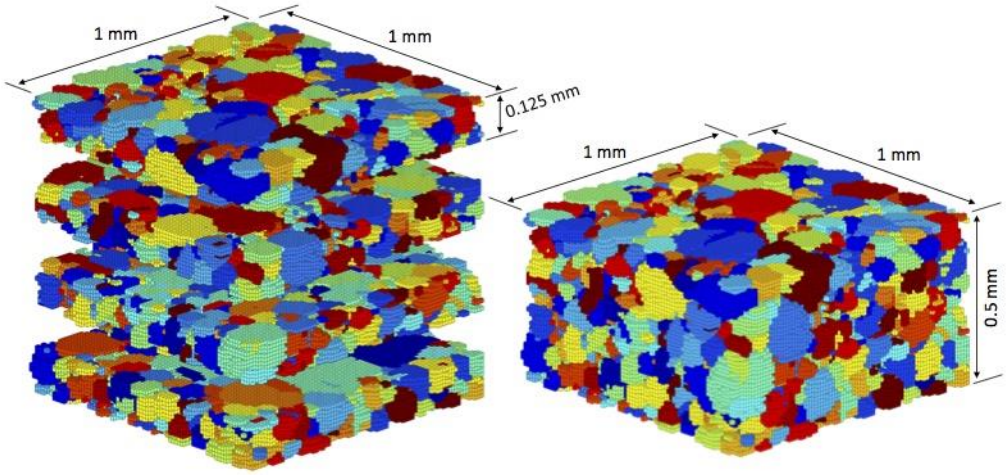

Figure 1. Grain map of the OFHC copper sample interrogated in the HEXD experiment depicting the four slices acquired during individual diffraction experiments (left) and the assembled aggregate (right).

Figure 2 depicts the macroscopic stress strain response of the OFHC sample at 2 cycles and at 256 cycles. The fully reversed experiments were conducted in strain control between endpoints of +- 0.3%. The differences between the stress levels of the hysteresis loops are due to the cyclic hardening that occurs in the material. Diffraction experiments were conducted at 8 points around the hysteresis loop.

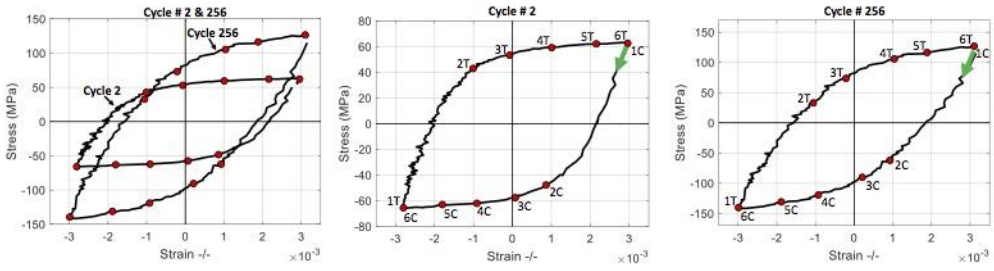

Figure 2. Macroscopic stress-strain response of the OFHC copper sample. The red spots are points where HEXD experiments were conducted.

We created a new way of analyzing the HEXD data. Instead of examining spread in orientation using the azimuthal Full Width at Half Maximum (FWHM) of each peak, we now examine the "cloud" of orientations associated with each crystal and define a scalar measure of misorientation. We then fit these values to a Weibull distribution. The distributions for each of the red points in Figure 2 are shown in Figure 3. The misorientation magnitudes are much larger in cycle 256 but we see significant evolution taking place during cycle 2. The misorientation actually reaches its minimum value in between the loop tips on both the tension- and compression-going parts of the cycle. By cycle 256 we see very little evolution of the distributions around the hysteresis loops, consistent with the saturation we see in the macroscopic stress-strain curves.

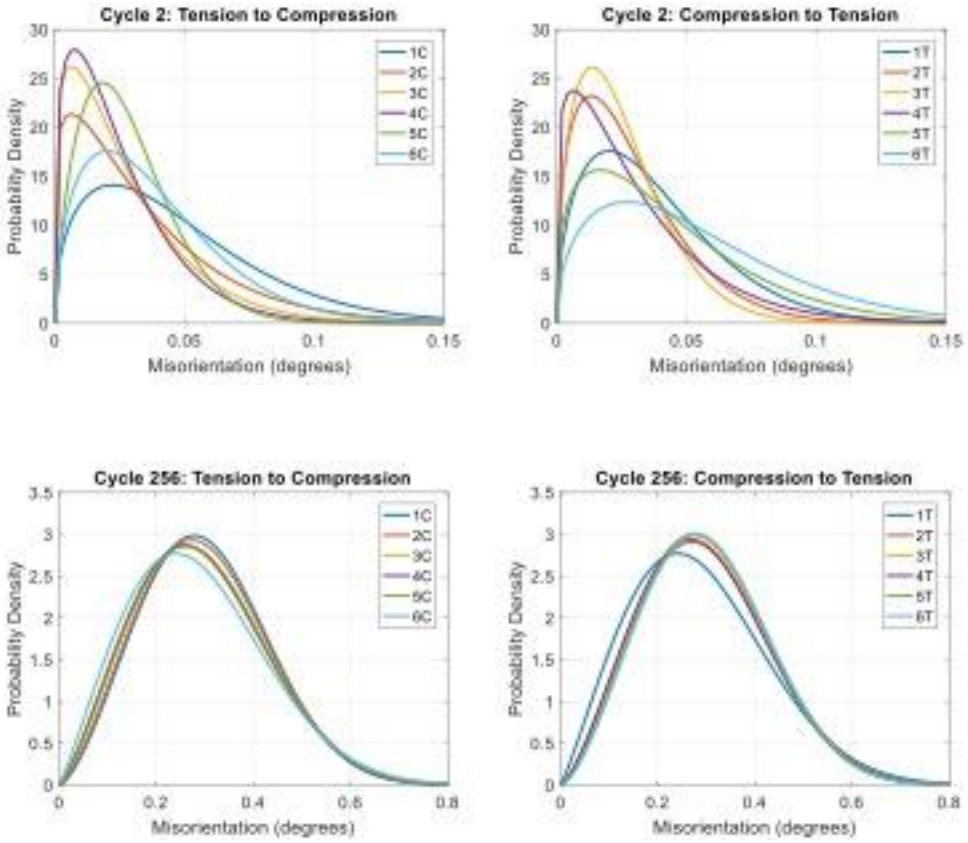

Figure 3. The Weibull distributions of intra-crystal spread in orientation for the OFHC aggregate on cycle 2 (top) and cycle 256 (bottom). The colors of the curves correspond to red points on the stress-strain curves shown in Figure 2.

Modeling In our previous work on this project, we developed the virtual diffractometer capability for comparing experiments to simulation; real diffraction data were compared simulation by projecting through the finite element model. We sought measures similar to the FWHM that would come directly from the material model itself that would provide measures of orientation heterogeneity. We used the OMC data to develop these new metrics. The OMC macroscopic strain data along with model predictions are shown in Figure 4. Three new metrics for lattice orientation heterogeneity are given in Figure 5.

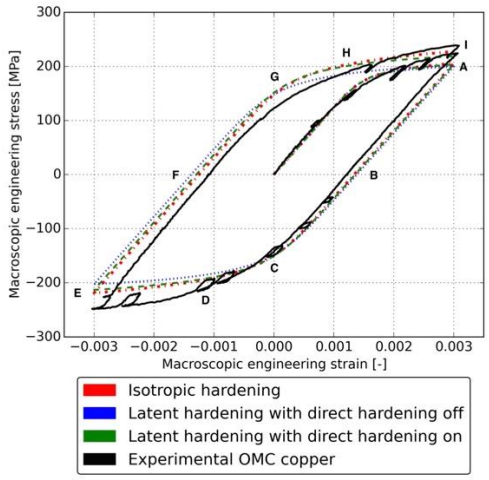

Figure 4. OMC stress strain response from the HEXD experiment and using various hardening models.

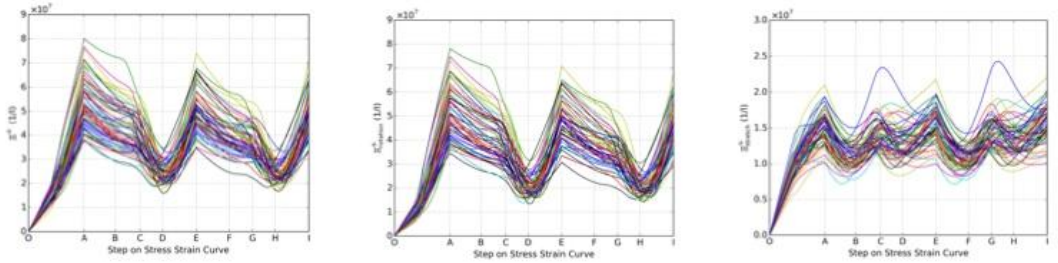

Figure 5. The mean lattice orientation heterogeneity for each grain within the OMC aggregate subjected the loading history given in Figure 3. Heterogeneity based on (left) elastic stretch and rotation, (middle) rotation only and (right) elastic stretch only.

Publications

1. S.L.Wong, M.O. Obstalecki, M.P. Miller, and P.R. Dawson, "Stress and deformation heterogeneity in individual grains within polycrystals subjected to fully reversed cyclic loading," Journal of the Mechanics and Physics of Solids, **79**, 157-185, 2015
2. Carson, R., Obstalecki, M., Miller, M., and Dawson, P., "Characterizing het- erogeneous intragranular deformations in polycrystalline solids using diffraction-based and mechanics-based metrics," Modelling and Simulation in Materials Science and Engineering, 25(5):055008, 2017.
3. Obstalecki, M., Carson, R., Dawson, P., and Miller, M., "Observing mesoscale structural heterogeneity under fully reversed plastic cycling through high energy x- ray diffraction and its implications for crystal plasticity modeling," Acta Materialia., in Review, 2017.

Transformation and Deformation Mechanisms in High-Temperatures Shape Memory Alloys with Nano-precipitates

Principal Investigators: Profs. Michael J. Mills, Peter M. Anderson, and Yunzhi Wang.
The Ohio State University, Department of Materials Science and Engineering

Program Scope

The focus of this program is on an emerging class of high temperature shape memory alloys (HTSMAs) that are exciting candidates for actuators and adaptive components in a wide range of energy and transportation applications. At present there is only a rudimentary understanding of the important microstructure-property relationships in these materials. The goals of this effort therefore are to (1) develop a fundamental understanding of the inherent microstructure-property behavior of high temperature shape memory alloys, including the interaction of precipitates with plasticity and martensite, and (2) develop computational models that capture these structure-property relationships and provide novel insights into the important transformation and plasticity mechanisms that govern their behavior.

Two HTSMA alloy systems have been at the core of the effort during the previous year, Ni(Ti,Hf) and (Ni,Au)Ti alloys. Both of these alloys can exhibit high transformation temperatures, large transformation strain, and small permanent strain. These beneficial properties can be strongly influenced by the formation of nanoscale precipitates. Binary NiTi has also been studied in an effort to understand the origin of permanent strain accumulation during load-biased thermal cycling. The program is spearheaded by an array of advanced characterization techniques, including high resolution HAADF imaging, 4D STEM diffraction, transmission Kikuchi diffraction (TKD), and in situ high energy X-ray diffraction microscopy (HEDM). These characterization efforts have motivated phase field and finite element simulations to explore the interaction of precipitates with martensite at lower temperature, dislocation activity at higher temperature, and grain reorientation after load biased thermal cycling testing. The program is benefitting substantially from extensive interaction with NASA Glenn Research Center, Colorado School of Mines, the Molecular Foundry/National Center for Electron Microscopy, the Cornell High Energy Synchrotron Source (CHESS), and Monash University.

Recent Progress

Aging has an extraordinarily potent effect on mechanical behavior in Ni-rich Ni(Ti,Hf) alloy systems while four near-stoichiometric NiTiAu alloys are remarkably insensitive to composition and heat treatment. We have uncovered the microstructural origins of this divergent behavior using a STEM, EDS, and XRD techniques. The NiTiAu alloys exhibit the highest transformation temperature with useful work output of any known alloy system. Its shape memory behavior is largely unaffected by changes in alloy composition from 49Ti to 51Ti. This is likely caused by the presence of two types of secondary phases, Ti_3Au and $Ti(Au0.66Ni0.33)_2$, which have a moderating effect on matrix composition, and therefore the martensitic transformation behavior.

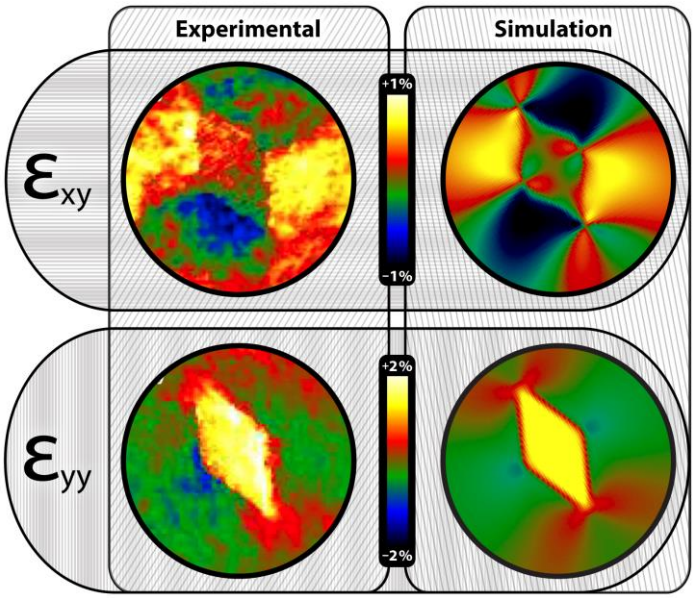

Fig. 1. Comparison of 4D STEM measurement and phase field simulation of strain fields around an H-phase particle (zone direction [110]), showing excellent quantitative agreement.

Fundamental understanding of the strong effect of H-phase precipitates on transformation behavior of Ni-rich Ni(Ti,Hf) has motivated the application of the "4D STEM" nanobeam electron diffraction strain mapping technique via a successful Molecular Foundry proposal. Using this technique, the strain fields around the H-phase nanoparticles have been characterized quantitatively through both advanced experimental characterization and phase field modeling. According to the experimental results, the nano-sized H-phase precipitate has a diamond shape with {113} type facets and keeps coherent with the parent B2 phase matrix. The strain field around such an H-phase particle is calculated using the phase field approach. In the above figures, the long and short diagonal of the diamond shape is along the [-110] and [001] directions, respectively. The calculated strain fields are in excellent quantitative agreement with the experimental measurements.

Two types of finite element simulations have been developed over the past several years and deployed for specific studies over the past year. The first technique – phase-field finite element (PFFE) – employs the phase field method and crystal plasticity to study the formation of individual martensite variants at the sub-micron scale. The second technique – microstructural finite element (MFE) – employs averaging techniques to study the formation of numerous twinned martensite plates at the super-micron scale. Both PFFE and MFE simulations have been applied to understand the dual nature of nm-scale precipitates: they impart large resistance to large-scale plastic deformation yet they allow the martensitic transformation to seamlessly propagate around thousands of precipitates, creating continuous martensite plates rather than fractionated ones. It is found that when a precipitate with no misfit strain is introduced, it disrupts the formation of martensite whereas when a precipitate with a misfit strain is introduced, it serves as a strong nucleation site that patterns the martensite. The results underscore the key role that misfitting precipitates, including H-phase precipitates, can play in the patterning of martensite.

Two possible sources of permanent strain during stress cycling or load biased thermal cycling are (a) dislocation plasticity induced by the martensite and (b) symmetry-dictated non-phase-transformation pathways (SDNPTPs), which leads to the "birth" of crystalline defects during transformation cycling. Both of these contributions may be generic to SMAs and are being studied presently for NiTi due to the dramatic "walking" behavior exhibited by the simple binary

alloy. The PFFE simulations for stress-induced martensite (Figure 2) show that the phase transformation leaves nm-scale arrays of plastically deformed material in the wake of the transformation—located along the twin interfaces in martensite. This outcome, coupled with transmission electron microscope images of material that has been cycled through the phase transformation, reveals that specific arrays of dislocation loops can be "written" into the material by the transformation process. The results underscore that the process of training SMAs involves the development of nm-scale dislocation structure that is indexed to each of the 24 twinned plate types that can form in systems with the B2-B19' phase transformation.

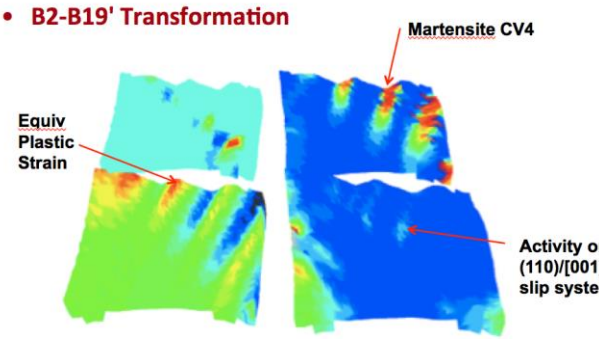

Fig. 2: Predictions of phase field – finite element (PFFE) simulations at the interface between austenite (at the forefront of each image) and twinned martensite (in the background of each image), showing: active plastic regions (upper left); volume fraction of martensite correspondence variant 4, shown by regions of red intensity (upper right); equivalent plastic strain (lower right); instantaneous slip activity on the austenite (110/[001] slip system (lower right).

Regarding the SDNPTP hypothesis, we have sought direct evidence for the predicted grain reorientation during load-biased thermal cycling (LBTC). In essence, the premise of this hypothesis is that due to defects and stresses generated during LBTC, the martensite formed at lower temperature does not transform back to the original B2 austenite grain, but rather can nucleate a new grain orientation. Our previous work has provided evidence for this process using post-mortem analysis of samples, but the advent of high temperature loading coupled with in situ HEDM (with both near-field and far-field detectors) has offered an exciting possibility to directly observe the grain reorientation process. Exciting, preliminary results were obtained at CHESS with extensive aide from beam line scientist Darren Pagan, and in collaboration with Prof. Aaron Stebner and his group at

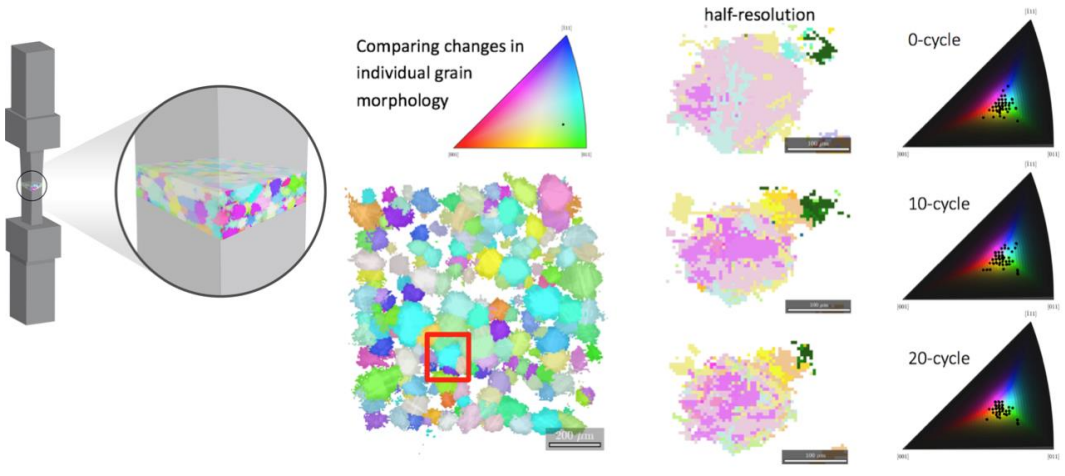

Fig. 3: Initial result form LBTC experiments on NiTi which are the first direct exploration of substructure development, and possible transformation-induced grain reorientation. Experiments conducted at CHESS with beam line scientist Darren Pagan and in collaboration with Prof. Aaron Stebner and Ashley Buscek at the Colorado School of Mines.

Colorado School of Mines. In situ LBTC experiments have been performed on both single crystal and polycrystalline NiTi samples. An example of a 3D reconstruction of grain and subgrain structures for a polycrystalline case is shown in Fig. 3. In this data set, a volume of 1 x 1 x 0.32 mm was sampled after reconstruction. Approximately 1500 grains have been identified and tracked during subsequent load-biased thermal cycles that take the sample above the martensite to austenite phase transition temperature (data was acquired at 120°C) under a constant bias stress of 100MPa. In the example shown in Fig. 3, the subdivision of a single grain in the volume is shown as a function of cycling, from 1 to 20. These exciting experiments are the first such experiments that combine near and far-field measurements at elevated temperature. Mining the datasets already acquired will continue over the next several months in order to develop a comprehensive understanding of substructure development during LBTC experiments.

Future Plans

We are presently calculating the interaction of the strain / stress field of such H-phase precipitates with martensite, both individual variants and internally twinned multi-variant combinations to quantify their effect on the nucleation of martensitic phase. The results will be incorporated in the nucleation model of the phase field simulation of the martensitic transformations to investigate the effect of these nanoprecipitates on the overall transformation behavior of the high-temperature SMAs. Data mining of the HEDM datasets that have been generated for both single crystal and polycrystalline NiTi samples will provide a comprehensive understanding of permanent strain development and accompanying substructure evolution during LBTC conditions. These results will be used to validate the competing hypotheses that have been proposed to explain this behavior.

Publications

1. Xiang Chen, From Nano-precipitates to Macroscale Composites: How Inclusion-Matrix Interactions Influence the Behaviors of Shape Memory Alloys and Structures, PhD Thesis, The Ohio State University (2015).

2. M.L. Bowers, Y. Gao, L. Yang, D.J. Gaydosh, M. De Graef, R.D. Noebe, Y. Wang, M.J. Mills. "Austenite grain refinement during load-biased thermal cycling of a Ni-Ti shape memory alloy." **Acta Materialia** 91 (2015), 318-329.

3. A. Hehr, X. Chen, J. Pritchard, M.J. Dapino and P.M. Anderson, "Al-NiTi Metal Matrix Composites for Zero CTE Materials: Fabrication, Design, and Modeling", **Advanced Composites for Aerospace, Marine, and Land Applications II**, (2015)13-28.

4. H. Paranjape, S. Manchiraju, P.M. Anderson, A phase field – Finite element approach to model the interaction between phase transformations and plasticity in shape memory alloys, International Journal of **Plasticity** 80 (2016) 1-16.

5. Y. Gao, R. Shi, J.F. Nie, S.A. Dregia, Y. Wang, "Group theory description of transformation pathway degeneracy in structural phase transformations", **Acta Materialia** 109 (2016), 353-363.

6. D. Wang, D. Lv, Y. Gao, Y. Wang, X. Ren, Y. Wang. "Defect strength and strain glass state in ferroelastic systems", **Journal of Alloys and Compounds** 661 (2016), 100-109.

7. Y.L. Hao, H.L. Wang, T. Li, J.M. Cairney, A.V. Ceguerra, Y.D. Wang, D. Wang, Y. Wang, H.L. Zhou, Q. Zhang, S.J. Li, R. Yang, "Superelasticity and tunable thermal expansion across a giant temperature range," **JMST** 32 (2016) 705-709.

8. D.R. Coughlin, L. Casalena, F. Yang, R.D. Noebe, M.J. Mills, "Microstructure–property relationships in a high-strength 51Ni–29Ti–20Hf shape memory alloy", **J. Mater. Sci.**, 51 (2016) 51, 766.

9. T. Yang, Y. Gao, D. Wang, R.P. Shi, Z. Chen, J.F. Nie, J. Li, Y. Wang, "Non-conservative dynamics of lattice sites near a migrating interface in a diffusional phase transformation", **Acta Materialia** 127 (2017), 481-490.

10. Kathryn Esham, *Precipitates and Nanoscale Templating of Martensite in Shape Memory Alloys*, MS Thesis, The Ohio State University (2017).

11. Y. Gao, S.A. Dregia, Y. Wang, "A universal symmetry criterion for the design of high performance ferroic materials", **Acta Materialia** 127 (2017), 438-449.

12. H. Paranjape, M.L. Bowers, M.J. Mills, P.M. Anderson, Mechanisms for phase transformation induced slip in shape memory alloy micro-crystals, **Acta Materialia** 132 (2017) 444-454.

13. J. Zhu, Y. Gao, D. Wang, T.Y. Zhang, Y. Wang, "Taming martensitic transformation via concentration modulation at nanoscale", **Acta Materialia** 130 (2017), 196-207.

14. Y. Gao, L. Casalena, M.L. Bowers, R.D. Noebe, M.J. Mills, Y. Wang, "An origin of functional fatigue of shape memory alloys", **Acta Materialia** 126 (2017), 389-400.

15. J. Zhu, H. Wu, D. Wang, Y. Gao, H. Wang, Y. Hao, R. Yang, T.Y. Zhang, Y. Wang, "Crystallographic analysis and phase field simulation of transformation plasticity in a multifunctional β-Ti alloy", **International Journal of Plasticity** 89 (2017), 110-129.

16. L. Casalena, G.S. Bigelow, Y. Gao, O. Benafan, R.D. Noebe, Y. Wang, M.J. Mills, "Mechanical Behavior and Microstructural Analysis of NiTi-40Au Shape Memory Alloys Exhibiting Work Output Above 400 °C," **Intermetallics** 86 (2017) 33-44.

17. L. Casalena, J.M. Sosa, D.R. Coughlin, F. Yang, X. Chen, H. Paranjape, Y.P. Gao, R.D. Noebe, G.S. Bigelow, D.J. Gaydosh, S.A. Padula, Y. Wang, P.M. Anderson, M.J. Mills, "Revealing Transformation and Deformation Mechanisms in NiTiHf and NiTiAu High Temperature Shape Memory Alloys Through Microstructural Investigations," **Microscopy and Microanalysis** 22 (S3), 1954-1955.

Plasticity of High-Strength Multiphase Metallic Composites

Amit Misra[1] (PI), Jian Wang[2] (co-PI), Jyoti Mazumder[1] (co-PI),

[1]University of Michigan, Ann Arbor; [2]University of Nebraska, Lincoln.

Program Scope

The goal of this research program is to elucidate the role of the microstructural scale, morphology and interphase boundary structure and crystallography in enabling plastic co-deformability in high-strength metallic composites containing disparate phases.

The proposed work aims to fill the gaps in knowledge in the fundamental understanding of plastic flow in metallic composites with soft/hard phases:

- Is plastic co-deformability favored as the interphase boundary spacing is reduced to nanoscale?

- Does the morphology (e.g., continuous vs degenerate lamellae or rods) of the hard phase influence plastic co-deformability?

- Can plastic co-deformability be achieved in composites with cubic/non-cubic phases?

- What is the role of the defect structure and crystallography of the interphase boundary in promoting plastic co-deformability?

Laser processed Al-Cu and Al-Cu-Si based eutectic systems are being used as model systems of metal-intermetallic composites with a range of sizes, morphologies and interface crystallography. Nanoindentation, micro-compression and tensile testing, and *in situ* nanoindentation and tension in high-resolution transmission electron microscope (TEM) are used to elucidate the mechanisms of slip transfer across and dislocation nucleation at interphase boundaries, and to quantify the local stresses that lead to plasticity in the intermetallic phase. The experimental research is conducted at University of Michigan with Prof. Mazumder leading the laser processing task and Prof. Misra leading the characterization task.

To develop fundamental understanding and predictive capability of the plastic co-deformation mechanisms, the experimental findings will be integrated with atomistic, meso-scale and crystal plasticity modeling, lead by Prof. Wang at Nebraska. Defect and interface-level properties obtained from atomistic modeling will be the input in the meso-scale model to compute strain hardening and local stress-strain response in a unit bi-crystal that will then be fed into the crystal plasticity finite element method to compute the macroscopic stress-strain response and compare with experimental measurements. The research will provide the scientific underpinning crucial to the design of ultra-strong metallic alloys (e.g., Al alloys with > 1 GPa strength levels) that exhibit significant plastic deformability at room temperature.

Recent Progress

This new program initiated in January 2017. In the first year, fine-scale binary Al-Cu and ternary Al-Cu-Si eutectics have been synthesized by laser surface remelting of arc-melted ingots. In the ternary system, a bimodal ultrafine eutectic structure is observed. By controlling the cooling rate of the laser solidification process, the relative volume fractions of coarse and fine eutectics in bimodal microstructure can be varied. Laser remelted microstructures with volume fractions of the fine eutectic varying from 25 to 40 % exhibit compressive flow strengths ranging from 500 to 900 MPa. In addition to the compression tests, the laser remelted alloys were rolled at room temperatures to reductions > 40% to examine the plastic co-deformability. While the as-cast alloys exhibited cracking around hardness indents as well as in compression tests and rolling, the ultra-fine scale laser remelted microstructures revealed evidence of plasticity in metallic as well as intermetallic phases. The line defects observed experimentally in the Al_2Cu phase of the deformed eutectics were analyzed using atomistic simulations. Seven potential slip systems $(110)\langle 001\rangle$, $(010)\langle 001\rangle$, $(310)\langle 001\rangle$, $(010)\langle 100\rangle$, $(110)\langle 110\rangle$, $(110)\langle 111\rangle$ and $(112)\langle 111\rangle$ in Al_2Cu with body centered tetragonal structure were studied. It was found that three edge dislocations with Burgers vector $\langle 001\rangle$ on glide planes (110), (010), and (310), show an extended core and are predicted to be glissile at room and moderate temperatures. Other four edge dislocations associated with slip systems $(010)\langle 100\rangle$, $(110)\langle 110\rangle$, $(110)\langle 111\rangle$ and $(112)\langle 111\rangle$ and three screw dislocations with Burgers vectors $\langle 001\rangle$, $\langle 110\rangle$, and $\langle 111\rangle$ show a condensed core, and exhibit significantly higher Peierls barrier for glide at room temperature. Plastically deformed laser processed Al-Al_2Cu eutectics exhibited {121}1/2<111> shear in nanoscale Al_2Cu lamellae (Fig. 1). This shear is presumably induced by the nanoscale confinement since it is energetically unfavorable in monolithic Al_2Cu at room temperature.

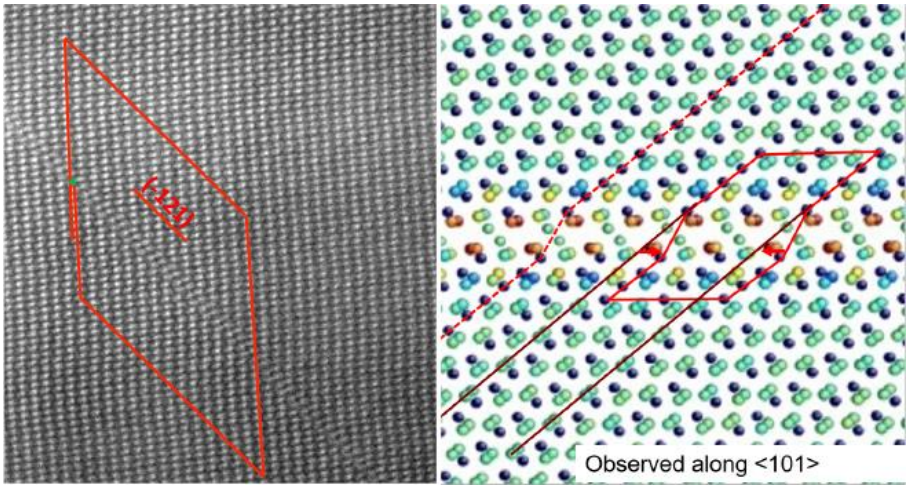

Figure 1. Left: High-resolution TEM image showing plastic shear induced stacking fault on the (-1 2 1) plane in Al_2Cu nanolayer in laser processed Al-Al_2Cu eutectic. Zone axis is [101] Al_2Cu. Right: Atomic structure of a stacking fault on (-1 2 1) plane, confirming the shear vector associated with the stacking fault is 1/2<111>. Cu atoms are colored in the blue. Others are Al atoms with different excess energy.

Future Plans

TEM characterization, including *in situ* indentation, will be used to elucidate the slip events and the activation of slip in the hard phase as a function of lamellae thickness and interface crystallographic orientation. The crystallography of the defects observed in the intermetallic phase will be correlated with the active slip systems in Al for both binary Al-Cu and ternary Al-Si-Cu systems.

Molecular dynamics simulations will be used to explore plastic deformation mechanisms in Al-Al_2Cu eutectics. The focus is on understanding the role of accumulated defects associated with plastic deformation in Al layers in facilitating plastic deformation in Al_2Cu with respect to lamellae thickness and interface crystallographic orientation that are observed in experiments.

Publications

Jian Wang, Qing Zhou, Amit Misra, Ping Huang, Fei Wang, and Kewei Xu, *Dislocation Interaction induced Structural Instability in Intermetallic Al_2Cu*, NPJ-Computational Materials, **3** (2017), 24. doi: 10.1038/s41524-017-0030-2

Qing Zhou, Jian Wang, Amit Misra, Ping Huang, Fei Wang, and Kewei Xu, *Atomistic study of fundamental character and motion of dislocations in intermetallic Al_2Cu*, International Journal of Plasticity, **87** (2016) 100-113. doi: 10.1016/j.ijplas.2016.09.005

Jian Wang, Qing Zhou, Shuai Shao, Amit Misra, *Strength and Plasticity of Nanolaminated Materials*, Materials Research Letters, **5** (2017) 1-19. doi: 10.1080/21663831.2016.1225321

High-throughput nano-indentation of polycrystalline FCC metals with in-situ plane tension

S. Papanikolaou (PI), Department of Mechanical and Aerospace Engineering, West Virginia University
K. Hemker (co-PI), Department of Mechanical Engineering, Johns Hopkins University

Program Scope

Nanoindentation of crystals at the ultra-nano regime (<100nm) is plagued by surface roughness randomness and by intrinsic material deformation random fluctuations (known as pop-ins) due to pre-existing dislocation microstructure. Both extrinsic and intrinsic randomness contribute to a very stochastic behavior that is commonly neglected by scientists and engineers. Is it possible to detect and classify dislocation microstructures through stochastic but high-throughput nano-indentation data?

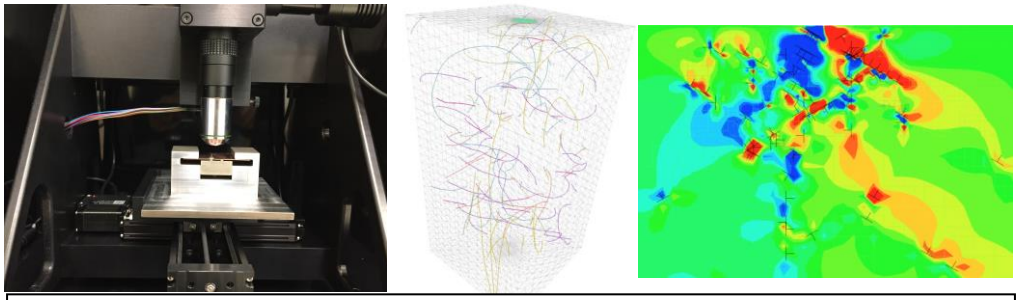

High-throughput Nanoindentation and Extensive Dislocation Dynamics Simulations: (Left): Nanoindentation of a Cu sample, under in situ tension, in austom-built 4-pt bending fixture. (Center): 3D Discrete Dislocation Dynamics of Nanoindentation, (Right): 2D Discrete Dislocation Dynamics of Nanoindentation.

The scope of this program is to investigate and characterize the multiscale character of crystal plasticity in FCC metals in the ultra-nano regime, using high-throughput nano-indentation experiments and multi-scale simulations (2D/3D Discrete Dislocation Dynamics (DDD) simulations, and Molecular Dynamics). The ultimate target is to identify: i) ways to mitigate the intrinsic and extrinsic randomness effects through the application of in-plane tension, ii) universal measures, beyond simple scalar quantities like hardness, that will allow nanoindentation to detect and characterize various dislocation microstructures in terms of their mobile/immobile quality.

The basic hypotheses of the project are that: a. Intrinsic indentation deformation originating in small grains of a polycrystal can be as abrupt as in micropillar compression experiments, b. In-plane stress can intrinsically reduce hardness and smoothen the overall plastic response during nanoindentation, mitigating extrinsically and intrinsically induced noise.

Recent Progress

During the first two years of the project, both experiments and simulations have advanced significantly. Our project builds upon prior research findings, especially Oliver and Pharr's basic indentation approach [1], the main results on the effects of in-plane stress on nanoindentation properties such as hardness and moduli [2,3], and the identification of pop-in loads in FCC crystals [2]. We have identified a set of generic effects of applied in-plane tension on the

indented surface that go beyond prior research on the topic, given that we focus on the ultra-nano <100nm regime. Nanoindentation experiments utilize custom 4-pt bending fixtures that have been manufactured with the purpose to impose tensile stress on the top surface of polished polycrystalline specimens. In this way, indentation can be performed in-situ and at nanoscale resolution. In the first two years, 3 versions of the 4-pt bending fixture have been built, gradually decreasing the dimensions. Currently, the state-of-art device applies tensile stress on 10mm x 10mm x 0.5mm specimens that are concurrently indented. Polycrystalline pure Cu, Al and Ni samples are tested at the 4-point bending fixture and consequently indented to 100nm. These experiments are clearly focused on the statistical effects that may emerge either from extrinsic or intrinsic disorder effects. Statistical correlations of nanoindentation in polycrystalline samples have been calculated in connection to the measured hardness values; in association, the **StatIndent Python** numerical software has been developed to analyze indentation data, derived from generic nanoindenter devices, in correlation with associated images, and perform data mining and machine learning. For this purpose, grain orientation maps (identified through electron backscatter diffraction (EBSD) measurements) are being correlated with indentation arrays on FCC polycrystalline samples (Ni, Cu, Al).

Experiments are corroborated by state-of-art indentation simulations using 2D-DDD [5] and 3D-DDD [6] methods. 2D

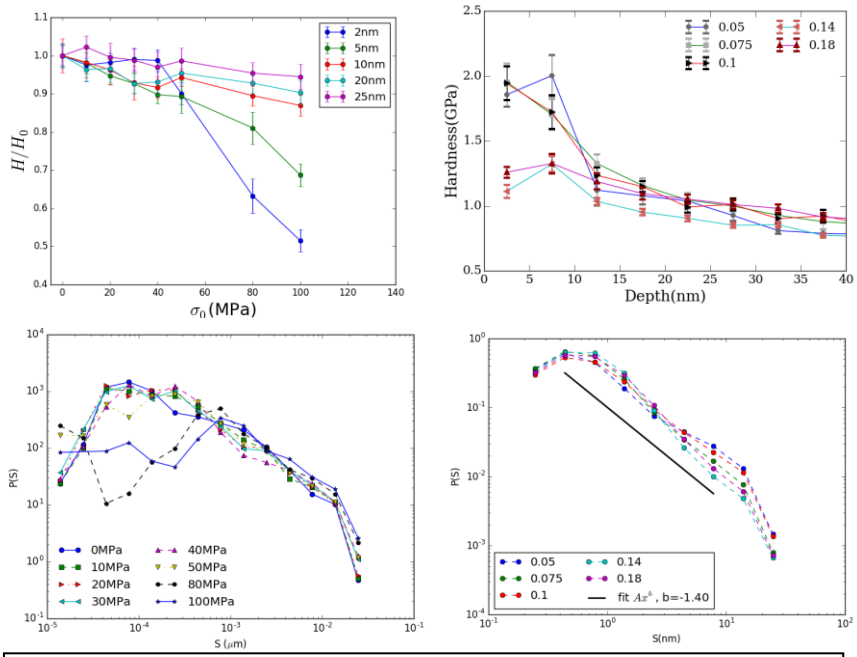

Hardness and pop-in statistics as function of applied load in experiments on pure polycrystalline Al and 2D DDD simulations: (Top Left): Hardness vs. applied stress for various depths in 2D DDD, (Top Right): Hardness vs. depth for various applied loads in pure Al, (Bottom Left): Abrupt event distributions in 2D-DDD indentation, (Bottom Right): Abrupt event distributions in pure Al experiments.

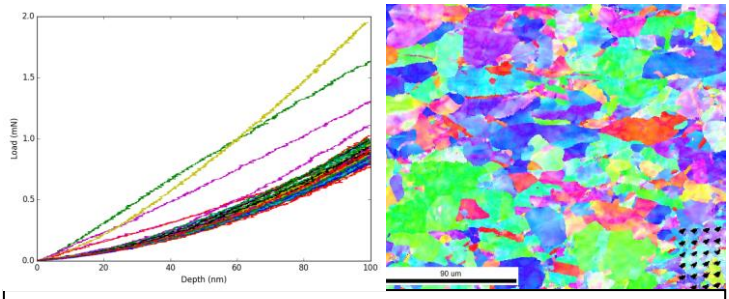

Nanoindentation force-depth curves (Left) and EBSD orientation maps(Right) of pure polycrystalline Ni, that are being mutually correlated using the **StatIndent** Python Package.

edge dislocation dynamics indentation simulations are used for insights, while 3D discrete dislocation dynamics indentation simulations are utilized to confirm findings and compare with experimental results.

In summary, we have identified that:

1. Indentation noise induced by extrinsic roughness is dramatically decreased by applied in-plane tension beyond the plastic yield point of the material.

2. Statistically, measured hardness through the continuous stiffness method is decreased in polycrystalline Al, for indentation depths below 20nm. This novel size effect finding has been justified by extensive 2D-DDD simulations and it is currently under thorough investigation in various FCC polycrystalline materials (Cu, Ni), single crystal FCC and BCC metals, and also 3D-DDD and MD simulations.

3. Pop-in events, induced by a Berkovich tip, measured in an unbiased manner for depths up to 100nm, display a universal (across stress level) power-law tail. Remarkably, increased tensile stress appears to have an effect at the probability for small pop-in events, being drastically reduced. In a way, these events resemble the abrupt events in uniaxially stressed pillars, even though there are distinct differences.

4. Nanoindentation timeseries is correlated with grain orientation and size in polycrystalline FCC metals (especially Ni, Cu, Al) and further investigation is currently pursued.

5. Preliminary statistical investigation, using machine learning methods, has been performed on synthetic nanoindentation timeseries, produced in simulations, towards a direct and swift dislocation density and grain orientation estimation.

Overall, through combined simulation and experiments, we have identified a novel sensitivity of indentation behavior to plane tension in generic FCC metals. These results are in consistency with the basic hypotheses of the project, even though further investigation is required.

Furthermore, the PI has promoted the importance of strain bursts in crystal plasticity, by co-authoring a review on strain bursts in crystal plasticity and also, co-authoring contributions on the detection of strain bursts using dynamical loading approaches and coarse-grained approaches to dislocation dynamics, in collaboration with other PIs (Cai, Greer) of the DOE-BES program.

Future Plans

The future plans in this project deepen further in the experimental and theoretical fronts, while promoting a unique integration of Large Data production and theoretical analysis that lead to the development of state-of-art open-source software that should be useful to experimental groups. Furthermore, we are rapidly pursuing the following tasks during the next year:

1. Single crystals and polycrystals Cu, Ni, Al, will be explicitly compared with respect to the newly found statistical indentation size effect. Similar measurements will be performed on BCC and HCP metals

2. Extensive 3D DDD indentation simulations will be performed in the presence of voids,

inclusions, and machine learning approaches will be trained in order to interpret high throughput experimental data from FCC metals.

3. 3D Molecular Dynamics simulations will be performed in order to identify the basic mechanisms and validate the ultra-nano size effect that we have identified using discrete dislocation dynamics.

4. The StatIndent software package will be developed further and will aim at including post-indent images in order to also include them in machine learning approaches.

References

1. Oliver, W.C. and Pharr, G.M., 1992. An improved technique for determining hardness and elastic modulus using load and displacement sensing indentation experiments. *Journal of materials research*, *7*(6), pp.1564-1583.
2. Tsui, T.Y., Oliver, W.C. and Pharr, G.M., 1996. Influences of stress on the measurement of mechanical properties using nanoindentation: Part I. Experimental studies in an aluminum alloy. *Journal of Materials Research*, *11*(3), pp.752-759.
3. Suresh, S. and Giannakopoulos, A.E., 1998. A new method for estimating residual stresses by instrumented sharp indentation. *Acta Materialia*, *46*(16), pp.5755-5767.
4. Shim, S., Bei, H., George, E.P. and Pharr, G.M., 2008. A different type of indentation size effect. *Scripta Materialia*, *59*(10), pp.1095-1098.
5. Balint, D.S., Deshpande, V.S., Needleman, A. and Van der Giessen, E., 2006. Discrete dislocation plasticity analysis of the wedge indentation of films. *Journal of the Mechanics and Physics of Solids*, *54*(11), pp.2281-2303.
6. Po, G., Lazar, M., Seif, D. and Ghoniem, N., 2014. Singularity-free dislocation dynamics with strain gradient elasticity. *Journal of the Mechanics and Physics of Solids*, *68*, pp.161-178.

Publications

1. Yavas, H., Song, H., Hemker, K.J. and Papanikolaou, S., 2017. Detecting in-plane tension induced crystal plasticity transition with nanoindentation. *arXiv preprint arXiv:1706.08910*.

2. Song, H., Yavas, H., Van der Giessen, E. and Papanikolaou, S., 2017. Discrete Dislocation Dynamics Simulations of Nanoindentation with Pre-stress: Hardness and Statistics of Abrupt Plastic Events. *arXiv preprint arXiv:1707.03915*.

3. Papanikolaou S., Tzimas M., Song H. , Reid A., Langer S. 2017 Learning Crystal Plasticity using digital image correlation: Examples from discrete dislocation dynamics. *arXiv: (submitted to JMPS)*

4. Papanikolaou, S., Song, H. and Van der Giessen, E., 2017. Obstacles and sources in dislocation dynamics: Strengthening and statistics of abrupt plastic events in nanopillar compression. *Journal of the Mechanics and Physics of Solids*, *102*, pp.17-29.

5. Papanikolaou, S., Cui, Y. and Ghoniem, N., 2017. Avalanches and Plastic Flow in Crystal Plasticity: An Overview. *arXiv preprint arXiv:1705.06843*. *(invited review, submitted to MSMSE)*

6. Ni, X., Papanikolaou, S., Vajente, G., Adhikari, R.X. and Greer, J.R., 2017. Probing Microplasticity in Small-Scale FCC Crystals via Dynamic Mechanical Analysis. *Physical Review Letters*, *118*(15), p.155501.

7. Akhondzadeh Sh., Sills R. B., Papanikolaou S., Van der Giessen, Cai W., Geometrically Projected Discrete Dislocation Dynamics, arXiv:

8. Ispanovity, P. D., Papanikolaou S., Groma I., The Emergence and Role of Dipolar Dislocation Patterns in Discrete and Continuum Formulations, submitted to Phys. Rev. Letters, arXiv: 1975404 (2017)

NanoMechanics: Friction and Elasticity of Nano-Objects

Elisa Riedo

City University of New York (CUNY) Advanced Science Research Center

Program Scope

Nanosheets, nanotubes, nanowires, and nanoparticles are gaining a large interest in the scientific community for their exciting properties, and they hold the potential to become building blocks in integrated nano-electronic and photonic circuits, nano-sensors, batteries electrodes, energy harvesting nano-systems, and nano-electro-mechanical systems (NEMS). The vision of this DoE research program is to understand the mechanical properties of nanoscale materials by exploring new experimental methods and theoretical models at the boundaries between continuum mechanics and atomistic models, with the overarching goal of defining the basic laws of mechanics at the nanoscale.

The goal of our research program is to study the frictional properties and the transverse elasticity of 2D materials as a function of number of layers, substrate interaction, stacking, intercalates, and defects. We aim at investigating the mechanical interaction between atomically thin sheets, with the ultimate goal of manipulating their structure, stacking, and number of layers for producing nano-materials with tailored optimum mechanical, electro-mechanical and thermo-mechanical properties.

Recent Progress

The research activity during this first year has been divided in two main projects. In the first project we have investigated the elasticity of one- and two-layer graphene, and the buffer-layer of epitaxial graphene, in the second project the goal has been to investigate the Van der Waals forces, adhesion and frictional properties of MoS_2 and other 2D films as a function of number of layers, presence of piezoelectricity, stacking–e.g. orientation–, substrate, intercalates, and defects. Below we provide details about the main projects and related accomplishments.

1) **Inducing a diamond-stiff phase in two-layer graphene: the fingerprint of diamene [1, 2]**

The quest for materials with exceptional mechanical properties has been the focus of major efforts since the beginning of civilization. In particular, discovering materials stiffer and harder than diamond is an ongoing challenge. While graphite has an elastic modulus similar to diamond in the plane, it is much softer in the transverse direction— perpendicular to the planes. The discovery of graphene, a single atomic layer of graphite, has opened a new plethora of properties related to the two-dimensionality of this material, including unique electronic and mechanical

properties. Here, we show that upon indentation with a nano-size tip, two-layer graphene supported and grown on SiC (0001) displays a transverse stiffness and hardness equal or larger than that of bulk diamond. This phenomenon vanishes for graphene films thicker than 3 to 5 layers or for a single layer, demonstrating a unique phase diagram for two-layer epitaxial graphene. Density functional theory (DFT) calculations explain the experimental results, showing that pressures of the order of 1-10 GPa at room temperature can transform two-layer epitaxial graphene into an ultra-stiff diamond single layer, here called diamene. DFT calculations also indicate that this graphitic-to-diamond phase transition depends on the availability of mechanisms to saturate surface dangling bonds and it is hindered for more than two layers.

Here, we use modulated nanoindentation (MoNI) [2, 11] to measure force vs. indentation curves when an AFM tip indents epitaxial graphene (EG) films supported by a SiC substrate, for maximum indentation depths smaller than 1 Å. For 10-layer epitaxial graphene (10-L epitaxial graphene) the indentation curves are almost the same as for bulk Highly Ordered Pyrolytic Graphite (HOPG). We also measure the indentation curves for 5-layer EG on SiC (0001), as well as the indentation curves measured on bare SiC. The indentation curves measured on SiC can be perfectly fitted with the Hertz model for a Si sphere (the AFM tip) indenting a flat substrate (SiC). The fitting procedure gives as SiC Young's modulus E_{Hertz}^{SiC} = 400 GPa, which is in excellent agreement with values in literature. Compared to SiC, 5-L epitaxial graphene is much softer since we are still probing the soft *c*-axis out-of-plane modulus of a graphitic system. However, 5-L epitaxial graphene on SiC displays slightly steeper (stiffer) curves than 10-L epitaxial graphene, very likely because of the influence of the very stiff SiC substrate. When measuring the very first graphene-like layer on SiC (0001), which is strongly interacting with the SiC substrate, and it is referred to as buffer layer, we obtain almost the same, but slightly softer, indentation curves than in bare SiC. This behavior is in agreement with physical intuition and with previous indentation measurements in thin films, which show that when a film on a rigid

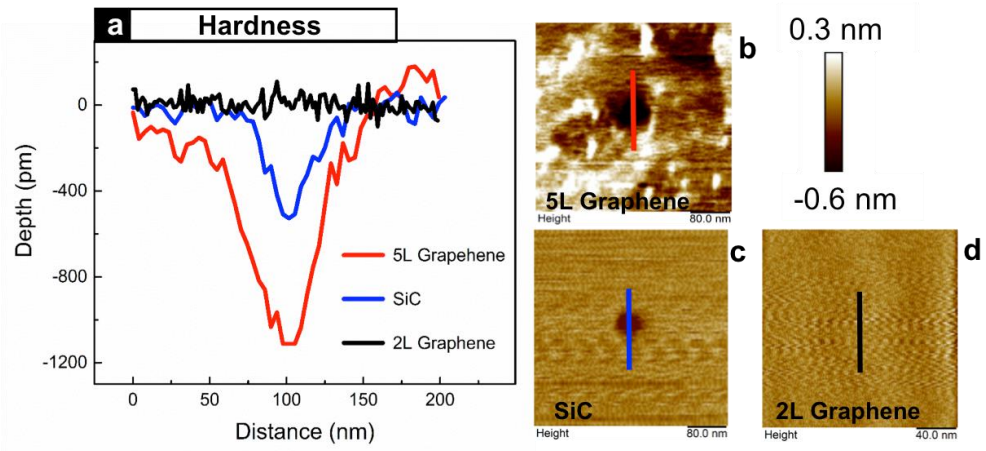

Figure 1 | Micro-hardness measurements. AFM topographical images of the residual indents in 2-L graphene (**d**), SiC (**c**), and 5-L graphene (**b**) upon indentation with a diamond indenter. **a**, Cross section profile of the residual indents in 2-L graphene, SiC and 5-L

substrate is thin enough the measured indentation curves sense the stiffness of the underlying substrate. Overall the indentation curves for 10-L, 5-L and buffer layer graphene on SiC follow a predictable behavior, and two-layer epitaxial graphene was expected to display indentation curves with intermediate values between 5-L and the buffer layer. However, very surprisingly when we indent two layers of graphene on SiC, we obtain force vs. indentation curves which are much steeper than the ones for 5-L or 10-L graphene and even steeper than on bare SiC. Such large stiffness, corresponding to a Young's modulus larger than 1 TPa, can only be understood with a structural change induced by the local pressure on two-layer graphene.

To further investigate the ultra-stiff phase induced in two-layer graphene, we have performed micro-hardness measurements with a diamond AFM indenter (Fig. 1). Upon indentation with a load of 6 □N and with subsequent imaging, we were able to identify a shallow residual indent in SiC, a larger indent in 5-layer graphene and no residual indent at all in two-layer graphene. When applying larger loads on two-layer graphene, the tip broke.

2) **Oscillatory friction for even and odd number of layers in polycrystalline MoS_2 [3]**

The frictional properties of 2D materials are attracting a large attention in the scientific community for their interesting and unusual behavior. Here, we have studied by atomic force microscopy (AFM) the frictional properties of MoS_2 in the form of polycrystalline CVD grown films and monocrystalline CVD grown triangular islands on sapphire. Interestingly, while friction forces monotonically decrease with increasing number of layers for monocrystalline CVD grown MoS_2, as it was previously observed in literature for MoS_2 exfoliated flakes, we observe that polycrystalline MoS_2 gives rise to a friction behavior that follows a odd-even oscillatory pattern with the number of layers. To understand this oscillatory frictional behavior for polycrystalline MoS_2, we have performed AFM friction and adhesion measurements in dry and humid conditions. We observed that in dry conditions the oscillatory behavior disappears and polycrystalline MoS_2 behaves as the monocrystalline sample. Furthermore, the force spectroscopy measurements indicated that the origin of the oscillations in friction could mainly be ascribed to the changes in adhesion forces as a function of odd and even number of layers. These results suggest that there is a different amount of water on the surface of odd or even number of layers in the polycrystalline MoS_2 sample due to the broken inversion symmetry when the number of layers in the film is an odd number, e.g. 1 and 3. When the structure is monocrystalline, the in-plane polarization may change the amount of water adsorbed at the edges of the triangular structure, without impacting the friction and adhesion forces with the surface. However, in the case of a polycrystalline film, each crystalline grain may display a different direction of the in-plane polarization, giving rise to uncompensated charges at the grain boundaries, which may induce a larger adsorption of water in the case of one- and three-layer films. These results have been further corroborated by XPS and Kelvin Probe Force Microscopy measurements, indicating an oscillatory behavior of the work function in the case of the polycrystalline films.

Future Plans

Firstly we plan to investigate more in detail the amazing bilayer-diamene phase transition that we have recently discovered. Secondly, we propose to investigate the perpendicular elasticity, e.g. the unique van der Waals elastic interaction, and frictional behavior of 2D heterostructures made of a variety of vdW materials, including mixing insulating, metallic and semiconducting layers. The research will start by focusing on MoS2 and other transition metal dichalcogenides 2D films. On a third side, we will continue our investigation on the relationship between defects, piezoelectricity and friction in TMDC films.

Publications

1. Y. Gao, T. Cao, C. Berger, W. de Heer, E. Tosatti, A. Bongiorno, E. Riedo "Inducing a diamond-stiff phase in two-layer graphene: the fingerprint of diamene", submitted.
2. Yang Gao, Filippo Cellini and Elisa Riedo "Modulated NanoIndentation, a new method for A-indentation experiments in stiff ultrathin films", in preparation.
3. Francesco Lavini, Annalisa Calo, Yang Gao, Carmela Aruta, Elisa Riedo "Oscillatory friction behavior for even and odd number of layers in polycrystalline MoS2", submitted.
4. E. Albisetti, D. Petti, M. Madami, S. Tacchi, P. Vavassori, E. Riedo, R. Bertacco "Nanopatterning spin-textures: A route to reconfigurable magnonics" AIP Advances, (7), 5, 10.1063/1.4973387 (2017)
5. A. Gurarslan, S. Jiao, T.- D. Li, G. Li, Y. Yu, Y. Gao, E. Riedo, Z. Xu, L. Cao, "Van der Waals Force Isolation of Monolayer MoS2" Advanced Materials, (2016) doi: 10.1002/adma.201601581
6. E. Albisetti, D. Petti, M. Pancaldi, M. Madami, S. Tacchi, J. Curtis, W.P. King, A. Papp, G. Csaba, W.Porod, P. Vavassori, E. Riedo, R. Bertacco, "Nanopatterning reconfigurable magnetic landscapes via thermally assisted scanning probe lithography" Nature Nanotechnology, 11, 545–551 (2016) doi:10.1038/nnano.2016.25 (Cover article)
7. R. V. Ulijn and E. Riedo "Learning to think systems" Nature Nanotechnology, 11 (9), 824-824 (2016)
8. Carroll, Keith; Wolf, Heiko; Knoll, Armin; Curtis, Jennifer; Zhang, Yadong; Marder, Seth; Riedo, Elisa; Duerig, Urs "Understanding how Charged Nanoparticles Electrostatically Assemble and Distribute in 1-D" Langmuir (2016) doi: 10.1021/acs.langmuir.6b03471
9. Albisetti, Edoardo; Carroll, Keith; Xi, Lu; Curtis, Jennifer; Petti, Daniela; Bertacco, Riccardo; Riedo, Elisa, "Thermochemical scanning probe lithography of protein gradients at the nanoscale" Nanotechnology, 27 (31), 315302 (2016)
10. Abdelghani Laraoui, Halley Aycock-Rizzo, Yang Gao, Xi Lu, Elisa Riedo, Carlos Meriles, "Imaging thermal conductivity with nanoscale resolution using a scanning spin probe" Nature Communications 6, 8954, (2015) doi:10.1038/ncomms9954
11. Y. Gao, Si Zhou, S. Kim, H.-C. Chiu, D. Nélias, C. Berger, W.de Heer, L. Polloni, R. Sordan, A. Bongiorno and E. Riedo, "Elastic coupling between layers in two-dimensional materials", Nature Materials 14, 714–721 (2015), DOI: 10.1038/nmat4322

Mechanical Behavior of Materials: Damage-Tolerant Structural Materials

Robert O. Ritchie, Mark Asta and Andrew M. Minor

Lawrence Berkeley National Laboratory

Program Scope

The attainment of strength and toughness is a vital requirement for structural materials; unfortunately, these properties are generally mutually exclusive. Indeed, the development of strong and tough materials has traditionally been a compromise between hardness *vs*. ductility. Using advanced metallic alloys, we examine strategies to solve this "conflict" by focusing on the interplay between the individual mechanisms that contribute to strength and toughness, that of plasticity and crack-tip shielding, noting that these phenomena originate at very different structural length-scales. Over the past two years, we have directed our studies to seeking an understanding, at atomistic to near-macroscopic length-scales, of the scientific origins of damage-tolerance in multi-element metallic alloys. Our focus has been on single-phase high-entropy alloys and metallic glasses, which can display exceptional damage tolerance, due to novel mechanisms that arise from their disordered structures. Our approach to understanding damage-tolerance in CrCoNi-based high-entropy alloys has involved fracture mechanics coupled with *in situ* SEM and TEM testing to discern the synergy of dislocation and twinning mechanisms responsible for their properties. For metallic glasses, we have focused on the existence of short and medium range ordering within the amorphous state and its role in triggering shear-band formation, which we believe represents the fundamental origin of plasticity and toughness in these alloys. Our ultimate aim is to uncover the relationships between atomic-scale phenomena and the macroscopic mechanical behavior of structural materials.

Recent Progress

Our research combines state-of-the-art experimental characterization, atomistic computational modeling, and theory to probe the mechanics and mechanisms of deformation and fracture at multiple dimensions in structural materials. We are currently focusing on nominally single-phase, multiple-element metallic alloys, which have limited recognizable structure over most length-scales - metallic glasses and high-entropy alloys - with the aim of discerning the fundamental mechanistic origins of damage tolerance, *i.e.*, toughness (resistance to fracture) without compromise in strength (resistance to deformation). An ability to undergo limited deformation is a crucial feature of toughness as this enables the local dissipation of stresses which would otherwise cause fracture; alloy design is thus a compromise of strength *vs*. ductility, properties that are invariably mutually exclusive.[1]

Metallic Glasses: We have studied bulk metallic glasses (BMGs) for many years and have developed the most damage-tolerant glass alloy on record, *e.g.*, a Pd-based BMG[2], with Bill Johnson at Caltech. Although BMGs tend to be strong (strengths >1-2 GPa), they deform by shear banding, which can lead to brittleness as a single shear band can cause failure at vanishingly small tensile strains. The key to attaining ductility in BMGs is to promote multiple shear banding and to inhibit cavitation within the bands to prevent cracks, a characteristic that we achieved in the Pd-based BMG with an alloy with a high bulk-to-shear modulus ratio.[2]

However, we have realized that the toughness of a specific BMG alloy tends to be highly variable, a property that we believe is a result of two distinct issues. Firstly, we have shown that the lack of strain hardening in BMGs curtails the existence of the unique singular crack-tip stress/displacement fields in a nonlinear-elastic (*J*-based) fracture mechanics test; as the local crack-tip stress and strains can no longer be presumed to be unique, fracture toughness measurements become compromised.[3] Secondly, it appears that the amorphous state itself is not uniform due to the presence of short- (SRO) to medium-range (MRO) order. We have initiated both theoretical and experimental work to probe structure-property relations in metallic glasses, with the goal of understanding if their properties can be determined by atomic-level structure. Based on atomistic computer simulations of the SRO within the second nearest-neighbor shells in BMGs, derived from atomic cluster connection schemes between linked coordination polyhedral, we have shown that cluster connections by face-sharing yield the stiffest elastic response during shear deformation, and are favored when changing from the liquid to glassy state.[4] We have also examined the effect of hydrostatic pressure on the rejuvenation of $Cu_{50}Zr_{50}$ glasses, finding anomalous structure-property relationships can result after removal of the pressure at room temperature; the glasses are less stable and display a lower shear modulus, despite having a denser packing structure, and a significant increase in full icosahedra SRO.[5]

High Entropy Alloys: Our work on high-entropy alloys (HEAs), which are a new class of nominally equiatomic, five or more element, metallic systems, has largely been conducted in close collaboration with Easo George at ORNL and has focused on CrCoNi-based alloy systems. The rationale for HEAs is that, in principle, the configurational entropy contribution to the total free energy from their multi-element composition should stabilize solid solutions relative to multi-phase microstructures.[6] We have examined two alloys to date, the CrMnFeCoNi (Cantor) HEA and the CrCoNi medium-entropy alloy (MEA), both single-phase, face-centered cubic materials which we have shown to exhibit truly remarkable mechanical properties.[7-10]

With the five-element CrMnFeCoNi HEA, we found exceptional damage tolerance, with tensile strengths >1 GPa and (crack-initiation) fracture toughnesses of K_{Ic} > 200 MPa√m, properties which were progressively enhanced at low temperature.[7] We also studied the three-element (medium-entropy) CrCoNi alloy, where we observed even better properties: at 77K, UTS >1.3 GPa, ductility ~ 90%, K_{Ic} values ~ 275 MPa√m, and a "valid" crack-growth toughness of 450 MPa√m, properties that approach the best of any material on record.[8] At low temperatures ~77K, both alloys exhibit increasing strain hardening which inhibits localization to give enhanced strength and ductility. To understand the nanoscale mechanisms underlying this behavior, *in situ* straining to fracture experiments in an aberration-corrected TEM revealed a synergy of deformation mechanisms that appear to be unique to these alloys. Both materials are characterized by high lattice friction; perfect dislocation motion is correspondingly slow along planar slip bands, which provides for strength.[9] They also display low stacking fault energies; as such partial dislocations move rapidly (Fig. 1), which is a source of ductility.[9,10] We also found that cracking appears is impeded by twinned, nano-scale bridges which span the near-tip crack faces and act to delay fracture by shielding the crack tip.[9] This synergism of intrinsic (plasticity-related) and extrinsic (shielding-related) toughening represents an effective means to enhance damage tolerance that differs from usual strategies where

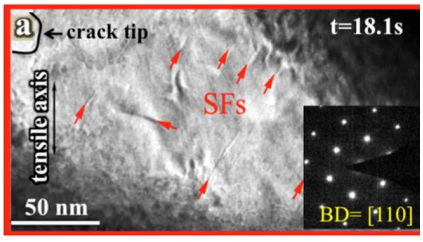

Fig. 1: *In situ* TEM[9] of crack-tip dislocation emission in CrMnFeCoNi.

secondary phases and hetero-interfaces are added. At 77K, deformation in the CrMnFeCoNi alloy[7] involves nano-twinning, but in CrCoNi, a hierarchical twin network forms at 298K, where the twin boundaries act as barriers to dislocation motion, providing for strength, whereas the partial dislocations can move rapidly along the boundaries themselves, which provides for ductility.[10]

Future Plans

Metallic Glasses: Our pursuit of the origins of damage-tolerance is now centered on computational work and state-of-art microscopy, spurred by an appreciation that specific SRO in the glassy state can be tuned to yield specific properties.[11] In light of this, we are focused on establishing structure-property links through the use of simulations to understand how the SRO influences shear banding. We believe that such insights will provide a fundamental understanding of the properties of BMGs.

Our hypothesis is that BMGs, while macroscopically uniform and single phase, have an inherently inhomogeneous structure with atoms in many local configurations: two extremes are characteristic SRO, the favored atomic coordination motifs[12] and geometrically unfavorable motifs (GUMs).[13] Many GUMs may simply be local configurations with less SRO retained during fast liquid cooling and containing excess "free volume". A link between the structural and mechanical heterogeneity is "soft spots", *i.e.*, aggregates of atoms that strongly participate in soft vibrational modes and correlate with GUM-rich regions, yet are heterogeneously localized into nano-scale regions. These soft spots directly reflect dynamic response that also scales with the possibility of shear transformation and thus may correlate with local groups of atoms that tend to undergo cascade deformation.[13] Our belief is that ductility will be enhanced by a proliferation of soft spots through different processing histories. Conversely, the lack of soft spots would stifle plastic flow, analogous to dislocation starvation that elevates strength in crystals. As it is unclear how GUMs induce yielding in a BMG, we propose to employ large-scale MD and mesoscale simulations to clarify these questions in BMGs with different GUM distributions. An example is shown in Fig. 2 from studies with Lin Li (Un. Alabama) to explore the role of elastic heterogeneity, induced by fluctuations in structural order, on shear banding.

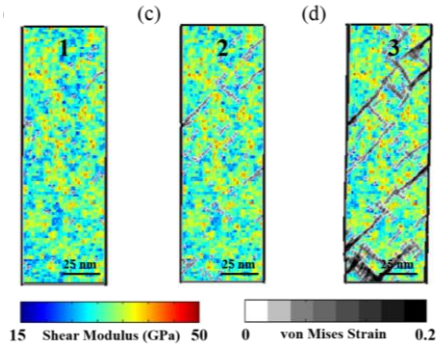

Fig. 2: Computational simulation of strain localization paths in a metallic glass.

To enable direct experimental validation of our numerical models, a central challenge is the experimental characterization of structural SRO and MRO. To characterize these states in BMGs, we are using fluctuation electron microscopy[14] and scanning nano-diffraction[15]. Aberration-corrected scanning transmission microscopes (STEM), coupled with fast direct electron detectors allow us to compare the variance in diffraction patterns from point to point to create a quantitative map of local order (Fig. 3). Here, we employ the 4DSTEM technique[15] that uses a series of 2D diffraction patterns collected at each position in a 2D STEM raster scan resulting in a 4D data set. As shown in Fig. 2b, by taking advantage of direct electron counting we can visualize "hot spots", or multi-pixel regions of similar symmetry in the diffraction patterns. These span 3-4 pixels, or 1.5-2 nm, and represent direct imaging of the medium range order of the sample.

Our intent is not only to be able to quantify the SRO for essentially macroscopic samples, but also to perform experiments in the TEM that explicitly link shear-band formation, and hence the origin of plasticity in BMGs, to regions of unstable short-range order (GUMs). Our goal is to establish

quantitative structure-property relationships between GUMs and mechanical behavior, which can lead to an understanding of the fundamental origins of damage-tolerance in metallic glasses.

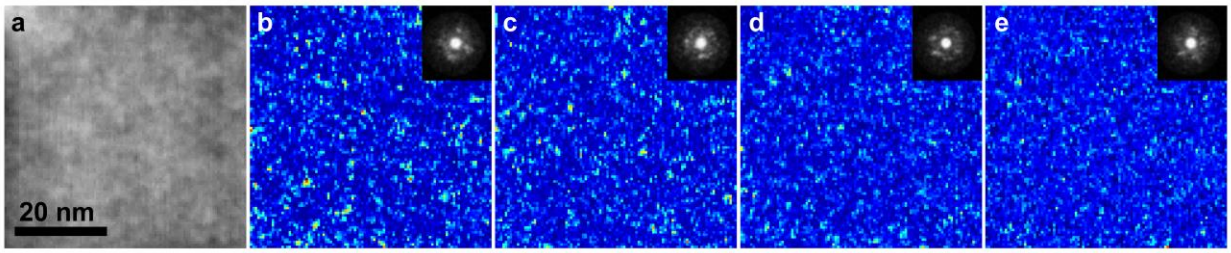

Fig. 3: a) Annular dark field image of the region of interest in an annealed Cu46Zr46Al8 BMG. b-e) Two, three, four and five fold in plane rotational symmetry maps, respectively, inset with a highly correlated diffraction pattern from the field of view with the same symmetry order. These maps are four-dimensional datasets, in which whole diffraction patterns are acquired in the field of view from every pixel. The scan size is 100 x100 pixels, with a 0.5nm step size.

High-Entropy Alloys: We plan to continue to examine the fundamental origins of the exceptional mechanical properties of HEAs, in collaboration with ORNL. Again, we believe that it is vital to combine mechanical property measurements and *in situ* TEM observations with dedicated theory to truly understand why HEAs display such remarkable properties. In light of this, we will perform detailed first-principles calculations to elucidate the relative energetics of planar faults governing slip and twinning. A primary focus will be to understand how chemical SRO in these multicomponent solid solutions may affect these planar fault energies and their role in governing deformation mechanisms, as much of the modeling of HEAs has been made without regard to chemical SRO. As with BMGs, to verify the computational results we will attempt, for the first time, to directly image short-range-ordering in HEAs utilizing the high-resolution STEM capabilities at NCEM. To our knowledge, SRO in HEA is as yet unconfirmed. We believe that STEM diffraction mapping with the Gatan K2-IS direct electron detector on the TEAM I TEM gives us a powerful new tool to investigate any SRO in the structure directly through nanoscale characterization. The outcome of our analysis will shed light on how defects ahead of crack tips and dislocations interact with local chemical ordering.

References

1. Ritchie RO. *Nature Mater* 2101;**10**:817.
2. Demetriou MD, Launey ME, Garret G, *et al*. RO. *Nature Mater* 2011;**10**;123.
3. Gludovatz B, Granata D, Thurston KVS, *et al. Acta Mater* 2017;**126**:494.
4. Ding J, Ma E, Asta M, *et al*. *Science Rep* 2015;**5**:17429.
5. Ding J, Asta M, Ritchie RO. *Phys Rev B* 2016;**93**:140204(R).
6. Yeh JW, Chen SK, Lin SJ, *et al*., *Adv Eng Mater* 2004;**6**:299.
7. Gludovatz B, Hohenwarter A, Cartoor D, *et al*. *Science* 2014;**345**:1153.
8. Gludovatz B, Hohenwarter A, Thurston KVS, *et al*. *Nature Commun* 2016;**7**:10602.
9. Zhang ZJ, Mao MM, Wang J, *et al*. *Nature Commun* 2015;**6**:10143.
10. Zhang Z, Sheng H, Wang Z, *et al*. *Nature Commun* 2017;**8**,14390.
11. Cheng YQ, Ma E. *Prog Mater Sci* 2011;**56**:379.
12. Ding J, Cheng YQ, Ma E. *Acta Mater* 2014;**69**:343.
13. Ding J, Patinet S, Falk ML, *et al. PNAS* 2014;**111**:14052.
14. Voyles P, Hwang *J. Charact Mater* 2012;**1**:7.
15. Ozdol VB, Gammer C, Jin XG, *et al. Appl Phys Lett* 2015;**106**:253107.

Publications

1. V. Naglieri, B. Gludovatz, A. P. Tomsia, R. O. Ritchie. Developing strength and toughness in bio-inspired silicon carbide hybrid materials containing a compliant phase, *Acta Materialia*, vol. 98, Oct. 2015, pp 141-51.
2. B. Gludovatz, E. P. George, R. O. Ritchie, Processing, microstructure and mechanical properties of the FeMnCoNiCr high-entropy alloy, *Journal of Materials*, vol. 67, Oct. 2015, pp 2262-70.
3. J. Ding, E. Ma, M. Asta, R. O. Ritchie, Second nearest-neighbor correlations from connection of atomic packing motifs in metallic glasses and liquids, *Scientific Reports*, vol. 5, pp.17429, Nov. 30, 2015. doi:10.1038/srep.17429.
4. Z-J. Zhang, M. M. Mao, J. Wang, H. Tian, B. Gludovatz, Z. Zhang, S. X. Mao, E. P. George, Q. Yu, R. O. Ritchie, Nanoscale origins of the damage tolerance of the high-entropy alloy CrMnFeCoNi, *Nature Communications*, vol. 6, pp. 10143, Dec. 9, 2015. doi:10.1038/ncomms10143.
5. H. Bai, Y. Chen, B. Delattre, A. P. Tomsia, R. O. Ritchie, Bioinspired large-scale aligned porous materials assembled with dual temperature gradients, *Science Advances*, vol. 1 (11), pp. e1500849, Dec. 4, 2015. doi:10.1126/sciadv.1500849.
6. H. Bai, F. Walsh, B. Gludovatz, B. Delattre, C. Huang, Y. Chen, A. P. Tomsia, R. O. Ritchie, Bioinspired hydroxyapatite/poly(methyl methacrylate) composite with nacre-mimetic architecture by a bidirectional freezing method, *Advanced Materials*, vol. 28 (1), pp. 50-56, Jan. 6, 2016.
7. A. Shekhawat, R. O. Ritchie, Toughness and Strength of Nanocrystalline Graphene, *Nature Communications*, vol. 7, pp. 10546, Jan. 2016. doi:10.1038/ncomms10546.
8. B. Gludovatz, A. Hohenwarter, K. V. S. Thurston, H. Bei, Z. Wu, E. P. George, R. O. Ritchie, Exceptional damage-tolerance of a medium-entropy alloy CrCoNi at cryogenic temperatures, *Nature Communications*, vol. 7, pp. 10602, Jan.2016. doi:10.1038/ncomms10602.
9. J. Ding, M. Asta, R. O. Ritchie, Anomalous structure-property relationships in metallic glasses through pressure-mediated glass formation, *Physical Review B*, vol. 93, April 8, 2016, pp. 140204(R).
10. A. Shekhawat, C. Ophus, R. O. Ritchie, A generalized Read-Shockley model and larger scale simulations for the energy and structure of graphene grain boundaries, *RSC Advances*, vol. 6, 2016 pp. 44489-97.
11. R. Wilkerson, B. Gludovatz, J. Watts, A. P. Tomsia, G. E. Hilmas, R. O. Ritchie, A novel approach to developing biomimetic ("nacre-like") metal-compliant-phase (nickel-alumina) ceramics through coextrusion, *Advanced Materials*, vol. 28 (45) Dec. 2016, pp. 10061–67.
12. J. Ding, Y.-Q. Cheng, H. Sheng, M. Asta, R. O. Ritchie, E. Ma, Flexibility volume as a universal structural parameter to quantitatively predict metallic glass properties, *Nature Communications,* vol. 7, 2016, p. 13733 (doi:10.1038/ncomms13733).
13. Z. Zhang, H. Sheng, Z. Wang, B. Gludovatz, Z. Zhang, E. P. George, Q. Yu, S. X. Mao. R. O. Ritchie, Dislocation mechanisms and 3-D twin architectures generate the exceptional strength, ductility and toughness in the CrCoNi Medium-Entropy Alloy, *Nature Communications*, vol. 8, Feb. 20, 2017, p. 14390 (doi:10.1038/ncomms14390).

14. B. Gludovatz, D. Granata, K. V. S. Thurston, J. F. Löffler, R. O. Ritchie, On the understanding of the dffects of sample size on the variability in fracture toughness of bulk-metallic glasses, *Acta Materialia*, vol. 126, March 2017, pp. 494-506.

15. J. Ding, M. Asta, R. O. Ritchie, On the question of fractal packing structure in metallic glasses, *Proceedings of the National Academy of Sciences (PNAS)*, published online, July 2017 (doi: 10.1073/pnas.1705723114).

16. K. V. S. Thurston, B. Gludovatz, A. Hohenwarter, G. Laplanche, E. P. George, R. O. Ritchie, Effect of temperature on the fatigue-crack growth behavior of the high-entropy alloy CrMnFeCoNi, *Intermetallics*, vol. 88, Sept. 2017, pp. 65-72.

Doping Metallic Grain Boundaries to Control Atomic Structure and Damage Tolerance

Timothy J. Rupert
University of California, Irvine

Program Scope

Grain boundaries and other interfaces often act as nucleation sites for cracks and voids that lead to failure during plastic deformation of metallic materials. While it is known that interface character and structural state can greatly influence this damage nucleation process, the current level of understanding and control over such details is relatively limited. The objective of this research is to obtain a fundamental understanding of how grain boundary structure can be controlled by locally and selectively adding other elements, with the idea of inducing planned grain boundary phases or ***complexions*** [1]. The effect of complexion structure on dislocation accommodation mechanisms will also be studied, to improve the field's understanding of damage nucleation at interfaces and identify materials design strategies for extremely tough materials. This research will use a combination of computational, experimental, and characterization techniques to isolate and understand the importance of atomic grain boundary structure as well as interfacial chemistry. The fundamental insights provided by this research will enable the creation of advanced engineering metals with improved damage tolerance.

Recent Progress

The project has been ongoing for approximately two years, meaning this extended abstract touches on progress from the start of the project to the current time, albeit in a brief and incomplete manner. We have broken down our progress into (1) experimental and (2) computational subheadings. However, these task are intimately related, continually informing and guiding one another, so we also identify connections throughout. A number of publications have resulted from this work, with details provided at the end of this document.

Experimental

Our proof-of-concept results showed that disordered complexions, or amorphous intergranular films (AIFs), could serve as toughening features which improve both the ductility and strength of nanocrystalline Cu-Zr [2]. These structures allow for efficient dislocation absorption that delays crack nucleation and growth at internal interfaces [3], a process that would be beneficial for a wide range of materials. However, while we showed that AIFs could be incorporated into Cu-Zr, there was no systematic way to select other alloy systems where these amorphous complexions can be introduced. Hence, we began working on the creation of materials selection rules that can be used to identify metallic systems capable of sustaining amorphous intergranular complexions.

We started our study by emphasizing dopant segregation to grain boundaries and the creation of energetically favorable conditions for forming an amorphous phase. To test the robustness of these rules, a variety of Cu-rich systems with contrasting thermodynamic parameters were sputter

deposited. Two examples from Cu-Hf and Cu-Mo are shown in Fig. 1(a) and (b), respectively, where the first has AIFs and the second has only ordered grain boundaries. Generally, we found that the type of complexion formed at the grain boundaries of a polycrystalline binary metallic alloy can be controlled by an informed selection of enthalpy of segregation (ΔH^{seg}), enthalpy of mixing (ΔH^{mix}), and atomic radius mismatch, where AIF formation depends on dopant segregation to the grain boundary and the glass forming ability of the alloy. The behavioral patterns were then extended to predict the complexion formation behavior of a new Ni-based alloy, Ni-Zr, where AIFs had not yet been observed in prior work. Finally, we used our materials selection rules to make predictions for all binary transition metals (Fig. 1(c)), providing a roadmap for the widespread usage of AIFs.

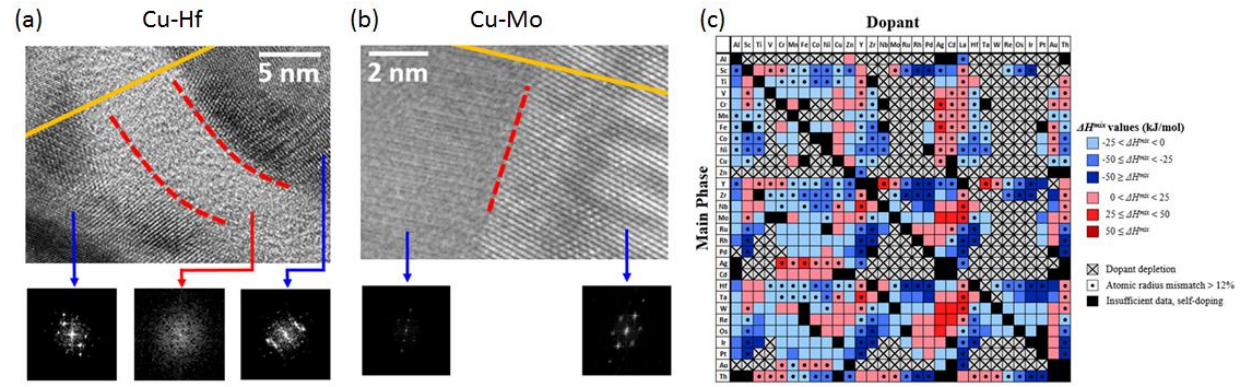

Figure 1. (a) Cu-Hf shows evidence of amorphous grain boundary complexions, while (b) Cu-Mo only has ordered boundaries. The observations in four Cu-based alloys and a Ni-based alloy were used to then make predictions for (c) all binary combinations of transition metals.

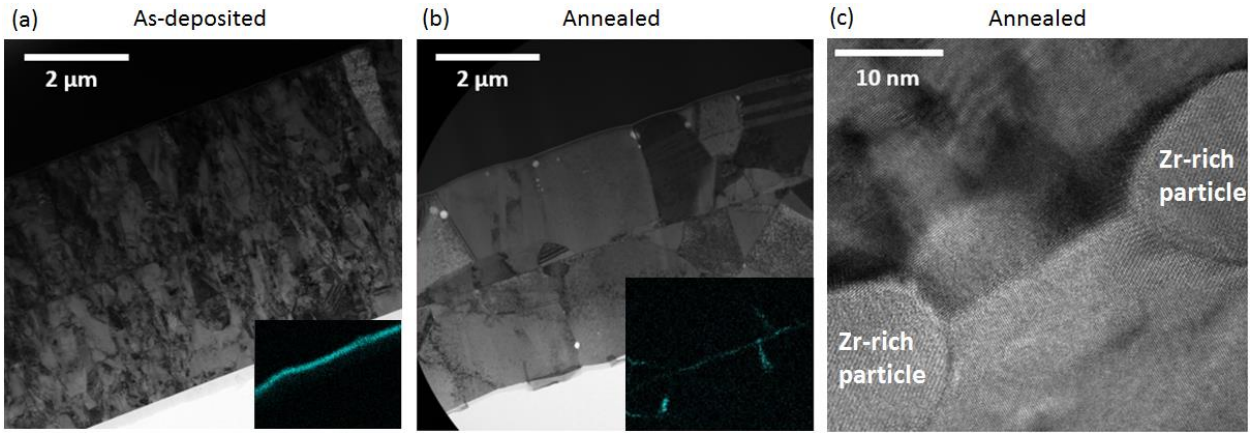

Figure 2. Sputter deposition was used to create two Cu films sandwiched around a thin, nanoscale Zr layer. (a) The as-deposited film had nanoscale grains that quickly coarsened into columnar grains after annealing (b). The insets to these figures are energy dispersive x-ray spectroscopy (EDS) maps of Zr, showing that the dopants start to migrate along grain boundaries. (c) An interface between two Zr-rich particles.

While our processing experiments above were run with the goal of having large grains for easy identification and testing of various complexions, we found that most of our samples still had grain sizes in the nanocrystalline range due to the segregation of stabilizing dopants. Since we are interested in probing the tolerance of individual boundaries to mechanical and radiation damage (see Future Work section), we have been using new sample geometries to try to obtain columnar

grain structures with micron-sized grains and different complexions. A preliminary example is shown in Fig. 2, where two Cu films were sandwiched around a Zr film, creating a structure that can act as a diffusion couple. Annealing causes the Cu-rich grains to become columnar and coarse, while the Zr begins to diffuse up the grain boundaries (Fig. 2(b)). There are also interesting regions where grain boundary diffusion is occurring between two Zr-rich particles, as shown in Fig. 2(c). These specimens are currently being used to identify different types of complexions at grain boundaries with different character, connecting to the simulations described below.

Computational

We have used atomistic modeling to guide experiments and to improve our understanding of atomic mechanisms. First though, we had to pinpoint the features of interatomic potentials that are necessary for the accurate modeling of grain boundary segregation and associated structural transitions. We performed a study of complexion transitions in a bicrystal sample containing Σ5 (310) grain boundaries, but used four different interatomic potentials and compared our simulations to the experiments described above. Perhaps unsurprisingly, only two of the potentials were able to faithfully recreate the real-world complexion transitions. We find that the potentials that are reliable for modeling complexions accurately recreate the enthalpy of mixing, interfacial energy, and bulk modulus values of the alloy system.

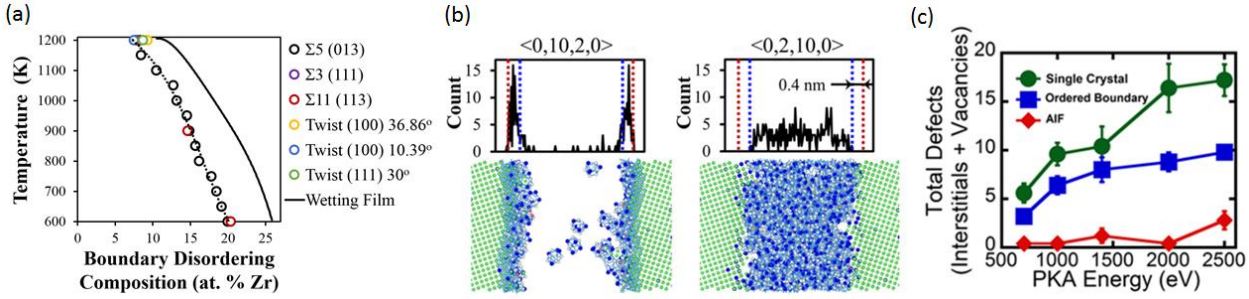

Figure 3. (a) Boundary disordering composition at different temperatures. (b) Distribution of two common polyhedral types along the thickness direction of a 4.5 nm thick AIF. (c) Total point defects left after a collision cascade.

We have also worked to understand fundamental issues associated with complexion transitions. First, we investigated the importance of grain boundary character. Experimental results show that not all boundaries have transformed to AIFs, and even those that have often have different thicknesses. By using hybrid molecular dynamics/Monte Carlo simulations on six different boundaries, we were able to show that the critical grain boundary composition for a disordered complexion is independent of boundary type (Fig. 3(a)). On the other hand, the global composition needed to achieve these states is very different due to segregation excesses that are character-dependent. Next, we studied the details of short-range ordering in amorphous complexions to demonstrate how these features differ from bulk amorphous phases. We find that amorphous complexions have three distinct regions: amorphous-crystalline interfaces, regions deep inside the films that have short-range order identical to a bulk amorphous phase, and transition regions that connect the first two regions. However, thin amorphous films contain only the amorphous-crystalline interface and the transition region, providing further evidence of the constraints

imposed by the abutting crystals. An example of this is shown in Fig. 3(b), where the ~0.4 nm thick amorphous-crystalline region is rich in <0,10,2,0> polyhedra but poor in <0,2,10,0> polyhedra. These details are expected to be related to the dislocation absorption and pinning mechanisms that control ductility and strength.

Concerning material performance, we have performed molecular dynamics simulations of radiation damage, which show that AIFs are damage tolerant grain boundary structures. The collision cascades induced by ion bombardment were simulated and residual point defect populations analyzed as a function of boundary type and primary knock-on atom (PKA) energy. While ordered grain boundaries easily absorb interstitials, these interfaces are inefficient vacancy sinks. Alternatively, amorphous intergranular films act as efficient, unbiased defect sinks. Fig. 3(c) presents data from these simulations. Finally, we have begun to use our simulations for materials discovery. Contrasting with the Cu-Zr system that experiences amorphization, we found that Cu-Nb forms crystalline nanoscale precipitates through heterogeneous nucleation and eventually full intergranular films at grain boundary sites. We have also observed that free surfaces can compete with the grain boundaries as potential segregation sites, depending on the dopant type.

Future Plans

Our future work will focus on additional materials discovery, as well as in-depth investigation of damage near various complexion types. We are beginning to explore the usage of ternary alloys, driven by a vast amount of literature from the bulk metallic glass community that suggests that glass forming ability can be greatly increased, hopefully leading to thicker and more stable amorphous complexions. Atomistic modeling is expected to be a key facilitator here, as we can make rapid predictions before running the more costly and time-consuming experiments. We have also obtained exciting preliminary results on linear complexions, a concept that is very new to the field [4]. We have also started collaborating with Sandia National Laboratories (Drs. Brad Boyce and Khalid Hattar) to perform nanomechanical and irradiation experiments at individual grain boundary sites. Jennifer Schuler, one of the graduate students working on this project, is expected to spend ~6 months visiting Sandia to perform this work. We hope to obtain atomic details of grain boundary-dislocation interactions from in situ nanoindentation, as well as point defect accommodation near different complexions through in situ irradiation. In situ mechanical tests are also starting at UC Irvine.

References

1. Cantwell, P. R. *et al.* "Grain boundary complexions." *Acta Mater.* **62**, 1-48, (2014).
2. Khalajhedayati, A., Pan, Z. and Rupert, T. J. "Manipulating the interfacial structure of nanomaterials to achieve a unique combination of strength and ductility." *Nature Communications* **7**, 10802, (2016).
3. Pan, Z. and Rupert, T. J. "Amorphous intergranular films as toughening structural features." *Acta Mater.* **89**, 205-214, (2015).
4. Kuzmina, M., Herbig, M., Ponge, D., Sandlöbes, S. and Raabe, D. "Linear complexions: Confined chemical and structural states at dislocations." *Science* **349**, 1080-1083, (2015).

Publications

- Ludy JE, Rupert TJ. "Amorphous intergranular films act as ultra-efficient point defect sinks during collision cascades," *Scripta Materialia*, 110, 37 (2016).

- Pan Z, Rupert TJ. "Effect of grain boundary character on segregation-induced interface structural transitions," *Physical Review B*, 93, 134113 (2016).

- Rupert TJ. "The role of complexions in metallic nano-grain stability and deformation," *Current Opinion in Solid State & Materials Science*, 20, 257 (2016).

- Pan Z, Rupert TJ. "Formation of ordered and disordered intergranular films in immiscible metal alloys," *Scripta Materialia*, 130, 91 (2017).

- Pan Z, Rupert TJ. "Spatial variation of short-range order in amorphous intergranular complexions," *Computational Materials Science*, 131, 62 (2017).

- Pham QN, Larkin LS, Lisboa CC, Saltonstall CB, Qiu L, Schuler JD, Rupert TJ, Norris PM. "Effect of Growth Temperature on the Synthesis of Carbon Nanotube Arrays and Amorphous Carbon for Thermal Applications," *Physica Status Solidi A*, 1600852 (2017).

- Schuler JD, Rupert TJ. "Materials selection rules for amorphous complexion formation in binary metallic alloys," *Acta Materialia*, In Press (2017).

- Hu Y, Schuler JD, Rupert TJ. "Identifying interatomic potentials for the accurate modeling of interfacial segregation and structural transitions," (Submitted to *Computational Materials Science*).

Strengthening Nanotwinned Metals Beyond the Hall-Petch Limit

Frederic Sansoz
Department of Mechanical Engineering, The University of Vermont, Burlington VT (USA)

Program Scope

The primary goal of the project is to study the roles of trace element segregation as a fundamentally new mechanism of grain-boundary (GB) and twin-boundary (TB) strengthening in nanotwinned metals, in order to push the limits of strength, ductility and thermal stability in face-centered-cubic (fcc) metals and alloys for extreme environments in energy-related applications. Experiments and simulations have demonstrated that strengthening metals through GB and TB interfaces into nanoscale region is manifested by a maximum strength, a phenomenon that is known as Hall-Petch breakdown [1-6]. Although the underlying mechanisms of this observation have been investigated extensively, an unresolved grand challenge is to continue hardening nanostructured materials beyond this strength limit while preserving other attractive properties, e.g. the electrical conductivity.

To address this challenge, the present project combines a wide range of resources and scientific expertise to create new nanotwinned (nt) alloys with potential for unprecedented properties to be discovered at the atomic scale. This program is leveraged by the PI's expertise in theoretical and computational materials research for nt material systems, and a long-term partnership with two experimentalists, Dr. Morris Wang at Lawrence Livermore National Laboratory (LLNL) and Dr. Ryan Ott at the Ames Laboratory (Ames). Dr. Mikhail Mendelev (Ames) also collaborates with us in the development of new interatomic potentials to be used in atomistic simulations.

Our preliminary results suggested that significant improvement in the thermal stability of small twins could be made by introducing solute atoms to block the mobility of TB defects, and thus prevent strength softening with small twins. We have investigated the effects of doping on hardness of nt-Ag, because this metal has a low stacking fault energy (~16 mJ/m^{-2}) and is known to form copious growth twins during magnetron sputtering. We discovered that annealing of nt-Ag with trace concentrations of Cu solute atoms (<1.0 wt. %) results in grain sizes and twin spacings well below those previously obtained in nt-Ag. At a Cu concentration level of 0.81wt. %, we observed a grain size of 49 nm and a twin spacing of 3.6 nm after annealing. We termed this new material as ***nanocrystalline-nanotwinned*** **(nnt) Ag.**

To date, the majority of atomic mechanisms related to Hall-Petch softening has been garnered by MD simulations. It has long been challenging to experimentally verify or disapprove these mechanisms due to the technological difficulty of synthesizing nanostructured materials with microstructures that are as ideal as those used in MD models. For example, the grain sizes of as-synthesized nt-Cu and nt-Ag metals are typically larger than 100 nm, therefore precluding experimental investigations of the truly nanocrystalline region (<100 nm) where deformation mechanisms have been investigated by simulations. **Our new Cu-doped nnt Ag metals make possible to interrogate the strength behavior in nt materials with grain sizes well below 100 nm.**

The specific objectives of this partnership program are three-fold:

(1) To use hybrid monte-carlo (MC)/molecular-dynamics (MD) atomistic simulations and density-functional-theory (DFT)-based calculations to study the roles of solute atom segregation on twin stability and plastic deformation in doped nnt metals.

(2) To develop a mechanism-based theoretical framework for predicting how doping element addition influences yielding and plastic flow stresses in nnt fcc metals.

(3) To integrate computational simulations, theory, and experiments at the atomic scale for rapid prototyping of new doped nnt alloys with optimum strength and electrical properties.

Recent Progress

1. Cu Segregation Affected Twin Stability and Yield Strength in Nanotwinned Ag

The goal of this task was to study how solute atom segregation may affect twin stability and yielding mechanisms in Cu-doped nnt-Ag. Large-scale 43-million-atom MC/MD simulations [7] were created in the software LAMMPS using an ab-initio-based interatomic potential for Cu-Ag alloys [8] as shown in Figure 1a. To investigate twin stability, our models included nanoscale TB kink defects (Figure 1b and c). In a past study [9], we proved that TB defects are mobile and easily migrate along TBs under stress, leading to detwinning. It was found in the current study that adding trace concentrations of Cu below 1 at. % dramatically increases the stability of nanotwins containing kinked TBs, and the resistance against GB sliding and migration, under high stress. Cu segregation affected yield strength was found to result from pronounced segregation of dilute Cu atoms towards both GBs and TB defects during high-temperature annealing (Figure 1d).

We also obtained DFT-based VASP calculations in Ag showing that segregation enthalpies of Cu atoms inside TB kink steps (Figure 1c) are up to twice as high as those predicted for segregation at GBs. Furthermore, in-situ x-ray diffraction heating analysis conducted by our LLNL and Ames partners showed that nnt-Ag doped with 0.19 wt.% Cu exhibited structure stability up to 415^{o}C, i.e. more than 200^{o}C higher than that in pure nt-Ag, which confirmed the theoretical predictions.

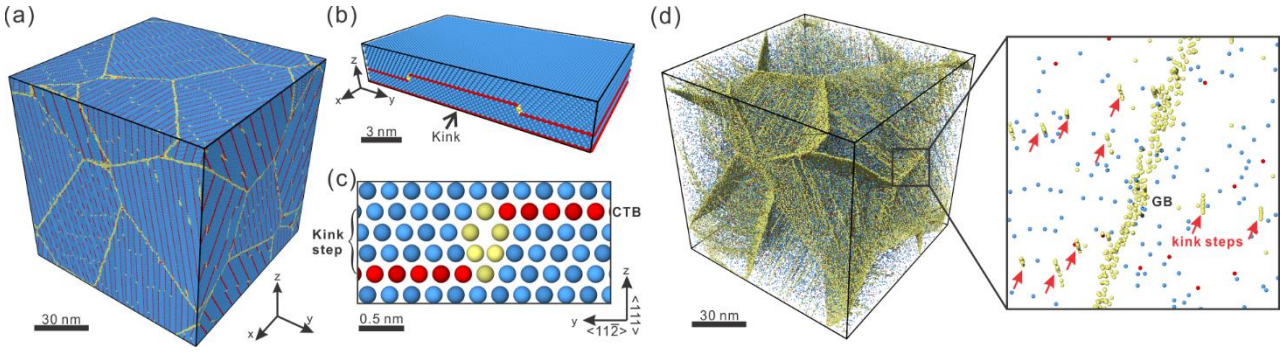

Figure 1. Hybrid Monte-Carlo/molecular-dynamics simulations of segregation of 0.8 at. % Cu atoms in nanotwinned Ag at 500 K. **(a)** 43-million-atom nt-Ag model with kinked TBs of 2.8 nm in thickness and an average grain size of 45 nm. **(b)** Small-scale nt-Ag bicrystal containing only one single TB kink defect. **(c)** Atomic structure in a TB kink of 0.7 nm in height and 10 nm in width. **(d)** Equilibrium Cu atom distribution in large-scale nt-Ag model showing simultaneous Cu segregation to GBs and TB defects. Cu atoms segregated to kink steps and GBs are colored in yellow, atoms moved to coherent TB segments in red, and other atoms staying in solution in blue.

2. Hall-Petch Plastic Flow Stress Limit in Cu-doped Nanotwinned Ag

The second objective was to use hybrid MC/MD simulations to study the influence of twin spacing (λ) and grain size (*d*) on plastic flow stress in doped and undoped nnt-Ag. A series of large-scale simulations with 10 different twin spacings (1.4 – 22 nm), 5 grain sizes (6 – 45 nm) and 4 dopant concentrations (0 – 0.8 at% Cu) were conducted in this program. For a 45-nm grain size close to that synthesized experimentally in annealed Cu-doped nnt-Ag, Figure 2a showed two distinct regimes of plasticity, i.e. tensile yielding below 5% strain and plastic flow above 5% strain. The influence of λ was found to be more significant on the plastic flow regime. Figure 2b showed that the flow stress limit at 300 K occurs at TB spacing λ = 7 ± 0.7 nm, accompanied with a smooth transition from strengthening to softening, in both undoped and Cu-doped nnt-Ag. Also, we found that GB sliding plays a critical role on Hall-Petch softening in undoped and Cu-doped nt-Ag when λ and *d* decrease, as shown in Figure 2c. Therefore, an effective strategy to push the Hall-Petch limit must involve a reduction of GB sliding deformation at small TB spacing by doping.

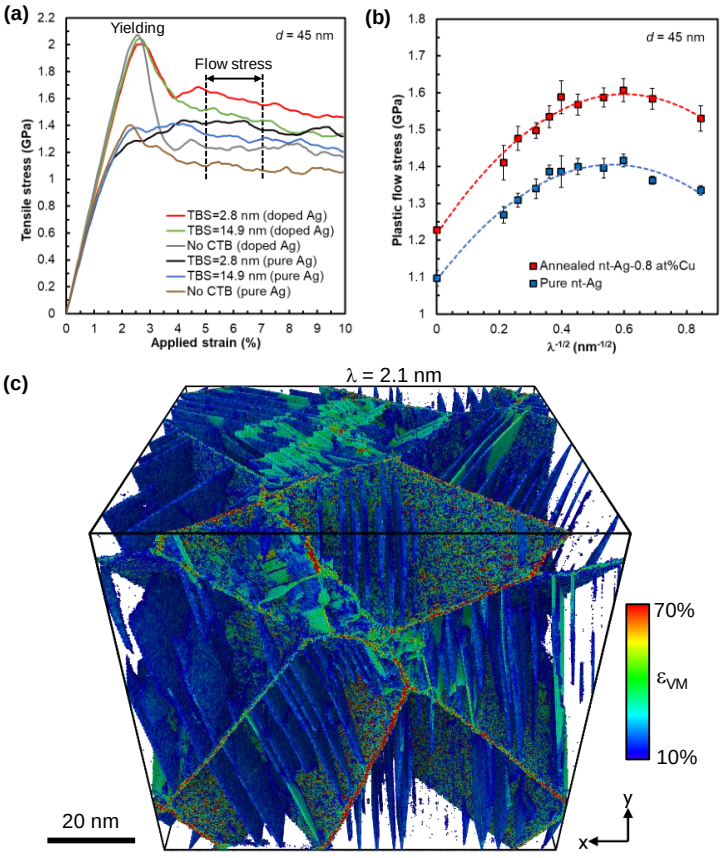

Figure 2. Hall-Petch hardening and softening mechanisms in undoped and Cu-doped nnt-Ag with mean grain diameter of 45 nm by molecular dynamics simulations. (a) Representative stress-strain curves showing two distinct regimes for tensile yielding and plastic flow between 5% and 7% strains. **(b)** Hall-Petch plots for plastic flow stresses as a function of TB spacing (λ) for undoped and doped nnt-Ag. **(c)** Local microstrain accumulated during plastic flow deformation from 5% to 7% strain at λ = 2.1 nm.

The above findings suggested that while Cu doping increased the overall strength in nnt-Ag, it did not significantly affect the mechanisms of strengthening and softening as a function of TB spacing. Our first-principles calculations using VASP, however, predicted that more pronounced segregation to GBs could be obtained with different dopants, e.g Ni in Ag, which is expected to change the interface-mediated plastic deformation mechanisms in nnt-Ag.

3. Development of a New Ab-Initio-based EAM Potential for Nanotwinned Ag-Ni Alloys

Our preliminary results suggested that Ni-doping has stronger strengthening efficiency than Cu doping in nnt-Ag. Our ab-initio calculations have also confirmed that the enthalpy for atom segregation at GBs and TB kink steps are higher with Ni than Cu. First, we have developed a new embedded-atom-method (EAM) potential for MD simulation of pure Ag, giving better predictions

of melting point, stable and unstable stacking-faults, and energy values on Σ9 (221) GB and kink (112) defects, as compared to ab-initio results. Second, we have created an ab-initio database for fitting a new EAM potential for the Ag-Ni system, which makes it possible to study the strengthening mechanism of Ni dopant with classical MD simulations. The new potential includes liquid structure of Ag and Ag20Ni80, generalized stacking fault energy, coherent TB energy, Σ9(221) GB energy, kink (112) energy, and dopant segregation energy. The potential fitting process was performed by Dr. Mikhail Mendelev at Ames. The first tests are underway.

Future Plans

Our plans are to study the strengthening efficiency of different dopants in nnt-Ag. Preliminary ab-initio results suggested that Ni solute segregation to GBs and TB defects is more strongly favored than Cu solute segregation, while Al segregation was found to be weak. Therefore, the new Ag-Ni interatomic potential developed in this program will enable us to study the small-scale mechanics of trace Ni segregation in nnt-Ag and its impact on strengthening and softening mechanisms.

Furthermore, we plan to fundamentally study how local stress concentrations at GB-TB triple junctions influence plasticity in doped and undoped nnt-Ag. Finite-element analysis using linear anisotropic elasticity and atomistic simulations will be used to quantify the local elastic strain intensity at a TB-GB triple junction in Ag as a function of grain size, twin spacing and dopant concentration. These results will be integrated into a size-dependent criterion for strengthening of nt-Ag based on Rice theory of partial dislocation emission from a local stress intensity.

References

1. Li, X. Y., et al. Dislocation nucleation governed softening and maximum strength in nano-twinned metals. *Nature* 464, 877-880 (2010).
2. Lu, L., et al. Revealing the Maximum Strength in Nanotwinned Copper. *Science* 323, 607-610 (2009).
3. Schuh, C. A., Nieh, T. G. & Yamasaki, T. Hall-Petch breakdown manifested in abrasive wear resistance of nanocrystalline nickel. *Scr. Mater.* 46, 735-740 (2002).
4. Schiotz, J., Di Tolla, F. D. & Jacobsen, K. W. Softening of nanocrystalline metals at very small grain sizes. *Nature* 391, 561-563 (1998).
5. Shan, Z. W. et al. Grain boundary-mediated plasticity in nanocrystalline nickel. *Science* 305, 654-657 (2004).
6. Chokshi, A. H., Rosen, A., Karch, J. & Gleiter, H. On the validity of the Hall-Petch relationship in nanocrystalline materials. *Scr. Metall.* 23, 1679-1683 (1989).
7. Caro, A., et al. Effects of microalloying on the mobility and mechanical response of interfaces in nanocrystalline Cu. *Mater. Sci. Forum* 633-634, 21-30 (2010).
8. Wu, H. H. & Trinkle, D. R. Cu/Ag EAM potential optimized for heteroepitaxial diffusion from ab initio data. *Comput. Mater. Sci.* 47, 577-583 (2009).
9. Wang, Y. M., Sansoz, F., Ott R., et al. Defective twin boundaries in nanotwinned metals. *Nature Mater.* 12, 697-702 (2013).

Publications (participants directly supported by this program are highlighted in bold font)

1. **X. Ke** and **F. Sansoz**. Segregation Affected Yielding in Nanotwinned Silver by Microalloying (in preparation).
2. J. Ye, **X. Ke**, **Z. Pan**, J. Geng, M.F. Besser, F. Liu, D. Qu, J. Marian, E. Martinez, A. Caro, R. T. Ott, **F. Sansoz**, Y. M. Wang. Exploring the Strength Limit of Interface-controlled Metallic Nanomaterials (in preparation).
3. **Z. Pan**, M. Mendelev, V. Borovikov, **F. Sansoz**. Development of a semi-empirical potential for simulation of Ni solutes segregated in Ag grain boundaries (in preparation).

Bulk Metallic Glasses: A narrow but steep path to success

Jan Schroers, Yale University

Program Scope

The majority of metallic glasses are limited by fracture toughness and not by strength. However, accurate studies and deeper inside in the origin of fracture toughness of metallic glasses have been hampered by challenges with the fabrication of test samples and by the limited understanding of the numerous factors affecting fracture toughness. Within this program we have been developing an understanding of fracture toughness of BMGs and how it depends on BMGs' composition and processing (often quantified by the fictive temperature). We use a method that we have developed during previous funding period to precisely fabricate well defined and reproducible fracture toughness samples. The method allows us to study fracture toughness of metallic glasses at unprecedented precision. Our study will build on our research during the previous funding periods. We will develop and test quantitative theories, that we intend to develop during this funding period against the vast number of precise data that we will create here. We will consider an unprecedented number of BMGs as our proposed method permits us to fabricate and characterize ~1,000 BMG test samples. The wide range of behaviors represented in this sample size will enable us to identify correlations with other properties, such as elastic constants, structure measurements, and enthalpy recovery measurements.

Recent Progress

We have identified a mechanical glass transition revealed by the fracture toughness of metallic glasses. This fracture transition is present on the fictive temperature scale and reveals a dramatic transition from brittle to ductile with increasing fictive temperature. This transition is approximately 50 times more pronounced than the previously reported ductile to britle transition in metallic glasses. We developed a theory of fracture toughness dependence on fictive temperature based on a cross over of time scales. We compare this behavior with the ordinary glass transition and predict and then show experimentally that the fracture toughness in metallic glasses is a function of strain rate.

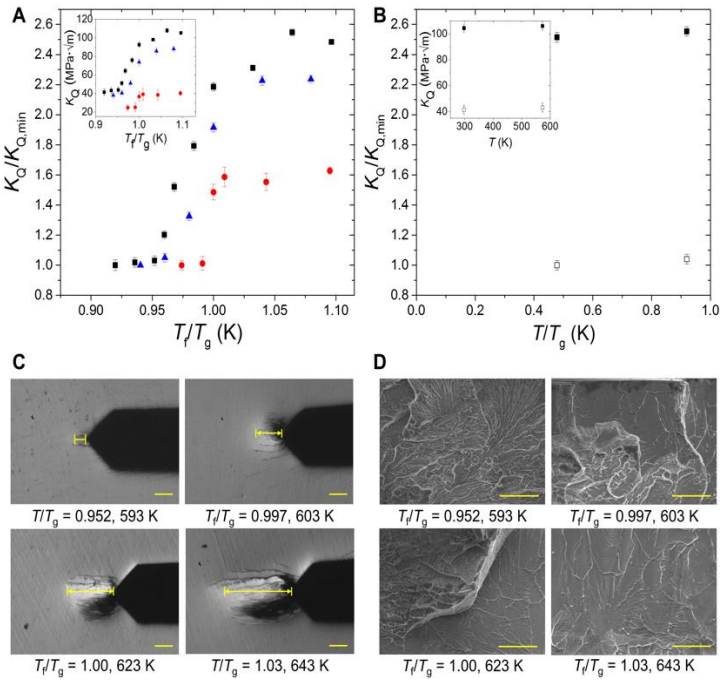

Normalized (notch) fracture toughness as a function of the normalized T_f for $Zr_{44}Ti_{11}Ni_{10}Cu_{10}Be_{25}$, $Pd_{43}Cu_{27}Ni_{10}P_{20}$, and $Pt_{57.5}Cu_{14.7}Ni_{5.3}P_{22.5}$. K_Q at given T_f is normalized by the minimum K_Q measured here and T_f is normalized by T_g. The inset shows the absolute K_Q as a function of T_f/T_g. Error bars represent one standard deviation, calculated using five samples per data point. Dash lines guides the eye. **(B)**. Normalized (notch) fracture toughness as a function of absolute testing temperature of a $Zr_{44}Ti_{11}Ni_{10}Cu_{10}Be_{25}$ metallic glass with $T_f > T_f^c$. **(C)**. Plastic zone prior to catastrophic fracture of $Zr_{44}Ti_{11}Ni_{10}Cu_{10}Be_{25}$ sample with varying T_f's. Dimension lines highlights the size of the plastic zone region, where samples of $T_f < T_f^c$ exhibit small plastic zone region, while glasses of $T_f > T_f^c$ exhibit visibly larger plastic zone size. The plastic zone contrast asymmetry can be visualized optically, which confirms that shear bands form symmetrically along the crack propagating direction as expected in mode-I or tensile fracture tests. Scale bars represent 100 μm **(D)**. Scanning Electron Microscopy images of the fracture morphology of $Zr_{44}Ti_{11}Ni_{10}Cu_{10}Be_{25}$ with varying T_f. As the threshold T_f^c is surpassed, fracture morphology changes from fractal-like structures of unstable fracture to river-like patterns, commonly found in stable fractures. Scale bar represents 50 μm.

We have in a separate activity also determined the effect of sample geometry on fracture toughness.

Future Plans

We are developing a theoretical understanding of the origin of the widely varying fracture toughness within the material class of metallic glasses.

Publications

- W Chen, H.Z., Z Liu, J Ketkaew, H Gao, J Schroers, *Test Sample Geometry for Fracture Toughness Measurements of Bulk Metallic Glasses.* Acta Materialia, in review, (2017).
- Ketkaew, J., H. Wang, W. Chen, G. Pereira, Z. Liu, W. Dmowski, E. Bouchbinder, C.S. O'Hern, T. Egami, and J. Schroers, a mechanical glass transition revealed by the fracture toughness of metallic glasses..in review, (2017).
- Sohn, S.W., Y.H. Liu, J.B. Liu, P. Gong, S. Prades-Rodel, A. Blatter, B.E. Scanley, C.C. Broadbridge, and J. Schroers, *Noble metal high entropy alloys.* Scripta Materialia, 126, 29-32, (2017).
- W Chen, H.Z., Z Liu, J Ketkaew, N Li, J Yurko, N Hutchinson, H Gao, J Schroers, *Processing effects on fracture toughness of metallic glasses.* Scripta Materialia 130, 152-156, (2017).

Microparticle Supersonic Impact: A Testbed for the Exploration of Metals under Extreme Conditions

Principal Investigators: Christopher A. Schuh[1] and Keith A. Nelson[2]
Massachusetts Institute of Technology, (1) Department of Materials Science and Engineering and (2) Department of Chemistry

Program Scope

Understanding material behavior under high velocity impact is the key to addressing a variety of fundamental phenomena including impact-induced plasticity, phase transformations, wear, erosion and ballistic penetration. More recently, adhesion has emerged in this spectrum since it has been found that micrometer-sized metallic particles can bond to metallic substrates under supersonic-impact conditions [1], even when there is no applied heat to inspire, e.g., melt formation or liquid-phase bonding.

In this area, researchers have repeatedly observed "critical velocities", thresholds above which supersonic particles transition their mode of interaction with the substrate. For example, there is a critical velocity at which they may adhere to the substrate instead of rebounding, and another where the adhesion gives way to erosion. A variety of mechanisms have been put forth to explain such empirical observations, but these have not been quantitatively supported by physical theories nor yet directly observed. In our view, the lack of consensus on the operative mechanisms traces to a lack of real-time studies of supersonic micro-particle impact. Such studies require spatial (micron) and temporal (nanosecond) resolutions much finer than those provided by existing experimental techniques. With such real-time studies, this project, which will begin in Fall 2017, seeks to provide a fundamental understanding of impact-induced adhesion and erosion across a range of metallic microparticles.

Experiment: We have been developing an in-house-designed setup to accelerate single micron-sized metallic particles, to track them, and to observe the entire deformation/adhesion/erosion process in real time as they impact a substrate [2]. In our setup, a laser excitation pulse is focused onto a launching pad assembly from which single metallic particles are ejected. Particles are accelerated to supersonic speeds, controllable (from 100 m/s to ~2 km/s) by adjusting the laser excitation pulse energy. The particle impacts a metallic target whose deformation is captured by a high frame rate camera that records up to 16 images with a time resolution as short as 3 ns. The time resolution is enough to capture the deformation event at such extreme impact, which typically takes place over a 50 ns time window. The setup uniquely enables us to study metals response to a wide range of impact velocity, pressure and deformation rate.

Simulation: Since the induced pressure during high velocity impact of micrometer-sized particles can greatly exceed the strength of the material (volumetric stress >> deviatoric stress), we are interested in focusing our studies on these conditions, where solid materials behave like fluids at the continuum level. This is a unique regime because we can use finite element models in which the particle is treated in an Eulerian domain, but where the substrate is treated in a Lagrangian domain. This approach is not widely used, but will enable us to systematically investigate deformation of the particle over a wide range of impact velocities without producing numerical artifacts. It will permit us to calibrate plasticity models directly to the observations of deforming particles, and can provide local information on the induced strain, strain rate and temperature during such experiments.

Preliminary Results

To illustrate the feasibility of our approach outlined above, a series of exploratory experiments and simulations have been performed on aluminum particles. Figure 1a shows snapshots taken for 45-micron Al particles impacting an Al target with a velocity of 600 m/s (i) and 800 m/s (ii). At the lower impact velocity, the particle rebounds with clear flattening and permanent deformation. At the higher impact velocity, there is significantly more deformation accompanied by very fast lateral material ejection at the periphery of the particle, formation of an interfacial jet, and material ejection. The particle does not rebound, but instead adheres to the substrate. Finite element simulation of impact at 800 m/s reveals that 300% plastic strain accumulates in the particle and its temperature rises up to 60% of the melting temperature within 50 ns. *These are truly extreme conditions, which we can now study in real-time and through direct observation of the particle deformation*. The response of metals to such extreme conditions is intimately connected with the mechanisms that become operative to dissipate energy during micro-impacts.

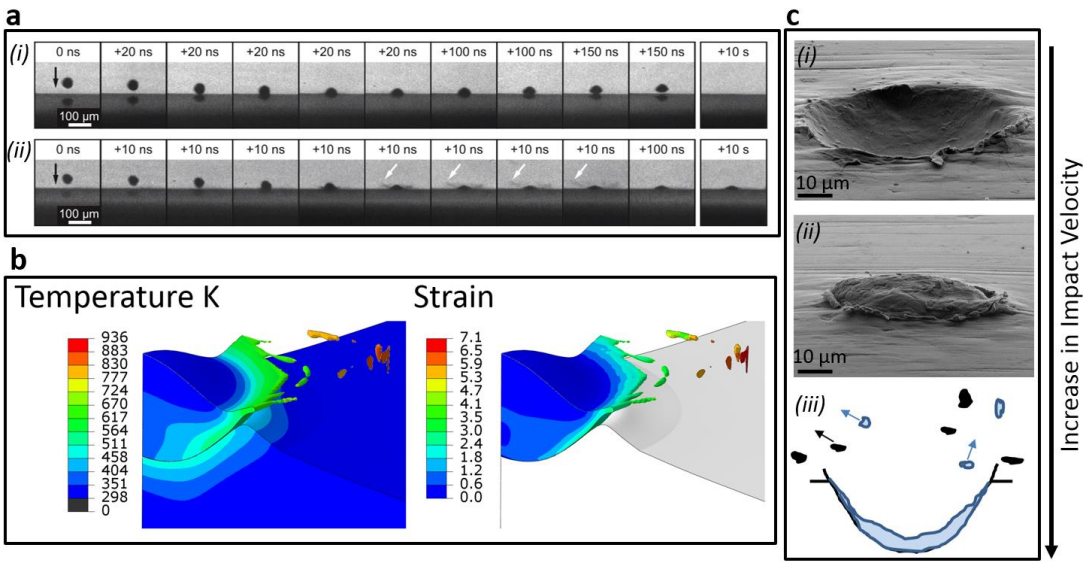

Figure 1. a) Multi-frame sequences with 5 ns exposure time and variable inter-frame time showing single Al particle impacts on Al targets. The inter-frame time relative to the previous frame is shown at the top the frames. (i) Impact at 600 m/s showing particle rebound. (ii) Impact at 800 m/s showing particle adhesion. Material ejection is indicated by white arrows. **b)** The deformation, temperature and strain distribution in Al particle as a result of impact at 800 m/s velocity, featuring extreme thermo-mechanical conditions induced at the contact region during a short amount of time (~50 ns). **c)** Surface deformation at different supersonic impact regimes: (i) rebound (SEM); (ii) adhesion (SEM); and (iii) erosion (schematic).

Future Plans

The above results are preliminary and unpublished, but they open a new perspective on metals at extremes, and raise several key scientific issues on the mechanisms that govern the response of metals under impact. The combination of a new particle-level experimental technique, a different simulation approach, in situ observations along with post mortem characterizations present a clear opportunity for focused study.

Rebound-adhesion transition: We plan to perform a systematic set of metallic particle impact tests on matched powder-substrate combinations of a variety of pure metals: Cu, Zn, Al, Ti, Fe, Ni, Ta and W. The impact tests will be conducted with increasing velocity starting with relatively low velocity (~200 m/s where we expect rebound) to then reach impact velocities where powders will no longer rebound,

but rather adhere to the substrate. This approach will enable us, for the very first time, to accurately measure the threshold velocity where adhesion occurs.

Adhesion mechanism: Based on our preliminary simulations we hypothesize that material jet formation is the result of a pressure induced instability that leads to adhesion. The nature of adhesion, however, is not known. That is to say there is no consensus whether the particle and the substrate are metallurgically bonded or mechanically interlocked to each other. To answer this fundamental question we plan to study impact behavior of dissimilar materials so that we can chemically track the interaction of their surfaces in post-mortem examination. We plan to use energy dispersive spectroscopy in a TEM to scan the atomic concertation along perpendicular lines crossing the interface. We will perform such measurements at different locations around the interface, from the impact center to its edge, and for different impact velocities. By tuning the mismatch in the metals to include pairs that are mechanically similar but clearly chemically different (i.e., Ni-Co, or Ti-Zr), we hope to discern the critical mechanisms that lead to bonding. We also hope to use micromachining and micromechanical testing to assess the local bond strength, e.g., as a function of position across the impact site and at different velocities above the threshold.

Adhesion-erosion transition: As shown in Figure 1c, in supersonic impacts, the first regime change with increasing velocity is the transition from rebound (i) to adhesion (ii), both featuring plastic deformation of the substrate. At still higher velocities, a second transition from plastic deformation of the substrate to hydrodynamic penetration is expected. In this case, the impacting particles might cause strong erosion of the substrate as schematically shown in Figure 1c (iii). We propose to explore the potential behavioral regime change from adhesion to erosion for two metals: Al and Zn. In addition to the real-time observations, we plan to investigate the morphology of the eroded tracks by SEM and TEM to elucidate the operative erosion mechanism and look for possible shear band formation due to localized plastic deformation and adiabatic heating.

Energy dissipation mechanisms: Plastic deformation is the most important mechanism for energy dissipation in our microparticle impact tests. Plastic deformation occurs nominally by the generation and movement of dislocations [3], which in turn can lead to grain formation by plasticity or by recrystallization owing to the adiabatic heat in the contact region. We plan to use site-specific cross-sectional TEM to examine the structure and its relation to impact pressure, plastic shear and temperature. The TEM specimens will be sampled from along the interface where the deformation mode changes from compression-dominated to shear-dominated from the impact center toward the edge. Combining the metallic substructure observations and numerical modeling results (local temperature and deformation rate), we will map the substructure to shear rate-temperature space for different impact pressures in different metals. In particular we are interested in the following questions: What is the extent or the limit of grain refinement attainable at deformation rates of 10^9 s^{-1}? Do recrystallization time-temperature-strain combinations from the literature on bulk metals simply extrapolate to the extreme conditions of microparticle impact? When does polymorphic transformation occur as a result of the high pressure shock passage in non-close packed metals?

References

1. H. Assadi, F. Gärtner, T. Stoltenhoff, H. Kreye, Bonding mechanism in cold gas spraying. *Acta Mat.* **51** 4379–4394 (2003).
2. D. Veysset, A. J. Hsieh, S. Kooi, A. A. Maznev, K. A. Masser, K. A. Nelson, Dynamics of supersonic microparticle impact on elastomers revealed by real-time multi-frame imaging. *Sci. Rep.* **6**, 25577 (2016).
3. C. A. Schuh, J. K. Mason, A. C. Lund, Quantitative insight into dislocation nucleation from high-temperature nanoindentation experiments. *Nature Materials.* **4**, 617 (2005).

Radiation Response of Low Dimensional Carbon Systems

Lin Shao, Texas A&M University

Program Scope

The project is aimed at understanding the fundamentals of radiation response of low dimensional carbon systems and irradiation-induced property changes, with focus on the unique phenomena caused by their geometry, boundary, and quantum size effects. Materials of key interests include graphene, carbon nanotubes (CNTs), CNT films, and CNT embedded composites.

Recent Progress

In situ characterization of graphene under ion irradiation

Significant efforts have been made to develop the technique to combine scanning tunneling microscope (STM) with ion accelerator to gain the unique capability of *in situ* characterization of defects under concurrent ion irradiation. Such capability is critical to study fundamentals of monolayer graphene and their boundary effects. This approach makes it possible to observe dynamic response of graphene under ion irradiation, and to characterize both domain and boundary configuration changes at atomic scales.

However, it is very challenging to introduce an ion beam into a STM chamber. The largest issue is the machine vibration. The STM cannot be housed in a vacuum chamber that uses any turbomolecular pumps for high vacuum due to pumping induced vibration and cannot be directly connected to a beam line due to the vibrations from other parts of an accelerator. As shown in Fig. 1, the following innovation is used by us to overcome the issue. First, a STM chamber is equipped with two pumping systems. Initially a turbomolecular pump is used to evacuate the chamber to a pressure of 1×10^{-6} torr. Then the pump is stopped, and an ion pump is used to maintain the vacuum at a pressure of 1×10^{-7} torr. The STM is positioned on a vibration dampening table. A 2 MeV proton beam is extracted from our 1.7 MV tandem accelerator into the air through a Ti widow. Then the beam immediately penetrates through a second Ti window on the STM chamber. This setup is able to remove the two primary sources of vibration affecting the STM. The use of an ion pump will eliminate any vibrations when maintaining high vacuum, and the physical disconnect from the main beamline will erase any vibrations coming from the accelerator. Within the STM chamber, an Au coated film is used to backscatter the proton beam at an angle pointing to the graphene sample. Prior to bombarding the graphene, a collimator is used to shape the beam and a Mylar film is used to filter the low energy proton atoms scattered from non-Au substrate.

We achieved certain success but also experienced certain failure. For the successful part, we are able to observe defects formed on graphene plane and also are able to characterize defects nearby a grain boundary. Figure 2a shows STM image of a virgin defect-free graphene plane. Figure 2b shows a defective graphene observed after a prolonged ion irradiation. The defects are marked by dash circles. Figure 2c shows an irradiated graphene plane which has a grain boundary in the middle. On the other hand, the project meets the following challenge: (1) the concurrent STM characterization is difficult due to charge deposition on the graphene which disturbs the imaging process; (2) the dynamic defect-boundary interactions cannot be recorded because defects are lack of mobility. To alleviate issues, we propose two following approaches which are currently ongoing: (1) studying graphene deposited a Ni substrate which helps charge dissipation and (2) applying a laser to improve defect mobility through local energy deposition. The second approach requires optimization to adjust laser-deposited energy without over-heating and damaging STM.

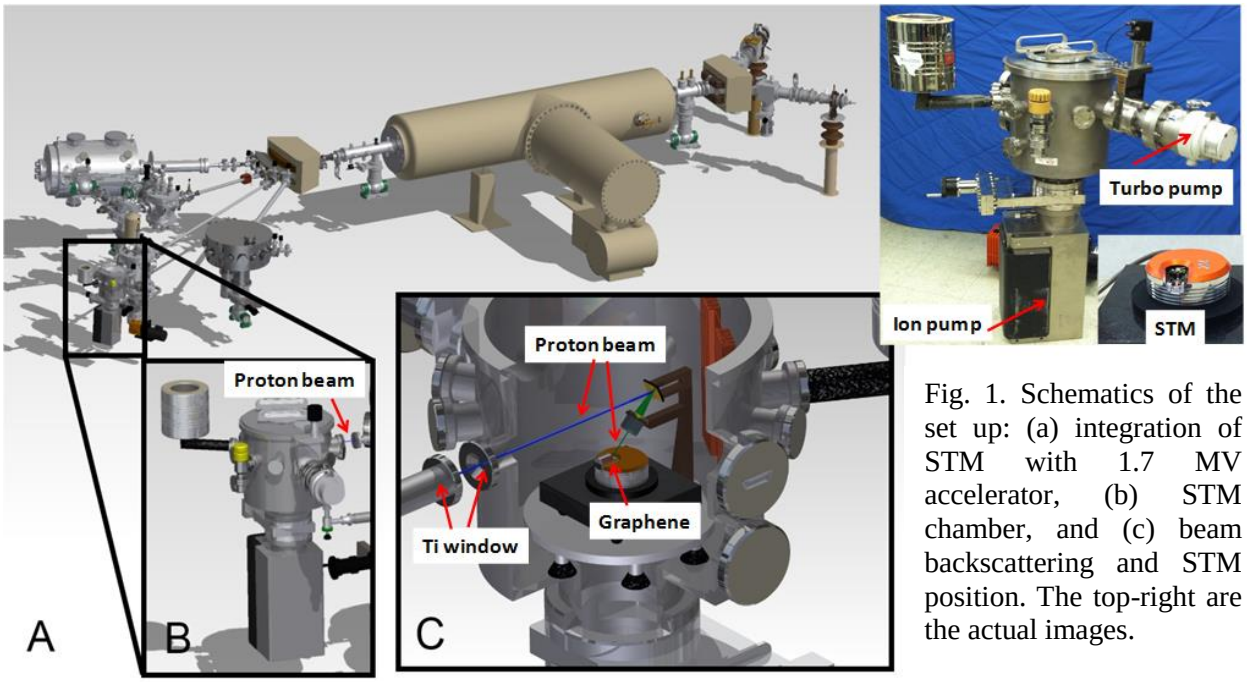

Fig. 1. Schematics of the set up: (a) integration of STM with 1.7 MV accelerator, (b) STM chamber, and (c) beam backscattering and STM position. The top-right are the actual images.

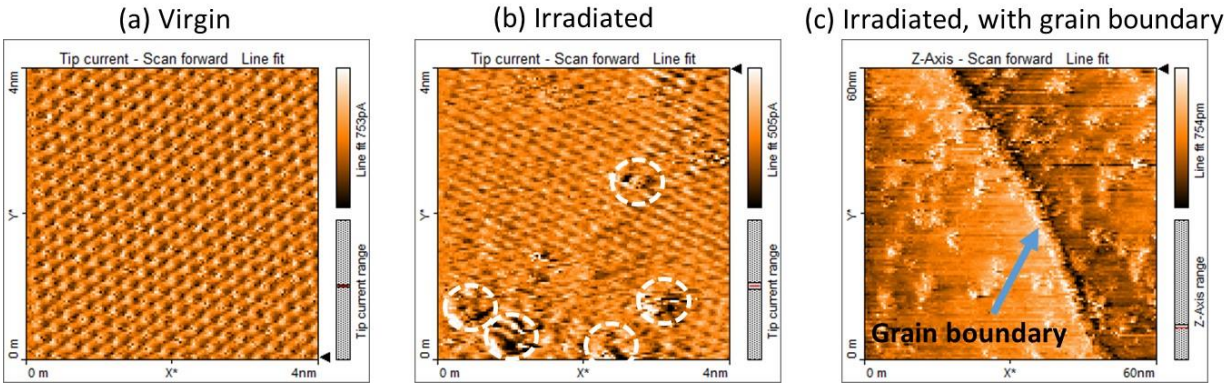

Figure 2. STM images of (a) irradiation-free graphene, (b) irradiated graphene and (c) irradiated graphene nearby a grain boundary.

Defect evolution on ion-irradiated graphene

Raman spectra were obtained from Si-ion-irradiated graphene and molecular dynamics simulations (MD) were performed to understand atomic scale details of structural evolution. As shown in Fig. 3, low fluence ion irradiation creates isolated vacancies defects, while high fluence irradiation induces coalescences of vacancies and formation of nanometer size pores on the surface. The pore formation is associated with trend changes of Raman D/G intensity ratio (first increase and then become saturated at higher fluences), due to the loss of six-fold rings and their reduced contribution in D mode vibration.

Resistive switching devices based on defective graphene

Our findings that ion irradiation can change defect morphology of defects, from vacancies at low ion fluences to nano-pores at high fluences, pave new ways of device applications. We have successfully applied the technique to fabricate cation-based resistive switching (RS) devices, driven by the needs for

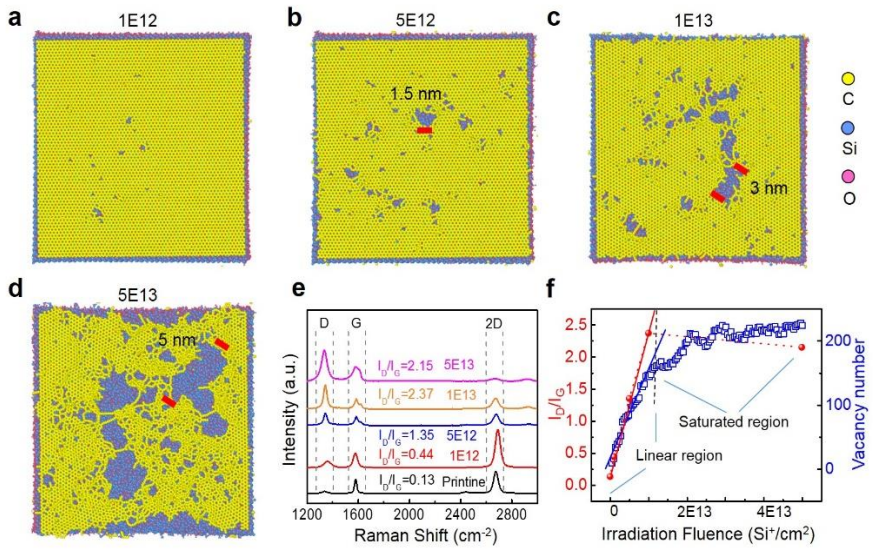

Fig. 3 MD simulations and Raman spectra of Si-ion-irradiated graphene. (a-d) MD simulations of graphene surface morphologies after 10 keV Si irradiation to fluences of 1×10^{12}, 5×10^{12}, 1×10^{13}, 5×10^{13} Si$^+$/cm^2, respectively, and (e) corresponding Raman spectra, and (f) Raman D/G intensity ratio changes as a function of Si fluences.

high-density random access memory. Fig. 4 shows schematically a cation-based resistive switching (RS) device proposed in our studies. The key design is to use graphene defects to control the size and density of the areas to form highly conductive filament channels when a sufficient voltage is applied. The morphology of channel directly determines device quality. Traditional devices rely on random formation of filament channels, leading to high power dissipation and device instability. In our approach, ion irradiation is used to induce either sub-nanometer channels (vacancy dominated) or large channels (nano-pore dominated), which is controllable through manipulation of defect clustering process on ion-irradiated graphene.

We realized both lower power dissipation and high ON-state current, which are not achievable by using other approaches. Figure 5 shows I-V characteristics of control device (Fig. 5a, no graphene) and devices having graphene irradiated to difference fluences. For the low irradiation fluences (Figs. 5b, and 5c), graphene defect numbers are limited and the numbers of active cation which migrate into the RS layer are insufficient to form a continuous conductive filament channel. For the device with a higher irradiation fluence (1×10^{13} Si$^+$/cm^2, Fig. 5d), larger amount of injected cation leads to a bidirectional volatile threshold switching (TS) behavior. For the highest fluence of 5×10^{13} Si$^+$/cm^2, graphene defects start to coalesce and induce formation of much stronger filaments, leading to a nonvolatile memory switching (MS) behavior.

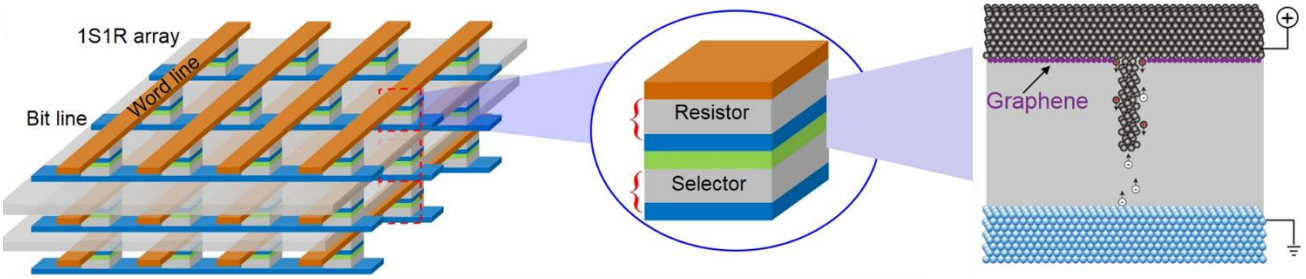

Fig. 4. Schematic illustrations of the 3D memory device, cell structure, and formation of filament channel when the device is applied with a high voltage. Cation migration occurs at the nanohole and lead to the localized formation of single or a few filament channels along the graphene nanohole, which contributes to relatively weaker atom diffusion and better filament stability.

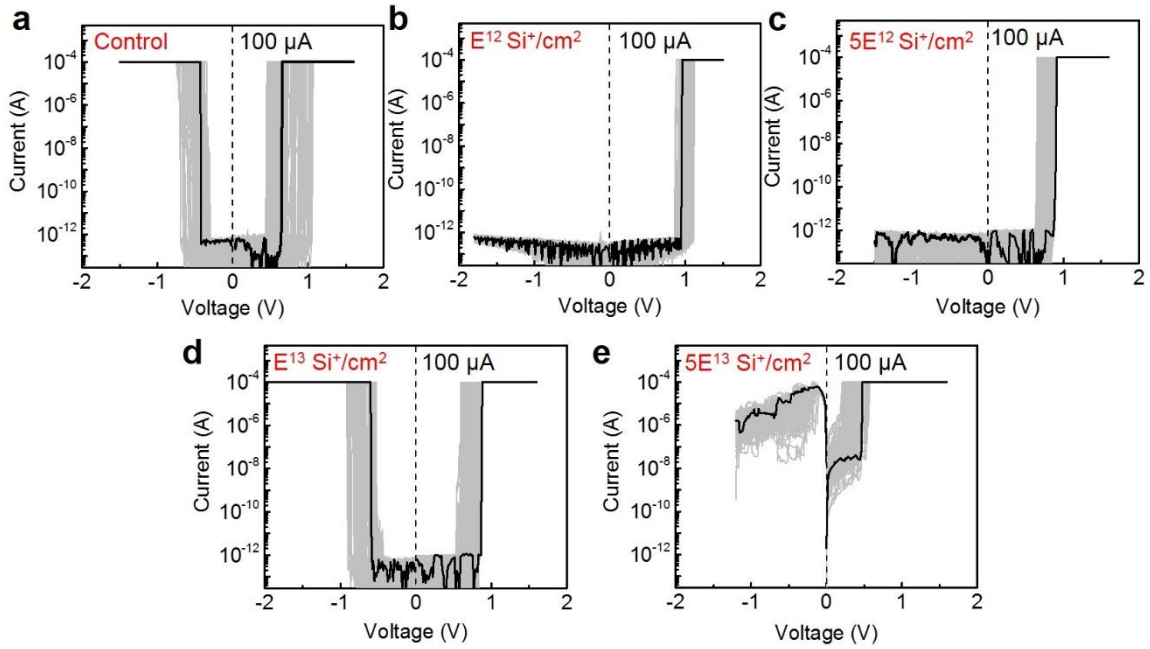

Figure 5. I-V characteristics of (a) bidirectional TS behavior of the control device, and (b,c) unidirectional TS characteristics of the device with lower irradiation fluences (1×10^{12}, 5×10^{12} Si^{+}/cm^{2}), and (d) bidirectional symmetrical TS characteristics of the device with 1×10^{13} Si^{+}/cm^{2} irradiation fluence, and (e) bipolar MS characteristics of the device with larger irradiation fluence (5×10^{13} Si^{+}/cm^{2}).

Future Plans

With aberration-corrected transmission electron microscope available on campus soon, we will focus on studying effects of stress on defect clustering of graphene under electron beam irradiation. MD simulations suggest that stress plays a critical role to change morphologies of cavities. The second focus is *in situ* characterization of defect-boundary interactions on graphene, to answer the key questions whether boundaries have a defect sink property and what are the correlations between sink strength and detail boundary configurations.

Publications for 2015-2017

1. K.P. So, D. Chen. A. Kushima, M. Li, S. Kim, Y. Yang, Z. Wang, J.G. Park, Y.H. Lee, R.I. Gonzalez, M. Kiwi, E.M. Bringa, L. Shao, J. Li, "Dispersion of carbon nanotubes in aluminum improves radiation resistance", *Nano Energy* 22, 319-327 (2016).
2. Joseph B. Wallace, Di Chen, Lin Shao, "Carbon displacement-induced single carbon atomic chain formation and its effects on sliding of SiC fibers in SiC/graphene/SiC composite", *Mater. Res. Lett.* 4, 55-61 (2016).
3. Jing Wang, Di Chen, Julia S. Bykova, Anvar A. Zakhidov, J. Gigax, Xuemei Wang, Lin Shao, "Thermal property tuning in aligned carbon nanotube films and random entangled carbon nanotube films by ion irradiation", *Appl. Phys. Lett*. 107, 151904 (2015).
4. Joseph Wallace, Lin Shao, "Defect-induced carbon nanoscroll formation", *Carbon* 91, 96 (2015).
5. Qiang Yan, Jing Wang, Di Chen, Jonathan Gigax, Lin Shao, "Displacement cross sections of electron irradiated graphene and carbon nanotubes", *Nuclear Instruments and Methods in Physics Research B* 350, 20 (2015).
6. X. Zhao, J. Ma, X. Xiao, Q. Liu, Lin Shao, Di Chen, S. Liu, J. Niu, X. Zhang, Y. Wang, R. Cao, W. Wang, Z. Di, H. Lv, S. Long, and M. Liu, *Nat. Communication*, submitted.

Toughening mechanisms in ceramic nanocomposites with one and two dimensional reinforcements

Brian W. Sheldon, Huajian Gao, Nitin Padture, Brown University, Providence, RI

Jun Lou, Rice University, Houston, Texas

Program Scope

Although ceramic materials have inherent advantages for applications at high temperatures and in chemically aggressive surroundings, their poor mechanical properties (relative to metals) often prevent implementation in these types of harsh environments. Thus, the research community has long focused on methods for improving these properties, particularly the fracture toughness. With this in mind the exceptional mechanical properties of some nanotubes and nanofibers have led to efforts to use these types of materials to produce new *composite* materials with substantially improved toughness. A number of these prior studies have now reported toughness improvements in carbon nanotube (CNT) reinforced ceramics [1-8]. Several recent studies have also shown evidence of substantial fracture toughness improvements in ceramic nanocomposites reinforced with graphene and reduced graphene oxide (r-GO) [9-11]. However, an understanding of the mechanisms that lead to increased toughness in these types of materials is lacking. In comparison with conventional ceramic composites, reducing the reinforcement dimensions by roughly two orders of magnitude leads to important new questions – in particular, the extent to which existing continuum mechanics laws are applicable. Because the scale over which fracture and decohesion occur are comparable to the reinforcement dimensions (e.g., nanotube diameter or number of graphene layers), phenomena at atomic or near-atomic length scales must now be carefully addressed. For example, in ceramic nanocomposites the idea of a distinct reinforcement-matrix interface must be reconsidered in light of the fact that the entire reinforcement is within a few atomic spacings of the matrix. Exploring the ways in which these inherently smaller size scales will impact toughening mechanisms is the central motivation of the work being pursued in this project.

In this research, several different processing methods are being employed to carefully control defects and other structural features. These well controlled materials are then being used to enable systematic experiments. The experimental investigations of toughening mechanisms employ *in situ* mechanical testing capabilities that have been developed at both Brown and Rice Universities. This approach allows us to observe and monitor fracture mechanisms in ways that go well beyond prior studies. All of these experimental investigations are also closely integrated with multiscale modeling efforts. Through this combination of careful processing, in situ mechanical testing, and modeling, we expect to greatly expand the existing understanding of nanoscale toughening in ceramic nanocomposites.

Future Plans

This project started in September 2017. Research plans for the first year are summarized below.

A. Controlled Investigations of Atomic Scale Defects

The relationship between point defects and fracture toughness in CNT-reinforced ceramics is unclear. General comparisons show that CNTs with higher defect densities lead to shorter pull-out lengths during nanocomposite fracture [12], however, this could be due to lower fracture strengths, to changes in the fiber/matrix interface, or both. We plan to investigate these effects with controlled modifications of "very high quality" MWCNTs. The central idea here is that the near-perfect structure of these starting materials can be altered with controlled surface modifications or by modifying the internal structure. The primary method that we plan to employ is to introduce defects with radiation damage. These efforts will be conducted in collaboration with Izabela Szulfarska's group at Wisconsin [13]. Fracture properties will be investigated with both microcantilever specimens at Brown, and single CNT pull-out measurements at Rice (see below). We will also initiate parallel investigations on graphene/r-GO reinforced nanocomposites, using the same polymer-derived ceramic (PDC) matrix.

B. Quantification of Nanocarbon – Ceramic Interfacial Interactions

Bonding at the interfaces between nanocarbon reinforcements and the ceramic matrices is expected to play a critical role in nanocomposite fracture. The Rice team has done pioneering work with *in situ* electron microscopy studies. These methods will be used to measure interface properties in CNT reinforced ceramics. We also plan to extend these *in situ* small-scale mechanical testing methods to mechanically/chemically exfoliated graphene and reduced graphene oxide (and eventually to chemical vapor deposition (CVD) grown graphene). Figure 1 shows the schematic of mechanical investigation of interfacial bonding between graphene and the PDC matrix. The complete pull-out test is recorded by a video to reveal the corresponding deformation and fracture processes, and to ensure the validity of such tests.

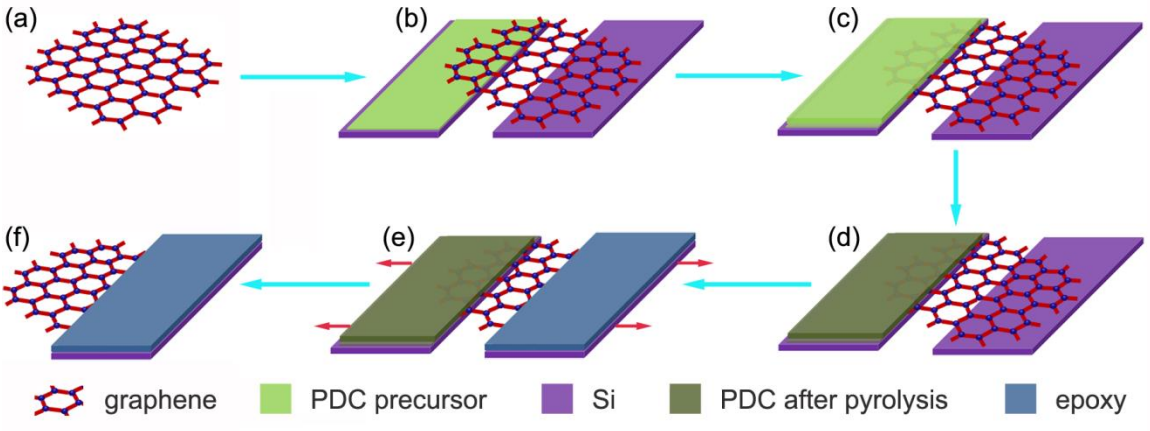

Fig. 1. Schematic of mechanical investigation of interfacial bonding between graphene and PDC.

C. Impact of Platelet Structures

Direct observations of crack-microstructure interactions will be investigated with the in situ SEM capabilities at Brown. The example in Figure 2 clearly shows r-GO sliding and pull-out from an SPS processed silicon nitride matrix. These experiments indicate that there is significant deformation occurring inside of the graphene platelets, behavior which appears to be substantially different from the sword-sheath failures that typically occur with multiwalled carbon nanotubes. Microcantilever testing of FIB notched specimens will also be employed to obtain accurate load-displacement measurements during fracture.

Reinforcement size effects are expected to be important in these materials. Nanoplatelet dimensions will be controlled through processing. The nanocomposites produced with SPS have platelets that are locally aligned, such that FIB cut microcantilevers with oriented structures can be obtained from these specimens. These will permit more effective comparisons between the experimental results and model predictions.

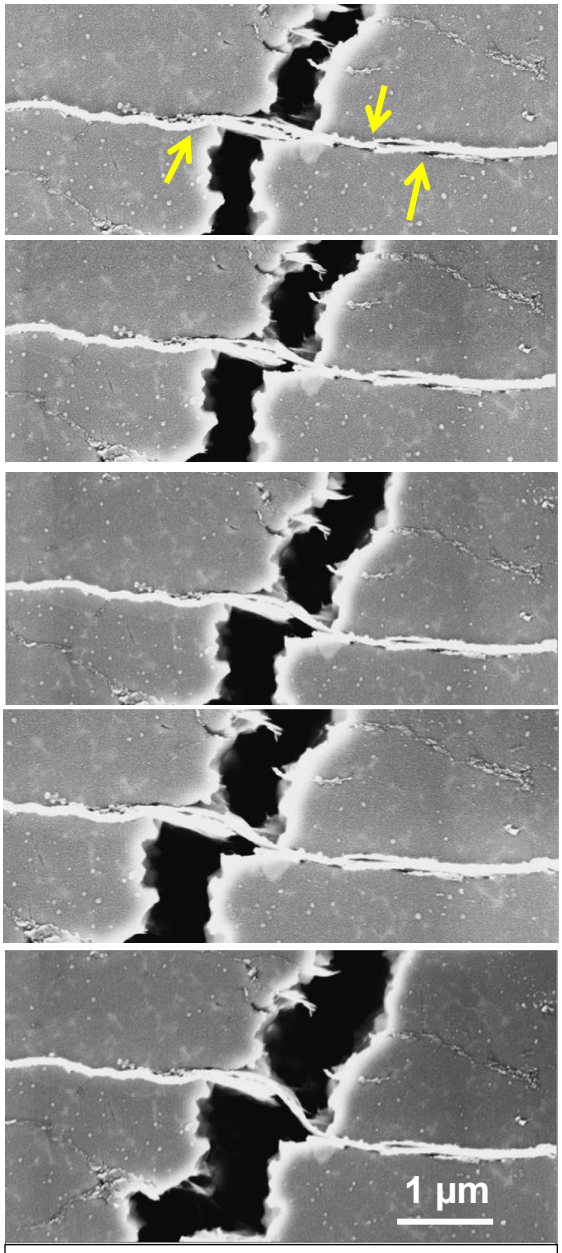

Figure 2. Sequence of SEM images (top to bottom) of the same r-GO bridge, as the crack propagates (downwards) in a Si3N4/4.5 vol% r-GO nanocomposite.

D. Multiscale modeling

The specific direction of the modeling will be closely linked to the ongoing experiments. Initial atomistic investigations of fracture will be conducted for both CNTs and graphene nanoribbons. This work will focus on the behavior of these materials as bridging inclusions in ceramic nanocomposites. In CNTs, it is believed that the tensile fracture of CNTs is accompanied by the formation of unraveling monatomic carbon chains (MACCs) [14,15]. We believe that besides MACCs, graphene nanoribbons might also occur and lead to a similar unraveling process. This type of spiral unraveling mechanism could potentially lead to improved toughness, due to the robustness of nanoribbons. In r-GO nanosheets, this behavior may also be influenced by the helicities, defects and chemisorbed O and H atoms. MD and ab initio MD simulations of tensile fracture will be carried out for CNTs and graphene-based nanosheets of different helicities and sizes.

We will also develop a two-layer cohesive model of brittle fracture in nanocomposite materials. This will be closely aligned with the experiments, and will permit direct comparisons with the data obtained from the in situ measurements. In this model, two layers of cohesive elements are overlapped and inserted into the composites. The fracture toughness of the matrix is assigned to one of the cohesive layers to simulate the brittle K-field near the crack tip. The other cohesive layer has higher strength and toughness in order to capture the strengthening and sliding effects of CNTs in the bridging zone. This two-layer cohesive model will be capable of reproducing the stable crack propagation observed in the experiments.

References

1. S. I. Cha, K. T. Kim, K. H. Lee, C. B. Mo, S. H. Hong, "Strengthening and toughening of carbon nanotube reinforced alumina nanocomposite fabricated by molecular level mixing process" *Scripta. Mater.* **53**, 793 (2005).

2. R. Ma, J. Wu, B. Wei, J. Liang, and D. Wu, "Processing and properties of carbon nanotubes–nano-SiC ceramic", *J. Mater. Sci.* **33**, 5243 (1998).

3. A.K. Kothari, K. Jian, J. Rankin, B. W. Sheldon, "Comparison between carbon nanotube and carbon nanofiber reinforcements in amorphous silicon nitride coatings", *J. Am. Ceram. Soc.* **91**, 2743-2746 (2008).

4. B.T.T. Chu, G. Tobias, C. G. Salzmann, B. Ballesteros, N. Grobert, R. I. Todd, M. L. H. Green, "Fabrication of carbon-nanotube-reinforced glass–ceramic nanocomposites by ultrasonic in situ sol–gel processing", *J. Mater. Chem.* **18** 18, 5344 (2008).

5. Z. Xia, L. Riester, W. A. Curtin, H. Li, B. W. Sheldon, J. Liang, B. Chang, J. . Xu, "Direct observation of toughening mechanisms in carbon-nanotube ceramic matrix composites", *Acta. Mater.* **52**, 931 (2004).

6. A. Peigney, C. Laurent, E. Flahaut, A. Rousset, "Carbon nanotubes in novel ceramic matrix nanocomposites", *Ceram. Int.* **26**, 677 (2000).

7. F. Chastel, E. Flahaut, A. Peigney, A. Rousset, "Carbon nanotube–metal–oxide nanocomposites: microstructure, electrical conductivity and mechanical properties", *Acta. Mater.* **48**, 3803 (2000).

8. A. Mukhopadhyay, B. T. T. Chu, M. L. H. Green, R. I. Todd, "Understanding the mechanical reinforcement of uniformly dispersed multiwalled carbon nanotubes in alumino-borosilicate glass ceramic", *Acta. Mater.* **58**, 2685 (2010).

9. L.S. Walker, V.R. Marotto, M.A. Rafiee, N. Koratkar, and E.L. Corral, "Toughening in Graphene Ceramic Composites," *ACS Nano*, **4** 3182-90 (2011).

10. L. Kvetkova, A. Duszova, P. Hvizdos, J. Dusza, P. Kun, and C. Balazsi, "Fracture Toughness and Toughening Mechanisms in Graphene Platelet Reinforced Si_3N_4 Composites," *Scripta Materialia,*

66 793-6 (2012).

11. C. Ramirez, P. Miranzo, M. Belmonte, M.I. Osendi, P. Poza, S.M. Vega-Diaz, and M. Terrones, "Extraordinary Toughening Enhancement and Flexural Strength in Si_3N_4 Composites Using Graphene Sheets," *Journal of the European Ceramic Society*, **34** 161-9 (2014).

12. X. Liang, Y.C. Yang, J. Lou, B.W. Sheldon, "The Impact of Core-Shell Nanotube Structures on Fracture in Ceramic Nanocomposites", *Acta Materialia* **122**, 82-91 (2017).

13. Y. Yang, C. Ramirez, X. Wang, Z. Guo, A. Tokranov, R. Zhao, I. Szlufarska, J. Lou, and B.W. Sheldon, **"**Impact of carbon nanotube defects on fracture mechanisms in ceramic nanocomposites", *Carbon* **115**, 402-408 (2017).

14. T. Ragab and C. Basaran, "The Unravelling of Open-Ended Single Walled Carbon Nanotubes Using Molecular Dynamics Simulations." Journal of Electronic Packaging 133 (2011).

15. B.I. Yakobson, et al. (1997). "High strain rate fracture and C-chain unraveling in carbon nanotubes." Computational Materials Science 8(4): 341-348 (1997).

Dynamic Fracture in Dealloying Induced Stress Corrosion Cracking

Karl Sieradzki
Fulton School of Engineering
Arizona State University, Tempe, Arizona 85287-6106

Program Scope

Stress-corrosion cracking (SCC) is a form of environmentally induced crack propagation leading to premature failure of elemental metals and alloys. It is believed to require the simultaneous presence of tensile stress and corrosion; however, the exact nature of this synergism has eluded experimental identification. In the case of noble metal alloys SCC is a consequence of dealloying that results in the spontaneous formation of epitaxial nanoporous layers that we hypothesize have the ability transmit high-speed cracks into un-dealloyed parent phase by a pure mechanical process. Importantly, often the measured rate of SCC is incompatible with a purely electrochemical process. In some cases the crack growth velocity has been reported to be factors of 20-100 times that which would be predicted from the measured current density [1-3].

This program is focused on examining SCC caused by dealloying with the aim of unambiguously identifying the synergism between stress and corrosion in an otherwise well characterized system. We are currently examining the behavior of Ag-Au alloys since metal dissolution in this system has been thoroughly studied [4-7], as have the mechanical properties of the nanoporous gold (NPG) that forms as a result of dealloying [8-13]. The critical question addressed is whether or not a dealloyed corrosion layer can, owing to mechanical effects, inject a high-speed crack into un-dealloyed parent phase material [14-16].

Recent Progress

In order to explore these issues we have been conducting crack injection experiments on single crystal and polycrystalline materials. These experiments are designed to separate a mechanical component of cracking from any stress-corrosion component, here identified as simultaneous dealloying and mechanical loading [17-21]. In these experiments a sample is dealloyed under a zero stress condition in order to form a dealloyed corrosion layer of prescribed thickness and then while the dealloying potential is maintained the sample is rapidly loaded causing fracture. The purpose of rapid loading is to minimize the time that stress and dissolution simultaneously operate. All the variants of this general scheme involve inserting a step (or steps) between dealloying and load application in order to further eliminate the occurrence of SCC during load application. For example, the voltage is changed to a value for which no faradaic reaction is possible and the sample is held at this condition for a prescribed period of time (of order seconds to

minutes) prior to load application. Other variants involve removing the sample from the electrolyte and placing it in to DI water or holding the sample in air for prescribed periods of time prior to loading.

Single crystal crack injection and SCC

Tensile crack injection experiments were performed on fully annealed and oriented single crystal $Ag_{0.77}Au_{0.23}$ samples of 125 μm in thickness. The typical dealloying protocol (electrolyte 1M $HClO_4$, 1.26 V, SHE for 10-60 s) produced a nominally 0.5-4 μm thick dealloyed nanoporous layer on the surface of samples that were subsequently rapidly pulled in solenoid-based tensile device. Scanning electron microscopy and electron backscatter diffraction (EBSD) was performed on the fracture surfaces. Figures 1A and 1B display results showing a SEM micrograph of a fracture surface and orientation map of a typical crack injection test. The tensile axis was close to the (001). These EBSD results displayed far less plasticity than the bending experiments described in last year's progress report as evidenced by the lack of streaking in the orientation maps.

Stress corrosion cracking tests were performed on samples oriented in the same manner as those examined in the crack injection experiments. Tests were conducted at a displacement rate of 10 μms^{-1} in 0.1 M $HClO_4$ + 0.01 M $AgClO_4$. Figures 1C and 1D shows an image of a fracture surface as well as the orientation. These results demonstrate that the fracture plane observed in the SCC tests is similar to that obtained in the crack injection tests. Furthermore, we found no tendency for the crack to follow a particular orientation other than that defined by the tensile axis.

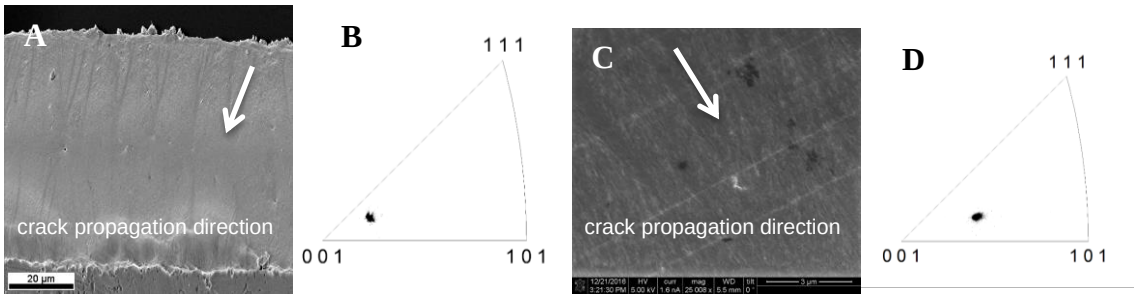

Figure 1. A, SEM and **B,** OIM of a fracture surface resulting from a crack injection experiment. **C** and **D** SEM and OIM of a SCC experiment performed under the identical electrochemical conditions used to produce the corrosion layer for the crack injection experiment.

Polycrystal crack injection and SCC

Dealloying was performed in 1M $HClO_4$ at either 1.26V NHE for 60s or 1.31 V for 60s for two alloy compositions, $Ag_{0.70}Au_{0.30}$ and $Ag_{0.72}Au_{0.28}$. These different protocols were used in order to vary the thickness of the dealloyed layer formed. For the first protocol the thickness of the dealloyed layer was ~500 nm while for the second protocol it was ~ 2.2 μm. In another series of tests, samples with dealloyed layers were not stressed (here termed no-load control samples) with

the aim of examining the extent of GB dealloying penetrations depths. Two general variants of experiments were performed. In one set of experiments following the no-load dealloying protocol, the potentiostat was switched to open circuit, samples were removed from the electrolyte, dipped into deionized water for ~10s, removed from the water and subsequently hand bent to a radius of curvature of ~ 500 μm. In the second set of experiments samples were removed from the dealloying electrolyte and held in air for times ranging from 3 – 180s prior to bending and subsequently immersed in water. None of the samples that were either immersed in water prior to bending or held in air for longer than 10s fractured, while virtually all of the samples that were held in air for less than 10s and bent fractured. We have previously characterized the results from the first testing protocol using atomic scale techniques of atom probe tomography and, aberration-correction scanning transmission electron microscopy in previous reports.

All of the eight crack injection experiments performed on samples that were removed from the electrolyte and bent within 10s resulted in sample fracture. Figure 2A shows a typical fracture surface obtained from these experiments and Fig. 4B compares this to that obtained in a conventional slow displacement rate SCC test. At the scale of the images the fracture surfaces are similar except that close inspection of the SCC surface shows porous structures on the grain facets. We emphasize that the only difference between samples that underwent fracture and those for which cracks were not injected through-thickness causing sample fracture was the length of the hold time in air or water immersion.

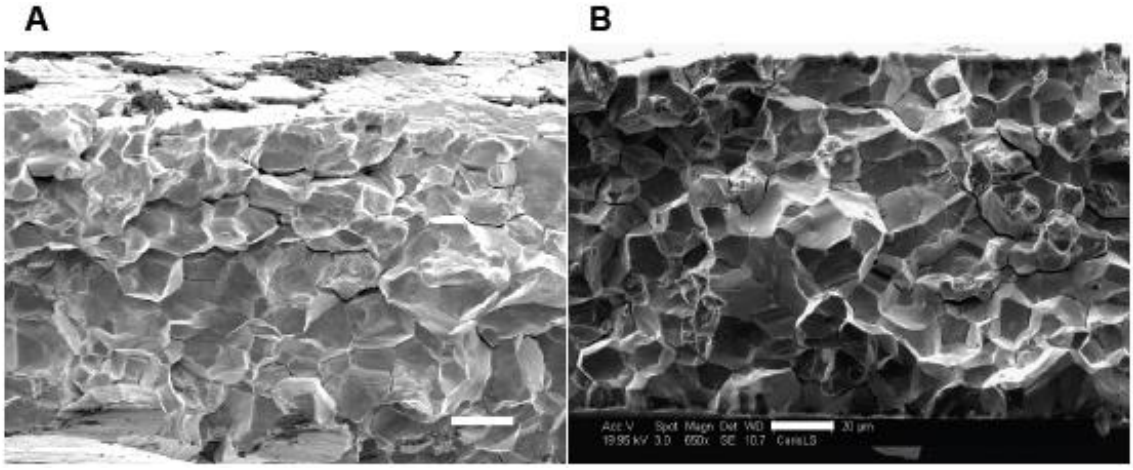

Figure 2. Crack injection and IGSCC fracture surfaces. A, Sample (125 μm thickness) dealloyed at 1.26 V, NHE for 60 s removed from the electrolyte and bent into a U-shape of approximate radius of 500 μm. This sample underwent through-thickness fracture. **B.** Stress-corrosion cracking result for a sample (125 μm thickness) under tensile loading at a displacement rate of 1.0 μm/s at 1.26 V, NHE. Contrast in this image has been enhanced in order to make visible at increased magnification the porosity on the fracture surface. In both cases, the fracture surfaces are primarily intergranular, with isolated regions of transgranular fracture. Scale bars are 20 μm.

Statistics of intergranular corrosion penetration and crack injection.

In order to develop a more general picture of the depth of intergranular corrosion penetration in the no-load control samples as well as GB crack injection distances, we examined cross-sections of samples to determine the statistics of penetration and crack injection. Following the formation of the dealloyed layer no-load control samples were immersed in DI water for one day. These samples were then stretched in a tensile device to ~15% elongation in order to tear open grain boundary dealloying penetrations to make them more easily visible. Crack injection samples followed the same no-load dealloying protocol after which they were mounted on a solenoid tensile device and impulsively loaded. The elapsed time between removal of these samples from the electrolyte and loading was ~180 s. Figures 3A and 3B show the histograms of grain boundary penetration distances and demonstrate that for the dealloying conditions employed the GB penetrations were less than 4 times the thickness of the dealloyed layer. In all, we examined the depth of ~ 10,000 penetrations and the mean and median of the distributions correspond to either the ~ 500 nm or ~2.2 μm thick nanoporous layers. Figure 3C is a histogram result for crack injection and reveals qualitative differences between the statistics of corrosion induced GB penetration and crack injection. The mean and median injection distances were 2.8 μm and the largest injection distance found was 12 μm, which is ~ 4 μm deeper than any no-load grain boundary corrosion penetration distance observed for the identical alloy composition and dealloying protocol.

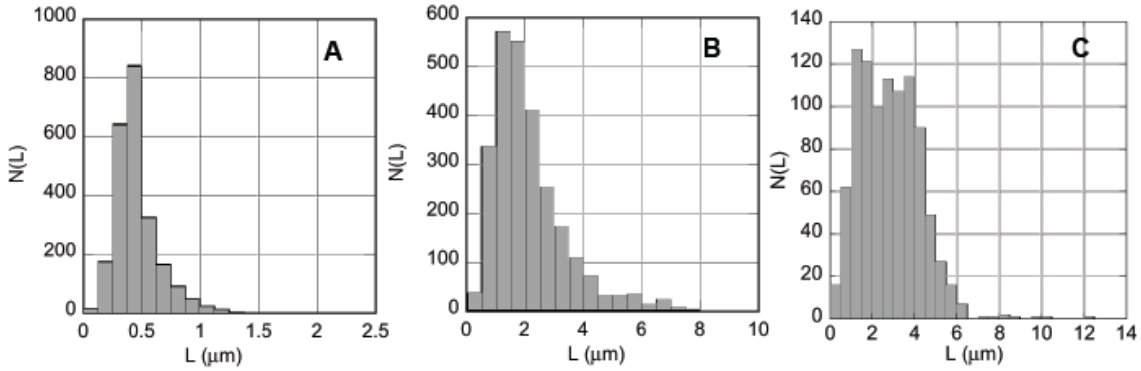

Figure 3. A, Crack penetration histogram for a $Ag_{70}Au_{30}$ sample treated at 1.26 V NHE for 60 s resulting in a ~500 nm deep nanoporous dealloyed layer. **B,** Crack penetration histogram for a $Ag_{72}Au_{28}$ sample treated at 1.31V NHE for 60 s resulting in a ~2.2 μm deep nanoporous dealloyed layer. **C,** Crack injection histogram for a $Ag_{72}Au_{28}$ sample treated at 1.31 V NHE for 60 s resulting in a ~2.2 μm deep nanoporous dealloyed layer.

In considering the qualitatively different behaviors observed in the crack injection experiments, we are left with the question of what happens to the ability of the dealloyed layer to inject a through-thickness crack following removal of a sample from the electrolyte? Coarsening of the layer occurs immediately following switching the potentiostat to an open circuit condition and at

one time we believed that such a coarsened NPG structure could not support high-speed cracking. However, recently published work by our group has shown that monolithic NPG coarsened over days, is able to support dynamic fracture at 200 ms^{-1} [13]. We believe that the different behaviors observed are related to the changes in the structure of the interface between the NPG layer and the un-dealloyed parent phase. Previous work has shown that The NPG layer in these crack injection experiments is composed of ligaments that are ~ 5 nm in diameter. The dealloyed layer/parent phase interface shows regions of large elongated voids of order 5 nm in width and 30 nm in length. This evidence suggests that these voids degrade interfacial adhesion and that this significantly impedes the ability of a NPG layer to inject a GB crack into the un-dealloyed parent phase.

In conclusion our results reveal that crack injection depends on the time-dependent morphology at the dealloyed layer/parent phase interface and that the mechanistic roles of stress and corrosion can be de-coupled. Our key finding is connected to coarsening of the nanoporous morphology occurring at the interface where relatively large elliptical voids evolve with their major axis aligned parallel to the interface severely degrading adhesion and consequently the ability of a NPG corrosion layer to inject GB cracks.

Future Plans

- Continued work on Ag-Au diffusion couples for examining crack injection in nominally pure single crystal gold.
- Continued work on single crystal Ag-Au crack injection experiments that will further examine tensile orientation effects to determine if there are favored fracture planes.
- Remarkably our work has shown that the current understanding of GB confined corrosion does not allow for predicting corrosion rates. We aim to develop models for this based on future results from experiments in Cu-Au alloys for which Cu is known to segregate to GBs.

References

1. K. Sieradzki, J.S. Kim, A.T. Cole, A.T., R.C. Newman, The relationship between dealloying and transgranular stress-corrosion cracking of CuZn and CuAl alloys, J. Electrochem. Soc. **134,** 1635-1639 (1987).
2. S.A. Serebrinsky, J.R. Galvele, Effect of the strain rate on stress corrosion crack velocities in face-centered cubic alloys. A mechanistic interpretation, Corros. Sci. **46,** 591-612 (2004).
3. T.B. Cassagne, W.F. Flanagan, B.D. Lichter, On the failure mechanism of chemically embrittled Cu3Au single crystals, Metall. Trans. **A 17**, 703-710 (1986).
4. J. Erlebacher, M.J. Aziz, A. Karma, N. Dimitrov, and K. Sieradzki, Evolution of Nanpoporosity in Dealloying, Nature, **410**, pp. 450-453 (2001).
5. J.Erlebacher, K. Sieradzki, Pattern formation during dealloying, Scripta Mat., **49,** 991-996 (2003).
6. J. Rugolo, J. Erlebacher, K. Sieradzki, Length scales in alloy dissolution and measurement of absolute interfacial free energy, Nat. Mater., 5, 946-949 (2006).

7. A. Dursun, D. V. Pugh, S G. Corcoran, Probing the Dealloying Critical Potential, J. Electrochem. Soc., **152,** B65-B72 **(**2005**).**
8. R. Li, K. Sieradzki, K. Ductile-brittle transition in random porous Au, *Phys. Rev. Lett.* **68**, 1168 (1992).
9. N. J. Briot, T. Kennerknecht, C. Eberl & T. J. Balk, Mechanical properties of bulk single crystalline nanoporous gold investigated by millimetre-scale tension and compression testing, Philos. Mag. **94,** 847-866 (2014).
10. H-J Jin, L. Kurmanaeva ,J. Schmauch, Harald Rosner, Y.Ivanisenko, J Weissmuller, Deforming nanoporous metal: Role of lattice coherency, Acta Mater. 57, 2665-2672 (2009).
11. N. Huber, R.N. Viswanath, N. Mameka, J. Markmann a,c, J. Weissmuller, Scaling laws of nanoporous metals under uniaxial compression, Acta Mater**., 67**, 252-265 (2014).
12. N. Badwe, X. Chen, K. Sieradzki, Mechanical properties of nanoporous gold in tension, Acta Mater., **129,** 251-258 (2017).
13. S. Sun, X. Chen, N. Badwe, K. Sieradzki, "Potential Dependent Dynamic Fracture in Nanoporous Gold", Nat. Mater., **14,** pp. 894-898 (2015).
14. K. Sieradzki, R.C. Newman, Stress-corrosion cracking, J. Phys. Chem. Solids, 48, 1101-1113 (1987).
15. S. Sun, X. Chen, N. Badwe, K. Sieradzki, Potential Dependent Dynamic Fracture in Nanoporous Gold, Nat. Mater., 14, pp. 894-898 (2015).
16. K. Sieradzki, R.C. Newman, Brittle behavior of ductile metals during stress-corrosion cracking, Philos. Mag A. 51, 95-132 (1985).
17. J.D. Fritz, B.W. Parks, H.W. Pickering, Stress corrosion cracking of Cu-18% Au in 1N Na_2SO_4 - 0.01N H_2SO_4. Scripta. Metall. **22**, 1063–1068 (1988).
18. R.G. Kelly, A.J. Frost, T. Shahrabi, T. R.C. Newman, R. C. Brittle-fracture of an Au/Ag alloy induced by a surface-film. Metall. Trans. A-Physical Metall. Mater. *Sci.* **22**, 531–541 (1991).
19. J.S. Chen, M. Slameron, M., T.M. Devine,Intergranular and transgranular stress corrosion cracking of Cu-30Au. Corros. Sci. **34**, 2071–2097 (1993).
20. M. Saito, G.S. Smith, R.C. Newman, Testing the film-induced cleavage model of stress-corrosion cracking. Corros. Sci. **35**, 411–413 (1993).
21. F. Friedersdorf,, K. Sieradzki, Film-induced brittle intergranular cracking of silver-gold alloys. Corros. Sci. **52**, 331–336 (1996).
22. A. Barnes, N.A. Senior, R.C. Newman, R. C. Film-induced cleavage of Ag-Au alloys. Metall. Mater. Trans. A **40A**, 58–68 (2009).

Publications (2-year list of publications SUPPORTED BY BES)

Nilesh Badwe, Xiying Chen, Karl Sieradzki, "Mechanical Properties of nanoporous Gold in Tension", Acta Materialia, **129,** pp. 251-258 (2017).
doi.org/10.1016/j.actamat.2017.02.040

Shaofeng Sun, Xiying Chen, Nilesh Badwe, Karl Sieradzki, "Potential Dependent Dynamic Fracture in Nanoporous Gold", Nature Materials, 14, (September), pp. 894-898 (2015). doi:10.1038/nmat4335

Understanding, controlling and creating martensitic phase transformations in nanostructured polycrystals and metamaterials

Alejandro Strachan

School of Materials Engineering, Purdue University

Program Scope

Martensitic phase transformations are exploited to enhance the performance and to achieve otherwise inaccessible functionalities in a wide range of advanced materials. Examples range from TRIP steels [1] to shape memory alloys (SMAs) [2] used for environmental-friendly energy conversion [3] and refrigeration, [4] as well as sensors and actuators for medicine and vibration damping. Despite many decades of research and a host of successful applications, recent advances indicate that this class of materials possesses a significant untapped potential. Nano-engineered composites and metamaterials with at least one component capable of undergoing martensitic transformation can open the door to remarkable mechanical properties. Examples include composites that combine ultra-high elastic limit with high-strength [5] and our group's work on shape memory metamaterials (SMMs) with tunable transformation hysteresis and temperature.[6] The objective of this project is to use atomistic simulations to design **metamaterials with novel mechanical properties** by building on the concept of *energy landscape engineering*, represented schematically on Figure 1. By epitaxially integrating appropriately chosen materials with complementary free-energy vs. lattice parameter landscapes one can create metamaterials with properties not achievable otherwise. Specific goals are to: i) achieve ultra-low and tunable stiffness and thermal conductivity by stabilizing negative phase at the nanoscale and ii) optimized shape memory metamaterials (SMMs) from non-transforming constituents with desirable transformation characteristics.

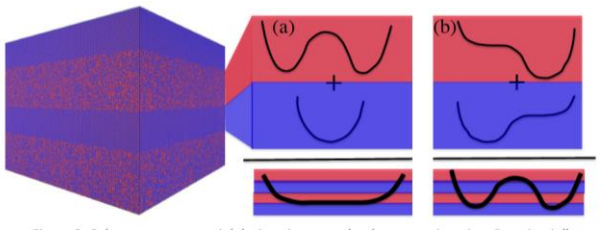

Figure 1. Coherent metamaterial design via energy landscape engineering

Recent Progress

We recently demonstrated, computationally, ultra-low stiffness in fully dense metallic nanowires and laminates via the stabilization of a negative stiffness state using epitaxy. These novel metamaterials exhibit Young's moduli over one order of magnitude lower than either constituent, defying long-standing bounds of composite design. Key to achieving this unprecedented property is a martensitic alloy constrained to a mechanically unstable phase by its coherent integration with a compatible, stable second component. Explicit large-scale molecular dynamics simulations using state of the art interatomic potentials confirm the low stiffness expected from the competing response of the two components and provide insight into the

mechanisms behind ultra-low stiffness. Figure 2 shows snapshots of the deformation of a pure martensitic nanowire with standard stiffness (top snapshots) and the coherent metamaterial (bottom). Atoms are colored based on the local environment (blue indicates austenite and red martensite) and we observe interpenetrating domains in the metamaterials as a wide range of lattice parameters have similar energies. Upon deformation the system can change lattice parameters under low stresses resulting in ultra-low stiffness.

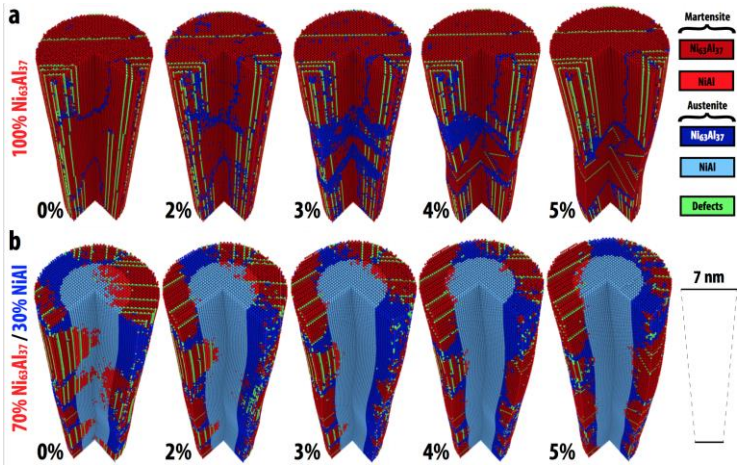

We find moduli as low as 2 GPa, a value typical of soft materials, while maintaining full strength; these properties together with metallic conduction could enable new functionalities in flexible electronics and implantable devices. The concept of stabilizing unstable nanoscale phases via coherent integration is generally applicable and the ability to harness such states significantly enhances the design space available to materials scientists.

Future Plans

Ongoing and future work is along two lines. i) We are performing ab initio calculations using density functional theory to develop a library of energy landscapes (energy as a function of lattice parameters) for a wide range of metals. We will then search the landscapes for pairs of materials that, when epitaxially combined, result in the properties of interest described above. ii) We have demonstrated ultra-low stiffness in epitaxial nanolaminates and nanowires, we are now exploring whether other geometries would also exhibit the same effect. Specifically, we are interested in whether coherent nano-precipitates within a matrix could be stabilized in negative stiffness phases and lead to softening.

References

[1] Grässel, O., L. Krüger, G. Frommeyer, and L. W. Meyer. "High strength Fe–Mn–(Al, Si) TRIP/TWIP steels development—properties—application." *International Journal of Plasticity* 16, no. 10 (2000): 1391-1409.

[2] *Phase Transformations of Nanocrystalline Martensitic Materials*, T. Waitz, K. Tsuchiya, T. Antretter, and F.D. Fischer, MRS Bulletin, 34, 814 (2009).

[3] Srivastava, Vijay, Yintao Song, Kanwal Bhatti, and R. D. James. "The direct conversion of heat to electricity using multiferroic alloys." *Advanced Energy Materials* 1, no. 1 (2011): 97-104.

[4] Liu, Jian, Tino Gottschall, Konstantin P. Skokov, James D. Moore, and Oliver Gutfleisch. "Giant magnetocaloric effect driven by structural transitions." *Nature materials* 11, no. 7 (2012): 620-626.

[5] Hao, Shijie, et al. "A transforming metal nanocomposite with large elastic strain, low modulus, and high strength." *Science* 339.6124 (2013): 1191-1194.

[6] Vishnu, Karthik Guda, and Alejandro Strachan. "Shape memory metamaterials with tunable thermo-mechanical response via hetero-epitaxial integration: A molecular dynamics study." *Journal of Applied Physics* 113.10 (2013): 103503.

Publications

- Samuel Temple Reeve, Alexis Belessiotis-Richards, Alejandro Strachan, "*Harnessing mechanical instabilities at the nanoscale to achieve ultra-low stiffness metals*" Nature Communications (in press).
- Keith R Morrison, Mathew J Cherukara, Hojin Kim, Alejandro Strachan, "*Role of grain size on the martensitic transformation and ultra-fast superelasticity in shape memory alloys*" Acta Materialia 95, 37-43 (2015).

Coupled Effects of Radiation and Chemical Environment on Interfaces in SiC

PI: ***Izabela Szlufarska***
Department of Materials Science & Engineering, University of Wisconsin – Madison

Program Scope

We use an integrated approach that includes multi-scale simulations and state of the art experimental characterization techniques to develop understanding of radiation induced segregation (RIS) and radiation assisted corrosion (RAC) in SiC. This understanding and these models will provide design principles for future synthesis of radiation-tolerant covalent ceramics. The main themes of this project are: (i) dependence of RIS on grain boundary (GB) type; (ii) structural evolution of GBs under RIS; (iii) impact of RIS on RAC; and (iv) radiation effects on bonding and O_2/H_2O permeability through a protective oxide scale.

Recent Progress

While grain boundaries (GBs) can act as sinks of defects in irradiated materials, much less is known about the effects of radiation on the evolution of atomic structure and consequently on the sink strength of GBs. In addition, in multi-component materials, such as silicon carbide, there can be an unbalanced flux of different species to the GBs, raising questions about potential compositional changes of GBs under irradiation and the effects of these changes on the continuing ability of GBs to absorb defects. In order to predict time-evolution of sink strength, we investigated the defect kinetics, structural and chemical changes taking place in GBs during irradiation using a combination of multi-scale simulations and experimental characterization.

On the simulation side, we first demonstrated that the diffusion of interstitials along tilt GBs in SiC is slower as compared to lattice diffusion, which is in contrast to the common assumption adapted from metals that GBs are fast diffusion channels for defect transport. To account for the competing processes of (i) interstitial diffusion along GBs and annihilation at other sinks such as triple junctions or surfaces; (ii) defect clustering; (iii) jog nucleation from clusters; and (iv) growth of new lattice planes in the GB, we have developed a continuum level "dislocation-line model" and performed simulations for different temperatures and different irradiation conditions. Our model predicts (Fig. 1a) that the fate of defects within a GB depends on the grain size as well as the irradiation conditions and it implies that to predict evolution under irradiation, it important to consider the mutual effects of defects on interfaces and of interfaces on defects. This work has been published in Ref.[1]

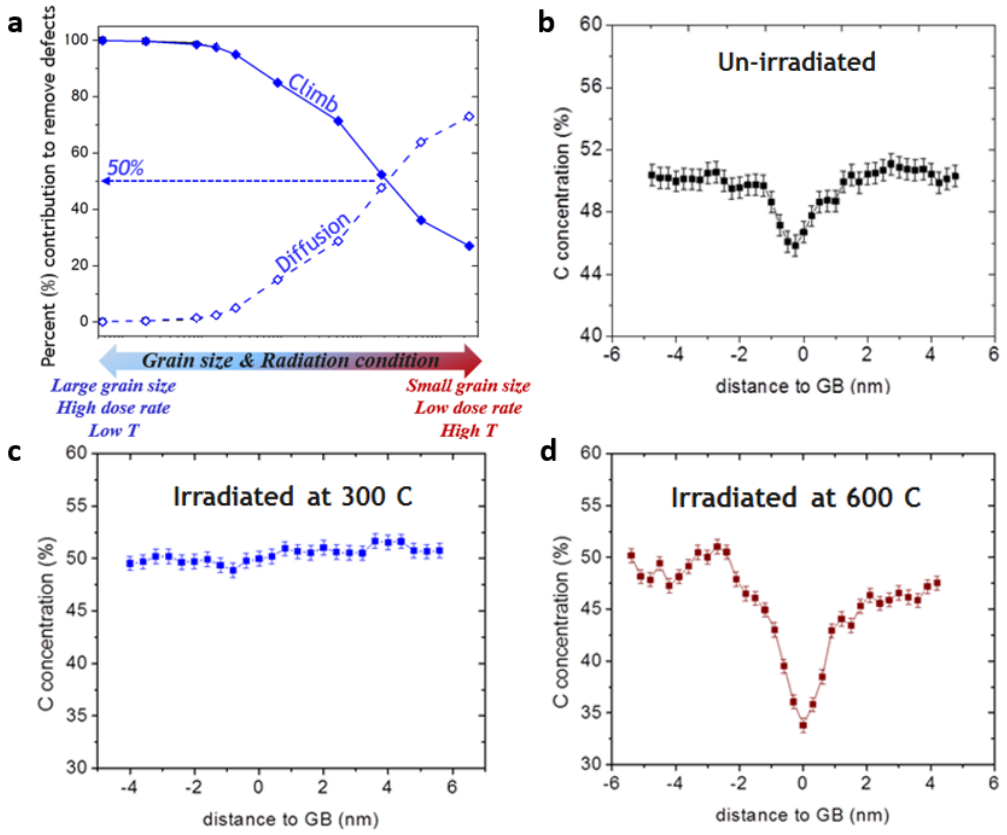

Figure 1 | **a**, Percent of interstitials annealed by diffusion along GB to other sinks and by dislocation climb under different irradiation conditions in tilt GBs. Local relative C concentration profile near GBs measured by 200 kV EELS in **b**, unirradiated; **c**, 300 C ion-irradiated; and **d**, 600 C ion-irradiated SiC samples.

Effects of irradiation on structural evolution of twist GBs have also been investigated in terms of evolution of GB dislocation networks. Unlike tilt GBs, where defect annihilation mechanisms based on dislocation climb mechanisms are relatively well established,[2] at present it is unknown how twist GBs accommodate defects and how these accommodation mechanisms are affected if the defect flux is off-stoichiometric. We used a combination of molecular dynamics, kinetic Monte Carlo, and grand canonical Monte Carlo simulations to unravel defect kinetics and structural evolution in {001} and {111} twist GBs. We found that because of the large driving fore for segregation of interstitials (binding energy lower than -1.5 eV for both C and Si interstitials) at dislocation intersections, these sites provide strong traps for interstitials. This strong trapping effect has two main concequences. First of all, it surpresses the overall diffusion of interstitials along the dislocation grid in twist GBs. The surpressed interstitial mobility at twist GBs can lead to interstitial accumulation at GBs under conditions of large grain size (above 100 nm), or irradiated at high dose rate (higher than 10^{-5} dpa/s), or at low temperature (below 873 K).

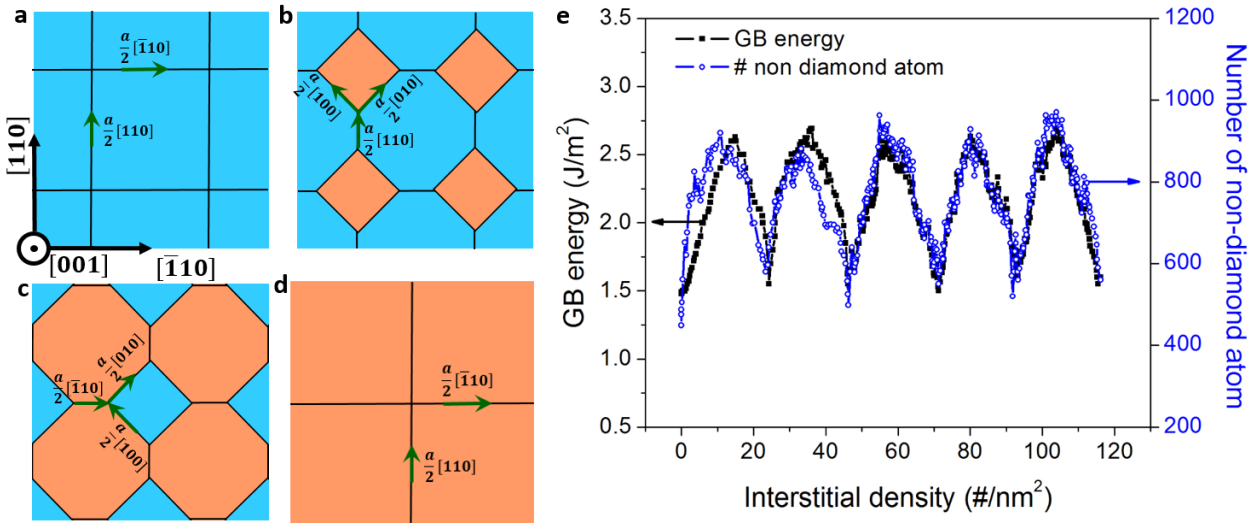

Figure 2 | **a-d**, Schematic representation of loop nucleation and extension in {001} twist GBs under interstitial flux. Black lines represent dislocations, and green arrows represent the screw components of the Burgers vector of each dislocation segment. Green arrows show the Burgers vector of the screw components of dislocation segments. **e**, the change of GB energy and number of non-diamond atoms as a function of interstitial density loaded into the interface.

In addition, the strong trapping of interstitials at intersections drives interstitial clustering and initiates structural evolution of GBs. The common features in evolution of GB dislocation networks of {001} and {111} twist GBs are the formation and climb of mixed dislocations, which take place to accommodate interstitials. The two GBs differ in the way they form mixed dislocations. In {001} twist GBs, interstitial clusters at dislocation intersections can nucleate interstitial loops (orange squares in Fig. 2b). These loops can extend by absorbing interstitials segregated to GBs (Fig. 2c) and the continuous extension of these loops can lead to the growth of one lattice plane at the interface (Fig. 2d). At this stage, the initial screw dislocation grid is reproduced at the interface and interstitial loops can nucleate again at dislocation intersections. This repeating pattern implies that {001} twist GBs do not saturate in their ability to absorb interstitials in SiC (Fig. 2e). In {111} twist GBs, which are composed of stacking faults (SFs) and partial dislocations (Fig. 3a), interstitials segregated to dislocation intersections drive the glide of partial dislocations to produce mixed dislocations. The glide of partial dislocations can remove initial SFs (unfaulting process in Fig. 3a-b) or produce SFs (faulting process in Fig. 3c-3d). The roughly linear relationship between mixed dislocation length and interstitial density loaded at GB in Fig. 3e provides further evidence of mixed dislocation formation. The formation and climb of these mixed dislocation can accommodate interstitials into lattice sites in {111} twist GBs. The evolution of dislocation networks in twist GBs under irradiation is valid for both stoichiometric flux and off-stoichiometric flux. In the latter case, we observed the formation of carbon antisites because carbon interstitials are incorporated into lattice sites by dislocation climb. The antisite-rich interfaces are structurally stable within the timescale of molecular dynamics (hundreds of nanoseconds) at temperature as high as 1500 K.

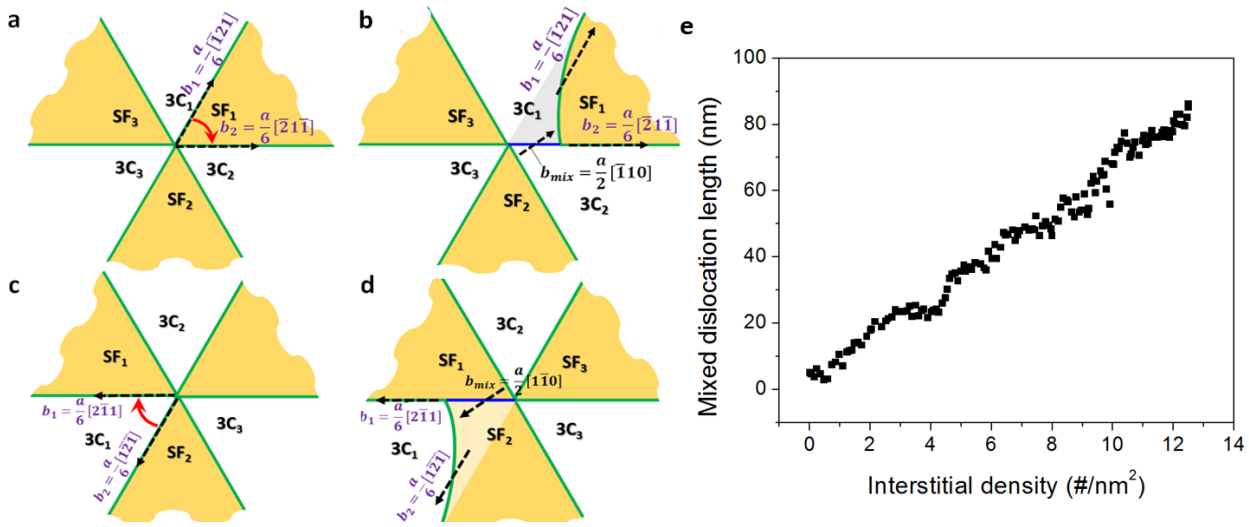

Figure 3 | Mixed dislocations formation in $(11\bar{1})$ twist GB. **a** before unfaulting and **b** after unfaulting process; **c** before faulting and **d** after faulting process. Green lines are partial dislocations, and blue lines are mixed dislocations produced by the reaction of partials. Black dashed arrows show the direction of the Burgers vector of each dislocation segment. Red arrows in panels **a** and **c** show the glide direction of partials. **f**, mixed dislocation length as a function of interstitial density loaded at the interface.

On the experimental side, we employed scanning transmission electron microscopy (STEM) and electron energy loss spectroscopy (EELS) and found that GBs in CVD-SiC are intrinsically carbon-poor and the relative C composition can be as low as 45%. (Fig. 1b) This carbon depletion disappeared in samples irradiated to 1 dpa at 300 C, which is likely due to the unbalanced flux of C interstitials to defect sinks and low diffusivity of defects along GBs (Fig. 1c). Interestingly, the C depletion appeared again in samples irradiated at 600 C and the depletion was found to be more significant than in the non-irradiated samples (Fig. 1d). The off-stoichiometry of SiC is surprising given that it is a line compound.

Our results from both simulation and experiments indicate that the role of GBs as defect sinks can very depending on irradiation environments (e.g., from defect clustering reservoirs at low irradiation temperatures to defect diffusion channels at high irradiation temperatures in Fig. 1) and evolve as a function of radiation dose. Changes in GBs atomic structure and chemistry due to irradiation are critical to understand expected to impact such properties as its fracture strength, corrosion resistance, as well as the ability of materials to provide a barrier to diffusion of fission products in nuclear reactor applications.

Future Plans

The following research is either being currently pursued or will be pursued in the near future:

- Discover dependence of RIS on GB character in SiC. For this purpose we will use bicrystal samples prepared using direct wafer bonding technique. The bicrystal samples will provide better control of the GB characteristics (e.g., tilt, twist, and misorientations).
- Corrosion studies of non-irradiated and irradiated bicrystals: studies of different bicrystal misorientations will allow us to determine how the rate of oxidation depends on the GB type, providing fundamental understanding for future GB engineering. Experimental studies will be carried out both ex situ and in situ and these experiment will be complemented with multiscale simulations to discover fundamental mechanisms controlling corrosion. Comparison between non-irradiated and irradiated samples with the same GB misorientation will allow us to determine how much the oxidation is affected by irradiation and the GB type.

References

1. Jiang, H.; Wang, X.; Szlufarska, I., The Multiple Roles of Small-Angle Tilt Grain Boundaries in Annihilating Radiation Damage in SiC. ***Scientific Reports*** 2017**,** *7*, 42358.
2. Sutton, A. P.; Balluffi, R. W., ***Interfaces in crystalline materials***. Clarendon Press, Oxford: 1995.
3. Balluffi, R., Mechanisms of dislocation climb. ***Phys. Stat. Sol.*** 1969**,** *31* (2), 443-463.

Publications in the last 2 years of the project

- Kaczmarowski, A., Yang, S., Szlufarska, I. & Morgan, D. Genetic Algorithm Optimization of Defect Clusters in Crystalline Materials. ***Comp. Mater. Sci.*** 98, 234-244 (2015).
- Wang, X. *et al*. Evidence for cascade overlap and grain boundary enhanced amorphization in silicon carbide irradiated with Kr ions. ***Acta Materialia*** 99, 7-15 (2015).
- Jiang, H., Morgan, D., Voyles, P. M. & Szlufarska, I. Radiation-induced mobility of small defect clusters in covalent materials. ***Phys. Rev. B*** 94, 024107 (2016).
- Tangaptjaroen, C., Grierson, D., Shannon, S., Jakes, J. & Szlufarska, I. Size effects in nanoscale wear of silicon carbide. ***ACS Applied Materials and Interfaces*** 9, 1929-1940 (2017).
- Y. Yang, C. Ramirez, X. Wang, Z. Guo, A. Tokranov, R. Zhao, I. Szlufarska, J. Luo, B. W. Sheldon, Impact of Carbon Nanotube Defects on Fracture Mechanisms in Ceramic Nanocomposites, ***Carbon*** 115, 402-408 (2017)
- Jiang, H., Wang, X. & Szlufarska, I. The Multiple Roles of Small-Angle Tilt Grain Boundaries in Annihilating Radiation Damage in SiC. ***Scientific Reports*** 7, 42358 (2017).
- M-J. Zheng, X. Wang, I. Szlufarska, D. Morgan, *Continuum model for hydrogen pickup in zirconium alloys of LWR fuel cladding* ***J. Appl. Phys.*** 121, 135101 (2017)
- Sahoo, D. R., Szlufarska, I., Morgan, D. & Swaminathan, N. Role of pre-existing point defects in primary damage production and amorphization in silicon carbide. ***Submitted***

- X. Wang, H. Jiang, J-C Idrobo, D. Morgan, P. M. Voyles, I. Szlufarska, Radiation-induced composition evolution of grain boundaries in SiC, ***Submitted***

- Ko, H., Kaczmarowski, A., Szlufarska, I. & Morgan, D. Optimization of self-interstitial clusters in 3C-SiC with genetic algorithm. ***J. Nucl. Mater.*** 492, 62-73 (2017)

A 3D perspective on twinning: interfacial defects and collective interactions in HCP

C.N. Tomé (PI), L. Capolungo (co-PI), R. J. McCabe, M. Arul Kumar, E. Martinez, B. Clausen

Materials Science and Technology Division
Los Alamos National Laboratory, Los Alamos NM 87545

Program Scope

Twinning accommodates strain during plastic deformation of HCP materials via the formation of reoriented 3D domains. Twin growth involves the 3D kinetics of interfaces containing complex Interfacial Defects (IDs) such as disconnections, faults, and disclinations. The Material Science community, surprisingly, has focused on twin morphology and interface mobility from only a 2D perspective. Our Program addresses, for the first time, the full 3D character of twin domains and aims at elucidating the collective role of IDs on the growth kinetics of twin domains. We use Mg and Ti as paradigm systems. It is hypothesized that the growth kinetics of twin domains is driven by the ability of IDs to rearrange their atomic scale structure without affecting the long-range strain fields. This hypothesis will be tested in the case of both isolated and interacting domains by leveraging several advanced techniques, such as in-situ TEM, 3D EBSD, high-energy X-ray diffraction, molecular dynamics. A novel Generalized Discrete Defect Dynamics (GD^3) approach will be introduced to study the dynamics of IDs induced by local stress fields. We expect GD^3 to profoundly change our understanding and description of transformation-mediated plasticity, in much the same way as Discrete Dislocation Dynamics changed the understanding of dislocation structures and their role in plasticity.

Recent Progress

In the last two years we have devised methods to establish statistical correlations between twin morphology and microstructure, in order to advance our knowledge of twining in HCP materials. An automated EBSD analysis software, METIS [1], was developed and used to provide correlations between twin features (twin thickness, variant selection, number of twins per grain, etc) and microstructural features (parent grain size, neighboring grain orientation, transmissibility across grain boundaries, etc). Using local elasto-plastic calculations based on the Fast Fourier Transform we were able to elucidate the mechanisms responsible for most of these correlations [2-5]. A central concept of this research is the internal stress induced by the twin shear transformation, and how the latter strain is accommodated both, in the parent and in the neighboring grains. In parallel to these efforts, atomistic scale simulations and experimental HR-TEM observations have been performed with the objective of unraveling the structure of defects

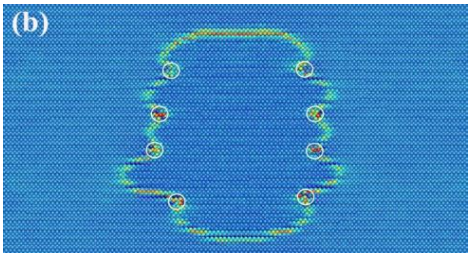

Figure 1: Atomistic simulation of the lateral growth of (10-12) twins in pure Mg. Simulations reveal the potential nature of interfacial defects on the lateral side of the twin (see Ref 7)

at twin interfaces. Among others, the presence of steps on twin boundaries, such as basal-prismatic interfaces, have been revealed and analyzed in the context of topological defect theory. These findings and their relevance to diffusionless transformations (e.g. twinning, phase transformations) are discussed in a recent review [6].

The aforementioned computational and experimental work focused on two-dimensional aspects of twinning from planes containing the normal and shear direction). In a recent publication [7], we pioneer the analysis of the 3rd dimension (lateral side of twins). Both molecular dynamics (MD) and HR-TEM provided evidence of another type of twist interfaces across the twin boundary, whereby prism-prism and pyramidal-pyramidal twist interfaces separate twin from parent. Figure 1 illustrates typical results obtained via atomistic simulations, and Figure 2 provides a schematic representation of a faceted 3D twin domain.

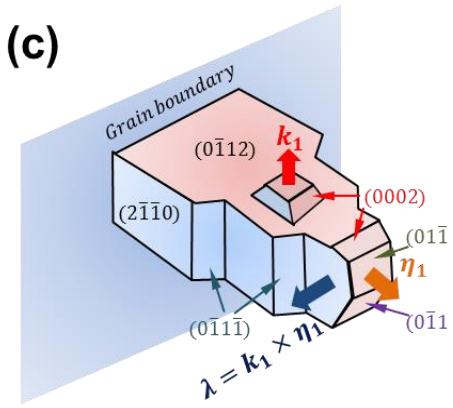

Figure 2: schematic representation of a faceted three dimensional twin domain. Each facet is made up of IDs.

In transitioning the current program towards the study of the nature and properties of IDs, and their role on twin propagation and growth, four distinct, yet connected, research tasks are being pursued. All such tasks acknowledge the need to consider IDs as generating three-dimensional facets (Figure 2) bounding the twin domain. The general objective is to reconcile both lateral and transverse views of IDs along twin boundaries. First, leveraging the previously developed automated EBSD microstructure analysis software (METIS), a series of EBSD maps were obtained in deformed pure titanium so as to gather statistically representative information as to the shape of twins as seen from a viewpoint normal to the coherent twin plane. Figure 3 shows a subset of an EBSD map. The study suggests that twins have low or limited line tension for propagating laterally [8]. In parallel to these findings, an experimental characterization campaign was conducted with the intent to non-destructively quantify the stress field within crystals containing twins. The work leveraged the facilities available at the Advanced Photon Source. An Mg AZ31 sample was loaded in-situ and the measurement successfully revealed both, stress and strain gradient variations across a twinned grain [9]. The work described above focused on capturing grain scale information about twin shapes and stress states in twinned domains, so as to provide valuable data sets for model validation.

Simultaneously, theoretical and computational work was conducted both at the atomistic length and at the single crystal length scales. First, atomistic simulations were performed to quantify the formation energy of interfacial defects present on (10-12) interfaces in pure Mg [10]. The simulations revealed the multiplicity of ID types and characters on twin interfaces. The original 2D study was then extended to three-dimensions. The work revealed the particular ease in nucleation of ID islands, referred to as terraced pop up events, on twin interfaces. Further, the

nature of the lack of temperature dependence associated with twin growth was rationalized on the basis of the low activation barrier for terrace pop-ups and of associated small activation volume (in the order of a few twinning dislocations Burgers vector magnitude). Finally, an existing Discrete Dislocation Dynamics (DDD) numerical framework was extended to introduce three main capabilities: (i) modeling the dynamics of disclinations, (ii) modeling lattice reorientation resulting from the motion of line defects, (iii) simulating deformation in polycrystalline samples by including the capability of treating material interface / bulk dislocation interactions. These developments are detailed in a series of submitted papers [11-13].

Future Plans

In the upcoming year, four connected research tasks will be emphasized. The generalized defect dynamics (GD^3) code previously developed will be exercised to reproduce the findings of the 3D atomistic simulations discussed in the above. Key here is to calibrate the rate of nucleation of twin islands and the mobility of interfacial defects in order to match atomistic simulations. Following this, GD^3 will be used to simulate the stress-driven growth of three-dimensional twin domains in polycrystals. The objective is to quantify the plastic dissipation occurring in the wake of twin domains as a function of pre-twinned microstructure. The intent is to establish a connection/rationalization of the experimental data gathered at the APS and discussed in the above. Clearly, these continuum level simulation need to address the fundamental question of bulk dislocation/ID interaction, which so far has not been explored.

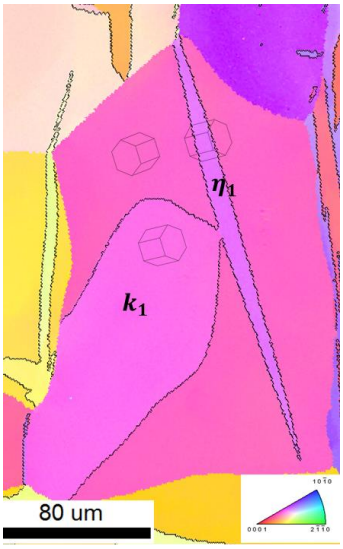

Figure 3: EBSD map of Ti revealing the qualitatively different shape of a twin section perpendicular to (η_1), and parallel to (k_1) the twinning plane.

To address these questions both in-situ and post-mortem TEM (HR) will be performed on pure titanium samples. Focus will be placed on the effect of bulk dislocations on twin growth and on the quantification of the strain field in the vicinity of twin boundaries. To this end, geometrical phase analysis will be employed. At the same scales, atomistic simulations will be conducted to quantify the formation energy and mobilities of IDs on the lateral side of the twin. This information will be passed onto GD^3. Further, fully three-dimensional domains –albeit of limited size- will be constructed within the context of atomistic simulations and their interactions with infinitely long dislocation segments will be simulated. The objective is to characterize both short-range interactions between ID and bulk dislocations as well as the contactless effects of dislocations on the growth of twin domains.

The last endeavor to be pursued aims at quantifying the three-dimensional geometry (i.e. shape, convexity, volume, thickness) and number densities of twins as a function of distinct features of the microstructure (e.g. grain orientation, grain size). To this end, sequential EBSD

mapping and serial sectioning will be performed on rolled titanium subjected to in plane compression loading. Further, METIS will be extended to generate a statistical description of twinned microstructure [9]. The data will be analyzed to extract potential correlations between microstructure and twinning. Further the dataset thus generated will be used as a benchmark to future GD^3 simulations of twin growth.

References

1- P.A. Juan, C. Pradalier, R.J. McCabe, L. Capolungo, "A graph theory based automated twin recognition technique for Electron Back-scatter Diffraction analysis", Modeling and Simulations in Materials Science and Engineering, submitted for publication

2- M. Arul Kumar, I.J. Beyerlein, R.J. McCabe, C.N. Tomé, "Grain neighbor effects on twin transmission in hexagonal close packed materials", Nature Communications 7:13826 (2016)

3- M. Arul Kumar, I.J. Beyerlein, C.N. Tomé, "A measure of plastic anisotropy for hexagonal close packed metals: application to alloying effects on the formability of Mg", J of Alloys and Compounds **695** (2017) 1488-97

4- M. Arul Kumar, I.J. Beyerlein, C.N. Tomé, "Effect of local stress fields on twin characteristics in HCP metals", Acta Materialia 116 (2016) 143-154

5- M. Arul Kumar, I.J. Beyerlein, C.N. Tomé, "Grain size constraints on twin expansion in hexagonal close packed crystals", J Applied Physics **120** (2016) 155105 1-11

6- J.P. Hirth, J. Wang, C.N. Tomé, "Disconnections and other defects associated with twin interfaces", Progress in Mats Science 80 (2016) 417-471

7- Y. Liu, N. Li, S. Shao, M. Gong, J. Wang, R.J. McCabe, Y. Jiang, C.N. Tomé, "Characterizing the boundary lateral to the shear direction of deformation twins in magnesium" Nature Communications 7,11577 (2016) 1-6

8- Y. Liu, N. Li, S. Shao, M.Y. Gong, J. Wang, R.J. McCabe, Y. Jiang, C.N. Tomé, "Characterizing the lateral twin boundary of {01-12} twins in magnesium", submitted for publication

9- M. Arul Kumar, R.J. McCabe, L. Capolungo, C.N. Tomé, "Study of 3D twin morphology in Ti via EBSD and serial sectioning", in preparation

10- E. Martínez, L. Capolungo, C.N. Tomé, "Atomistic analysis of the {01-12} twin stability and growth in α-Ti", in preparation

11- N. Bertin, L. Capolungo, "A FFT-based formulation for discrete dislocation dynamics in heterogeneous media", submitted for publication

12- N. Bertin, L. Capolungo, "On the effect of dislocation-twin boundary interactions: a study by discrete dislocation dynamics in FCC metals", submitted for publication

13- V. Taupin, L. Capolungo, "Generalized discrete defect dynamics ", in preparation

Publications FWP E401 supported by BES during 2016-2017

* H. Wang, Y. Jeong, B. Clausen, Y. Liu, R.J. Mccabe, F. Barlat, C.N. Tomé, "Effect of martensitic phase transformation on the behavior of 304 austenitic stainless steel under tension" Materials Science & Engineering A649 (2016) 174-183

* H.C. Wu, A. Kumar, J. Wang, X.F. Bi, C.N. Tomé, Z. Zhang, S.X. Mao, "Rolling-induced face centered cubic Ti in hexagonal close packed Ti at room temperature", Scientific Reports 6:24370 (2016)

* H. Wang, B. Clausen, L. Capolungo, I.J. Beyerlein, J. Wang, C.N. Tomé, "Stress and strain relaxation in Mg AZ31 rolled plate: in-situ neutron measurement and elastic viscoplastic polycrystal modeling", Intl J of Plasticity 79 (2016) 275-292

* Y. Liu, N. Li, S. Shao, M. Gong, J. Wang, R.J. McCabe, Y. Jiang, C.N. Tomé, "Characterizing the boundary lateral to the shear direction of deformation twins in magnesium" Nature Communications 7,11577 (2016) 1-6

* J.P. Hirth, J. Wang, C.N. Tomé, "Disconnections and other defects associated with twin interfaces", Progress in Mats Science 80 (2016) 417-471

* M. Arul Kumar, I.J. Beyerlein, C.N. Tomé, "Effect of local stress fields on twin characteristics in HCP metals", Acta Materialia 116 (2016) 143-154

* M. Arul Kumar, I.J. Beyerlein, C.N. Tomé, "Grain size constraints on twin expansion in hexagonal close packed crystals", J Applied Physics **120** (2016) 155105 1-11

* M. Arul Kumar, I.J. Beyerlein, R.J. McCabe, C.N. Tomé, "Grain neighbor effects on twin transmission in hexagonal close packed materials", Nature Communications 7:13826 (2016)

* M. Arul Kumar, I.J. Beyerlein, C.N. Tomé, "A measure of plastic anisotropy for hexagonal close packed metals: application to alloying effects on the formability of Mg", J of Alloys and Compounds **695** (2017) 1488-97

* H. Wang, L. Capolungo, B. Clausen, C.N. Tomé, "A crystal plasticity model based on transition state theory", Intl J of Plasticity **93** (2017) 251-268

* Y. Liu, N. Li, M. Arul Kumar, S. Pathak, J. Wang, R.J. McCabe, N.A. Mara, C.N. Tomé, "Experimentally quantifying critical stresses associated with basal slip and twinning in magnesium using micro-pillars", Acta Materialia 135 (2017) 411-421

* M. Arul Kumar, I.J. Beyerlein, R.A. Lebensohn, C.N. Tomé, "Modeling the effect of neighboring grains on twin growth in HCP polycrystals", Modeling and Sim in Mats Sc and Engineering 25 (2017) 064007 (25pp)

Chemomechanics of Far-From-Equilibrium Interfaces (COFFEI)

[1]Harry L. Tuller, [1]Yet-Ming Chiang, [1]Craig Carter, [1,3]Krystyn Van Vliet, [1,2]Bilge Yildiz, Departments of [1]Materials Science and Engineering, [2]Nuclear Science and Engineering, and [3]Biological Engineering, Massachusetts Institute of Technology

Program Scope

Brittle oxide functional materials, such as those utilized in solid oxide fuel cells, permeation membranes and lithium-ion batteries, exhibit significant operational stresses induced via chemical and electrochemical diffusion across material interfaces which can promote fracture, decrease charge capacity, and reduce SOFC energy conversion efficiencies. At the same time, certain types of highly defective ionic compounds can relieve stresses by defect redistribution, dislocation formation, or phase changes, and thereby tolerate larger deformations and/or induce enhanced charge and mass transport near interfaces. In this program we address these important issues by (*a*) applying advanced *in-situ* and *ex-situ* characterization tools to characterize model materials and interfaces synthesized with molecular-level control, under both laboratory-controlled and extreme environments representative of energy device operation; and (*b*) employing computational modeling and simulation frameworks to predict transport mechanisms, reactivity and stability of these model materials and interfaces under significant chemical, electrochemical and mechanical strains typical of energy device operation. The goals of this program are addressed in two inter-related thrusts. Thrust I focuses on chemomechanics due to cation transport and interactions with solid electrolytes in battery transition metal oxides, while Thrust II focuses on chemomechanics of anion transport at solid oxide fuel cell transition and rare earth metal oxides and interfaces.

Recent Progress

We established direct and fundamental correlations between fracture of active electrode ($Li_{1-y+x}Mn_{2-x}O_{4-\delta}$ or LMO cathode) particles and growth in the impedance of lithium ion batteries during electrochemical cycling, thereby providing a detailed understanding of electrochemical fatigue: the process by which various impedance contributions are affected by mechanical fracture under different electrochemical cycling conditions. We expanded this work to investigate the effect of fracture on lithium ion diffusion, to decouple transient and permanent impedance changes after electrochemically triggered fracture events, that can now be correlated with our predictive simulations.

Through one of several direct connections with Thrust II, we adapted density functional theory simulations developed for oxygen-ion conductors, to show that oxygen loss in both Li-excess and Li-stoichiometric forms of LMO can be expected to cause increased material volume, leading to irreversible changes in the stress state of LMO films during their first electrochemical charge-discharge cycle.

Using our analysis and a non-contact adaptation of dynamic chemical expansion measurement that we originally developed in Thrust II, we showed that stress within LMO cathode materials depends directly on charge rate or C-rate. Specifically, we showed that C-rate (voltage oscillation frequency) significantly modulates both the maximum stress experienced by LMO films during a single electrochemical cycle, and the degree to which asymmetry is apparent in the stress-voltage waveform.

We also measured the elastoplastic properties of Co- and Al- doped Li_XNiO_2 (NCA) cathode materials, and found that mechanical stiffness was significantly reduced by delithiation. This finding is consistent with our prior work in other lithium intercalating cathode materials, and suggests a general trend that can now be incorporated into our quantitative electrochemomechanical models of lithium ion batteries.

All-solid-state batteries include Li-ion conductive, solid electrolytes for which mechanical behavior is an important but less explored design constraint. We quantified the elastic, plastic, and fracture properties of the air-sensitive Li_2S-P_2S_5 (LPS) solid electrolyte, enabled by stabilization of the compounds with mineral oil within a specialized cell for instrumented nanoindentation. The extremely low stiffness (E < 20 GPa) and brittle (K_{Ic} < 0.25 MPa-m $^{1/2}$) behavior of this material suggests susceptibility to fracture and lithium dendrite penetration. These experiments and integrated computational models show that fracture resistance is now an important design criterion, in addition to conductivity, for electrolytes of all-solid-state batteries.

We conducted the first quantitative analysis of mechanical reliability of all-solid state batteries. We implemented a coupled electrochemomechanical model to quantify the key material properties that cause an electrolyte to fracture. In the numerical tests, fracture was suppressed when electrode particle volumetric expansion was <7.5% (typical for most Li-intercalating compounds) and the solid electrolyte fracture energy >4 J m^{-2}. Perhaps counterintuitively, and informed by our experiments on solid electrolytes such as LPS, the analyses show that compliant solid electrolytes are more prone to microcracking.

In a combined experimental and modeling approach, we showed that intentionally introduced dislocations in the model single crystalline $SrTiO_3$ system lead to a markedly lower (hole) electronic conductivity and oxygen diffusivity (approx. ~50 x and 1000 x, respectively, at 600 ^oC) compared to pristine specimens with few (experimental) or zero (computational) dislocations. Through this approach, we connected the depletion of majority charge carries (e.g. holes and oxygen vacancies) within the space charge regions surrounding dislocations to their positively charged cores, which we predicted from atomistic simulations earlier in this project. This has broad implications given the ability to tunable oxygen diffusion and electronic conduction over orders of magnitude without change in chemical composition.

We demonstrated and published the first concept of high temperature, low electrical bias oxide actuators using $Pr_{0.1}Ce_{0.9}O_{2-<>\delta}$ (PCO) as a model system for such actuation and for thin film solid oxide fuel cells (SOFC) At 650 °C, strain >0.1% could be achieved with electrical bias <0.1 V for, a far lower voltage than required in typical piezoelectrics for comparable strains at the same size scale. This study was enabled by the coincident development of a novel high temperature, displacement-sensing indenter method developed in this program, with nm-scale displacement detection up to 650 °C, and our fabrication of PCO films with integrated electrodes to "pump" oxygen vacancies while measuring PCO film displacement. We introduced *nanoscale electrochemomechanical spectroscopy* (NECS), and showed that these measurements give direct access to mechanical impedance spectra reminiscent of electrochemical impedance spectra, and by analysis to activation energies of key unit processes.

Using cross-sectional, aberration corrected transmission electron microscopy (ac-TEM) of PCO films grown on yttria-stabilized zirconia (YSZ) substrates, we designed and piloted experiments to show oxygen breathing of electrochemically pumped PCO films *in situ*.

We computed the biaxial elastic constant of bulk $Pr_xCe_{1-x}O_{2-\delta}$ (PCO) via density functional theory (also adapted for analysis of LMO in Thrust I), and showed that this stiffness decreases

with increased non-stoichiometry or oxygen vacancy concentration for both Pr-doped (x>0) and undoped (x=0) materials due to chemical expansion.

We have undertaken an analysis of vertically aligned nanostructures (VANs), which unlike conventional heterostructures, place the solid/solid interfaces in parallel with the ion transport path within a realistic SOFC geometry. Our Thrust I continuum mechanics modeling was applied in Thrust II to predict the stress state in alternating columns of PCO and $SrTiO_3$ (~80 nm wide), whereby the relatively inert $SrTiO_3$ is demonstrated to clamp the PCO, reducing its tendency to chemically expand. In order to experimentally evaluate the effect of this stress control on electrochemical properties, we are applying optical and electrical based techniques to characterize defect concentrations and transport.

Future Plans

We are completing two publications showing first full correlation between fracture and impedance growth in LMO in lithium ion batteries with liquid electrolytes. To expand on these findings for the next stage of research, we will expand our studies to include depth of discharge variations in addition to cycling rate variations; explore longer time scales to decouple transient effects from permanent fracture effects. Future results will also include time-domain diffusivity studies in addition to the high-frequency impedance techniques. We will continue and complete measurement of the mechanical behavior of NCA cathodes as a function of state-of-charge. Remaining tasks on this project include additional mechanical measurements and X-ray and microscope characterization.

As solid state electrolyte mechanical properties are key to solid state battery durability, safety, and also energy density as we recently showed, we will complete the first measurements of key elastoplastic mechanical properties of a wide range of solid electrolytes. We will build on our studies establishing mechanistic links between fracture and electrochemical impedance growth, by extending them to all-solid-state batteries. We will assemble solid-state battery cells and evaluate their fracture via in situ acoustic emissions and side-by-side electrochemical impedance spectroscopy. Next, insight from these studies as well as the solid electrolyte mechanical properties we measure will serve as input to the solid electrolyte finite element simulations we have developed over the past year. These simulations, in conjunction with our experimental *in situ* fracture and electrochemical fatigue testing, will facilitate our multi-scale microstructural understanding of all-solid-state battery degradation.

Via random walk analysis we are studying the effect of mechanical degradation on the transport properties of all-solid state electrodes. In our previous work we have shown that brittle electrolytes are prone to micro-cracking in response to intercalation-induced stresses. Because fracture causes discontinuities that block Li-ion transport, we quantify the loss in rate performance caused by mechanical damage. Our preliminary results show a linear correlation between fracture surface and the average diffusivity of Li within the electrode microstructure.

We are investigating the mechanical stability of interfaces in solid-state-electrode microstructures. Mechanical instability is characterized by a non-equilibrium transition from the coherent state to a fully delaminated interface. Contact at solid electrolyte-electrode interfaces, if not well preserved, may become the kinetic bottleneck to achieve high power density. We derive criteria for the design of composite electrodes resistant to sudden mechanical degradation. Our analyses lead to guidelines for the engineering of particle size, volume ratio of active material and the mechanical properties of electrolyte and interfaces.

A key limitation of the battery performance is the structural instability of the electrodes

with continuous usage, resulting in its failure. In a battery cycle the electrode microstructures typically operate in a two-phase window that comprises of a moving coherent interface. Theoretical studies indicate that a moving coherent interface causes anisotropic expansion of electrode and affects Li-ion kinetics. These factors affect battery performance, and motivates us to explore how interfaces form. The aim is to study the role of material crystallography in the formation of coherent interfaces in lithium ferrous phosphate (LFP) electrodes. In a typical LFP electrode, lithiated crystals with different orientations nucleate heterogeneously and little is known about how they interact to form coherent interfaces. In the present work, we apply a phase field crystal model to investigate the formation of coherent interfaces in LFP electrodes. These models offer the advantage of describing microstructures with atomic features, while solving diffusive time equations. The current work provides insights on how lithiated crystals interact with each other to form grain boundaries, and how lattices elastically relax during phase transformation. Overall, the model aims to serve as a design tool to chemically engineer material crystallography to tailor electrode properties.

To the maximum extent possible, computational models, data analytics, and experimental methods developed in Thrust I will be utilized also in Thrust II, as we have illustrated through specific examples in this current budget year.

Edge dislocations and threading dislocations will be modeled to understand the role of different dislocation core structures and different types of strain field on surface reactions. We will continue implementing the QM/MM technique with the software Lammps and Quantum espresso, to assess reaction kinetics at dislocations in and on oxides. We will generalize the protocol that we developed for CeO_2 to other oxide materials, including classical force field fitting, construction of extended defects and QM convergence test. We plan to use QM/MM technique model the surface reduction, oxidation, and CO, CO_2, H_2O adsorption, desorption and dissociation at the surface termination of dislocations in ceria.

Our simulations of the interfacial stresses in VANs have indicated that these composites may be less reducible and therefore less prone to the deleterious effect of chemical expansion. Future studies to experimentally investigate the lattice parameter change of VANs using high temperature XRD are underway. Additionally, electrochemical measurements are being performed to explore the role this stress plays on the oxygen reduction reaction. The in-plane multilayer samples represent an excellent model system to study the effects of interfaces on the defect concentration, conductivity, and chemical capacitance of mixed conductors. Experiments are continuing on this system using the *in situ* optical absorption, electrochemical pumping, and pO_2 dependent conductivity measurements discussed above.

Simultaneous use of optical and electrochemical characterization for studying nonstoichiometry and chemomechanics of thin films in situ under bias. This will be extended to aid in understanding the rate limiting processes active in electrode performance. Chemical capacitance is a useful technique for evaluating non-stoichiometry and defect chemistry of thin films. However in many perovskite materials of interest for SOFCs C_{chem} values may be affected by dominant interfacial contributions. Comparison of electrochemically measured C_{chem} in thin films of STF (e.g.) with that derived by electro-chemo-mechanical spectroscopy will enable us to separate bulk from interface effects and more comprehensively extend the C_{chem} technique to study thin film perovskite defect chemistry *in situ*.

Publications

1. Swallow, J.G.; Kim, J.J.; Bishop, S.R.; Smith, J.F.; Tuller, H.L.; and Van Vliet, K.J. *Elastoplastic properties of (Pr,Ce)$O_{2-\delta}$.* ECS Transactions. 68, 847-855 (2015).
2. Swallow, J.G.; Kim, J.J.; Chen, D.; Bishop, S.R.; Smith, J.F.; Tuller, H.L.; and VanVliet, K.J. *Quantifying chemical expansion of non-stoichiometric oxide thinfilms: Challenges and opportunities.* ECS Transactions. 68, 599-607 (2015).
3. Marrocchelli, D., Sun, L. & Yildiz, B. *Dislocations in $SrTiO_3$: Easy To Reduce but Not so Fast for Oxygen Transport*. J. Am. Chem. Soc. (2015). doi:10.1021/ja513176u.
4. Sun, L., Marrocchelli, D. & Yildiz, B. *Edge dislocation slows down oxide ion diffusion in doped CeO_2 by segregation of charged defects.* Nat Commun 6, (2015). doi:10.1038/ncomms7294.
5. P. Knauth, H. Saltsburg, J. Engel, H.L. Tuller, *In-Situ Dilatometric And Impedance Spectroscopic Study Of Core-Shell Like Structures: Insights Into The Exceptional Catalytic Activity Of Nanocrystalline Cu-Doped CeO_2,* J. Mat. Chem. A, **3**, 8369-8379 (2015). DOI: 10.1039/c4ta07181f.
6. Nicola H. Perry, Jaejin Kim, Sean R. Bishop, and Harry L. Tuller, *Strongly Coupled Thermal and Chemical Expansion in the Perovskite Oxide System Sr(Ti,Fe)$O_{3-\alpha}$,* J. Mat. Chem. A, **3** [7], 3602-3611 (2015). DOI: 10.1039/c4ta05247a
7. N. H. Perry, D. Pergolesi, S. R. Bishop, and H. L. Tuller, *Defect Chemistry and Surface Oxygen Exchange Kinetics of La-Doped Sr(Ti,Fe)$O_{3-\alpha}$ in Oxygen-Rich Atmospheres,* Solid State Ionics, **273**, 18-24 (2015).
8. J. J. Kim, D. Chen, S. R. Bishop, S. N. Cook and H. L. Tuller, *Mass Transport in Oxide Thin Films - Visualization and Control*, ECS Transactions 69, Symposium on Ionic Conducting Thin Films, 228th ECS Meeting, Phoenix AZ, Oct 11-16, 2015. ECS Trans. 69, [16] 3-10 (2015*).* doi: 10.1149/06916.0003ecst.
9. S. N. Cook and H. L. Tuller, *The Direct Measurement of Ionic Piezoresistance,* Symposium N, Frontiers in Complex Oxides, Chairs J.D. Baniecki, N.A. Benedek, G. Catalan, J.E. Spanier, MRS Symp. Proc. 1730, 7 pp., 2015. DOI: 10.1557/opl.2015.266.
10. W. Ma, J. J. Kim, N. Tsvetkov, Y. Kuru, Z. Cai; Y. Chen, H. L. Tuller; B. Yildiz, *Vertically Aligned Nanocomposite $La_{0.8}Sr_{0.2}CoO_3/(La_{0.5}Sr_{0.5})_2CoO_4$ Cathodes – Electronic Structure, Surface Chemistry and Oxygen Reduction Kinetics,* J Mat. Chem. A, **3 [1]**, 207-219 (2015). **DOI:** 10.1039/C4TA04993D.
11. N. H. Perry, D. Pergolesi, S. R. Bishop, and H. L. Tuller, *Defect Chemistry and Surface Oxygen Exchange Kinetics of La-Doped Sr(Ti,Fe)$O_{3-\alpha}$ in Oxygen-Rich Atmospheres,* Solid State Ionics, **273**, 18-24 (2015). http://dx.doi.org/10.1016/j.ssi.2014.09.013.
12. G. Bucci, Y.-M. Chiang, and W.C. Carter. *Formulation of the coupled electrochemical-mechanical boundary-value problem, with applications to transport of multiple charged species.* Acta Materialia, 62:33-51, 2016.
13. Swallow, J.G.; Kim, J.J.; Kabir, M.; Smith, J.F.; Tuller, H.L.; Bishop, S.R.; and Van Vliet, K.J. *Operando reduction of elastic modulus in (Pr, Ce)$O_{2-\delta}$ thin films.* Acta Materialia. 105, 16-24 (2016).

14. McGrogan, F.P., Chiang, Y.-M., and Van Vliet, K.J. *Effect of Transition Metal Substitution on Elastoplastic Properties of $LiMn_2O_4$ Spinel*. *J. Electroceram.*, (in press, 2016).
15. Metlenko, V., Jung, W.-C., Bishop, S.R., Tuller, H.L., De Souza, R.A., *Oxygen Diffusion and Surface Exchange in the Mixed Conducting Oxides $SrTi_{1-y}Fe_yO_{3-\delta}$*, Phys.Chem.Chem.Phys., 18, 29495-29505 (2016) DOI: 10.1039/c6cp05756j
16. Swallow, J.G., Kim, J.J., Kabir, M., Smith, J.F., Tuller, H.L., Bishop, S.R., and Van Vliet, K.J., *Operando Reduction Of Elastic Modulus In (Pr, Ce)$O_{2-\delta}$ Thin Films*, Acta Mater. 105, 16-24 (2016), doi:10.1016/j.actamat.2015.12.007
17. Sheth, J., Chen, D., Bowman, W.J., Crozier, P., Tuller, H.L., Misture, S.T., Zdzieszynski, S., Sheldon, B.W., Bishop, S.R., *Coupling Of Strain, Stress, And Oxygen Non-Stoichiometry In Thin Film $Pr_{0.1}Ce_{0.9}O_{2-\delta}$*, Nanoscale 8, 16499 – 16510 (2016). DOI: 10.1039/C6NR04083G (BES support; I2CNER & Progress 100)
18. Knauth, P., Harrington, G., Bishop, S.R., Saltsburg, H., Tuller, H.L., *CeO_2 Nano-Rods and-Nanocubes: Impact of Nanoparticle Shape on Dilatometry and Electrical Properties*, J. Am. Ceram. Soc, 99 [7], 2415–2421 (2016), DOI: 10.1111/jace.14257
19. Bucci, G., Swamy, T., Bishop, S.R., Sheldon, B.W., Chiang, Y.-M., and Carter, W.C., *The Effect Of Stress On Battery-Electrode Capacity*, J. Electrochem. Soc. 2017 volume 164, issue 4, A645-A654
20. Adepalli, K.K., Yang, J., Maier, J., Tuller, H.L., and Yildiz, B., *Tunable Oxygen Diffusion and Electronic Conduction in SrTiO3 by Dislocation-Induced Space Charge Fields*, Advanced Functional Materials, DOI: 10.1002/adfm.201700243 (2017).
21. Bucci, G., and Carter, W.C., Mechanics of Materials. Micro-mechanics in electrochemical systems (book chapter, ready for production). Springer, 2017
22. McGrogan, F.P., Swamy, T., Bishop, S.R., Eggleton, E., Porz, L., Chen, X., Chiang, Y.-M., and Van Vliet, K. J. *Compliant yet Brittle Mechanical Behavior of Li_2S-P_2S_5 Lithium-Ion Conducting Solid Electrolyte*. Adv. Energy Mater., 1602011, 2017.
23. Swallow, J.G., Kim, J.J., Maloney, J.M., Chen, D. Smith, J.F., Bishop, S.R., Tuller, H.L., and Van Vliet, K.J. Dynamic chemical expansion of thin-film non-stoichiometric oxides at extreme temperatures. *Nature Materials* (2017 online and DOI: 10.1038/nmat4898).
24. Tuller, H.L., ***Solar to Fuels Conversion Technologies – A** Perspective*, Mater Renew Sustain Energy 6:3 (2017), 16 pgs. DOI 10.1007/s40243-017-0088-2
25. Kim, J.J., Bishop, S.R., Chen, D., and Tuller, H.L., *Defect Chemistry of Pr Doped Ceria Thin Films Investigated by in Situ Optical and Impedance Measurements*, Chem. Mat. 29 [5] 1999-2007 (2017)
26. Perry, N., Harrington, G., Tuller, H.L., *Ionic Conductors: Electrochemical Ionic Interfaces, Invited Chapter in* Metal Oxide-based Thin Film Structures: Formation, Characterization and Application of Interface-based Phenomena, Editors N. Pryds and V. Esposito, Elsevier Publ, 2017, in press.
27. Sheth, J., Chen, D., Tuller, H.L., Misture, S.T, Bishop, S.R., Sheldon, B., *Role of Grain Size in Redox Induced Compositional Stress in Pr Doped Ceria Thin Films*, Phys. Chem. Chem. Phys., DOI 10.1039/C7CP00088J

The Relationship Between Defect Kinetics and Crystalline Disorder

Blas Pedro Uberuaga, Los Alamos National Laboratory

Program Scope

Understanding mass transport in materials is critical for understanding, predicting and designing materials for future applications. In particular, complex oxides such as pyrochlores and spinels have application in nuclear energy systems, as fuel cell and battery materials, and as armor materials. In these applications, mass transport is often a key factor enabling performance. However, in these materials, given their chemical complexity, the kinetics of transport is very sensitive to the detailed chemical arrangement of cations. Thus, crystalline disorder, typified by mixing of cations, can dramatically alter mass transport and thus performance, motivating significant research into the structure-property relationship between crystal chemistry and atomic kinetics. However, there are still many unresolved questions. For example, in pyrochlores, reports find enhanced ionic conductivity in either ordered [1] or disordered materials [2]. In this program, we use irradiation to controllably induce cation disorder in the material to identify the precise relationship between the distribution of cations and the kinetics of atoms. These experiments are complemented by state-of-the-art atomistic modeling such as accelerated molecular dynamics to understand the fundamental relationship between cation structure and atomic dynamics in complex oxides.

Recent Progress

Over the last two years, we have focused on two themes: (1) understanding the relationship between crystal structure, crystal chemistry, and the response to radiation and (2) examining the impact of site disorder (mixing of cations) on both cation and anion transport in complex oxides. Much of our work has used pyrochlore ($A_2B_2O_7$) as a model material, both because of its history in radiation studies and its relevance to nuclear energy and as a fast ion conductor. However, we have also examined the behavior of another important engineering ceramic, spinel (AB_2O_4). Our efforts have led to new insight into how crystal structure and chemistry impact the radiation damage evolution in complex oxides.

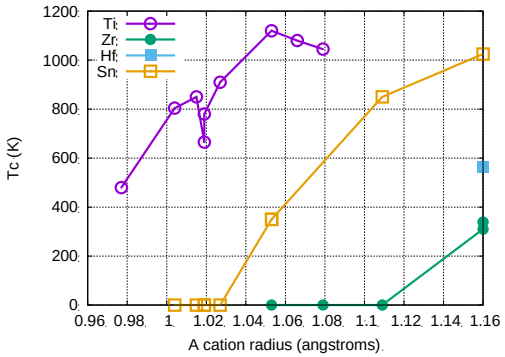

Figure 1. Experimentally measured critical temperature to amorphize as a function of pyrochlore chemistry.

The relationship between crystal structure, crystal chemistry, and radiation tolerance

There is a long history studying the response of complex oxides to irradiation with the goal of identifying factors that dictate the irradiation response of these materials. In perhaps the most systematically studied complex oxides – pyrochlores – various groups have examined the amorphization susceptibility as a function of chemistry and have found great variability in the

ability of the pyrochlore to withstand irradiation as a function of both the A and B cation [3]. This behavior is summarized in Figure 1. At the same time, groups have identified factors that govern this behavior, including the ability of the material to accommodate disorder [4], ionic radius and electronegativity [5], and the enthalpy of formation of the compound [6]. In our recent work, we have added to this understanding by examining the same relationships in another compound – spinel – and by applying machine learning (ML) modeling approaches to identify factors that best correlate with amorphization resistance.

In work published in *Nature Communications* [7], we have performed irradiations in three Mg-bearing spinels, $MgAl_2O_4$, $MgGa_2O_4$, and $MgIn_2O_4$, and compared the relative susceptibility for amorphization in these three materials. Just as for pyrochlores, we observe a systematic dependence on irradiation response with chemistry. However, when we calculate the energy to disorder these compounds with density functional theory (DFT), we found that the compound that is most resistance to amorphization is the one that is hardest to disorder. This was a surprise, as this is the opposite correlation observed for pyrochlores (Figure 2). Temperature accelerated dynamics simulations reveal that the fundamental difference between pyrochlores and spinels resides in the structural cation vacancies in spinel. These provide an efficient relaxation mechanism for damage that does not intrinsically exist in pyrochlore, as pyrochlore does not contain structural cation vacancies.

Thus, as for pyrochlores, we correlated the response of spinels with the energy to disorder the cations. However, in the case of pyrochlores, this correlation is incomplete. Compounds with a high energy to disorder (B=Sn) can exhibit higher radiation tolerance than those with a lower energy to disorder (B=Ti). In work published in *Chemistry of Materials* [3], we used machine learning to quantify the ability of different properties to correlate with radiation resistance. When we apply machine learning techniques to the B=Ti compounds, we find that those compounds that are most resistant minimize the energy to disorder but maximize the energy to amorphize.

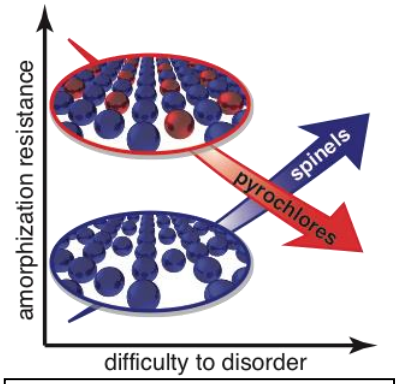

Figure 2. Dependence of amorphization resistance in spinels vs pyrochlores as determined from experiment and modeling.

The impact of site disorder on transport

The efforts described above focus on the basic response of complex oxides to irradiation, developing correlations between basic material properties and radiation tolerance. However, more fundamental laws would require knowing how defect transport is impacted by the changes in material structure induced by irradiation. To that end, we are using simulation and experiment to interrogate how cation disorder impacts mass transport.

First, we have irradiated thin films of pyrochlore with various fluences of low energy He ions to gradually induce disorder. To do this, we have grown the first thin film of a rare-earth

pyrochlore, using magnetron sputtering. Using grazing incidence x-ray diffraction, we characterized the change in cation disorder with fluence. Using AC impedance spectroscopy, we measured the change in ionic conductivity with fluence. Combining these two measurements, we arrive at the results presented in Figure 3, which show how the ionic conductivity changes with cation disorder. We first note a sharp increase in conductivity with only a small amount of cation disorder. The conductivity then plateaus over a wide range of cation disorder before it once again rises at high levels of disorder, corresponding to when the film begins to amorphize. These results show conclusively that cation disorder increases ionic conductivity in this system.

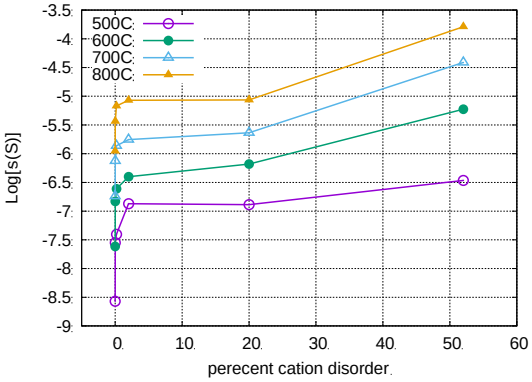

Figure 3. Dependence of ionic conductivity on cation disorder as induced by He irradiation in $Gd_2Ti_2O_7$ thin films.

In parallel, we have been applying accelerated molecular dynamics simulations to study cation transport in disordered pyrochlore. In these simulations, we introduce one cation vacancy into simulation cells with varying degrees of disorder. We found that the overall diffusivity of cations is non-linear with disorder, with an initial regime that is insensitive to the level of disorder. In fact, as shown in Figure 4, it is only when about 25% cation disorder is introduced that the cation diffusivity increases. This suggests that cation transport is dictated by the formation of a percolation network of disorder. Indeed, further analysis shows that cation vacancies (a) prefer disordered regions of the material, (b) hop faster when they are in those regions, and (c) do experience a connected network of disorder at disorder levels of about 25%. This has implications for the relationship between cation disorder, cation transport, and the response to irradiation. These results were recently accepted for publication in *Nature Communications* [8].

Future Plans

Our ongoing and future work can be summarized in three Focus Areas:

- Focus Area 1: Cation diffusion in chemically complex pyrochlores
- Focus Area 2: Interplay between grain boundaries and disorder
- Focus Area 3: Percolation networks and conductivity

These Focus Areas grow directly out of our recent results. We have already seen that cation disorder dramatically changes ionic conductivity in pyrochlore. Most past studies have induced cation disorder by mixing multiple A or B cations into the material. We expect that these more chemically complex systems exhibit their own surprises in terms of ionic conductivity. To understand these systems, we are using both modeling and experiment to understand the structure and kinetics associated with these more complex systems.

Further, we have recently shown how microstructural features such as surfaces [9] and grain boundaries [10] can change the local level of disorder and thus the mass transport characteristics of the system. Our future work involves examining this behavior in more detail. In particular, we hypothesize that, under irradiation, disorder will preferentially occur at grain boundaries and thus these will act as fast diffusion pathways for oxygen. This offers a novel route to engineering materials for fast ion conductor applications.

Finally, we have already seen how percolation networks in disorder can lead to enhanced cation transport [8]. However, percolation networks can occur at various length scales. In the work discussed above, a percolation network was formed on the atomic scale. In complex pyrochlores with multiple A or B cations, literature results have found that two-phase structures can form on larger length scales [11,12]. We hypothesize that the transport of mass can be sensitively controlled by controlling this phase microstructure.

Most of our work has focused on pyrochlores. More recently, however, in collaboration with CASL – The Consortium for Advanced Simulation of Light Water Reactors – we have begun studying the properties of Ni-bearing spinels (AB_2O_4) that form when steel components in nuclear reactors corrode. Depending on the chemistry of the spinel, they can be either ordered (normal) or disordered (random or inverse). Mass transport in these spinels dictate the release of species that ultimately deposit as CRUD on the fuel rods. The same considerations that dictate mass transport in pyrochlore is relevant for these spinels. We are helping develop physical models of species release from spinels to inform the source term for CRUD formation.

References

[1] K. J. Moreno, et al., *Physical Review B* **75**, 184303 (2007).
[2] H. Tuller. *J. Phys. Chem.* Solids **55**, 1393 (1994).
[3] G. Pilania, et al., *Chemistry of Materials* **29**, 2574 (2017).
[4] K. E. Sickafus, et al., *Science* **4**, 748 (2000).
[5] G. R. Lumpkin, et al., *Journal of Solid State Chemistry* **180**, 1512 (2007).
[6] K. B. Helean, et al., *MRS Proceedings* **824**, 22 (2004).
[7] B. P. Uberuaga, et al., *Nature Communications* **6**, 8750 (2015).
[8] R. Perriot, et al., *Nature Communications*, in press.
[9] J. Wen, et al., *Acta Materialia* **110**, 175 (2016).
[10] R. Perriot, et al., *Nanoscale* **9**, 6826 (2017).
[11] K. R. Whittle, et al., *Journal of Solid State Chemistry* **182**, 442 (2009).
[12] M. P. van Dijk, et al., *Journal of Solid State Chemistry* **62**, 377 (1986).

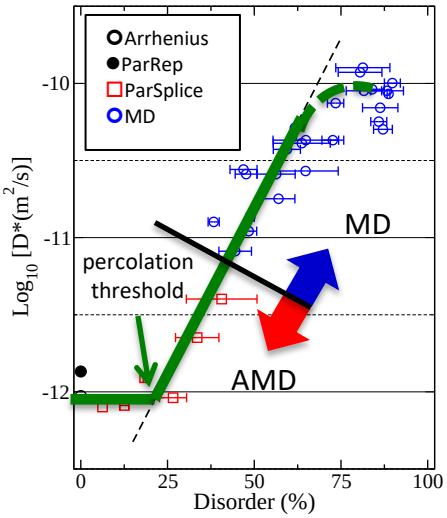

Figure 4. Dependence of cation diffusion on cation disorder in $Gd_2Ti_2O_7$ as determined from conventional and accelerated molecular dynamics simulations.

Publications

Intellectually led by this FWP

2017

1. CR Kreller, R Mukundan, EL Brosha, T Williamson, JA Valdez, TG Holesinger, Y-Q Wang, and BP Uberuaga, Characterization of $Gd_2Ti_2O_7$ thin films deposited using RF magnetron sputtering, submitted to *Solid State Ionics*. http://arxiv.org/abs/1608.00081
2. R Perriot, PP Dholabhai, and BP Uberuaga, Disorder-induced transition from grain boundary to bulk dominated ionic diffusion in pyrochlores, *Nanoscale* **9**, 6826 (2017).
3. R Perriot, BP Uberuaga, RJ Zamora, D Perez, and AF Voter, Evidence for Percolation diffusion of cations and material recovery in disordered pyrochlore from accelerated molecular dynamics simulations, *Nature Communications*, in press.
4. G Pilania, KR Whittle, C Jiang, RW Grimes, CR Stanek, KE Sickafus, BP Uberuaga, Using machine learning to identify factors that govern amorphization of irradiated pyrochlores, *Chemistry of Materials* **29**, 2574 (2017).

2016

5. PP Dholabhai, R Perriot, and BP Uberuaga, Atomic-scale Structure and Stability of the Low-index Surfaces of Pyrochlore Oxides, *Journal of Physical Chemistry C* **120**, 10485 (2016).
6. MM Hasan, PP Dholabhai, RHR Castro, BP Uberuaga, Stabilization of $MgAl_2O_4$ spinel surfaces via doping, *Surface Science* **649**, 138 (2016).
7. R Perriot, PP Dholabhai, and BP Uberuaga, The Role of Surfaces, Chemical Interfaces, and Disorder on Plutonium Incorporation in Pyrochlores, *Physical Chemistry Chemical Physics* **18**, 22852 (2016).
8. M Tang, JA Valdez, J Zhang, YQ Wang, BP Uberuaga, and KE Sickafus, Ion irradiation-induced phase transformations in fully inverse spinel $MgIn_2O_4$, *Scripta Materialia* **125**, 10 (2016).
9. RJ Zamora, AF Voter, D Perez, R Perriot, and BP Uberuaga, The effects of cation-anion clustering on defect migration in $MgAl_2O_4$, *Physical Chemistry Chemical Physics* **18**, 19647 (2016).
10. BP Uberuaga, Complex oxides: Intricate disorder, *Nature Materials* **15**, 496-497 (2016).

2015

11. R Perriot and BP Uberuaga, Structural vs. intrinsic carriers: contrasting effects of cation chemistry and disorder on ionic conductivity in pyrochlores, *Journal of Materials Chemistry A* **3**, 11554 (2015).

Collaborative publications

2017

1. L. Bayerjargal, W. Morgenroth, N. Schrodt, B. Winkler, V. Milman, C. R. Stanek, and B. P. Uberuaga, Synthesis of Hf_8O_7, a new binary hafnium oxide, at high pressures and high temperatures, *High Pressure Research* **37**, 147 (2017).
2. MM Hasan, PP Dholabhai, S Dey, BP Uberuaga, and RHR Castro, Reduced grain boundary energies in rare-earth doped $MgAl_2O_4$ spinel and consequent grain growth inhibition, *Journal of the European Ceramic Society* **37**, 4043 (2017).
3. L Wu, PP Dholabhai, TG Holesinger, BP Uberuaga, RHR Castro, Temperature dependent discontinuity in the stability of manganese doped ceria nanocrystals, *Crystal Growth and Design* **17**, 446 (2017).

2016

4. JA Aguiar, S Wozny, TG Holesinger, T Aoki, MK Patel, M Yang, JJ Berry, M Al-Jassim, W Zhou, K Zhu, In situ investigation on the formation and metastability of formamidinium lead tri-iodide perovskite solar cells, *Energy & Environmental Science* **9**, 2372 (2016).
5. JA Aguiar, S Wozny, NR Alkurd, M Yang, L Kovarik, TG Holesinger, M Al-Jassim, K Zhu, W Zhou, JJ Berry, Effect of Water Vapor, Temperature, and Rapid Annealing on Formamidinium Lead Triiodide Perovskite Crystallization, *ACS Energy Letters* **1**, 155 (2016).
6. S Dey, J Mardinly, YQ Wang, JA Valdez, TG Holesinger, BP Uberuaga, JJ Ditto, JW Drazin, RHR Castro, Irradiation-induced grain growth and defect evolution in nanocrystalline zirconia with doped grain boundaries, *Physical Chemistry Chemical Physics* **18**, 16921 (2016).
7. MM Hasan, S Dey, N Nafzin, J Mardinly, PP Dholabhai, BP Uberuaga, RHR Castro, Improving the Thermodynamic Stability of Aluminate Spinel Nanoparticles with Rare Earths, *Chemistry of Materials* **28**, 5163 (2016).
8. C Jiang and BP Uberuaga, Efficient Ab initio Modeling of Random Multicomponent Alloys, *Physical Review Letters* **116**, 105501 (2016).
9. G Pilania, A Mannodi-Kanakkithodi, BP Uberuaga, R Ramprasad, JE Gubernitis, and T Lookman, Machine learning bandgaps of double perovskites, *Scientific Reports* **6**, 19375 (2016).
10. J Wen, C Sun, PP Dholabhai, Y Xia, D Chen, M Tang, D Yang, YH Li, BP Uberuaga, and YQ Wang, Temperature dependence on the radiation tolerance of nanocrystalline pyrochlores, *Acta Materialia* **110**, 175 (2016).
11. (invited) RJ Zamora, BP Uberuaga, D Perez, and AF Voter, The Modern Temperature Accelerated Dynamics Approach, *Annual Review of Chemical and Biomolecular Engineering* **7**, 87 (2016), DOI: 10.1146/annurev-chembioeng-080615-033608.

2015

12. J Wen, YH Li, M Tang, JA Valdez, YQ Wang, M Patel, and KE Sickafus, Heavy and light ion irradiation damage effects in □-phase $Sc_4Hf_3O_{12}$, *Nuclear Instruments and*

Methods in Physics Research Section B **365**, 325 (2015), DOI: 10.1016/j.nimb.2015.04.011.
13. L Wu, JA Aguiar, PP Dholabhai, T Holesiger, T Aoki, BP Uberuaga, and RHR Castro, Interface Energies of Nanocrystalline Doped-Ceria: Effects of Manganese Segregation, *Journal of Physical Chemistry C* **119**, 27855 (2015).
14. SK Yadav, BP Uberuaga, M Nikl, C Jiang, and CR Stanek, Band-gap and band-edge engineering of multicomponent garnet scintillators: a first-principles study, *Physical Review Applied* **4**, 054012 (2015).

Atomistic study of plastic deformation of transition metals and their alloys including high entropy alloys

V. Vitek

Department of Materials Science and Engineering, University of Pennsylvania, Philadelphia, PA 19104

Program Scope

The major goal of this research is to enrich and put on a firm physical basis our understanding of mechanical properties of refractory metals (V, Nb, Ta, Cr, Mo, W) and Fe, as well as the alloys comprised from these metals, including compositionally complex alloys (also called high entropy alloys, HEAs). The common physical characteristic of these materials is that they all crystalize in the body-centered cubic (bcc) structure and their atomic bonding is mixed, nearly free electron and covalent. In the case of Fe the ferromagnetism plays a major role since it stabilizes the bcc structure.

½ <111> screw dislocations, owing to the non-planarity of their cores [1] govern the plastic deformation of all these materials. Consequently, the center theme of this research program is computer modeling of the structure and behavior of ½<111> screw dislocations in the above bcc metallic materials. The fundamental precursor for such studies is a description of atomic interactions that allows for the use in modeling atomic blocks composed of thousands of particles in pure metals and even millions in the case of alloys. This cannot be realized using the density-functional theory (DFT) and for this reason one of the major objectives of our research has been advancement of interatomic potentials that reflect correctly the basic quantum mechanical aspects of bonding and in the case of Fe also magnetism. This has been attained by developing the bond order potentials (BOPs) with d-band mediated bonding. In this scheme the cohesive energy is

$$E^{coh} = E^{cov} + E^{rep} + E^{mag}.$$

The covalent energy, E^{cov}, arising from the partially filled d band is

$$E^{cov} = \sum_{\sigma=\uparrow,\downarrow} \sum_{i,\alpha} \sum_{i \neq j,\beta} \rho^{\sigma}_{i\alpha,j\beta} H^{\sigma}_{j\beta,i\alpha},$$

where $r^{s}_{ia,jb}$ is the density matrix element for the bond between the orbital α at atom i and the orbital β at atom j and $H^{s}_{jb,ia}$ is the corresponding element of the Hamiltonian matrix; σ represents the two possible spin states. Hamiltonian elements are expressed via bond angles and corresponding bond integrals (BIs). E^{mag} is treated within the Stoner model of the itinerant magnetism and the repulsive part, E^{rep}, is formulated empirically such that the resulting BOP reproduces exactly the experimental values of the lattice constant, cohesive energy and three elastic constants. The potentials were thoroughly tested by comparing a variety of results with either experiments or DFT calculations.

Using the developed BOPs the structure of the cores of ½<111> screw dislocations and their transformations under the applied stress have been studied and the results published in a number of papers during this supported research, e.g. [2-9]. Presently we have been using the BOPs to investigate and decipher the physical reason for the anomalous slip in bcc refractory metals and to develop EAM potentials for study of structurally complex alloys (HEAs), which replicate the most significant aspects of dislocation cores revealed by BOPs. This development is described in the sections on recent progress and future plans.

Recent Progress

1. Bond order potentials

In BOPs only the bonding mediated by the d electrons is included explicitly. However, we have shown recently that the effect of s electrons with orbitals centered on atoms neighboring the corresponding dd bond is not negligible [8]. This effect has been emulated by the screening of corresponding dd bond integrals and it was found that the impact of screening is most significant when the distortion of the local atomic environment is inhomogeneous, such as in the case of phonons, point defects and dislocation cores. As an example phonon spectra calculated for Mo with and without screened bond integrals are compared in Fig. 1. Near the symmetry point *N*, the phonon frequency drops abruptly when screening is not employed, which indicates a possible instability. Along the [111] H-P-Γ cross section experiments show that the frequency of the L mode is considerably lower than that of the T mode. This is very well reproduced by BOPs with screened bond integrals but not without screening.

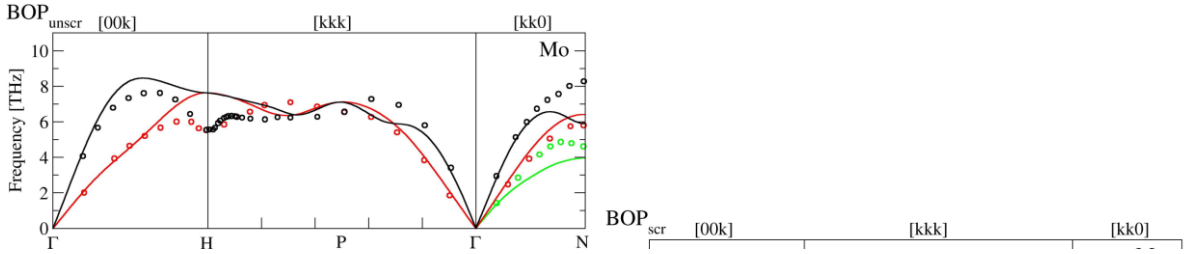

Fig. 1. Phonon dispersion curves for Mo. Lines: Calculations without screening right and with screening left. Dots: Experimental data. Different colors correspond to different vibrational modes; black longitudinal modes (L), red transversal modes (T or T1), green transversal mode T2.

In the case of Fe the same type of screening of bond integrals was introduced and the corresponding BOP is of the same quality as for the non-magnetic transition metals [9]. As an example, Fig. 2 shows the calculated phonon dispersion curves for Fe compared with relevant experimental data. Clearly the agreement is outstanding.

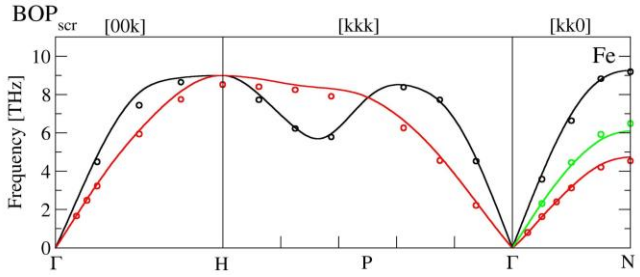

Fig. 2. Phonon dispersion curves for bcc ferromagnetic Fe. The notation is the same as in Fig. 1.

As in any available DFT calculations, the structure of the cores of ½[111] screw dislocations was found to be non-planar with non-degenerate symmetry (invariant with respect to the [111] three-fold screw axis and $[\bar{1}01]$ diad). The slip planes vary from material to material for a given loading and this variation depends on whether screening of bond integrals is or is not included. Moreover, the slip plane, while always of the {101} type, may not be the plane with the maximum resolved shear stress (MRSSP). This may be significant for explanation of the so-called anomalous slip discussed below.

2. Anomalous slip in transition bcc metals

The anomalous slip refers to the very localized deformation at cryogenic temperatures that occurs on the slip systems with Schmid factors much lower than several other available slip systems, in particular the most highly stressed <111>{101} system. As mentioned above, atomistic studies of the

glide of ½<111> screw dislocations show that these often glide on planes other than the MRSSP. While this is suggestive of the anomalous slip, the glide of individual screw dislocations does not explain this phenomenon. However, the explanation may be sought in combined glide of two distinct but similarly loaded ½<111> screw dislocations on a common slip plane. For tension/compression with the loading axes within the standard triangle (corners [001, $[\bar{1}11]$ and [011]) the two systems with the highest Schmid factors are $[111](\bar{1}01)$ and $[\bar{1}11](\bar{1}0\bar{1})$. Hence, upon loading the screw dislocations with Burgers vectors ½[111] and ½$[\bar{1}11]$will be generated on the $(\bar{1}01)$ and $(\bar{1}0\bar{1})$ planes, respectively, with about the same frequency. If both ½[111] and ½$[\bar{1}11]$ move in their common slip plane $(0\bar{1}1)$, the 'anomalous' slip occurs. We conjecture that whether the glide of both these screw dislocations continues on the corresponding most highly stressed {101} planes or whether both ½[111] and ½$[\bar{1}11]$ dislocations move in the $(0\bar{1}1)$ plane depends on the relative magnitudes of the activation enthalpies for the two processes. Since the glide of screw dislocations takes place via formation and propagation of pairs of kinks, corresponding activation enthalpies have been calculated using the modified nudged elastic band method developed in our earlier studies [10]. As an example we show here the results for Nb and Fe loaded in tension along the $[\bar{2}38]$ when the MRSSP for the ½[111] dislocation is $(\bar{1}01)$. The applied tensile stress corresponds to 0.75 of the load at which the dislocation moves at 0K.

In Nb the calculated ratio of activation enthalpies for the glide of the ½[111] dislocation on the $(0\bar{1}1)$ and $(\bar{1}01)$ plane is 0.84 and for the glide of the ½$[\bar{1}11]$dislocation on the $(0\bar{1}1)$ and $(\bar{1}0\bar{1})$ 0.92. This implies that in tension the anomalous slip should always occur. In Fe the calculated ratio of activation enthalpies for the glide of the ½[111] dislocation on the $(0\bar{1}1)$ and $(\bar{1}01)$ plane is 2.06 and for the glide of the ½$[\bar{1}11]$dislocation on the $(0\bar{1}1)$ and $(\bar{1}0\bar{1})$ 1.14. Hence, it is unlikely that ½[111] and ½$[\bar{1}11]$dislocations will move simultaneously on the $(0\bar{1}1)$ plane and thus the anomalous slip is improbable. Experimentally, the anomalous slip dominates at low temperatures in Nb while no such slip has been observed in Fe. Hence, this preliminary study suggests that the approach, in which the atomic level aspects of the glide of two different screw dislocations are included, is the way to explain the long lasting mystery of the anomalous slip. This study is now in progress for all refractory bcc metals and different orientations of tensile/compressive loading.

3. Dislocations and their glide in bcc compositionally complex alloys (HEAs)

The bcc HEAs are usually composed of refractory metals and the alloys studied experimentally most recently were $Nb_{25}Mo_{25}Ta_{25}W_{25}$ and $V_{20}Nb_{20}Mo_{20}Ta_{20}W_{20}$ [11,12]. In principal, dislocations in these alloys might be studied using the developed BOPs. However, the essential difference between HEAs and single element metals is that the distribution of their components is random and to consider this randomness appropriately the block of atoms used in any atomistic modeling must be very significantly larger than in the case of a single element. Thus, in the case of dislocations in single element crystals the periodicity along the dislocation line is commonly identified with the corresponding crystal period. While a periodicity along the dislocation will have to be introduced for numerical reasons even in the case of HEAs, it has to be large enough so that it does not affect significantly the dislocation behavior. Hence, while when studying ½<111> screw dislocations in single element crystals the total number of atoms in the block is sufficient to be of one or a few thousands, in the case of HEAs it may be needed to attain or exceed a million. Such calculations are obviously not feasible using DFT but even with BOPs could only be made using biggest available supercomputers. Hence, EAM type potentials were used in the only recent study of dislocations in bcc HEAs [13]. However, the EAM potentials usually lead to the degenerate (not invariant with respect to

the [$\bar{1}$01] diad) core of ½<111> screw dislocations, which is the case in [13]. But it is reasonable to assume that in HEAs made of refractory metals the average core structure will be non-degenerate as in elemental refractory metals. This is a very important aspect of the dislocation core since the degenerate and non-degenerate cores may lead to very different slip behavior.

Nevertheless, realistic modeling of dislocations in HEAs can at present be done only with relatively simple potentials such as EAM. For this reason we have advanced new EAM potentials for the refractory bcc metals for which the cores of ½<111> screw dislocations are non-degenerate and thus it is very likely that the cores of these dislocations in the corresponding HEAs will posses, on average, the same symmetry. Using these potentials the ½<111> screw dislocations and their glide are being studied for $Nb_{25}Mo_{25}Ta_{25}W_{25}$ and $V_{20}Nb_{20}Mo_{20}Ta_{20}W_{20}$ alloys.

Future plans

Our future research will be based on the developments summarized in the section on Recent Progress. The dislocations studies made using the BOPs [2,4-9] will be employed in advancing a minimal continuum dislocation dynamics model for slip in bcc metals that accounts explicitly for non-Schmid behavior of screw dislocations in these materials. In this model the dislocation substructure is represented by continuum distribution of ½<111> screw dislocations moving on their possible {101} slip planes according to the flow rule that describes the response of isolated screw dislocations to external loads. The goal is to show that the non-Schmid behavior persists to the continuum level.

The study of the anomalous slip will proceed to include all the refractory metals for which BOPs have been developed and for several different orientations of the tension/compression loading axes within the standard triangle. The goal of this research is to explain fully the anomalous slip observed at low temperatures in group V refractory metals, as well as the lack of this slip in group VI and Fe.

Using the newly developed EAM potentials for refractory bcc metals, which assure the non-degenerate cores of screw dislocations, the structure and glide of ½<111> screw dislocations in bcc HEAs will be modeled. The goal is to find the principal physical differences in deformation between bcc single elements and HEAs composed from these elements.

Finally, we will continue our collaboration with ICAMS at the Bochum University, Germany, in the development of analytical BOPs that will allow for full molecular dynamics calculations.

References

[1] V. Vitek and V. Paidar, in *Dislocations in Solids*, edited by J. P. Hirth (Elsevier, Amsterdam, 2008), pp. 439.

[2] R. Gröger, A. G. Bailey, and V. Vitek, Acta Mater. **56**, 5401 (2008).

[3] R. Gröger, K. J. Dudeck, P. D. Nellist, V. Vitek, P. B. Hirsch, and D. J. H. Cockayne, Philos. Mag. **91**, 2364 (2011).

[4] R. Gröger and V. Vitek, Mater. Sci. Eng. A **643**, 203 (2015).

[5] R. Gröger and V. Vitek, Acta Mater. **56**, 5426 (2008).

[6] R. Gröger and V. Vitek, International Journal of Materials Research **100**, 315 (2009).

[7] Y. S. Lin, PhD Thesis, University of Pennsylvania, 2015.

[8] Y. S. Lin, M. Mrovec, and V. Vitek, Model. Simul. Mater. Sci. Eng. **24**, 22, 085001 (2016).

[9] Y. S. Lin, M. Mrovec, and V. Vitek, Phys. Rev. B **93**, 11, 214107 (2016).

[10] R. Gröger and V. Vitek, Model. Simul. Mater. Sci. Eng. **20**, 035019 (2012).

[11] O. N. Senkov, G. B. Wilks, J. M. Scott, and D. B. Miracle, Intermetallics **19**, 698 (2011).

[12] D. B. Miracle and O. N. Senkov, Acta Mater. **122**, 448 (2017).

[13] S. I. Rao, C. Varvenne, C. Woodward, T. A. Parthasarathy, D. Miracle, O. N. Senkov, and W. A. Curtin, Acta Mater. **125**, 311 (2017).

PUBLICATIONS BASED OB BES SUPPORTED RESEARCH: 2015-2017

R. Gröger and V. Vitek: Determination of positions and curved transition pathways of screw dislocations in BCC crystals from atomic displacements, *Materials Science and Engineering A* **643**, 203, 2015.

Yi-Shen Lin, M. Mrovec and V. Vitek: Bond-order potential for magnetic body centered cubic iron and its transferability, Phys. Rev. B **93**, 214107, 2016.

Yi-Shen Lin, M. Mrovec and V. Vitek: Importance of inclusion of the effect of s electrons into bond-order potentials for transition bcc metals with d-band mediated bonding, *Modelling Simul. Mater. Sci. Eng*. **24**, 085001, 2016.

V. Vitek, Y. S. Lin, M and M. Mrovec: Development of bond-order potentials for BCC transition metals, *Solid State Phenomena* **258**, 3, 2017.

Localized Deformation and Intergranular Fracture of Irradiated Alloys under Extreme Environmental Conditions

Gary S. Was
2355 Bonisteel Blvd., University of Michigan, Ann Arbor, MI 48109 gsw@umich.edu

Ian M. Robertson
1415 Engineering Drive, University of Wisconsin-Madison, Madison WI 53706
ian.robertson@wisc.edu

Diana Farkas
201A Holden Hall, Virginia Tech, Blacksburg, VA 24061, diana@vt.edu

Program Scope

The overall objective of this project is to determine the basic processes by which localized deformation in irradiated materials leads to intergranular cracking in alloys in aggressive environments at high temperature. We will utilize a mesoscale science approach that provides linkage from atomistic simulations of dislocation responses to the accommodation and emission of dislocations from grain boundaries, through direct observation of dislocations with irradiation defects and grain boundaries, to macroscale experiments. The consequence of this combined effort will be the identification of the factors most likely responsible for establishing not only the local stress state at grain boundaries prone to failure but also their location with respect to the macroscopic applied stress. The grain boundaries and local conditions at which disruption of the surface oxide and hence, exposure to the water environment is most probable, have been identified. Having isolated these conditions, we are poised to address why this failure does not occur at every grain boundary that is favorably oriented, why it remains isolated at one channel over others along the same grain boundary, and what is the role of environment in inducing the cracking. We are focusing on the following sub-objectives are designed to bring us closer to determining the mechanism of irradiation assisted stress corrosion cracking, IASCC.

- Does a threshold stress for initiation of IASCC exist and if so, how can the magnitude of it be determined? Is the likelihood of IASCC initiation determinable from the value of the local normal stresses at dislocation channel-grain boundary intersections, and if so, what is that value and how does it depend on the slip systems active in the dislocation channel (DC) impinging on the grain boundary (GB), the grain boundary character, and the composition of the alloy?
- The water environment plays a critical role in the cracking process because straining at the same temperature and strain rate in an inert environment does not result in grain boundary cracking. What is the role of the environment/oxide film on the initiation of IASCC cracks coupled with high local stresses on the grain boundary? Does the oxidation process create a susceptibility to cracking which is initiated by the high local stresses where dislocation channels intersect grain boundaries? What is the nature of the induced "sensitivity" of the grain boundary to cracking and why is it location specific?

Recent Progress

We conducted high resolution electron backscattering detection (HREBSD) scans of a Fe-13Cr-15Ni tensile bar, which had been strained to 3.5% plastic strain in an argon environment at 288°C after being irradiated to 5 dpa at 360°C at the Michigan Ion Beam Laboratory. To date 15 scans at discontinuous channel – grain boundary interaction sites and 10 continuous channel – grain boundary interaction sites have been successfully analyzed using the CrossCourt3 EBSD pattern cross correlation software package. As shown in Figure 1, it is clear that the residual stress near the different types of DC-GB interaction sites is fundamentally different. For each of the 15 scans near discontinuous channels, a high residual tensile stress is present in the adjacent grain where localized deformation is not present. The stress is always highest at the point of intersection and dissipates further into the grain. This elevated stress typically penetrates only 2-3 μm into the grain before reaching background stress values. Using a least squares fitting algorithm, each of the 15 scans can be fit using an $r^{-1/2}$ dependence curve with good accuracy.

Unlike the discontinuous channel cases, there seems to be no appreciable residual stress at the intersection site for continuous dislocation channels. The tensile stress profile is flat, showing small amounts of variation, across the length of the grain. Compiling all of these results, a clear distinction is evident between the two interaction types and the increased tensile stress at the discontinuous channel sites could potentially be key for describing the crack initiation process in austenitic stainless steels.

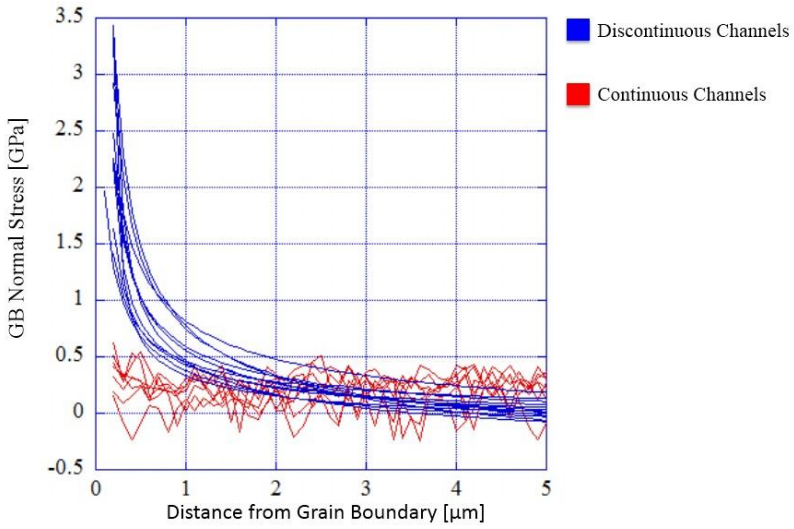

Figure 1. Compilation of stress normal to the trace of the grain boundary as a function of distance from the grain boundary for 15 discontinuous channel sites and 10 continuous channel sites in a 13Cr15Ni alloy after 3.5% strain in argon at 288°C.

Computational efforts have concentrated on the role of local grain boundary structure on the deformation response of the overall polycrystal. As part of this effort, a novel way to analyze grain boundary structure in random boundaries was developed that takes into account the dislocation content of the boundary structure itself. This analysis can better relate local grain boundary structure to the emission of dislocations from the boundaries, relevant to the dislocation channels studied in this project. In another milestone in our progress, we devised a computational technique for introducing additional disorder in the boundary structure. This additional disorder can constitute a way to mimic the effects of irradiation on grain boundary structure.

Figure 2 shows two examples of grain boundary structure viewed using the new analysis technique. To detect and quantify dislocations in the digital samples we used the Dislocation Extraction Algorithm (DXA) in the OVITO software package. DXA detects dislocations by first identifying the perfect lattice, constructing an "interface mesh" and then constructing a Burgers circuits to identify Shockley partials (⅙<112> type), perfect dislocations (½<110> type), stair-

rod dislocations (⅙<110> type), Hirth partials (⅓<100> type), and Frank partials (⅓<111>type). Dislocations that are not one of these types are labeled as "other". This analysis was run on our digital sample and results showed that there is a wide variation in the observed density of dislocations observed as part of the grain boundary structure. These variations point to the importance of local grain boundary structure when understanding deformation response.

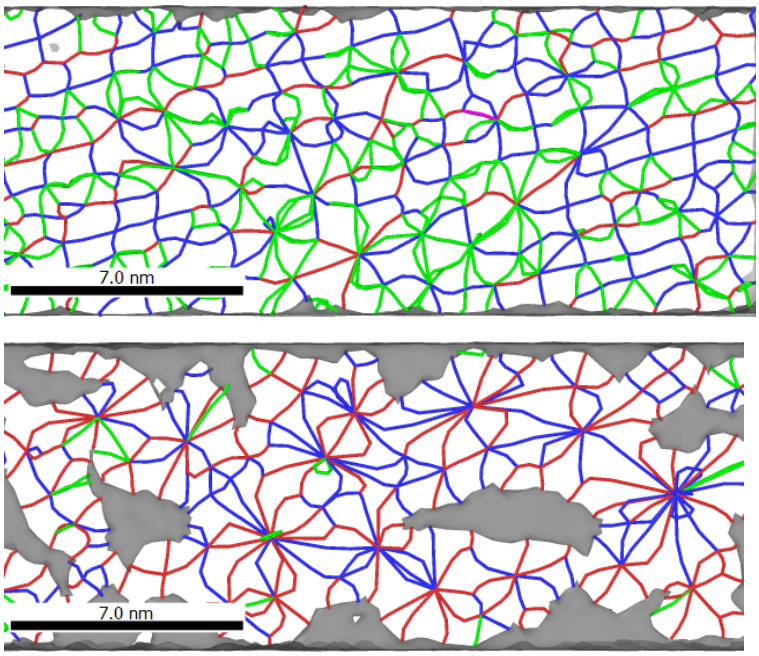

Figure 2. Renderings of DXA output of two relaxed boundaries viewed perpendicular to grain boundary plane showing examples of dislocation networks contained in random grain boundaries. Shockley partials in green, perfect ½<110> dislocations in blue and "other" in red.

To determine the role of local GB properties (e.g., composition, structure, and stress/strain) in governing the IASCC susceptibility of a specific GB site, multiple cracked and un-cracked sites in a Fe-13Cr-15Ni model alloy subjected to proton irradiation and straining in a high-temperature water environment are comparatively characterized by using transmission electron microscopy techniques. Figure 3 shows representative cracked and un-cracked sites (extracted from different GBs), respectively. For the first time, a quantitative correlation is revealed between the local composition of GBs (i.e., depletion of Cr and enrichment of Ni, as expected due to radiation-induced segregation) and their susceptibility to IASCC. Unexpectedly, GB sites beyond the crack tip always present a higher Cr and lower Ni content than the un-cracked sites on the same GB. In the meantime, the inner oxide behind the crack tip is always thinner or has a lower Cr content than that above the un-cracked sites. Overall, the efficiency of Cr transport along GBs and thus the protectiveness of inner oxide are found to play a critical role, apart from the depletion of Cr at GBs, in governing the crack initiation and propagation at a specific GB site. These effects of local composition may be coupled with local structure of the random high-angle GBs.

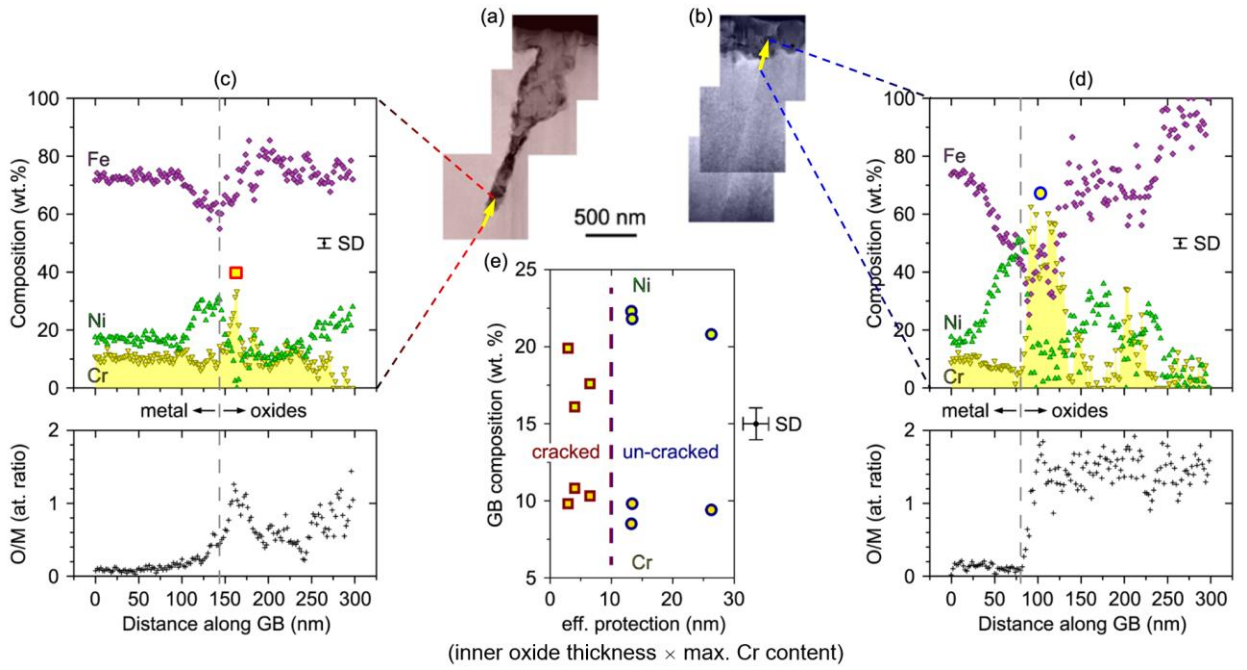

Figure 3. Representative characterization of inner oxide and its role in IASCC susceptibility of GB sites. (a, b) Annular dark-field STEM images of cross-sectional specimens extracted from (a) cracked and (b) un-cracked sites, respectively. (c, d) Compositional profiles along arrows in (a) and (b), respectively, as measured by energy dispersive spectroscopy (EDS) line-scan. The Cr profiles are highlighted in yellow, and the inner oxide layer is indicated with square in (c) and circle in (d). (e) Summary of all measurements to date shows the correlation between GB composition (upper: Ni; lower: Cr) at the far field and the effectiveness of protection, evaluated as the product of thickness and maximum Cr content, of the inner oxide layer.

Future Plans

HREBSD is being applied to an irradiated sample after pre-straining in Ar, but prior to cracking in high temperature water, to collect information on the true local residual tensile stresses at DC-GB intersections. The plan is to collect data on some 50-75 intersections to determine the relationship between local tensile stress and cracking propensity.

The slip transfer mechanisms at DC-GB intersections may not be sufficiently characterized based on the observation of surface morphology since the continuity of DCs at the far field can be distinct to that near the reaction front. Thus, we attempt to characterize the local stress/strain at GBs by using automated orientation mapping inside a transmission electron microscope. Current efforts focus on the comparing several cracked and un-cracked GB sites to determine the consistency of the initial observation.

The local development of strain and stress in these intersections is also being studied using the simulation techniques. The results of the simulations are compared with the experimental measurements of stress localization. The current simulations also focus on comparing the behavior of similar grain boundaries with different internal defect content and different states of relaxation, as a way to mimic the effects of radiation in the atomistic technique.

Recent Publications

L. Smith, D. Farkas, "Deformation Response of Grain Boundary Networks at High Temperature," J. Mater. Sci., submitted.

Mo-Rigen He, D. C. Johnson, G. S. Was, I. M. Robertson, "The Role of Grain Boundary Microchemistry in Irradiation-Assisted Stress Corrosion Cracking of a Fe-13Cr-15Ni Alloy," Acta Mater. 138 (2017) 61-71.

D. C. Johnson, B. Kuhr, D. Farkas, G. S. Was, "Quantitative Analysis of Localized Stresses in Irradiated Stainless Steels using High Resolution Electron Backscatter Diffraction and Molecular Dynamics Modeling," Scr. Mater. 116 (2016) 87-90.

B. Kuhr, Diana Farkas and Ian Robertson "Atomistic studies of hydrogen effects on grain boundary structure and deformation response in FCC Ni," Comp. Mater. Sci. 122 (2016) 820101.

I. M. Robertson, B. Cui, M.-R.He. "Dislocation-Grain Boundary Interactions in Irradiated Metals.," MINOS 2nd International Workshop, Irradiation of Nuclear Materials - Flux and Dose Effects. EPJ Web of Conferences: 2016, 115: 04001.

M. D. McMurtrey, B. Cui, I. Robertson, D. Farkas, G. S. Was, "Mechanism of Dislocation Channel-Induced Irradiation Assisted Stress Corrosion Crack Initiation in Austenitic Stainless Steel," Curr. Opin. Sol. Stat. Mater. Sci. 19 (2015) 305-314.

Electronic and Atomic Response of Ceramic Structures to Irradiation

William J. Weber[1,2], Yanwen Zhang[1], Eva Zarkadoula[1] and Fuxiang Zhang[1]

[1]Materials Science & Technology Division, Oak Ridge National Laboratory
[2]Department of Materials Science & Engineering, University of Tennessee

Program Scope

The overarching goal of this research is to understand, predictively model, and ultimately control the dynamic response of ceramic structures to energy deposition from irradiation at the level of electrons and atoms. The design of radiation tolerant materials and creation of new functional materials by ion beam modification demand a comprehensive understanding and predictive models of energy transfer and exchange processes between the electronic and atomic structures. To achieve this goal, this research focuses on two specific aims: (1) the dynamic and coupled response of the electronic and atomic structures to single ion events; and (2) the collective effects from energy deposition and dissipation processes on damage accumulation, nanostructure formation, phase transformations, and recovery processes from multiple ion events over a broad range of conditions. Novel experimental and computational approaches are integrated to investigate the separate and coupled dynamics of electronic and atomic processes over a range of irradiation conditions to elucidate the underlying mechanisms. This research utilizes unique new experimental capabilities for *in situ* luminescence measurements to characterize defect evolution in ceramics under ion irradiation. Scientific advances from the work will lead to new design principles for self-healing and radiation tolerant materials in extreme radiation environments, as well as provide the atomic-level foundation for the design and control of new functionalities in oxide electro-ceramics to enable broad advances in sustainable energy technologies and national security.

Recent Progress

Our previously work demonstrated that pre-existing defects in SiC can be annealed by irradiation with highly-ionizing ions due to energy transfer from the electronic structure to the atomic lattice, via electron-phonon coupling, that leads to highly localized heating (i.e, thermal spike) [1]. More recent studies have revealed that in-cascade ionization is also effective in suppressing the accumulation of irradiation damage in SiC due to the spatial and temporal overlap of electronic energy and ballistic damage energy deposition. The results indicate a significant dependence of irradiation damage accumulation on the ratio of total ionization energy to ballistic damage energy deposition for a range of ions. This is illustrated in Fig. 1 for SiC irradiated with 1.5 MeV Si ions [2], where the inverse dose for amorphization is linearly

dependent of the ratio of ionization energy to damage energy. The results in Fig. 1 indicate that for negligible ionization energy a unique dose for amorphization of SiC is predicted for a given ion irradiation condition. Furthermore, at sufficiently high values of the ratio of ionization to damage energy deposition (~170 for Si ions in SiC), the results indicate that the dose for amorphization will go to infinity, and full amorphization cannot be achieved. More recently [unpublished], we have found similar behavior for Au ions in SiC. The study of in-cascade ionization effects in SiC irradiated with 1.5 MeV Si also found that the threshold for in-cascade ionization-induced annealing is an electronic energy loss of ~1.0 keV/nm, which is slightly less than that previously determined (1.4 keV/nm) for highly ionizing ions in a separate effects study [1]. This work has identified a significant mechanism for self-healing of radiation damage in SiC for nuclear and space applications, and has demonstrated the important effects of energy transfer to electrons for repair of ion implantation damage in advanced electronics and for predicting material performance in extreme radiation environments where ionization and defect production occur simultaneously

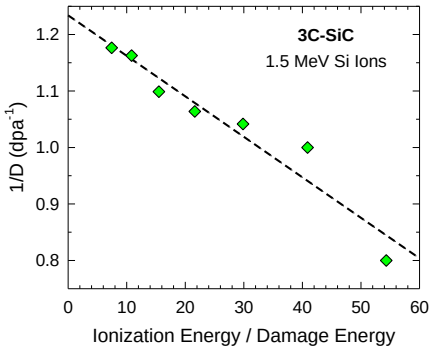

Fig. 1. Inverse amorphization dose ($1/D$) as a function of the ratio of ionization energy to damage energy deposition (adapted from Ref. 2).

A previously discovered synergy [3] between electronic energy loss by ions and pre-existing atomic defects in single-crystal $SrTiO_3$ has been investigated over a wide range of electronic energy loss [4]. The pre-existing defects decrease the electronic and lattice thermal conductivities and increase the electron-phonon coupling, which cause a highly localized thermal spike along the path of each ion that creates a nanoscale cylindrical amorphous track, but only in the region with pre-existing defects. Low energy irradiations with 0.9 MeV Au ions were used to create pre-damaged defect states corresponding to relative disorder levels of 0.10 to 0.15, as measured by Rutherford backscattering spectrometry in channeling geometry (RBS/C). Subsequent irradiations with highly ionizing ions (12 and 20 MeV Ti, 21 MeV Cl and 21 MeV Ni) revealed the formation of amorphous tracks, with track diameters that increased with increasing electronic energy loss of the ions, which is consistent with molecular dynamic simulations based on the two-temperature model [5]. The electronic stopping power threshold for ion track formation is found to be 6.7 keV/nm for the pre-damaged defect states studied, as shown in Fig. 2, which is significantly below the threshold of 10 keV/nm determined for pristine $SrTiO_3$ [6]. Below the 6.7 keV/nm threshold, ionization-induced annealing of the pre-damage $SrTiO_3$

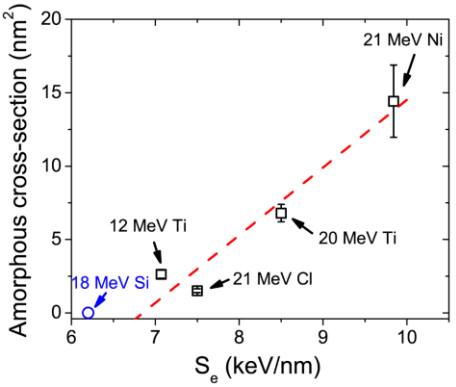

Fig. 2. Amorphous cross-sections of ion tracks as a function of S_e, for 21 MeV Ni, 12 and 20 MeV Ti, and 21 MeV Cl ion irradiations of $SrTiO_3$ with an initial disorder fraction of 0.10 to 0.15 [4].

is observed, similar to that observed in SiC. Since $SrTiO_3$ is a foundational material in functional microelectronics, the work provides new insights for creating novel interfaces and nanostructures to functionalize thin-film structures, including tunable electronic, magnetic and optical properties in thin films of epitaxial $SrTiO_3$.

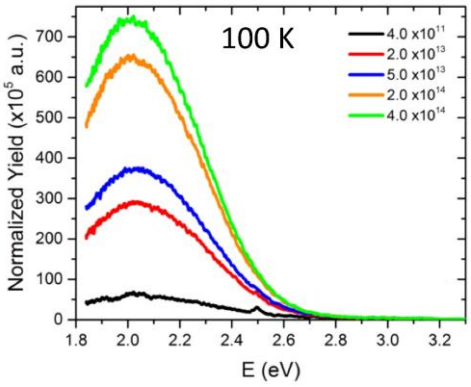

Fig. 3. Ionoluminescence spectra obtained from $SrTiO_3$ under 3 MeV H ion irradiation at 100 K to different ion fluences [7].

In-situ ionoluminescence measurements in real time during ion irradiation provide information on the evolution of emission bands with ion fluence, which can be used to establish correlations between point defect kinetics and phase stability. Novel visible luminescence in stoichiometric $SrTiO_3$ has been identified under irradiation at 100, 170 and 300 K [7]. The ionoluminescence spectra can be resolved into three main Gaussian bands at 2.0, 2.5 and 2.8 eV, whose relative contributions strongly depend on irradiation temperature, electronic energy loss and irradiation fluence. The 2.8 eV band is attributed to recombination of free electrons with an in-gap level, possibly related to self-trapped holes. Self-trapped excitons are considered responsible for the 2.5 eV emission band, which would imply a large energy relaxation in comparison to the intrinsic edge transition. The dynamics of electronic excitation govern a rapid increase in intensity of the 2.8 eV band; whereas, accumulated irradiation damage (competing non-radiative recombination channels) accounts for a subsequent intensity decrease. A previously invoked role of isolated oxygen vacancies for the blue luminescence (2.8 eV) is not consistent with our data. A well-resolved band at 2.0 eV dominates below 170 K. The increase in intensity of this band with increasing ion fluence at 100 K is shown in Fig. 3. This 2.0 eV band has been previously observed only in heavily strained and amorphous $SrTiO_3$; however, based on ab initio theoretical calculations, we attribute it to *d-d* transitions from electrons that are self-trapped as relaxed Ti^{3+} centers in distorted TiO_6 octahedra, which are stabilized by a high concentration of irradiation-induced oxygen vacancies. This interpretation has been confirmed in a more recent study using Cr-doped $SrTiO_3$ [unpublished], where decay of the Cr^{3+} luminescence (due to hole trapping) is correlated to the growth of the 2.0 eV emission band. This work demonstrates that defect evolution can be monitored in real-time using ionoluminescence and that the 2.0 eV emission band can be used to monitor the evolution of O vacancies in $SrTiO_3$ under irradiation and annealing.

The effects of electronic excitations on $SrTiO_3$ have been investigated using first-principles calculations. The results suggest that electronic excitation induces a metallic transition and charge redistribution in $SrTiO_3$. Upon electronic excitation, phonon frequencies in $SrTiO_3$ become highly localized and a new peak appears in the phonon density of states with negative frequencies, an indication of lattice instability. Further dynamics simulations confirm that $SrTiO_3$ undergoes a transition to an amorphous structure under strong electronic excitations. The

luminescence of $SrTiO_3$ under electronic excitation is consistent with the evolution of atomic structures, which supports using luminescence to probe structural changes.

Future Plans

Based on synergistic effects observed in $SrTiO_3$ [1,2] above a threshold and evidence for ionization-induced annealing below the threshold, experimental and computational studies are planned to advance the understanding of ionization processes in $SrTiO_3$. Emphasis will focus on understanding ionization-induced annealing at low levels of electronic energy loss, where thermal spikes are minimal, using electron and light ion beams (H, He, O). Similar behavior is expected to occur in $KTaO_3$ and $LiTaO_3$, and experimental and computational studies are planned to understand the effects of chemical changes on synergistic processes. These model ceramics have strong luminescence signatures for vacancy defects, and *in situ* luminescence measurements at cryogenic temperatures (down to 20 K) will be used to study the production and recovery of vacancy defects from the energy loss to electrons and atomic nuclei by energetic ions. The outcome from these studies will be essential to advance our understanding on electronic and atomic response of ceramic structures to irradiation.

The computational effort will focus on evaluating the fidelity of the two-temperature model as applied to ceramics and on employing ab initio MD methods to explore the effects of high electronic excitation densities on defect stability, defect mobility and phase transformations.

References

1. Y. Zhang, R. Sachan, O. H. Pakarinen, M. F. Chisholm, P. Liu, H. Xue, W. J. Weber, "Ionization-induced annealing of pre-existing defects in silicon carbide," *Nature Commun.* **6**, 8049 (2015).
2. H. Xue, Y. Zhang, W. J. Weber, "In-cascade ionization effects on defect production in 3C SiC," *Mater. Res. Lett.* (2017) in press. http://dx.doi.org/10.1080/21663831.2017.1334241
3. W. J. Weber, E. Zarkadoula, O. H. Pakarinen, R. Sachan, M. F. Chisholm, P. Liu, H. Xue, K. Jin, Y. Zhang, "Synergy of elastic and inelastic energy loss on ion track formation in $SrTiO_3$," *Scientific Reports* **5**, 7726 (2015).
4. H. Xue, E. Zarkadoula, P. Liu, K. Jin, Y. Zhang, and W. J. Weber, Amorphization due to electronic energy deposition in defective strontium titanate," *Acta Mater.* **127**: 400 (2017).
5. E. Zarkadoula, H. Xue, Y. Zhang, and W. J. Weber, "Synergy of inelastic and elastic energy loss: Temperature effects and electronic stopping power dependence," *Scripta Materialia* **110**: 2-5 (2016).
6. M. Karlusic et al. "Swift heavy ion track formation in $SrTiO_3$ and TiO_2 under random, channeling and near-channeling conditions," *J. Phys. D: Appl. Phys.* **50**: 205302 (2017).
7. M. L. Crespillo, J. T. Graham, F. Agulló-López, Y. Zhang, and W. J. Weber, "Role of oxygen vacancies in light emission mechanisms in $SrTiO_3$ induced by high-energy particles," *J. Physics D: Appl. Phys.* **50** [15]: 155303 (2017).

Publications

H. Xue, Y. Zhang, W. J. Weber, "In-cascade ionization effects on defect production in 3C SiC," *Mater. Res. Lett.* (2017) in press. http://dx.doi.org/10.1080/21663831.2017.1334241

N. Sellami, M. L. Crespillo, H. Xue, Y. Zhang, and W. J. Weber, "Role of atomic-level defects and electronic energy loss on amorphization in $LiNbO_3$ single crystals," *J. Physics D: Applied Physics* **50** [32]: 355103 (2017).

H. Xue, E. Zarkadoula, P. Liu, K. Jin, Y. Zhang, and W. J. Weber, "Amorphization due to electronic energy deposition in defective strontium titanate," *Acta Materialia* 127: 400-406 (2017).

M. L. Crespillo, J. T. Graham, F. Agulló-López, Y. Zhang, and W. J. Weber, "Role of oxygen vacancies in light emission mechanisms in $SrTiO_3$ induced by high-energy particles," *J. Physics D: Appl. Phys.* **50** [15]: 155303 (2017).

R. Sachan, Y. Zhang, X. Ou, C. Trautmann, M. F. Chisholm, and W. J. Weber, "New insights on ion track morphology in pyrochlores by aberration corrected scanning transmission electron microscopy," *J. Materials Research* **32** [5]: 928-935 (2017).

J. Xi, H. Xu, Y. Zhang, and W. J. Weber, "Strain effects on oxygen vacancy energetics in $KTaO_3$," *Phys. Chem. Chem. Phys.* **19** [8]: 6264-6273 (2017).

E. Zarkadoula, K. Jin, Y. Zhang, and W. J. Weber, "Synergistic effects of nuclear and electronic loss in $KTaO_3$ under ion irradiation," *AIP Advances* **7** [1]: 015016 (2017).

R. Sachan, V. R. Cooper, B. Liu, D. S. Aidhy, B. K. Voas, M. Lang, X. Ou, C. Trautmann, Y. Zhang, M. F. Chisholm, and W. J. Weber, "Forging Fast Ion Conducting Nanochannels with Swift Heavy Ions: The Correlated Role of Local Electronic and Atomic Structure," *J. Physical Chemistry C* **121** [1]: 975-981 (2017)

K. Imada, M. Ishimaru, H. Xue, Y. Zhang, S. C. Shannon, and W. J. Weber, "Amorphization resistance of nano-engineered SiC under heavy ion irradiation," *J. Nuclear Materials* **478**, 310-314 (2016).

J.-M. Costantini, G. Lelong, M. Guillaumet, W. J. Weber, T. Seiya, and K. Yasuda, "Color-center production and recovery in electron-irradiated magnesium aluminate spinel and ceria," *J. Physics: Condensed Matter* **28**, 325901 (2016).

M. L. Crespillo, J. T. Graham, Y. Zhang, and W. J. Weber, "In-situ luminescence monitoring of ion-induced damage evolution in SiO_2 and Al_2O_3," *J. Luminescence* **172**: 208-218 (2016).

R. Sachan, E. Zarkadoula, M. Lang, C. Trautmann, Y. Zhang, M. F. Chisholm, and W. J. Weber, "Insights on dramatic radial fluctuations in track formation by energetic ions," *Scientific Reports* **6**: 27196 (2016).

E. Zarkadoula, H. Xue, Y. Zhang, and W. J. Weber, "Synergy of inelastic and elastic energy loss: Temperature effects and electronic stopping power dependence," *Scripta Materialia* **110**: 2-5 (2016).

D. S. Aidhy and W. J. Weber, "Microstructure design for fast oxygen conduction," *J. Materials Research* **31** [1]: 2-16 (2016).

T. Oda, W. J. Weber, and H. Tanigawa, "Two-body potential model based on cosine series expansion for ionic materials," *Computational Materials Science* **111**: 54-63 (2016).

P. Liu, Y. Zhang, H. Xue, K. Jin, M. L. Crespillo, X. Wang, and W. J. Weber, "A coupled effect of nuclear and electronic energy loss on ion irradiation damage in lithium niobate," *Acta Materialia* **105**: 429-437 (2016).

C. L. Fontana, C.-H. Chen, M. L. Crespillo, J. T. Graham, H. Xue, Y. Zhang, and W. J. Weber, "Stopping power measurements with the Time-of-Flight (ToF) technique," *Nucl. Instrum. and Methods in Physics Research* **B 366**: 104-116 (2016).

D.S. Aidhy, R. Sachan, E. Zarkadoula, O. Pakarinen, M. F. Chisholm, Y. Zhang, and W. J. Weber, "Fast ion conductivity in strained defect-fluorite structure created by ion tracks in $Gd_2Ti_2O_7$," *Scientific Reports* **5**: 16297 (2015).

E. Zarkadoula, M. Toulemonde, and W. J. Weber, "Additive effects of electronic and nuclear energy losses in irradiation-induced amorphization of zircon," *Applied Physics Letters* **107** [26]: 261902 (2015).

K. Imada, M. Ishimaru, K. Sato, H. Xue, Y. Zhang, S. Shannon, and W. J. Weber, "Atomistic structures of nano-engineered SiC and radiation-induced amorphization resistance," *J. Nuclear Materials* **465**: 433-437 (2015).

E. Zarkadoula, O. H. Pakarinen, H. Xue, Y. Zhang, and W. J. Weber, "Predictive modeling of synergistic effects in nanoscale ion track formation," *Phys. Chem. Chem. Phys.* **17** [35]: 22538-22542 (2015).

Deformation mechanisms of nanotwinned Al and binary Al alloys

Xinghang Zhang
School of Materials Engineering, Purdue University, West Lafayette, IN 47907
Phone: (765) 494-1641; Email: xzhang98@purdue.edu

Program Scope

The objective of this project is to investigate, at a fundamental level, the deformation mechanism of nanotwinned (nt) Al and binary Al alloy films with high density **twin boundaries (TBs)** and **stacking faults (SFs)**. To achieve this goal, we will test the following hypotheses:

1) ***Nanotwinned (nt) Al with high stacking fault energy (SFE) may have strengthening mechanisms drastically different from those of nt Cu with low SFE.*** *In particular, the high SFE implies that incoherent twin boundaries (ITBs) in Al may be less mobile comparing to ITBs in Cu with low SFE during deformation. Also softening observed in nt Cu (at smaller twin spacing) due to ITB migration may be absent in nt Al.*
2) ***ITBs and SFs may enable high ductility in nt Al.*** Although there are abundant studies that show CTBs promote work hardening in nt Cu, there are few studies that investigate the influence of ITBs and SFs on tensile ductility of nt Al. Furthermore the mechanisms of dislocation-ITB interactions in nt Al, which may be crucial to accomplish tensile ductility in nt Al, are poorly understood.
3) ***Certain solutes in nt Al alloys may enable substantial increase of strength and plasticity and significantly enhance the mechanical and thermal stability of TBs in nt Al alloys.*** *The addition of certain solutes may enable us to tailor (reduce) the SFE of Al alloy, so that we can introduce greater density of twins/SFs in nt Al alloys, tailor strengthening and deformation mechanisms in nt Al alloys and accomplish significant increase of strength with little loss in ductility in nt Al alloys.*

Recent Progress

1. The formation mechanisms of growth twins in polycrystalline Al with high stacking fault energy (S. Xue et al, Acta Mater., 2015)

Fabrication of growth twins in Al is a challenge due to the high stacking fault energy of Al. Recently high-density growth twins and stacking faults have been fabricated into Al by introducing nanotwined Ag buffer layers by the magnetron sputtering technique. The Al film grown epitaxially on Ag replicates the microstructures including twins from the Ag seed layer because Ag and Al has identical lattice parameter and crystal structure. In this study, however, we report the observation of growth twins in sputtered polycrystalline Al films on amorphous substrates without Ag seed layer as shown in Fig. 1. Most growth twins are inclined to the growth direction.

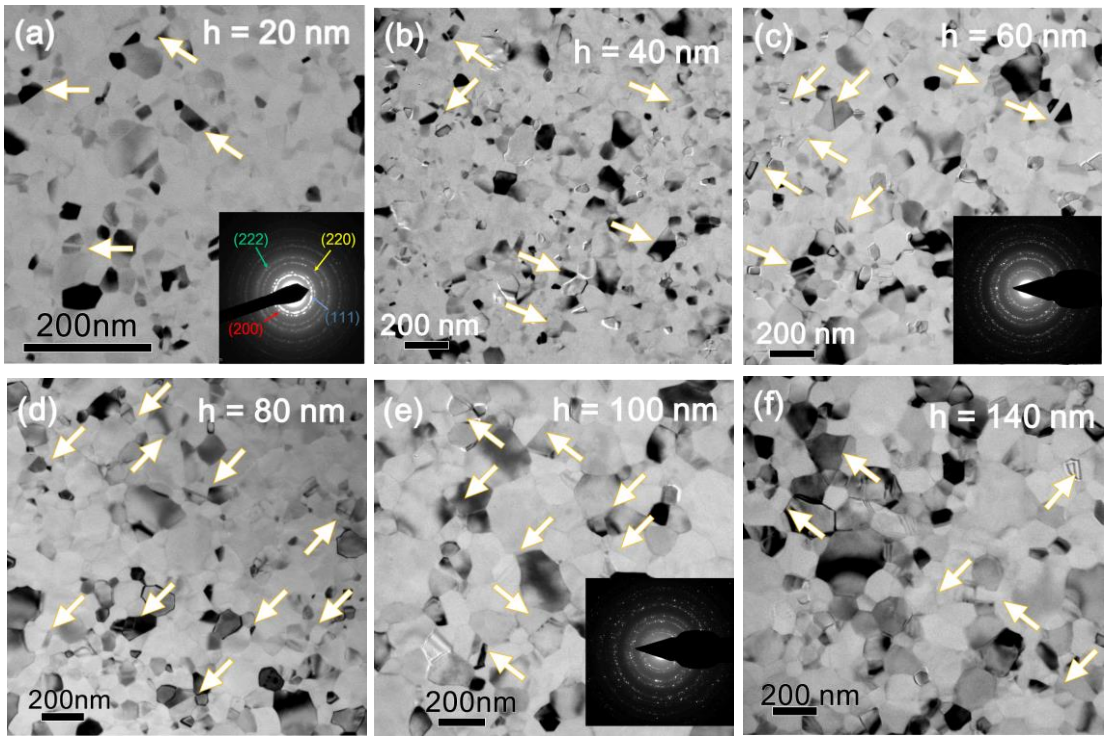

Figure 1. Figure 1. Transmission electron microscopy (TEM) micrographs of Al films with different film thickness showing the formation of growth twins. (a) h = 20 nm, (b) h = 40 nm, (c) h = 60 nm, (d) h = 80 nm, (e) h = 100 nm, (f) h = 140 nm. Twins were frequently observed as labeled selectively by arrows in the micrographs. The inserted selected area diffraction (SAD) patterns indicate the formation of polycrystalline Al films.

Although the fraction of twinned grains is low, it increases monotonically with increasing film thickness, reaches a maximum (9%, Fig. 2A) at the film thickness of 80 nm, and decreases thereafter in the thicker films. The nucleation mechanism for the inclined twins is compared with that of the parallel growth twins in Al as shown schematically in Fig. 2B. Basically the nucleation of an inclined twin may be preferred over a twin nuclei parallel to the substrate (matrix). This study provides an alternative perspective to evaluate the formation of growth twins in metals with high stacking fault energy.

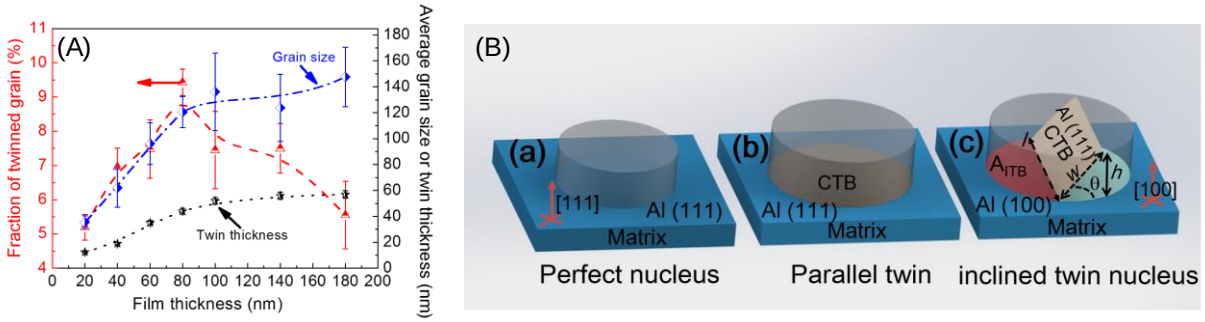

Figure 2. (A) The evolution of fraction of twinned grains, average twin thickness and grain size with Al film thickness. The fraction of twinned grains increases continuously with increasing film thickness, reaches a maximum of ~ 9% when h = 80 nm, and decreases thereafter in thicker films. The average twin thickness and grain sizes increase monotonically with film thickness and approach plateaus when h = 100 nm. (B) Schematic diagrams comparing the nucleation of (a) a perfect nucleus, (b) a parallel twinned nucleus and (c) a nucleus with inclined growth twin on Al matrix. (a) The perfect nucleus and the matrix has the same <111> crystal orientation. (b) The parallel twin nucleus forms (111) CTB on the (111) matrix. (c) A nucleus contains both inclined CTB and incoherent twin boundary (ITB) with the matrix. Note an example of (100) matrix is used to illustrate the concept without losing the generality of the model. A fraction of the matrix-nucleation interface contains ITB with an area of A_{ITB}, whereas the remaining of the nucleus has the same crystal orientation as the matrix.

(2) Texture-directed twin formation propensity in Al with high stacking fault energy (in review)

There are limited approaches to promote the formation of nanotwins in Al films. Here, we show that twin morphology and twin density can be altered by tailoring the texture of films. TKD-EBSD experiments were systematically performed to show detailed crystallographic and microstructural information. Epitaxial Al (111) has only two {111} twin variants, matrix and twins, resulting in small isolated twin islands due to abnormal grain growth (Fig. 3b). Epitaxial Al (112) film has the highest density of ITBs, because the {112} and {212} twin variants are separated by Al (102) islands, promoting the formation of ITBs (Fig. 3c). The smaller domain size can thus be achieved by introducing high angle grain boundaries (HAGBs) into the twinned structure to inhibit the abnormal growth of single twin variant. Two designing criteria are identified to fabricate high density twins in Al. These in-depth microstructure analyses supported by extensive EBSD and TEM studies provide an alternative way to promote the formation of highly twinned Al.

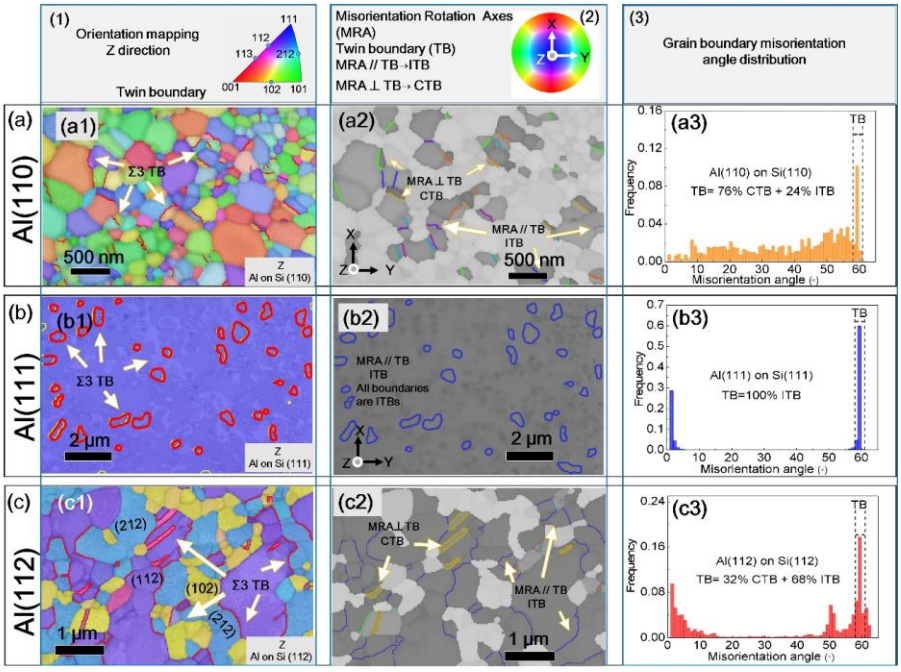

Figure 3. Orientation mapping and grain boundary misorientation angle distribution for as-deposited Al thin films by using TKD technique. Row a, b and c show the crystallographic information of Al (110), Al (111), Al (112) separately. Column 1, 2, 3 show the orientation mapping, twin boundary rotation axis, and GB misorientation angle distribution respectively. (a1, b1, and c1) The Al film orientation map (OM) along the Z direction with red lines arising from the Σ3 TB. (a2, b2 and c2) The misorientation rotation axis (MRA) maps reveal the method to differentiate ITBs from coherent twin boundaries (CTBs). For ITBs, the MRA//TBs, and for CTBs, MRA⊥TBs. See supplemenery information for details to differentiating ITBs and CTBs. (a3, b3 and c3) The distribution of GB misorientation angle of Al thin films with different texture.

Future Plans

In the next fiscal year, we plan to undertake the following tasks:

1) Study deformation and strengthening mechanisms of different twin structures in Al.
2) Explore the solute effect on twin formation in binary Al alloy systems.
3) Investigate different deformation mechanisms and nt Al and Al alloys.
3) Explore the thermal stability of nanotwins in Al and Al alloys.

Publications-patent through this program, 2015-2017

1. Y. Liu, N. Li, D. Bufford, J. Wang, J.H. Lee, H. Wang, and X. Zhang, *In situ* nanoindentation studies on detwinning and work hardening in nanotwinned monolithic metals", *JOM* (invited review article), 68 (2016) 127.

2. J. Li, K. Y. Yu, Y. Chen, M. Song, H. Wang, M.A. Kirk, M. Li, and X. Zhang, *In situ* Study of Defect Migration Kinetics and Self-Healing of Twin Boundaries in Heavy Ion Irradiated Nanotwinned Metals, *Nano Letters*, *15* (2015), pp 2922–2927, **DOI:** 10.1021/nl504677z.

3. Y. Chen, Y. Liu, S. Shao, H. Wang, M.A. Kirk, J. Wang and X. Zhang, Damage tolerant nanotwinned metals with nanovoids under radiation environments, *Nature Communications*, 6, 7036, 2015.
4. Xinghang Zhang, Daniel Bufford, Yue Liu and Haiyan Wang, Method for producing high stacking fault energy metal films and coatings with high density nanotwins, US patent filed in spring 2015.
5. S. Xue, Z. Fan, Y. Chen, J. Li, H. Wang and X. Zhang, the formation mechanisms of growth twins in polycrystalline Al with high stacking fault energy, *Acta Mater.*, 101 (2015), 62-70.
6. Daniel C. Bufford, Y. Morris Wang, Yue Liu, and Lei Lu, Synthesis and microstructure of electrodeposited and sputtered nanotwinned face-centered-cubic metals, MRS Bulletin, 41 (2016) 286-291.
7. Jian Wang, Xinghang Zhang, Twinning effects on strength and plasticity of metallic materials, **MRS Bulletin**, 41 (2016) 274-281 (Guest editor).
8. S. Xue, W.C.H. Kuo, Q. Li, J. Ding, R. Su, H. Wang, and X. Zhang, Texture-directed twin formation propensity in Al with high stacking fault energy, under review.

Author Index

Participant List

Name	Organization	Email
Aifantis, Katerina	University of Florida	kaifanti@mtu.edu
Allison, John	University of Michigan	johnea@umich.edu
Anderson, Peter	The Ohio State University	anderson.1@osu.edu
Beach, John	University of Illinois, Urbana-Champaign	jabeach2@illinois.edu
Bellon, Pascal	University of Illinois, Urbana-Champaign	bellon@illinois.edu
Boehlert, Carl	Michigan State University	boehlert@egr.msu.edu
Boyce, Brad	Sandia National Laboratories	blboyce@sandia.gov
Brinson, Catherine	Northwestern University	cbrinson@northwestern.edu
Bruemmer, Stephen	Pacific Northwest National Laboratory	stephen.bruemmer@pnnl.gov
Byun, Thak Sang	Pacific Northwest National Laboratory	thaksang.byun@pnnl.gov
Cai, Wei	Stanford University	caiwei@stanford.edu
Capolungo, Laurent	Los Alamos National Laboratory	laurent@lanl.gov
Crimp, Martin	Michigan State University	crimp@egr.msu.edu
Daly, Samantha	University of California, Santa Barbara	samdaly@engineering.ucsb.edu
Dauskardt, Reinhold	Stanford University	dauskardt@stanford.edu
DeWitt, Stephen	University of Michigan	stvdwtt@umich.edu
Ding, Jun	Lawrence Berkeley National Laboratory	ding@lbl.gov
El-Azab, Anter	Purdue University	aelazab@purdue.edu
Farkas, Diana	Virginia Tech	diana@vt.edu
Foiles, Stephen	Sandia National Laboratories	foiles@sandia.gov
Fullwood, David	Brigham Young University	dfullwood@byu.edu
Gan, Jian	Idaho National Laboratory	Jian.Gan@INL.gov
George, Easo	Oak Ridge National Laboratory	georgeep@ornl.gov
Ghazisaeidi, Maryam	The Ohio State University	ghazisaeidi.1@osu.edu
Greer, Julia	California Institute of Technology	jrgreer@caltech.edu
Hackney, Steve	Michigan Technological University	hackney@mtu.edu
Hemker, Kevin	Johns Hopkins University	hemker@jhu.edu
Homer, Eric	Brigham Young University	eric.homer@byu.edu
Kacher, Joshua	Georgia Institute of Technology	josh.kacher@mse.gatech.edu
Karasz, Erin	Arizona State University	ekkarasz@asu.edu
Krogstad, Jessica	University of Illinois, Urbana-Champaign	jakrogst@illinois.edu
LeSar, Richard	AMES Laboratory	lesar@iastate.edu
Li, Lin	University of Alabama	lin.li@eng.ua.edu
Li, Qizhen	Washington State University	qizhen.li@wsu.edu
Lou, Jun	Rice University	jlou@rice.edu
McGrogan, Frank	Massachusetts Institute of Technology	mcgrogan@mit.edu
Miller, Matthew	Cornell University	mpm4@cornell.edu
Mills, Michael	The Ohio State University	mills.108@osu.edu
Misra, Amit	University of Michigan, Ann Arbor	amitmis@umich.edu
Morris, James	Oak Ridge National Laboratory	morrisj@ornl.gov
Papanikolaou, Stefanos	West Virginia University	stefanos.papanikolaou@mail.wvu.edu
Pekin, Thomas	Lawrence Berkeley National Laboratory	tcpekin@berkeley.edu
Perriot, Romain	Los Alamos National Laboratory	rperriot@lanl.gov

Riedo, Elisa	The City University of New York	elisa.riedo@asrc.cuny.edu
Ritchie, Robert	Lawrence Berkeley National Laboratory	roritchie@lbl.gov
Rupert, Timothy	University of California, Irvine	trupert@uci.edu
Sangid, Michael	Purdue University	msangid@purdue.edu
Sansoz, Frederic	University of Vermont	frederic.sansoz@uvm.edu
Schreiber, Daniel	Pacific Northwest National Laboratory	daniel.schreiber@pnnl.gov
Schroers, Jan	Yale University	jan.schroers@yale.edu
Schuh, Christopher	Massachusetts Institute of Technology	schuh@mit.edu
Sellami Bouachir, Neila	Oak Ridge National Laboratory	sellamibouan@ornl.gov
Shao, Lin	Texas A&M University	lshao@tamu.edu
Sheldon, Brian	Brown University	brian_sheldon@brown.edu
Sieradzki, Karl	Arizona State University	karl.sieradzki@asu.edu
Song, Hengxu	Johns Hopkins University	hsong30@jhu.edu
Stebner, Aaron	Colorado School of Mines	astebner@mines.edu
Szlufarska, Izabela	University of Wisconsin	szlufarska@wisc.edu
Tomé, Carlos	Los Alamos National Laboratory	tome@lanl.gov
Uberuaga, Blas	Los Alamos National Laboratory	blas@lanl.gov
Vetrano, John	US Department of Energy	john.vetrano@science.doe.gov
Vitek, Vaclav	University of Pennsylvania	vitek@seas.upenn.edu
Wang, Jian	University of Nebraska, Lincoln	jianwang@unl.edu
Was, Gary	University of Michigan	gsw@umich.edu
Weber, William	Oak Ridge National Laboratory	wjweber@utk.edu
Yildiz, Bilge	Massachusetts Institute of Technology	byildiz@mit.edu
Zhang, Xinghang	Purdue University	xzhang98@purdue.edu
Zhang, Yanwen	Oak Ridge National Laboratory	Zhangy1@ornl.gov
Zhang, Yongfeng	Idaho National Laboratory	Yongfeng.zhang@inl.gov